

Complementary-DNA-strand crosslinked polyacrylamide hydrogels

by

Cong Du

Department of Chemical Engineering

McGill University

Montreal, Quebec, Canada

October, 2018

A thesis submitted to McGill University in partial fulfillment of the requirements
for the degree of

Doctor of Philosophy

© Cong Du, 2018

Acknowledgements

I would like to express my deepest gratitude to my family for their unconditional love, and my friends for their encouragement and support.

Many thanks to my supervisor, Professor Reghan J. Hill, who gave me the precious opportunity to study at McGill University. His patient guidance and encouragement gave me confidence. Accomplishing this thesis would not have been possible without his invaluable knowledge and ideas, careful editing, and excellent feedback.

I want to thank all past and present members of Prof. Hill's research group, especially Vahid Adibnia who provided useful advice on my rheology experiments, Marziye Mirbagheri who was a very responsible safety officer, and my office mates: Mikhail Morunov, Luc Hudon, Liji Le, and Gbolahan Afuwape. Also, I want to thank Ahmed Khan for helping me with the French abstract.

I am sincerely grateful to Frank Caporuscio who is very resourceful and always willing to help, Andrew Golsztajn who helped me identify sources of error in my gel synthesis experiment, Gerald Lepkyj and Luciano Cusmich who helped me with electrode welding, Ranjan Roy who answered my questions in instrumentation, Lisa Volpato who is always patient in the store, Louise Miller-Aspin and Jo-Ann Gadsby for their administrative assistance, and all technical and administrative staff in the department of Chemical Engineering for their help.

Finally, thanks to a McGill Engineering International Tuition Award, NSERC Discovery and Research Tools and Instruments grants, and NSERC Sentinel Bioactive Paper Network for financial support of this research.

Abstract

Polyacrylamide hydrogels physically crosslinked by double-stranded DNA have demonstrated potential for drug delivery, biosensing, and tissue engineering due to their programmability, mechanical tunability, molecular-recognition, and temperature reversibility. For some applications, introducing chemical crosslinks (*e.g.*, bis-acrylamide) to the gel network is necessary. This thesis provides fundamental understanding of bis-, DNA-, and dual-crosslinked gels from macrorheology and swelling. In the rheological studies, dynamic shear moduli in the linear viscoelastic regime were measured during and following gelation, followed by creep-recovery. Swelling tests were undertaken to investigate the gel durability in the solvent. It was found that gelation with DNA crosslinker is faster and more efficient than chemical crosslinking. Time-temperature superposition was adopted to extend dynamic spectra and furnish the activation energy. For bis-crosslinked gels, the activation energy is interpreted as the potential barrier required for disentanglement, whereas, for DNA-crosslinked gels, the activation energy is the potential barrier for DNA-crosslink disengagement. DNA-crosslinked gels behave like solids on short timescales and become liquid-like on long timescales. These gels dissolve in the solvent, and the swelling ratio (prior to dissolution) increases with the gel plateau modulus. For dual-crosslinked gels, permanent crosslinks arrest creep and prevent gel dissolution in the solvent. Insights into the microstructures of the three types of gels, such as entanglements and pore sizes, are provided.

Abrégé

Les hydrogels de polyacrylamide physiquement réticulés par de l'ADN double brin ont démontré un potentiel pour l'administration de médicaments, la biodétection et l'ingénierie tissulaire en raison de leur programmabilité, leur accordabilité mécanique, leur reconnaissance moléculaire et leur réversibilité de la température. L'introduction de réticulations chimiques (par exemple bis-acrylamide) sur le réseau de gel est nécessaire pour certaines applications. Cette thèse apporte une compréhension fondamentale des gels bis-, ADN-, et double-réticulés de la macrorhéologie et du gonflement. Dans les études rhéologiques, les modules de cisaillement dynamique dans le régime viscoélastique linéaire ont été mesurés pendant et après la gélification, suivi de la récupération par fluage. Des essais de gonflement ont été entrepris pour étudier la durabilité du gel dans le solvant. Il a été trouvé que la gélification avec un agent de réticulation d'ADN est plus rapide et plus efficace qu'une réticulation chimique. La superposition de temps-température a été adoptée pour étendre les spectres dynamiques et fournir l'énergie d'activation. Pour les gels bis-réticulés, l'énergie d'activation est interprétée comme la barrière potentielle requise pour le démêlage. Pour les gels réticulés par ADN, l'énergie d'activation est la barrière potentielle pour le désengagement de l'ADN réticulé. Les gels réticulés par l'ADN se comportent comme des solides sur des échelles de temps courtes et deviennent liquides sur de longues périodes. Ces gels se dissolvent dans le solvant, et le ratio de gonflement (avant la dissolution) augmente avec le module du plateau de gel. Pour les gels à double réticulation, les réticulations permanentes arrêtent le fluage et empêchent la dissolution du gel dans le solvant. Un aperçu des microstructures des trois types de gels, tels que les enchevêtrements et les tailles de pores, sont fournis.

Contents

Acknowledgements	i
Abstract	ii
Abrégé	iii
List of figures	viii
List of tables	xviii
Abbreviations	xix
Symbols	xx
1 Introduction	1
1.1 Motivation	1
1.2 Thesis objectives	2
1.3 Thesis organization	2
1.4 Contributions of authors	3
2 Properties and characterization of hydrogels	4
2.1 Hydrogels	4
2.1.1 Polyacrylamide hydrogels	7
2.1.2 DNA-crosslinked hydrogels	9
2.1.3 Dual-crosslinked hydrogels	11
2.2 Rheology	11
2.2.1 Viscoelasticity	15
2.2.2 Creep-recovery	18
2.2.3 Large amplitude oscillatory shear (LAOS)	19
2.3 Swelling	20

2.3.1	Equilibrium swelling ratio	20
2.3.2	Swelling kinetics	21
2.3.3	Drug delivery	23
3	Linear viscoelasticity of bis-acrylamide crosslinked polyacrylamide hydrogels with low crosslinker ratio	24
3.1	Preface	24
3.2	Introduction	25
3.3	Materials and methods	27
3.4	Results and discussion	29
3.4.1	Gelation kinetics	29
3.4.2	Dynamic moduli spectra and time-temperature superposition	32
3.4.3	Activation energy and scaled effective crosslink number	38
3.4.4	Creep and recovery in the linear viscoelastic regime	40
3.5	Conclusions	42
	Appendices	45
3.A	Detailed protocols for bis-crosslinked hydrogel synthesis and rheology	45
3.B	Bis-crosslinked gels with higher crosslinker ratio	47
3.C	Sensitivity of rheological measurements to instrument setup	48
3.D	Gap-compensation factor	52
3.E	Transformation between creep compliance and dynamic moduli spectra	56
4	Linear viscoelasticity of complementary-DNA-strand crosslinked polyacrylamide hydrogels	57
4.1	Preface	57
4.2	Introduction	58
4.3	Materials and methods	60
4.4	Results and discussion	62
4.4.1	Gelation kinetics	62
4.4.2	Dynamic moduli spectra and time-temperature superposition	66
4.4.3	Activation energy and scaled effective crosslink number	73
4.4.4	Roles of physical and chemical crosslinks in dual-crosslinked networks	80
4.4.5	Creep and recovery in the linear viscoelastic regime	80
4.5	Conclusions	85

Appendices	88
4.A Detailed protocols for DNA- and dual-crosslinked hydrogel synthesis and rheology	88
4.B Dynamic moduli spectra of gels before and after time-temperature superposition	90
4.C Experimental condition effect on dynamic moduli spectra and time-temperature superposition	91
4.D Creep compliance model	95
4.E Transformation between creep compliance and dynamic moduli spectra . . .	96
4.F Strain-sweep test	97
5 Swelling of complementary-DNA-strand crosslinked polyacrylamide hydrogels	102
5.1 Preface	102
5.2 Introduction	103
5.3 Materials and methods	106
5.4 Results and discussion	107
5.4.1 Swelling of bis-crosslinked hydrogels	107
5.4.2 Swelling of DNA- and dual-crosslinked hydrogels	109
5.4.3 Theoretical interpretation	118
5.5 Conclusions	122
Appendices	124
5.A Dissolution and reformation of DNA-crosslinked gels	124
5.B Accumulated UV-vis spectra	124
5.C Conversion of mass swelling ratio to volume swelling ratio	124
5.D Calibration of DNA absorbance and determination of the DNA combination time	129
5.E Effect of solvent on the swelling ratio	131
5.F Comparing the swelling of DNA-crosslinked gels synthesized varying TEMED concentration	131
6 Conclusions and future work	139
6.1 Summary	139
6.2 Original contributions to knowledge	140
6.3 Future work	141

List of Figures

2.1	Top: Schematic of a polymer network with inhomogeneous crosslinking density and connectivity defects. The short arrow marks a typical mesh size, whereas the long arrow indicates the typical length scale of spatial variation of the crosslinking density. Bottom: Schematics of (A) randomly distributed crosslinks (red dots) in a deswollen polymer network and (B) the same network swollen in a good solvent. Highly crosslinked local domains (red segments) swell less than the rest of the network, leading to pronounced static spatial polymer-segmental concentration fluctuations on length scales of several tens to hundreds of nanometers ¹ . Reprinted with permission.	6
2.2	Relationship between crosslinker (bis-acrylamide) concentration and elastic modulus with various total monomer (acrylamide) concentrations ² . Reprinted with permission.	9
2.3	ARES-G2 rheometer with an advanced Peltier system for temperature control. The schematic shows the parallel-plate geometry used in this study.	14
2.4	Storage and loss modulus versus frequency with logarithmic scales for different polymer systems. Replotted according to Ferry ³	15
3.1	Gel-composition map: separation of solutions and gels (black curve); identification of constant crosslinker to monomer ratios (black lines); the monomer and crosslinker concentrations for this study (green), Adibnia and Hill ⁴ (blue), Adibnia ⁵ (red), Trompette et al. ⁶ (grey), Calvet et al. ⁷ (violet), Basu et al. ⁸ (yellow), and Denisin and Pruitt ² (orange).	27
3.2	Storage modulus G' (top left), least-squares fit of Eqn. (3.5) (top right), loss modulus G'' (bottom left), and loss tangent (bottom right) for bis-crosslinked gels during gelation: $\omega = 1 \text{ rad s}^{-1}$, $T = 21^\circ\text{C}$. Disturbances from the application of silicone oil have been removed.	30

3.3	Left: The mid-point slope P (left axis) and gelation half time θ (right axis) for bis-crosslinked gels with varying crosslinker ratio: $\omega = 1 \text{ rad s}^{-1}$, $T = 21^\circ\text{C}$. Right: The network-formation rate of bis-crosslinked gels with crosslinker ratios 0.2–0.9 mmol/mol (circles, $c_a \approx 1.3 \text{ mol l}^{-1}$) at $\omega = 1 \text{ rad s}^{-1}$ and crosslinker ratios 4–46 mmol/mol (squares, $c_a \approx 0.42 \text{ mol l}^{-1}$) at $\omega = 10 \text{ rad s}^{-1}$. The line identifies the linear region with crosslinker ratio less than 10 mmol/mol.	31
3.4	Left: G' at $\omega = 0.1 \text{ rad s}^{-1}$ (left axis) and crosslinking efficiency (right axis) at $T = 21^\circ\text{C}$ for bis-crosslinked gels with varying crosslinker ratio. Right: G' versus $\tan \delta$ at $\omega = 1 \text{ rad s}^{-1}$ for bis-crosslinked gels with crosslinker ratios 0.2–0.9 mmol/mol (circles, $c_a \approx 1.3 \text{ mol l}^{-1}$) and crosslinker ratios 4–46 mmol/mol (squares, $c_a \approx 0.42 \text{ mol l}^{-1}$) ⁴ .	33
3.5	G'' at $\omega = 0.1, 10, 100 \text{ rad s}^{-1}$ (top left) and loss tangent at $\omega = 0.1 \text{ rad s}^{-1}$ (top right) for bis-crosslinked gels with varying crosslinker ratio at $T = 21^\circ\text{C}$. Bottom: Loss-tangent spectra for bis-crosslinked gels with varying crosslinker ratio (increasing from blue to red) at $T = 21^\circ\text{C}$.	34
3.6	G' (circles) and G'' (squares) spectra for bis-crosslinked gels following TTS with reference temperature 21°C (temperature increases from blue to red).	36
3.7	Loss-tangent spectra for bis-crosslinked gels following TTS with reference temperature 21°C (temperature increases from blue to red).	37
3.8	G' (circles) and G'' (squares) spectra (left), and loss-tangent spectrum (right) for sample $B_{0.1}$: $T = 21^\circ\text{C}$.	38
3.9	Left: Time-concentration superposition of G' (circles) and G'' (squares) for bis-crosslinked gels with crosslinker ratios 0.2–0.9 mmol/mol, referenced to sample $B_{0.9}$. Right: The horizontal and vertical shift factors are plotted versus $\epsilon = (c_{\text{bis}} - c_c)/c_c$ with the critical bis-acrylamide concentration at the gel point $c_c/c_a = 0.127$. Lines are power-laws (to guide the eye) with exponents -3.5 and -1.3 for a and b .	39
3.10	Horizontal shift factors a_T (with WLF fits, left) and temperature-dependent apparent activation energy (lines are Eqn. (3.7) and symbols are calculated from local Arrhenius fits to data triplets in the left panel, right) for bis-crosslinked gels: $B_{0.2}$ (circles), $B_{0.4}$ (squares), $B_{0.6}$ (triangles), $B_{0.8}$ (diamonds).	40
3.11	Scaled effective crosslink number versus temperature according to the vertical shift factor b_T for bis-crosslinked gels: $B_{0.2}$ (circles), $B_{0.4}$ (squares), $B_{0.6}$ (triangles), $B_{0.8}$ (diamonds).	41

3.12 Creep-recovery for bis-crosslinked gels: $T = 21^\circ\text{C}$	43
3.B.1 G' (violet) and G'' (red) during gelation at $\omega = 1 \text{ rad s}^{-1}$ (left) and G' and G'' spectra (right) for a bis-crosslinked gel: monomer concentration $\approx 3\%$ w/v; crosslinker ratio $\approx 24 \text{ mmol/mol}$ at 21°C	48
3.C.1 Left: G' (filled) and G'' (open) for $B_{0.7}$ formed with increasing nitrogen flow rate (from bottom to top) at $T = 21^\circ\text{C}$. Right: G' and G'' (linear-log) of $B_{0.4}$ under different axial forces (-2, 0, 2, 4 N from bottom to top) at $T = 21^\circ\text{C}$	49
3.C.2 Left: G' (violet) and G'' (red) during gelation without the evaporation blocker (silicone oil was applied to the sample perimeter at 3500 s): $\omega = 1 \text{ rad s}^{-1}$, $T = 21^\circ\text{C}$. Right: Comparison of gelation kinetics when using RO water (black) and DNA suspension buffer (red) to form pre-gel solutions: $\omega = 1 \text{ rad s}^{-1}$, $T = 21^\circ\text{C}$	50
3.C.3 Analysis of errors in the dynamic moduli and loss-tangent (data from 5 samples) spectra for bis-crosslinked acrylamide hydrogels with composition the same as for sample $B_{0.7}$. G' from 15 samples are shown in the top-right panel. Error bars identify the maximum and minimum values.	51
3.D.1 Gap-compensation factor with a normal/axial force 0 N (left) and 0.75 N (right). Reds lines are the average.	52
3.D.2 Comparison of gaps obtained by subtracting thickness increment in each temperature range obtained in calibration from the apparent gaps under a constant force (circles) and gaps calculated according to the thermal expansion of water (squares).	54
3.D.3 Comparison of the apparent activation energy (left) and scaled effective number density of partial chains (right) under a constant force (circles) and under a constant gap-compensation factor (squares) for sample $B_{0.4}$	55
3.D.4 The ratio of gap thickness at each temperature and at 21°C for bis-crosslinked (black triangles) and DNA-crosslinked (red triangles) gels without calibration. Black circles are ratios for a bis-crosslinked gel obtained by the constant axial force calibration method.	55
3.E.1 Comparison of G' (filled) and G'' (open) spectra obtained from TTS (black) and Fourier transformation of creep compliance data (red) for bis-crosslinked gels.	56
4.1 Schematics of the chemical-, physical-, and dual-crosslinked hydrogel formation.	61

4.2	Left: DNA- and dual-crosslinked polyacrylamide hydrogels after rheological testing. Right: Ductility of a dual-crosslinked polyacrylamide hydrogel demonstrated before (top) and after (bottom) stretching.	63
4.3	Storage modulus G' (top left), least-squares fit of Eqn. (3.5) (top right), loss modulus G'' (bottom left), and loss tangent (bottom right) for DNA-crosslinked gels during gelation: $\omega = 1 \text{ rad s}^{-1}$, $T = 21^\circ\text{C}$. Disturbances attributed to the application of silicone oil have been removed.	64
4.4	Storage modulus G' (top left), least-squares fit of Eqn. (3.5) (top right), loss modulus G'' (bottom left), and loss tangent (bottom right) for dual-crosslinked gels during gelation: $\omega = 1 \text{ rad s}^{-1}$, $T = 21^\circ\text{C}$. Disturbances attributed to the application of silicone oil have been removed.	65
4.5	Top left: Mid-point slope P (left axis) and gelation half time θ (right axis) versus crosslinker ratio for bis- (circles) and DNA-crosslinked (squares) gels: $\omega = 1 \text{ rad s}^{-1}$, $T = 21^\circ\text{C}$. Top right: P for dual-crosslinked gels with a fixed total crosslinker ratio equal to that for sample B ₀ D _{0.8} . Bottom left: Network-formation rate versus crosslinker ratio for bis-crosslinked gels (circles), DNA-crosslinked gels (squares), bis-crosslinked gels with a higher TEMED concentration (triangles), DNA-crosslinked gels with a higher TEMED concentration (diamonds), bis-crosslinked gels with monomer concentration 1.3 mol l^{-1} (asterisk): $\omega = 1 \text{ rad s}^{-1}$, $T = 21^\circ\text{C}$. Bottom right: The network-formation rate for dual-crosslinked gels with a fixed total crosslinker ratio equal to that for sample B ₀ D _{0.8}	67
4.6	G' (circles) and G'' (squares) spectra for DNA-crosslinked gels following TTS with reference temperature 21°C (temperature increases from blue to red).	68
4.7	G' (circles) and G'' (squares) spectra for dual-crosslinked gels following TTS with reference temperature 21°C (temperature increases from blue to red).	69
4.8	Left: Plateau modulus (left axis) and crosslinking efficiency (right axis) at $T = 21^\circ\text{C}$ versus crosslinker ratio for bis- (circles) and DNA-crosslinked (squares) gels. Right: The plateau modulus (left axis) and crosslinking efficiency (right axis) for dual-crosslinked gels with a fixed total crosslinker ratio equal to that for sample B ₀ D _{0.8} at $T = 21^\circ\text{C}$	71
4.9	τ_X (circles) and τ_c (squares) of DNA-crosslinked gels at $T = 21^\circ\text{C}$ versus effective crosslink density. The inset compares τ_X for DNA-crosslinked (circles) and dual-crosslinked (triangles) gels.	73

4.10	G' (filled) and G'' (open) moduli at the frequencies furnishing G_N^0 at 21°C plotted versus temperature. Left: DNA-crosslinked gel samples $B_0D_{0.2}$ (circles), $B_0D_{0.4}$ (squares), $B_0D_{0.6}$ (triangles), and $B_0D_{0.8}$ (diamonds). Right: dual-crosslinked gel samples $B_{0.6}D_{0.2}$ (circles), $B_{0.4}D_{0.4}$ (squares), $B_{0.2}D_{0.6}$ (triangles), and $B_{0.1}D_{0.4}$ (diamonds).	74
4.11	Loss tangent spectra for DNA-crosslinked gels following TTS with reference temperature 21°C (temperature increases from blue to red).	75
4.12	Loss tangent spectra for dual-crosslinked gels following TTS with reference temperature 21°C (temperature increases from blue to red).	76
4.13	Arrhenius plots of the horizontal shift factor (left) and apparent activation energy versus temperature (right) for DNA-crosslinked gels: $B_0D_{0.2}$ (circles); $B_0D_{0.4}$ (squares); $B_0D_{0.6}$ (triangles); $B_0D_{0.8}$ (diamonds).	77
4.14	Arrhenius plots of the horizontal shift factor (left) and apparent activation energy versus temperature (right) for dual-crosslinked gels: $B_{0.6}D_{0.2}$ (circles); $B_{0.4}D_{0.4}$ (squares); $B_{0.2}D_{0.6}$ (triangles); $B_{0.1}D_{0.4}$ (diamonds).	78
4.15	Left: Crossover temperature for G' and G'' (circles) and transition temperature from Arrhenius to non-Arrhenius behaviour (triangles) versus DNA-crosslinker ratio for samples $B_0D_{0.2}$ (blue), $B_0D_{0.4}$ (green), $B_0D_{0.6}$ (red), $B_0D_{0.8}$ (black). Right: Temperature at which G' and G'' reach a constant (circles) and transition temperature from Arrhenius to non-Arrhenius behaviour (triangles) versus DNA-crosslinker ratio for samples $B_{0.6}D_{0.2}$ (blue), $B_{0.4}D_{0.4}$ (green), $B_{0.2}D_{0.6}$ (red), $B_{0.1}D_{0.4}$ (black).	79
4.16	Scaled effective crosslink number versus temperature according to the vertical shift factor b_T for DNA-crosslinked (left) and dual-crosslinked (right) gels. Symbols are the same as in figures 4.13 and 4.14.	79
4.17	Adding G' (circles) and G'' (squares) spectra for bis-crosslinked gels to DNA-crosslinked gels at $T = 21^\circ\text{C}$. Top left: $B_{0.6}D_{0.2}$ (lines); adding $B_{0.6}D_0$ to $B_0D_{0.2}$ (symbols). Top right: $B_{0.4}D_{0.4}$ (lines); adding $B_{0.4}D_0$ to $B_0D_{0.4}$ (symbols). Bottom left: $B_{0.2}D_{0.6}$ (lines); adding $B_{0.2}D_0$ to $B_0D_{0.6}$ (symbols). Bottom right: $B_{0.1}D_{0.4}$ (lines); adding $B_{0.1}D_0$ to $B_0D_{0.4}$ (symbols).	81

4.18	Subtracting G' (circles) and G'' (squares) spectra for DNA-crosslinked gels from those for dual-crosslinked gels at $T = 21^\circ\text{C}$. Top left: $B_{0.6}D_0$ (lines); subtracting $B_0D_{0.2}$ from $B_{0.6}D_{0.2}$ (symbols). Top right: $B_{0.4}D_0$ (lines); subtracting $B_0D_{0.4}$ from $B_{0.4}D_{0.4}$ (symbols). Bottom left: $B_{0.2}D_0$ (lines); subtracting $B_0D_{0.6}$ from $B_{0.2}D_{0.6}$ (symbols). Bottom right: $B_{0.1}D_0$ (lines); subtracting $B_0D_{0.4}$ from $B_{0.1}D_{0.4}$ (symbols).	82
4.19	Creep-recovery for DNA-crosslinked gels: $T = 21^\circ\text{C}$	83
4.20	Creep-recovery for dual-crosslinked gels: $T = 21^\circ\text{C}$	84
4.B.1	G' (filled) and G'' (open) spectra for bis-, DNA-, and dual-crosslinked gels at $T = 21^\circ\text{C}$ before (black) and after (red) TTS.	92
4.C.1	G' (circles) and G'' (squares) spectra for DNA-crosslinked gels with different sample gap thicknesses (top left, top right, and bottom left). Arrhenius plots (bottom right) for DNA-crosslinked gels with different sample gap thicknesses and/or TEMED concentrations (circles: $g = 0.2$ mm; squares: $g = 0.3$ mm; triangles: $g = 0.5$ mm; diamonds: $g = 0.5$ mm with lower TEMED concentration). An arbitrary factor 2 separates otherwise overlapping lines.	93
4.C.2	The angular velocity at which G'' is at the local minimum for DNA-crosslinked gels (circles), DNA-crosslinked gels with a high TEMED concentration (squares), dual-crosslinked gels (triangles), and dual-crosslinked gels with a high TEMED concentration (diamonds).	94
4.C.3	Top left: Comparisons of gaps obtained from subtracting gap compensation factors at difference temperatures from the apparent gaps under a constant force (squares) and gaps obtained according to the expansion of water for a DNA-crosslinked gel (circles). Comparison of the apparent activation energy (top right) and scaled effective number density of partial chains (bottom left) under a constant force (squares) and under a constant gap compensation factor (circles). Bottom right: G'' during gelation for pre-gel solution with a low (black) and high (red) TEMED concentration.	95
4.D.1	Creep for a bis-crosslinked $B_{0.8}D_0$ (left) and a dual-crosslinked $B_{0.4}D_{0.4}$ (right) gels fitted by one Maxwell element in series with one Kelvin-Voigt element (violet) and one Maxwell element in series with two Kelvin-Voigt elements (red) at $T = 21^\circ\text{C}$	97

4.E.1 Comparison of G' (filled) and G'' (open) spectra obtained from TTS (black) and Fourier transformation of creep compliance data (red) for DNA-crosslinked gels.	98
4.E.2 Comparison of G' (filled) and G'' (open) spectra obtained from TTS (black) and Fourier transformation of creep compliance data (red) for dual-crosslinked gels.	99
4.F.1 Strain-sweep tests performed at $\omega = 6.28$ rad/s for bis-crosslinked gel samples $B_{0.2}D_0$ (circle), $B_{0.4}D_0$ (squares), $B_{0.6}D_0$ (triangles), and $B_{0.8}D_0$ (diamonds); at $\omega = 1$ rad/s for DNA-crosslinked gel samples $B_0D_{0.2}$ (circles), $B_0D_{0.4}$ (squares), $B_0D_{0.6}$ (triangles), and $B_0D_{0.8}$ (diamonds); at $\omega = 1$ rad/s for dual-crosslinked gel samples $B_{0.6}D_{0.2}$ (circle), $B_{0.4}D_{0.4}$ (squares), $B_{0.2}D_{0.6}$ (triangles), and $B_{0.1}D_{0.4}$ (diamonds) at $T = 21^\circ\text{C}$	100
4.F.2 Stress versus strain during oscillatory cycles in the linear viscoelastic region at $T = 21^\circ\text{C}$. Top row from left to right: bis-crosslinked gel samples from $B_{0.2}D_0$ to $B_{0.8}D_0$; middle row from left to right: DNA-crosslinked gel samples from $B_0D_{0.2}$ to $B_0D_{0.8}$; bottom row from left to right: dual-crosslinked gel samples $B_{0.6}D_{0.2}$, $B_{0.4}D_{0.4}$, $B_{0.2}D_{0.6}$, $B_{0.1}D_{0.4}$	101
5.1 Schematics of DNA- and dual-crosslinked polyacrylamide hydrogel swelling, and dual-crosslinked polyacrylamide hydrogel cylinders before (top) and after (bottom) swelling.	105
5.2 Top left: Swelling of bis-crosslinked gels with $G_N^0 = 250$ Pa (circles), $G_N^0 = 400$ Pa (squares), and $G_N^0 = 730$ Pa (triangles) in PBS. Lines are least-squares fits of Eqn. (5.5). Top right: Cooperative diffusion coefficient versus G_N^0 . Bottom left: Swelling relaxation time versus G_N^0 . Bottom right: Pore size from D in the top-right panel (Eqn. (5.7)) versus G_N^0	108
5.3 Top left: Fitting of Eqn. (5.6) to the initial stage of swelling $G_N^0 = 250$ Pa (circles and blue line), $G_N^0 = 400$ Pa (squares and green line), and $G_N^0 = 730$ Pa (triangles and red line). Top right: Cooperative diffusion coefficient calculated with $\nu = 0.33$ (open circles) and $\nu = 0.5$ (filled circles) versus G_N^0 . Bottom: Pore (mesh) size obtained from D in the top-right panel with $\nu = 0.33$ (open circles) and $\nu = 0.5$ (filled circles), from D in the top-right panel of figure 5.2 (squares), and from $l = (2k_B T/G_N^0)^{1/3}$ (triangles) versus G_N^0	110

5.4	Swelling and dissolution of DNA-crosslinked gels in PBS: $B_0D_{0.4}$ (top left); $B_0D_{0.6}$ (top right); $B_0D_{0.8}$ (bottom left). Bottom right: Swelling of dual-crosslinked gels in PBS before the swelling-ratio decrease: $B_{0.6}D_{0.2}$ (circles); $B_{0.4}D_{0.4}$ (squares); $B_{0.2}D_{0.6}$ (triangles). Lines are least-squares fits of empirical Eqn. (5.8).	112
5.5	Top left: Fitting of Eqn. (5.6) to the initial stage of swelling $B_0D_{0.4}$ (circles and blue line), $B_0D_{0.6}$ (squares and green line), and $B_0D_{0.8}$ (triangles and red line). Top right: Cooperative diffusion coefficient calculated with $\nu = 0.33$ (open circles) and $\nu = 0.5$ (filled circles) versus G_N^0 . Bottom left: Pore (mesh) size from D in the top-right panel with $\nu = 0.33$ (open circles) and $\nu = 0.5$ (filled circles), and from $l = (2k_B T/G_N^0)^{1/3}$ (squares) versus G_N^0 . Bottom right: Swelling relaxation time from empirical Eqn. (5.8) versus G_N^0	113
5.6	Time series of the volume swelling ratio (left axis) and the fraction of DNA strands released to PBS (right axis) for samples $B_0D_{0.4}$ (top left), $B_0D_{0.6}$ (top right), and $B_0D_{0.8}$ (bottom).	114
5.7	Top left: Fitting of Eqn. (5.6) to the initial stage of swelling $B_{0.6}D_{0.2}$ (circles and blue line), $B_{0.4}D_{0.4}$ (squares and green line), and $B_{0.2}D_{0.6}$ (triangles and red line). Top right: Cooperative diffusion coefficient calculated with $\nu = 0.33$ (open circles) and $\nu = 0.5$ (filled circles) versus G_N^0 . Bottom left: Pore (mesh) size from D in the top-right panel with $\nu = 0.33$ (open circles) and $\nu = 0.5$ (filled circles), and from $l = (2k_B T/G_N^0)^{1/3}$ (squares) versus G_N^0 . Bottom right: Swelling relaxation time from fitting Eqn. (5.8) versus G_N^0	116
5.8	Time series of the volume swelling ratio (left axis) and the fraction of DNA strands released to PBS (right axis) for samples $B_{0.6}D_{0.2}$ (top left), $B_{0.4}D_{0.4}$ (top right), and $B_{0.2}D_{0.6}$ (bottom) during swelling.	117
5.9	The fraction of DNA strands/polymer chains left in dual-crosslinked gels from drying the gels (circles); UV-vis (squares); the decrease of S_v (triangles); the crosslinking efficiency (diamonds).	118
5.10	Swelling ratio at equilibrium/prior to dissolution/prior to decreasing versus plateau modulus for bis-crosslinked gels (red circles), DNA-crosslinked gels (blue squares), and dual-crosslinked gels (green triangles) in PBS. The curve is the least-squares fit of Eqn. (5.1) (solid: average; dashed: maximum; dash-dot: minimum). Violet squares and triangles are the swelling ratio at equilibrium for bis-crosslinked gels from Livney et al. ⁹ and Konda et al. ¹⁰	119

5.11	Top: Phenomenological probability function p versus λ with $\delta = 0.1\text{--}1.6r_0$ (from red to blue). Bottom left: $\partial A/\partial\phi$ versus ϕ/ϕ_0 with $\delta = 0.3\text{--}2.1r_0$ (from blue to red). Bottom right: $\partial A/\partial\phi$ versus ϕ/ϕ_0 for $B_{0.6}D_{0.2}$ with $\delta = 0.1r_0$ and $f = 2/5$ (blue), $B_{0.4}D_{0.4}$ with $\delta = 0.15r_0$ and $f = 2/3$ (green), and $B_{0.2}D_{0.6}$ with $\delta = 0.15r_0$ and $f = 6/7$ (red).	121
5.12	The correlation between λ and $\Delta\epsilon$ (top left); λ and δ (top right); λ and χ (bottom left). Solid and dashed lines are from the stable and unstable roots. Bottom right: Swelling ratio at equilibrium $S_v = \phi_0/\phi$ versus gel plateau modulus G_N^0 for DNA-crosslinked gels (black lines) and dual-crosslinked gel samples $B_{0.6}D_{0.2}$ with $f = 2/5$ (blue), $B_{0.4}D_{0.4}$ with $f = 2/3$ (green), and $B_{0.2}D_{0.6}$ with $f = 6/7$ (red). Squares and triangles are experimental swelling ratios for DNA- and dual-crosslinked gels.	122
5.A.1	Swelling of DNA-crosslinked polyacrylamide hydrogels before (a) and after adding 0.5 ml (b), 1 ml (c), and 1.5 ml (d: after 2 weeks; e: after 5 weeks) RO water. From left to right: $B_0D_{0.2}$, $B_0D_{0.4}$, $B_0D_{0.6}$, and $B_0D_{0.8}$	125
5.B.1	Accumulated UV-vis spectra for PBS containing gels during swelling (from blue to red) for $B_0D_{0.4}$ (top left), $B_0D_{0.6}$ (top right), and $B_0D_{0.8}$ (bottom).	126
5.B.2	Accumulated UV-vis spectra for PBS containing gels during swelling (from blue to red) for $B_{0.6}D_{0.2}$ (top left), $B_{0.4}D_{0.4}$ (top right), and $B_{0.2}D_{0.6}$ (bottom).	127
5.D.1	Left: UV-vis absorbance for DNA solution at 260 nm versus DNA concentration for Strand A (top), Strand B (middle), and “LinkerAdap” (bottom). Right: UV-vis spectra for DNA solution with concentration increasing from blue to red.	132
5.D.2	Top left: UV-vis absorbance for PA solution at the peak versus PA concentration. Top right: UV-vis absorbance for PA solution at 260 nm versus PA concentration. Bottom: UV-vis spectra for PA solution with concentration increasing from blue to red.	133
5.D.3	Left: UV-vis absorbance for acrylamide solution at the peak versus acrylamide concentration. Right: UV-vis absorbance for acrylamide solution at 260 nm versus acrylamide concentration.	134
5.D.4	Left: Kinetics of Strand A, Strand B, and “LinkerAdap” forming DNA crosslinker. Right: The solid curve is the least-squares fit of the $d(1 - X)/dt$ versus $1 - X$ correlation for a third-order reaction, and the dashed curve is the least-squares fit of the $d(1 - X)/dt$ versus $1 - X$ correlation for a second-order reaction.	134

5.E.1	Top: Swelling of bis-crosslinked gels in RO water (left) and PBS (right). Bottom: Fitting of swelling ratio at equilibrium in RO water (solid) and PBS (dashed) versus G_N^0 with Eqn. (5.1).	135
5.F.1	Swelling ratio prior to dissolution for DNA-crosslinked gels synthesized with a low (circles) and high (squares) TEMED concentration versus crosslinker ratio.	135
5.F.2	Swelling and dissolution of DNA-crosslinked gels B ₀ D _{0.6} (top left), B ₀ D _{0.7} (top right), and B ₀ D _{0.89} (bottom) formed with a high TEMED concentration in PBS. Lines before S_v decrease are least-squares fits of empirical Eqn. (5.8). Lines after S_v decrease are used to objectively estimate the maximum S_v . . .	136
5.F.3	Top left: Fitting of Eqn. (5.6) to the initial stage of swelling B ₀ D _{0.6} (circles and blue line), B ₀ D _{0.7} (squares and green line), and B ₀ D _{0.89} (triangles and red line). Top right: Cooperative diffusion coefficient calculated with $\nu = 0.33$ (open circles) and $\nu = 0.5$ (filled circles) versus G_N^0 . Bottom left: Pore (mesh) size from D in the top-right panel with $\nu = 0.33$ (open circles) and $\nu = 0.5$ (filled circles), and from $l = (2k_B T/G_N^0)^{1/3}$ (squares) versus G_N^0 . Bottom right: Swelling relaxation time from fitting Eqn. (5.8) versus G_N^0	137
5.F.4	Time series of the volume swelling ratio (left axis) and the fraction of DNA strands released to PBS (right axis) for DNA-crosslinked gels formed with more TEMED B ₀ D _{0.6} (top left), B ₀ D _{0.7} (top right), and B ₀ D _{0.89} (bottom) during swelling.	138

List of Tables

3.1	Compositions of bis-crosslinked polyacrylamide gels.	28
3.2	Best-fit parameters of the Burgers model and Weibull function at 21°C.	42
3.A.1	Solution volumes for bis-crosslinked gel synthesis.	47
3.C.1	Error propagation analysis for pre-gel solution preparation.	50
4.1	Compositions of DNA- and dual-crosslinked polyacrylamide gels.	62
4.2	Analysis of gel samples at 21°C.	86
4.3	Best-fit parameters for the Burgers model and Weibull function at 21°C.	87
4.A.1	Solution volumes for DNA- and dual-crosslinked gel synthesis.	91
4.D.1	Best-fit parameters for two creep models: Eqn. (3.9) and Eqn. (4.1).	96

Abbreviations

A	Acrylamide
APS	Ammonium Persulfate
bis	bis-acrylamide
PA	Polyacrylamide
RO	Reverse Osmosis
TCS	Time-Concentration Superposition
TEMED	<i>N,N,N',N'</i> -tetramethylethylenediamine
TTS	Time-Temperature Superposition
WLF	Williams-Landel-Ferry

Symbols

D	Cooperative diffusion coefficient
E_a	Apparent activation energy
G'	Storage modulus
G''	Loss modulus
G_N^0	Plateau modulus
J	Compliance
l	Mesh (pore) size
S_w	Mass swelling ratio
S_v	Volume swelling ratio
$\tan \delta$	Loss tangent
χ	Flory-Huggins interaction parameter

Introduction

1.1 Motivation

DNA-crosslinked polyacrylamide hydrogels have demonstrated considerable potential for drug delivery^{11,12}, biosensing^{13,14}, and tissue engineering^{15,16}. Such specialized and wide ranging applications are due to the unique programmability, mechanical tunability, molecular-recognition, and temperature reversibility of DNA-crosslinking^{17,18}. To date, mechanical studies of DNA-crosslinked gels have focussed on how the crosslinker concentration and DNA strand length affect the elastic modulus as inferred from microrheology at a single frequency^{19,20,21}. Many fundamental processes that control performance have not yet been studied, and are therefore poorly understood; these include gelation kinetics, the time dependence of linear and non-linear rheology, and swelling.

DNA-crosslinked gels are physical gels, so the timescales on which they behave as elastic solids, and how they respond to stress, greatly impact their properties and performance. One obvious and special characteristic of DNA crosslinking is the multiple base-pair structure. It may therefore be anticipated that, unlike physical gels with low dissociation activation energy, the gel relaxation mechanism may vary from the Maxwell model. Such relaxation mechanisms are probed by dynamic rheology, and so comprehensive rheological studies have the potential to provide fundamental insights into the potentially unique and distinctly different swelling characteristics of DNA-crosslinked gels from their covalently crosslinked counterparts.

Combining permanent covalent crosslinks with physical DNA-crosslinks provides yet another means of tailoring hydrogel properties. For example, when physical and chemical crosslinks coexist, the relaxation of DNA crosslinks and the dissociation activation energy might vary from DNA-only crosslinked gels. Efforts to understand how the DNA crosslinker concentration affect swelling and dissolution of DNA-only and dually crosslinked gels are undertaken in this thesis, many for the first time.

1.2 Thesis objectives

The principal objective of this thesis is to achieve a fundamental understanding of polyacrylamide hydrogels crosslinked by complementary-DNA-strand. This is pursued by the following sequence of experimental studies and interpretations:

- rheological tracking of gelation kinetics;
- time-temperature superposition of dynamic moduli spectra;
- linear mechanical responses under constant stress and during recovery;
- rheological determination of the activation energy for DNA crosslinking dissociation;
- gravimetric and spectroscopic tracking of swelling and dissolution .

1.3 Thesis organization

An overview of the science and methods adopted in the thesis is provided in chapter 2. DNA-crosslinked hydrogels and hydrogel physics are introduced, and rheometry and swelling are presented as techniques with which to study bulk mechanical properties and their connection to microstructure.

Polyacrylamide is the polymer used to synthesize DNA- and dual-crosslinked hydrogels in this thesis. Despite extensive studies in the literature on the viscoelasticity and crosslinking efficiency of polyacrylamide hydrogels covalently crosslinked by bis-acrylamide, few studies have been undertaken on gels with very low crosslinker ratio. Therefore, as a prelude to the studies of DNA-crosslinking, rheological characterizations of very weakly bis-crosslinked polyacrylamide gels are reported in chapter 3. Here, the focus is on gelation kinetics and dynamic moduli spectra. The results provide useful benchmarks with which to assess DNA- and dual-crosslinked gels in the following chapters.

Gelation kinetics and viscoelasticity of DNA- and dual-crosslinked gels are studied in chapter 4. Time-temperature superposition is undertaken to probe the dissociation of DNA crosslinks and establish rheological characteristics of these gels, particularly at long timescales (low frequencies). Such materials have been loosely classified in the literature as being hydrogels. The rheological examination undertaken here reveals that DNA-only crosslinked gels are viscous fluids on sufficiently long time scales. This motivated the studies in chapter 5 on swelling and dissolution. Creep-recovery tests are adopted to investigate the

response of these gels to a constant stress, and the influence of chemical crosslinking on dual networks.

The swelling kinetics of DNA- and dual-crosslinked gels are studied in chapter 5. A correlation between the swelling ratio and the plateau modulus is established, and a theoretical model is proposed to interpret unique swelling characteristics. This chapter also reports swelling data for bis-crosslinked gels. Similarly to the rheological studies, these data establish benchmarks with which to assess DNA- and dual-crosslinked gels.

Chapter 6 summarizes the thesis and the original contributions to knowledge.

1.4 Contributions of authors

The author (C. Du) conducted all the experiments and data analysis. Chapters 1–6 were written by the author, and chapters 1–6, with the exception of section 6.3, were edited by the author’s supervisor (R. J. Hill). R. J. Hill, guided the research and assisted with the experimental design and interpretation of the results. The thesis is presented in traditional format, with chapters 3–5 as the basis of manuscripts that will be submitted for publication with C. Du (first author) and R. J. Hill as coauthor.

Properties and characterization of hydrogels

2.1 Hydrogels

Gels are often defined as three-dimensional polymer networks that absorb solvent. Their network structure is typically achieved by crosslinking polymers. However, the term “gel” is used in many contexts, and there are numerous opinions on how to define a gel. Among the definitions are the requirement not to flow after a long time: “if the gel flows after a long time, it should not be called a gel”²², and to swell in a solvent, but not dissolve, even in a good solvent: “a polymer gel consists of a three dimensional crosslinked network and swells in a solvent to a certain finite extent, but does not dissolve even in a good solvent”²³. These characteristics generally limit the definition to covalently crosslinked polymers (chemical gels).

Gels can be identified based on structural features and rheological behaviour. For example, Flory²⁴ classified gels based on a well-ordered lamellar microstructure, a covalent polymeric network, a polymer network formed by physical aggregation, or a particulate structure. Almdal et al.²⁵ defined gels as solid-like materials that comprise two or more components, one of which is a liquid. Gels were required not to flow under their own weight, and to have a storage modulus that exhibits a pronounced plateau extending to at least the order of seconds, with the loss modulus considerably smaller than the storage modulus. According to the definition of Nishinari²³, gels should have a plateau region in the frequency range 10^{-3} – 10^2 rad s⁻¹, where the loss tangent is smaller than 0.1.

“Hydrogels” are generally considered three-dimensional hydrophilic polymer networks that can absorb a large quantity of water. Gupta et al.²⁶ suggested that, unlike gels, hydrogels should be restricted to polymer networks that maintain their three-dimensional structure upon swelling. Chirani et al.²⁷ stated that “hydrogels are polymeric matrixes that swell but don’t dissolve (in the short term) in water”. Note that differences in the foregoing definitions often hinge on the observation timescale, so the definitions are particularly relevant and necessary for describing physically crosslinked gels, which have dynamic crosslinks.

Because of their soft elastic properties and high tunability, hydrogels have many com-

mercial applications in industry, biomedicine, and daily life. For example, hydrogels are routinely used as drag-reduction agents, soil stabilizers, dressings that provide a moist and cool environment for wounds, and scaffolds for cell culture. Biomedical applications are possible because of “biocompatibility”, which is an ability to be in contact with a living system without producing an adverse effect²⁸. Hydrogels can also be used as contact lenses, or masks that release active ingredients when hydrogels transform from the solid to liquid state at skin temperature. Some polyelectrolytes, such as sodium polyacrylate gels, are used as “superabsorbents”.

Note that various polymer-backbone architectures, such as hydrophobic groups, ionic groups, and weak acid or base components, can excite a volume phase transition in response to chemical and/or physical stimuli, such as temperature, salt concentration, pH, and voltage²⁹. Hydrogels having crosslinkers that can bind specific molecules may exhibit volume changes arising from the presence of specific molecules, so volume changes can be linked to molecular concentration. Most volume responses to external stimuli are reversible, so hydrogels can be considered transducers that convert chemical energy into mechanical energy. These provide tremendous potential for use as sensors, actuators, and artificial muscle²⁹. Tunable porosity and stimuli responsiveness are highly desirable for drug delivery^{26,30}.

Most polymer networks formed by free-radical copolymerization are heterogenous on the nanoscale, imparting a distribution of mesh sizes (the distances between adjacent crosslinks), as well as topological defects, such as dangling chain ends, loops, and crosslinker-crosslinker shortcuts¹. Heterogeneity of crosslinking density is enhanced by swelling due to varying degrees of swelling in domains with contrasting densities, as illustrated in figure 2.1. Cyclization and localized multiple crosslinking reactions form “microgels”³¹, which are more pronounced with larger ratios of crosslinker to monomer³². The degree of inhomogeneity is also affected by the polymerization temperature. Inhomogeneity can be reduced by forming gels with pre-polymerized chains that contain crosslinkable moieties¹. Here, the crosslinker has no preference to react with itself or the monomer, and the segment length between two crosslinks is fixed, producing more homogenous networks. Nanostructural heterogeneity can be probed using light scattering (hundreds of nanometers), small angle X-ray and neutron scattering (a few Ångstroms), optical microscopy, electron and X-ray microscopy (a few Ångstroms), and atomic force microscopy (AFM) (a few Ångstroms)¹.

Polymeric gel deformation is generally described using the *affine network model*³, which assumes that all crosslinks deform with the macroscopic network. When the crosslinker

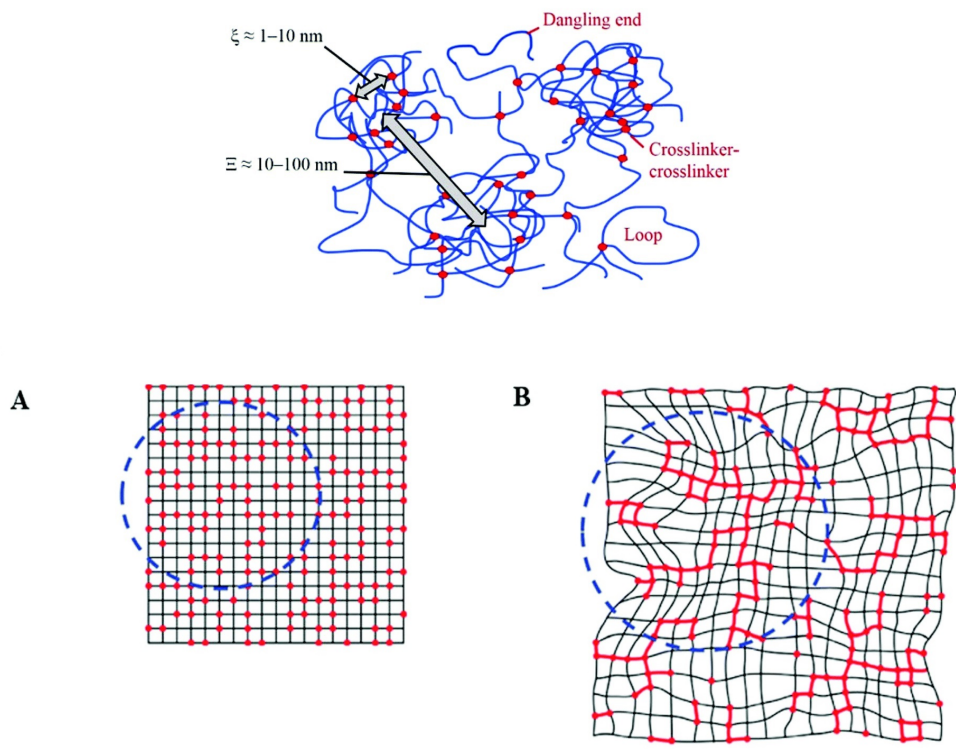


Figure 2.1: Top: Schematic of a polymer network with inhomogeneous crosslinking density and connectivity defects. The short arrow marks a typical mesh size, whereas the long arrow indicates the typical length scale of spatial variation of the crosslinking density. Bottom: Schematics of (A) randomly distributed crosslinks (red dots) in a deswollen polymer network and (B) the same network swollen in a good solvent. Highly crosslinked local domains (red segments) swell less than the rest of the network, leading to pronounced static spatial polymer-segmental concentration fluctuations on length scales of several tens to hundreds of nanometers¹. Reprinted with permission.

functionality f is equal to 4, the plateau storage shear modulus is

$$G_N^0 = \nu k_B T = f n k_B T / 2 = 2 n k_B T, \tag{2.1}$$

where ν is the network strand (polymer segments between two neighbouring crosslinks) number density, n is the crosslink number density, and $k_B T$ is the thermal energy. The *phantom network model*³ allows for thermal fluctuations of partial chains about the mean positions of the crosslinks, giving

$$G_N^0 = (1 - 2/f) \nu k_B T = n k_B T. \tag{2.2}$$

Akagi et al.³³ found that the transition between the phantom and affine network models occurs at the concentration at which polymer coils begin to overlap (polymer-overlap concentration). Basu et al.⁸ found the degree of polyacrylamide gel nonaffinity to be independent of the monomer and crosslinker concentrations in the range they studied. Because of defects in the network, a portion of crosslinkers do not act as elastically effective crosslinks. For polyacrylamide gels having different monomer concentrations, the maximum crosslinking efficiency is achieved by seeking optimum crosslinker ratios. If the affine model was adopted to calculate the plateau modulus for ideal networks, the crosslinking efficiencies have been reported by Basu et al.⁸ as 0.12 for 7.5% w/v and 0.9 for 15% w/v gels; Gerlach and Arndt²⁹ reported maximum efficiencies of 0.01 for 3% w/v, 0.09 for 5% w/v, and 0.2 for 7% w/v gels; and Adibnia and Hill⁴ reported 0.012 for 3% w/v gels. The low crosslinking efficiency for very dilute gels reflects the low monomer concentration decreasing the probability of crosslinkers attaching to monomers before polymerization is complete. The reviews by Oyen³⁴ and Denisin and Pruitt² summarize systematic trends emerging from a vast literature. However, few studies of the crosslinking efficiency with respect to systematic variations in the monomer concentration and crosslinker-to-monomer ratio have been undertaken.

2.1.1 Polyacrylamide hydrogels

Gels are often classified according to their crosslinking³⁵. Chemical gels have permanent crosslinks, whereas physical gels, or associative polymers, have transient crosslinks. One of the most widely used and extensively studied chemical hydrogels is from the free-radical copolymerization of acrylamide with a tetra-functional crosslinker, such as bis-acrylamide. These uncharged gels have many practical uses: drag reduction agents, thickening agents, cutting fluids, and soil stabilizers³⁶. Moreover, polyacrylamide (PA) gel electrophoresis is

routinely used for characterizing and separating proteins and DNA³⁷. Due to its biocompatibility and potential to mimic biological tissue, PA has also been proposed as a cell-culture substrate². Whereas the acrylamide monomer is toxic, it becomes benign following polymerization³⁴. It is therefore important that un-reacted monomer can be removed before use in medical applications.

PA hydrogels crosslinked by bis-acrylamide have been studied extensively from many perspectives, including gelation kinetics⁷, nanoscale structures³¹, mechanical properties³⁸, and swelling/shrinking³⁹. The properties of PA hydrogels can be tuned by the monomer and crosslinker concentrations, the amount of initiator (ammonium persulfate) and accelerator (TEMED), as well as preparation conditions, such as the polymerization temperature and deoxygenation process. For example, Trompette et al.⁶ reported that the complex shear modulus of PA gels increases as a power-law in the monomer concentration with an exponent 3.3. Denisin and Pruitt² summarized the elastic modulus of PA gels—with monomer concentrations in the range 0–22% w/v and crosslinker concentrations in the range 0.25–11% w/w—obtained from macrorheology and microrheology. They showed that the elastic modulus increases with increasing monomer concentration, whereas the values of elastic moduli for gels with the same compositions vary significantly. High variability may be attributed to different measurement methods, gel sample sizes, and gelation times. From the measurements of Denisin and Pruitt², the elastic modulus increased with crosslinker concentration until a critical concentration, beyond which the modulus decreased, as shown in figure 2.2. This is because heterogeneous networks are favoured by the high crosslinker concentration, as confirmed by field-emission scanning electron microscopy. At low crosslinker ratios, *e.g.*, 0.5–3.7% w/w (monomer concentration 8% w/v), the elastic modulus has been found to increase linearly with crosslinker ratio⁷. Similar linear correlations have been reported with crosslinker ratios between 0.03% w/w and 0.3% w/w (monomer concentration 15% w/v) or between 0.4% w/w and 1.6% w/w (monomer concentration 7.5% w/v)⁸. Basu et al.⁸ found that doubling the concentration of APS and TEMED speeds up the reaction, but yields an $\approx 20\%$ smaller modulus. Oyen³⁴ reviewed the intrinsic permeability of PA gels, which is proportional to the square of the mesh size. They found that the intrinsic permeability decreases with increasing monomer concentration, with no clear correlation between the permeability and crosslinker concentration. In the study of Lira et al.⁴⁰, however, the mesh size was found to decrease with increasing crosslinker concentration.

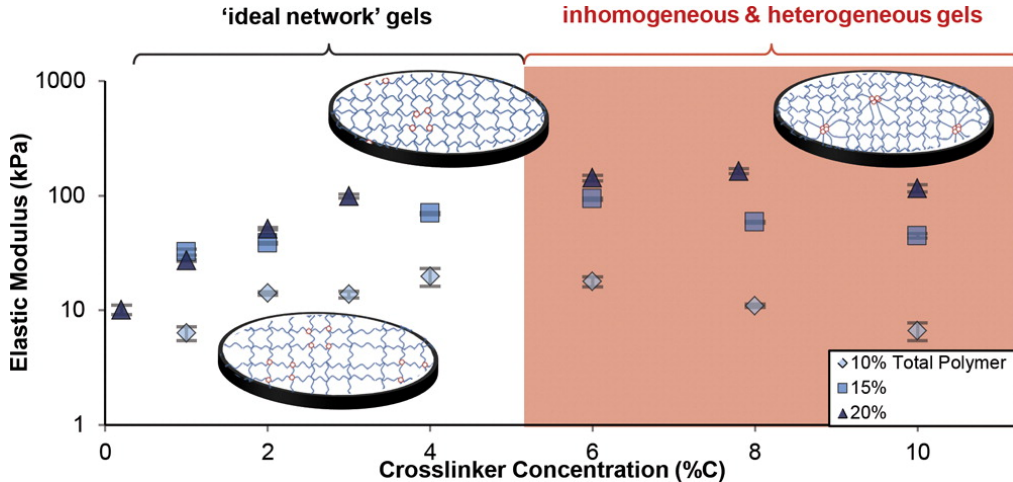


Figure 2.2: Relationship between crosslinker (bis-acrylamide) concentration and elastic modulus with various total monomer (acrylamide) concentrations². Reprinted with permission.

2.1.2 DNA-crosslinked hydrogels

In contrast to the foregoing covalently crosslinked gels, physical gels are crosslinked by polymer-chain entanglements or physical interactions, such as ionic bonds, crystallization, amphiphilic block and graft copolymers, hydrogen bonds, and protein interactions³⁵. Physically crosslinked gels have advantages in drug delivery, since toxic crosslinking agents might be avoided, and some physical gels are injectable⁴¹. The mechanical and swelling behaviours of physical gels are different from chemical gels. For example, the dynamic moduli of some physical gels are highly dependent on timescales, temperature, or pH. Agarose gels are found not to swell in water⁴², gellan gels with double-helix conformation^{43,23} and Ploxamer 407 gels crosslinked by a micellar microstructure³⁰ eventually dissolve in water.

Physical gels crosslinked by DNA hybridization have many favourable properties arising from the molecular recognition ability of DNA, its stable structure, and base-pair reversibility¹⁷. For example, the length and sequence of DNA strands adopted as crosslinkers are programmable, imparting controllable melting temperature¹⁸ and mechanical properties¹⁸. The gel formation can be reversed by heating⁴⁴ or the presence of a “removal” DNA strand (complementary to the crosslinker strand)¹⁹. These gels therefore have special potential for use in drug delivery^{11,12}, molecular separation⁴⁵, tissue engineering^{15,16}, and biosensing^{13,14}. Note that DNA strands can be easily modified and connected to polymer chains as a crosslinker⁴⁶.

Aptamers are single-stranded short DNA or RNA that can bind to a wide range of target

molecules—such as adenosine, thrombin, cocaine, and metal ions—with high affinity and specificity^{47,46}. Using aptamers, Yang et al.¹² constructed an adenosine-responsive PA hydrogel. Two acrydite-modified DNA strands are separately copolymerized with acrylamide. The mixture of polymer chains gels after adding a crosslinking strand containing an adenosine aptamer sequence. When adenosine is present and binds to aptamer, only five base pairs are hybridized, which is unstable at room temperature, leading to the gel dissolution. Using a similar principle, Zhu et al.⁴⁸ adopted the gel trapped with enzymes as a highly sensitive colorimetric visual detection platform. To separate molecules, He et al.⁴⁵ developed a reversible adenosine-5'-triphosphate aptamer-based hydrogel system, which acts as a hook that captures specific molecules, leaches out the nonspecific targets after gelation, and then releases target molecules by dissolving the gel using a complementary DNA strand. Another reversible aptamer-based hydrogel system was designed to capture and release thrombin, providing a promising tool for drug delivery and protein detection⁴⁹. With chemical crosslinkers, Wang and Wang¹³ fabricated a hydrogel diffraction grating with a sensitive response to thrombin. Unlike the three-strand systems, two DNA strands are used, one of which contains the thrombin aptamer and another that is partly complementary to the first. The gel swells when thrombin binds to the aptamer segment, inducing a change in the colour of diffracted light. Ye et al.¹⁴ developed a method to visually detect heavy metal ions using aptamer-functionalized colloidal photonic crystal hydrogel films. In this study, chemical-crosslinked hydrogels imbedding colloidal crystals were cast, and then Hg²⁺ or Pb²⁺ aptamer was incorporated into the networks. After binding to the specific heavy metal ions, the hydrogel shrinks because of the increase in crosslinker density, identified as a structural colour shift of the gel film. For the application of DNA-crosslinked gels in tissue engineering, the dynamic stiffness of DNA-crosslinked gels is achieved by introducing the “removal” DNA strand to mimic the highly dynamic microenvironment of cells^{20,15}.

There are two methods for DNA-crosslinked gel synthesis: (i) polymerizing monomer before DNA hybridization, and (ii) copolymerizing monomer and DNA strands simultaneously. The advantages of method (i) are that the gel network is more homogenous, and the material is injectable for drug-delivery applications. The limitations are that the gelation time cannot be controlled, and it is difficult to introduce covalent bonds into the network for two- or three-DNA strand systems. Literature reports of DNA-crosslinked gels have mainly focused on the feasibility of potential applications, as well as measurements of mechanical properties, including Young's modulus and the shear modulus from microrheology²¹.

2.1.3 Dual-crosslinked hydrogels

Self-healing gels have been developed to address the low mechanical toughness of many hydrogels⁵⁰, *e.g.*, their susceptibility to fracture at low stress intensity. Self-healing is achieved by introducing breakable crosslinks. Crosslink breakage and reformation dissipates energy, imparting a form of mechanical reinforcement. Many types of physical gels^{51,52,53}, chemical gels⁵⁴, double-network gels⁵⁵, and gels with physical and chemical crosslinks^{56,57} have been shown to exhibit self-healing characteristics. DNA-crosslinked gels have also been proposed as materials with potential for exhibiting self-healing characteristics⁵⁸.

Morphology, tensile strength, and rheological testing are typically used to identify self-healing characteristics. Gels crosslinked by two types of crosslinkers (either physical and chemical crosslinks or two physical crosslinks with different activation energies) are promising candidates: weak, reversible crosslinks preferentially yield, providing deformability, whereas stronger crosslinks provide reinforcement via scaffolding⁵⁸. Advantages of chemical gels, such as stability arising from the permanence of covalent bonds, are often needed for applications. For the biosensors highlighted in the previous section, covalent crosslinks in an otherwise physically crosslinked network can prevent the network dissolving after responding to target molecules.

A dual-crosslinked gel that has been studied extensively is polyvinyl alcohol (PVA) with borate ions as a physical crosslinker^{59,60,61,62}. Mayumi et al.⁶¹ found that PVA gels with physical crosslinks can be stretched at least twice that of PVA gels with only covalent crosslinks; they also have a distinctly different fracture-energy dependence on the stretch rate. From a large-strain constitutive model and the stretch-rate dependence from tensile tests, it was shown that enhanced toughness is due to the reversibility of dynamic crosslinks⁶².

2.2 Rheology

Rheology is the study of the flow and deformation of materials, including liquids and solids. It can also be considered the study of stress-strain material relationships. Rheology is routinely used to analyze polymer melts and solutions for formulation, quality control, and polymer processing⁶³. Material responses to stress and strain vary from purely viscous to purely elastic. For viscoelastic materials, such as polymers and gels, rheology is an indicator of microstructure. It provides qualitative and quantitative insights into whether a complex material is a gel or viscous fluid. As shown in figure 2.3, a commercial rheometer, such as the ARES-G2 (TA Instrument), has a separate motor (to induce deformation) and transducer

(to measure torque) that together link stress and strain over a wide range of stresses, strains, and strain rates.

The deformation or rate of deformation can be applied as compression, tension, or shear. To obtain dynamic shear moduli, a sinusoidal oscillation strain γ with a small amplitude (in the linear viscoelastic regime) is applied to the sample at an angular frequency ω . For ideally elastic materials, the resulting stress σ is perfectly in phase with γ , because these materials store and release elastic energy without dissipation. Under these ideal conditions, σ is independent of ω . For ideal viscous materials, σ is 90° out of phase with γ . There is no storage of energy, so the work of deformation is dissipated. Viscoelastic materials have elastic storage and viscous dissipative/loss mechanisms, both of which vary with ω . For a parallel-plate geometry (see figure 2.3), the storage (elastic) modulus G' , loss (viscous) modulus G'' , and phase angle δ are the fundamental measurements, defined as:

$$\gamma = \gamma_0 \sin(\omega t), \quad \gamma = \frac{R\theta}{H}, \quad (2.3)$$

$$\sigma = \sigma_0 \sin(\omega t + \delta), \quad \sigma = \frac{2M}{\pi R^3} \left(\frac{3}{4} + \frac{1}{4} \frac{d \ln M}{d \ln \dot{r}_R} \right), \quad (2.4)$$

where γ_0 and σ_0 are the maximum amplitude of the strain and stress, δ is the phase angle, R is the parallel plate radius, H is the parallel plate thickness, θ is the oscillation displacement, M is the generated torque, and \dot{r}_R is the shear rate at the plate rim. It can be shown that³

$$\sigma = \gamma_0 [G' \sin(\omega t) + G'' \cos(\omega t)], \quad (2.5)$$

where G' and G'' are in-phase and 90° out-of-phase with the strain, respectively. From Eqns. (2.3)–(2.5),

$$G' = (\sigma_0/\gamma_0) \cos \delta, \quad G'' = (\sigma_0/\gamma_0) \sin \delta, \quad \text{and} \quad G''/G' = \tan \delta,$$

and the complex modulus

$$G^* \equiv \sigma^*/\gamma^* = G' + iG'', \quad (2.6)$$

where $\sigma^* = \sigma_0 \exp[i(\omega t + \delta)]$, and $\gamma^* = \gamma_0 \exp(i\omega t)$ are the complex forms of the stress and strain, respectively. The complex viscosity

$$\eta^* = G^*/(i\omega) = \eta' - i\eta'' \quad (2.7)$$

is customarily used to describe the relationship between the stress and strain rate for viscoelastic liquids.

In addition to studies based on the foregoing mechanical rheometer, microrheology has come to play an important role in characterizing the mechanical properties of soft materials. Microrheology is generally classified as being passive or active⁶⁴. Passive methods, such as particle tracking microrheology (PTM) and diffusing wave spectroscopy (DWS), exploit thermal energy ($k_B T$) to induce particle motion; whereas active methods use an external force, *e.g.*, from a magnetic field (magnetic tweezers) or focused laser beam (optical tweezers). Novel techniques, such as electroacoustic spectroscopy⁶⁵ have also been applied to study gel rheology and nanoparticle dynamics.

Microrheology offers some advantages, including the ability to work with extremely small sample volumes, samples with low viscosity or elasticity, including extremely tenuous gels, and samples with non-conventional geometries, such as biological cells and membranes^{66,67,64}. Microrheology is suitable for probing the mechanical properties of heterogeneous systems, whereas bulk rheology provides averaged values. Another advantage is that microrheology can reach much higher frequencies (MHz). Nevertheless, there are important limitations^{66,67}.

In passive microrheological experiments on gels, the material stiffness is often too high to resolve particle dynamics. The maximum modulus is limited by the position-detection resolution of the experiment⁶⁷. The size of the tracer particles embedded in the sample can also affect the reported material properties. Beads must be large enough to accurately detect and quantify their Brownian or coherent external-force-driven motion, and small enough to resolve spatial variations in rheological properties. In active microrheology, viscosities and elastic moduli may be available in frequency ranges that are outside the range for which the results can be extrapolated to practical applications. Consequently, the response at low frequencies may be poorly resolved or inaccessible. For example, AFM microrheology can measure very stiff gels (MPa), but is limited to high frequencies (20–400 Hz)⁶⁸. The reported shear modulus obtained by manipulating magnetic beads embedded in hydrogels²⁰ has been found to exceed the ideal network modulus, possibly casting doubt on such measurements for the quantitative studies undertaken in this thesis using bulk mechanical rheometry.

Microrheology is not yet a standardized tool for quality control, because its ability to characterize materials on the macro-scale is still questionable, and careful calibrations are often required. The sol-gel transition can also be characterized using microrheology⁶⁹, but no comparison of macro- and micro-rheological measurements during the gelation of physical gels has been undertaken⁶⁶.

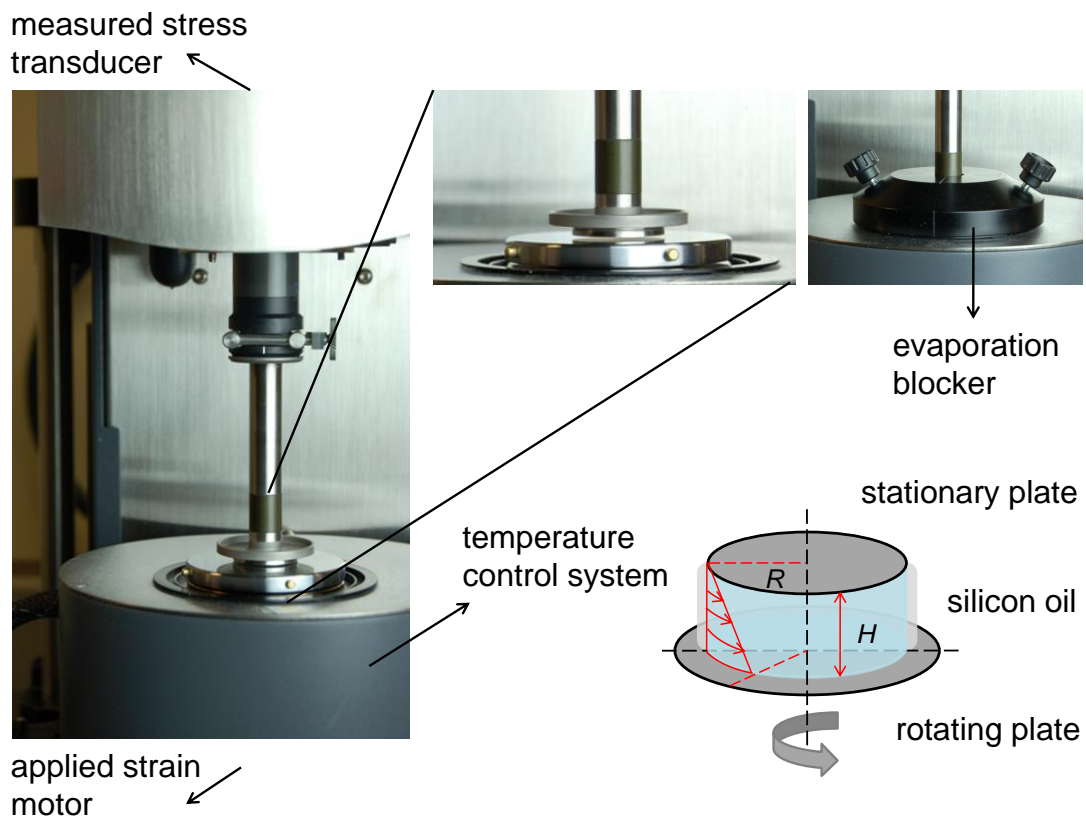


Figure 2.3: ARES-G2 rheometer with an advanced Peltier system for temperature control. The schematic shows the parallel-plate geometry used in this study.

2.2.1 Viscoelasticity

Materials can be characterized according to their linear viscoelastic response on various timescales³. As shown in figure 2.4, the terminal region of the storage and loss moduli for a chemically crosslinked network of polymers (VI) has $G' \sim G'' \sim \omega^0$. For polymers with very light crosslinks (VII), there is a slight increase in G' and G'' at higher frequencies; this is attributed to slipping of the entanglements on dangling branched structures, which are incompletely attached to the network. For high-molecular-weight polymer melts with long side groups (IV), G' and G'' in the terminal regime have larger exponents than polymer melts without long side groups (III); this is because coupling entanglements prolong the time required for long-range configurational changes.

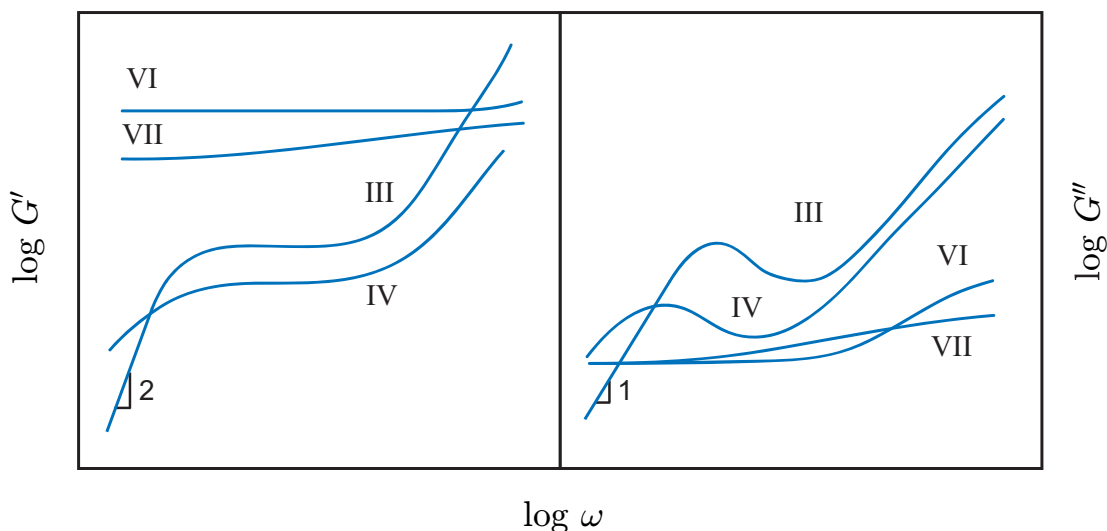


Figure 2.4: Storage and loss modulus versus frequency with logarithmic scales for different polymer systems. Replotted according to Ferry³.

The Maxwell model is a phenomenological model that captures principal viscoelastic characteristics using a series combination of springs and dashpots to model the frequency dependence of the storage and loss moduli, i.e., the viscoelastic spectra³. Many entangled polymer melts, entangled polymer solutions, and physical gels obey the Maxwell model, which predicts $G' \sim \omega^2$ and $G'' \sim \omega^1$ in the terminal regime.

The Rouse model is a molecular model of polymer dynamics that approximates polymer chains as a sequence of beads that are connected by linear springs. The beads have a friction coefficient ζ and interact with the other only through the springs. At low frequencies, the Rouse model predicts Maxwell relaxation, whereas at high frequencies, it predicts a power-law frequency dependence of $G' \sim G'' \sim \omega^{1/2}$ ⁷⁰.

For networks with fixed crosslinks, such as chemical gels, a modified Rouse model has been proposed³:

$$G' = \nu RT \left[1 + \sum_i \frac{\omega^2 \tau_i^2}{1 + \omega^2 \tau_i^2} \right], \quad (2.8)$$

$$G'' = \nu RT \sum_i \frac{\omega \tau_i}{1 + \omega^2 \tau_i^2}, \quad (2.9)$$

where ν is the molar (when R is the ideal gas constant) concentration of network strands, and τ_i is the relaxation time for each relaxation mode (with index i).

For physically crosslinked gels, a model (inspired by the theory of rubber elasticity) for a temporary network having a equal “break” and “re-form” rates predicts⁷⁰

$$G'(\omega) = \sum_i G_i \frac{\omega^2 \tau_i^2}{1 + \omega^2 \tau_i^2}, \quad (2.10)$$

$$G''(\omega) = \sum_i G_i \frac{\omega \tau_i}{1 + \omega^2 \tau_i^2}, \quad (2.11)$$

where τ_i and G_i are the relaxation time and modulus for each relaxation mode. This model is not applicable when the “break” and “re-form” rates are different.

Indei and Takimoto⁷¹ proposed an “associative Rouse model” that includes an intermediate regime in which the dynamic spectra scale as $G' \sim G'' \sim \omega^{1/2}$. In this model, the gel network comprises polymer chains having multiple associative stickers, and the terminal or longest relaxation time τ_A is proportional to $\tau_X \bar{N}^2$, where \bar{N} is the average number of associated stickers per chain, and τ_X is the time for an associated sticker to return to its equilibrium state. In the Maxwell model, τ_A and τ_X coincide (with small \bar{N}), so only the terminal relaxation mode is observed. However, the associative-Rouse model applies when \bar{N} is large (association rate higher than the dissociation rate), reducing the exponents at low frequencies ($\tau_A^{-1} \lesssim \omega \lesssim \tau_X^{-1}$). Indei and Takimoto⁷¹ obtained good agreement between their theoretical model and experimental data for poly(ethylene oxide) solutions with hydrophobic groups on backbones as associative stickers.

It is only in recent years that rheological properties of dual-crosslinked gels have been studied. Narita et al.⁶⁰ reported the frequency-sweep spectra of gels with and without chemical crosslinks. They showed that physically crosslinked PVA gels exhibit Maxwell behaviour at low frequencies. An associative-Rouse mode was identified after they subtracted chemical gel moduli from the dual-crosslinked gel moduli. They also proposed a stress-relaxation mechanism for dual-crosslinked gel networks to interpret an increase in the physical association lifetime with borate ion concentration.

Commercially available rheometers, such as the ARES-G2, probe frequencies from 10^{-3} to 628 rad s^{-1} . At low frequencies, however, the data collection time becomes too long, whereas at high frequencies, sample-geometry inertia can cause measurement error. Therefore, frequency-sweep tests are often undertaken in the range 10^{-1} – 10^2 rad s^{-1} . To examine viscoelastic properties of materials over a much wider frequency range, *time-concentration superposition* (TCS) or *time-temperature superposition* (TTS) are undertaken. Since a near-critical gel (a gel near its sol-gel transition) is geometrically self-similar, an increase in crosslinking merely changes the cluster scales and relaxation time⁷², thus permitting TCS. In addition to extending rheological spectra to a wider frequency range, TCS is a useful tool for studying viscoelastic materials at critical limits, such as the gel point, at which the bond probability reaches the critical value and an infinite cluster spans a macroscopic sample, inducing a transition from liquid- to solid-like characteristics⁷³.

In TTS, spectra measured at experimentally accessible frequencies and at different temperatures are *superposed*, furnishing a composite rheological spectrum. In the Rouse model, the elastic modulus and relaxation time for each spring is⁷⁰

$$G_i = G = \nu k_B T, \quad \tau_i = \frac{\zeta_b}{16k_B T \beta_s^2 \sin^2[i\pi(N_s + 1)/2]}, \quad (2.12)$$

where ν is the polymer molecules number density, ζ_b is the drag coefficient, β_s is related to the number of links at one end of a freely-jointed chain and the link length, and N_s is the number of springs in the Rouse chain. For τ_i , the most important temperature dependence is that of the monomer drag coefficient ζ_0 ($\zeta_b = N\zeta_0/(N_s + 1)$), which is the same for each τ_i . Therefore, on a log-log plot, a change in temperature merely shifts $G'(\omega)$ and $G''(\omega)$ along the frequency axis, without changing their shape. The spectra are also shifted along the modulus axis due to the dependence of G_i on T and ν . Because the effects of T and ν partially cancel (ν decreases with increasing T because of thermal expansion), the shift along the modulus axis is often small and, therefore, neglected. The horizontal a_T and vertical b_T shift factors are obtained via

$$b_T G^*(\omega, T) = G^*(\omega a_T, T_0), \quad (2.13)$$

where $G^*(\omega a_T, T_0)$ denotes the modulus at the reference temperature and shifted frequency ωa_T ⁷⁴. The correlation between a_T and T can be described by either the Arrhenius equation or Williams-Landel-Ferry (WLF) equation. According to Mark⁷⁵, the Arrhenius equation is more suitable for polymer solutions, and for polymer melts when T is well above the glass transition temperature T_g . The WLF equation is applicable for concentrated polymer solutions, and for polymer melts at temperatures between T_g and $T_g + 100 \text{ K}$.

2.2.2 Creep-recovery

Other dynamic experiments, such as creep and stress relaxation, can also be used to characterize viscoelastic materials. In a creep test, a constant shear stress σ is applied to the sample, and the time dependence of the resulting strain $\gamma(t)$ is recorded. The creep compliance is defined as

$$J(t) = \frac{\gamma(t)}{\sigma}. \quad (2.14)$$

After maintaining the stress for some time, the stress may be removed so that the sample returns toward its initial shape³. For ideal elastic solids, the strain during creep is instantaneous and independent of time, and upon removing the stress, the strain is fully recovered. For ideal viscous fluids, strain increases linearly with time while subjected to a constant stress, with no recoverable strain upon removing the stress. The time-dependence of viscoelastic materials, such as physical gels, during creep and recovery is a combination of the foregoing elastic and viscous deformations⁷⁶. In the linear viscoelastic regime (small strain), the creep compliance is independent of the stress. With increasing stress, however, the creep compliance changes, indicating a non-linear viscoelastic regime. At high enough stresses, creep curves may exhibit a so-called *tertiary creep* region, in which deformation accelerates until creep-rupture occurs⁷⁶. Creep tests are therefore used to study microstructural evolution⁷⁷. Models, such as the four-parameter Burgers model⁷⁷, have been developed to capture the time dependence of the creep compliance. In practical applications, creep tests are used to study long-term structural evolution, with recovery tests quantifying how much of the deformation is recoverable. A series of creep-recovery with increasing applied stress can be adopted to determine the yield stress: when a material with complete recovery under a small stress fails to recover completely, it has reached or exceeded the yield stress (TA Instruments user manual).

Creep-recovery for physical hydrogels has been used to understand gel structure and properties. For example, Cruz and Areas⁷⁸ showed that adding amylose to lysozyme physical gels increases the recoverable strain, because amylose enhances the gel strength. Abdurrahmanoglu and Okay⁷⁹ studied polymer-clay nanocomposite hydrogels using creep-recovery. They showed that gels formed by polymerizing acrylamide in a clay dispersion have a longer retardation time, when compared to other types of monomers, such as *N*-isopropylacrylamide. These indicate a higher crosslink-zone mobility, and therefore greater dissipated energy during deformation. Terech et al.⁵¹ used creep-recovery to show that physical gels with self-healing characteristics have a larger recoverable strain and a shorter retardation time.

The creep compliance in the linear viscoelastic regime can be transformed to dynamic moduli spectra via Fourier transform⁸⁰:

$$\frac{i\omega}{G'(\omega) + iG''(\omega)} = i\omega J_0 + (1 - e^{-i\omega t_1}) \frac{(J_1 - J_0)}{t_1} + \frac{e^{-i\omega t_N}}{\eta} + \sum_{k=2}^N \left(\frac{J_k - J_{k-1}}{t_k - t_{k-1}} \right) (e^{-i\omega t_{k-1}} - e^{-i\omega t_k}), \quad (2.15)$$

where k indexes the data points, J_0 denotes the initial compliance, and η is the steady-state viscosity. The range of transformed spectra depends on the response time for the first creep data point, and how long the creep test is performed ($t_N^{-1} < \omega < t_1^{-1}$).

This method is susceptible to the noise in data, *e.g.*, creep ringing caused by the coupling between instrumental inertia and material elasticity. Another method using the Laplace transform and the Havriliak-Negami model developed by Kim et al.⁸¹ can remove inertial effects. However, this method is not suitable for some polymeric materials, including gels. This limitation can be addressed by introducing new approximate functions for the Laplace transform of creep compliance⁸².

2.2.3 Large amplitude oscillatory shear (LAOS)

When the strain is large enough to place the deformation in the non-linear viscoelastic regime, the microstructure is dynamic, exhibiting strain dependent G' and G'' . Compared to small-amplitude oscillatory tests, LAOS is important because materials with linear viscoelastic properties may exhibit distinctly different non-linear characteristics. LAOS also has practical significance, because the deformation is often large and rapid in materials processing⁸³. Strain-sweep tests in the non-linear regime can also be adopted to identify the yield point. According to the microstructure, LAOS responses can be classified into the following four types: strain thinning, strain hardening, weak-strain overshoot, and strong-strain overshoot⁸³. Soft gels, such as Xanthan gum gel and associative polymer solutions, often follow weak-strain overshoot behaviour in the non-linear regime, in which G' decreases with increasing strain and G'' first increases and then decreases with respect to strain. The increase in G'' with strain can be attributed to increased network connectivity, which enhances dissipation. A loss of crosslinks dominates at larger strain amplitudes, leading to a decrease in G' and G'' .

The stress versus strain and stress versus strain rate in a sinusoidal cycle are adopted to qualitatively characterize the LAOS response and provide structural insight. For example, the stress versus strain curves are ellipses for viscoelastic materials in the linear regime, and are distorted ellipses in the non-linear regime⁸⁴. Moreover, systems with the same depen-

dence of G' and G'' on strain may have different shapes of stress versus strain due to their different microstructures⁸³. Moreover, Fourier transformation can be used to decompose the stress and produce a spectrum of relative intensity for higher-order odd harmonics, which increase from zero with increasing strain in the non-linear regime. An increase in the even harmonics indicates secondary flows or wall slip⁸⁵. To avoid the wall slip effect, cone-plate geometries are often used for LAOS tests. When using parallel-plate geometries, sand-paper coated plates⁸⁶ or serrated plates⁸⁷ may be required to eliminate wall-slip effects.

2.3 Swelling

2.3.1 Equilibrium swelling ratio

When a chemically-crosslinked polymer network is placed in a solvent, it absorbs the solvent and swells. According to the Flory-Rehner theory of polymer-network swelling, the gel expands due to a polymer-solvent mixing force, described by Flory-Huggins theory. The isotropic expansion is resisted by the network elasticity, described by the theory of rubber elasticity⁶⁶. The Flory-Huggins parameter χ measures the quality of the solvent. Because real networks deform between the localized phantom network limit and the affine network limit, the Flory-Rehner equation that describes the isotropic swelling of an uncharged gel can be written as

$$\frac{NV_1}{2N_A V_0} \phi^{1/3} = -[\ln(1 - \phi) + \phi + \chi\phi^2], \text{ (phantom limit)} \quad (2.16)$$

$$\frac{NV_1}{N_A V_0} (\phi^{1/3} - \phi/2) = -[\ln(1 - \phi) + \phi + \chi\phi^2], \text{ (affine limit)} \quad (2.17)$$

where N is the number of partial chains in the dry state, V_0 is the dried gel volume, V_1 is the molar volume of the solvent, N_A is Avogadro's number, and ϕ is the equilibrium polymer volume fraction²⁹.

The swelling of PA gels is well described by the Gaussian-chain model^{66,88} for which

$$G_e = \frac{Nk_B T \phi^{1/3}}{V_0}. \quad (2.18)$$

If the elastic shear modulus in the equilibrium state G_e is known, the crosslink density in the dry state may be obtained from the swelling ratio ($S = 1/\phi$). By fitting the osmotic pressure versus equilibrium swelling ratio for PA gels or solutions using the Flory-Huggins model, Li et al.⁸⁹ showed that χ ascertained from the fitting increases with G_e , whereas a

constant χ captures how the swelling ratio varies with osmotic pressure over four orders of magnitude in the osmotic pressure

Baselga et al.⁹⁰ showed that χ for PA gels decreases with increasing temperature. For nonionic gels, including PA gels, ions in the solvent increase solvent (water) uptake capacity. Boyde⁹¹ reported that the swelling ratio of PA gels increases with increasing sodium chloride concentration (0.2–2 M). Sivanantham and Tata⁹² found that χ for PA gels decreases with increasing salt concentration. Livney et al.⁹³ demonstrated that various anions and cations, and their concentrations, affect the swelling of PA gels.

Gels bearing charged moieties, often termed polyelectrolyte gels, have much larger swelling ratios. An additional contribution to the osmotic pressure can be modelled using Donnan theory⁹⁴. This additional swelling ability is suppressed with increasing salt concentration, because ions in the bulk solvent decrease the osmotic pressure difference between the inside and outside of the gel according to their influence on Donnan equilibrium²⁹. For PVA dual-crosslinked gels, Shibayama et al.⁵⁹ showed that the swelling ratio first decreases with increasing borate ion concentration, because of a larger intrachain crosslinking density, and then increases due to the increase of intrachain electrostatic repulsion.

2.3.2 Swelling kinetics

During swelling, solvent diffuses into the polymer network and the network expands. Tanaka and Fillmore⁹⁵ focused on the motion of polymer networks in solvents by developing a theory involving the displacement of a point in the network from its average position followed by a shear relaxation. Hakiki and Herz⁹⁶ showed that the swelling kinetics for a long cylindrical gel (the swelling rates in both radial and axial directions are assumed the same) follows:

$$-\ln \frac{u_r(a, t)}{u_r(a, 0)} = \frac{1}{\tau_1} - \ln B_1, \quad (2.19)$$

where u_r is the radial displacement, a is the gel radius in the equilibrium state, τ_1 is the relaxation time of the first-order swelling, and the fitting parameter

$$B_1 = \frac{2(3 - 4\nu)}{\alpha_1^2 - (4\nu - 1)(3 - 4\nu)}, \quad (2.20)$$

where ν is related to Poisson's ratio, and α_1^2 is related to eigenvalues that are prescribed by the boundary condition. The cooperative diffusion coefficient is

$$D = \frac{a^2}{\tau_1 \alpha_1^2}. \quad (2.21)$$

Although Hakiki and Herz⁹⁶ and Peters and Candau⁹⁷ proved that the values of D for cylinders or disks from swelling kinetics agree with those obtained from light-scattering spectroscopy, the theory still has limitations. For example, D is assumed constant, whereas D varies in space and time, because it depends on the changing polymer concentration. Thus, swelling data acquired near equilibrium are best described by this theory. Moreover, in the model, the gel is considered a mixture of a solid and a liquid, but the fluid displacement is neglected. Thus, deviations may arise when the effect of fluid transport on the gel network deformation is strong. For example, the swelling rate estimated from the model may be slower, especially in the initial stage of swelling or the last stage of deswelling. On the other hand, Biot’s theory of linear poroelasticity, originating from soil consolidation studies, can also be used to describe gel-swelling kinetics⁹⁸. Here, the solvent and network are considered as separate phases, and work done by the chemical potential of the solvent in the gel is considered. Hui and Muralidharan⁹⁹ included liquid-phase momentum transfer as an extension of Tanaka’s model, proving that the modified model is identical to Biot’s theory. There are assumptions made for both models, such as the volumetric strain in the gel cannot be too large, and the solid and liquid phases are incompressible.

The pore size (mesh size) of gel networks is an important parameter for gel applications, such as drug delivery. In addition to the permeability (see section 2.1.1) and swelling kinetics, light scattering, electron microscopy, porosimetry, rubber elasticity, equilibrium swelling theory, and electrophoresis of latex particles, DNA, or sucrose can also be used to infer pore sizes⁴⁰. These methods all present experimental challenges and their interpretation requires numerous assumptions. For instance, dehydrating a highly swollen network, as required for electron microscopy, can change the pore size and structure³⁴. From the reported pore sizes obtained from various methods, if the mesh size ξ_0 ascertained from the plateau modulus ($G' \approx 20$ kPa) is set as the reference, it has been shown that the pore size obtained from swelling kinetics⁹⁶ is half of ξ_0 ; the pore size obtained from equilibrium swelling theory⁴⁰ is 10 times smaller than ξ_0 ; the pore size from the electrophoretic mobility of DNA fragments¹⁰⁰ is about 3 times larger than ξ_0 ; and pore sizes obtained from the electrophoretic mobility of sucrose furnish $\xi = 1/\%T^{0.33}$ ($\%T$ is the monomer concentration)³⁷, which are 3 times smaller than ξ_0 . Pore sizes from scanning electron microscopy are 5–10 times larger than those from equilibrium swelling, indicating multiple coexisting porosity scales⁴⁰. Liedl et al.¹¹ reported that the DNA-crosslinked gels are capable of trapping nanoparticles smaller than the average pore size. They explained this based on a distribution of pore sizes, electrostatic interactions, and the high entropic cost of restricted nanoparticle dynamics in gel pores.

As highlighted in section 2.1.2, physically crosslinked gels have a variety swelling characteristics. An et al.¹⁰¹ developed a thermodynamic model for the swelling of physical gels. Elastic properties of the network and the transient nature of crosslinks are considered: a connectivity tensor is used to capture the crosslink reformation microscopically, and the total free energy is proposed as the sum of elastic, mixing, and bond energies. At equilibrium, the gel may dissolve into a polymer solution, because the bond energy is too weak to hold the polymer chains together, causing all crosslinks to break. It was shown that a sharp sol-gel transition occurs more easily for physical gels having a larger activation energy and larger polymer-solvent interaction parameter χ .

2.3.3 Drug delivery

The release of drug molecules from a delivery device can be controlled by molecular diffusion in water-insoluble gels, dissolution of water-soluble or biodegradable gels, advection by osmosis, and ion exchange¹⁰². These methods can only be used for continuous release with kinetics that is linear or burst-like. Hydrogels that can respond to external stimuli, such as pH or specific molecules, have potential for noncontinuous delivery. The stimulus needs to first permeate the gel to induce a volume/phase transition that will control release. When engineering an hydrogel drug-delivery system, the drug release rate, mechanical strength of the gel, drug-hydrogel affinity, and gel injectability need to be considered³⁰. Interpenetrating or dual networks have been adopted for prolonging the release, in addition to simply increasing the crosslink density.

Hoare and Kohane³⁰ pointed out that physical hydrogels have the advantage of gelling without adding crosslinking entities *in vivo*. Disadvantages arise from variables that are difficult to control, such as gelation time and network pore size. Moreover, physically crosslinked hydrogels dilute and disperse relatively fast due to water influx, restricting their use to short-acting release. Chemical gels, on the contrary, can prevent dilution and dissolution. However, most are not injectable, and toxic reagents are required for crosslinking, so these must be removed prior to hydrogel implantation.

Linear viscoelasticity of bis-acrylamide crosslinked polyacrylamide hydrogels with low crosslinker ratio

3.1 Preface

Chemically crosslinked polyacrylamide hydrogels have been studied extensively, but the microstructure of gels with low crosslinker ratio receives little attention. In this chapter, the rheology of bis-crosslinked polyacrylamide hydrogels with low crosslinker ratio ($c_a \approx 10\%$; c_{bis}/c_a is in the range 0.2–0.9 mmol/mol) is examined. Linear viscoelastic responses were measured during and following gelation. The formation rate of effective crosslinks increases with crosslinker ratio, and the plateau modulus is weakly quadratic in the crosslinker ratio. Gels with low crosslinker ratio exhibit distinctly different features from gels with higher crosslinker ratio. First, plateau regions in the dynamic moduli spectra are less pronounced. Second, the loss tangents are approximately several orders of magnitude higher than for polyacrylamide gels with higher crosslinker ratio but similar plateau modulus in the literature. Finally, time-concentration superposition of spectra above the apparent percolation threshold furnishes a critical relaxation exponent $\Delta \approx 0.38$ that is smaller than for the universal sol-gel transition. These distinct features may arise from physical entanglements formed in gel networks that can be released at long timescales. Time-temperature superposition shows that the apparent activation energy for disentanglement decreases from ≈ 25 to $\approx 6 k_B T$ with increasing temperature. This chapter also serves as a foundation for the study of DNA-crosslinked gels (physical gels) in chapter 4.

3.2 Introduction

Polyacrylamide (PA) hydrogels from the free-radical copolymerization of acrylamide monomer with bis-acrylamide (bis) crosslinker have been studied extensively. The literature includes studies of gelation^{7,103}, mechanical properties tuned by composition^{2,6}, and swelling^{40,89}. The monomer concentration c_a ¹ and crosslinker concentration c_{bis} ² are the principal parameters that can be adjusted to control gel properties, such as the shear modulus, water uptake capacity, permeability, and microstructural homogeneity. Unlike ideal networks, structural defects, including loops, dangling chains, entanglements, and crosslinker-crosslinker short-cuts, arise from a sub-optimal matching of c_a and c_{bis} .

The storage modulus G' of PA gels has been found to increase as a power-law in the monomer concentration c_a , with exponents 3.3⁶ and 3.5⁴. This is because the higher monomer concentration increases the probability for a bis-acrylamide to form an effective crosslink with a polymer chain in its neighbourhood⁸. The influence of c_{bis} is less pronounced than for c_a . With c_a fixed, Adibnia and Hill⁴ showed that the crosslinking efficiency first increases and then decreases with the crosslinker ratio c_{bis}/c_a ³ from 0.9 to 10% w/w ($c_a = 3\%$ w/v). Denisin and Pruitt² found that as c_{bis}/c_a increases from 0.2 to 11% w/w ($c_a \approx 10\text{--}20\%$ w/v), G' first increases, reaches a plateau, and then decreases. Inhomogeneous networks formed at higher crosslinker concentrations arise from aggregates (“microgels”) that are rich in bis-acrylamide and loosely connected by chains containing much less bis-acrylamide. It has been proposed that bis-acrylamide has a tendency to react with itself and that acrylamide has a preference to react with bis-acrylamide than with itself^{31,103}. Accordingly, clusters are expected to present fewer multi-functional groups than the same number of isolated bis-acrylamide junctions, thus decreasing the crosslinking efficiency. Due to the effects of c_a and c_{bis} on the gel network structure and crosslinking efficiency, an optimum value of c_{bis} can be determined when c_a is fixed. In low crosslinker ratio ranges such as 0.5–3.7% w/w with $c_a = 8\%$ w/v, G' has been found to increase linearly with the crosslinker ratio⁷. A similar linear correlation has been reported for gels with c_{bis}/c_a between 0.03% w/w and 0.3% w/w ($c_a = 15\%$ w/v), achieving a crosslinking efficiency as high as 0.9⁸.

In contrast to many studies of the storage modulus, little attention has been paid to the loss modulus G'' , which provides tremendous microstructural insight. According to the

¹ $\frac{\text{mass of acrylamide (g)}}{\text{volume of pre-gel solution (ml)}} \times 100\% \text{ (w/v)}$ or $\frac{\text{amount of substance of acrylamide}}{\text{volume of pre-gel solution}} \text{ (mol l}^{-1}\text{)}$.
² $\frac{\text{mass of bis-acrylamide (g)}}{\text{volume of pre-gel solution (ml)}} \times 100\% \text{ (w/v)}$ or $\frac{\text{amount of substance of bis-acrylamide}}{\text{volume of pre-gel solution}} \text{ (mmol l}^{-1}\text{)}$.
³ $\frac{\text{mass of bis-acrylamide (g)}}{\text{mass of acrylamide (g)}} \times 100\% \text{ (w/w)}$ or $\frac{\text{amount of substance of bis-acrylamide}}{\text{amount of substance of acrylamide}} \text{ (mmol/mol)}$.

percolation model^{104,105}, spatially isolated clusters form in the early stages of gelation. As the copolymerization of monomer and crosslinker proceeds, macroscopic gelation occurs by interconnecting these clusters to form a continuous network. In the early stages of gelation, G'' reflects cluster formation and connectivity. The higher dissipation accompanying larger values of G'' arises from polymer chains that are not connected to the percolating network. This has been observed in the gelation of DNA-crosslinked gels, which will be reported in chapter 4. Moreover, the study of Adibnia and Hill⁴ shows that increasing c_{bis}/c_a causes G'' for PA gels at a fixed frequency to first reach a maximum before decreasing to a lower steady-state value, suggesting the rearrangement of polymer chains and clusters during polymerization.

The storage modulus G' of PA gels is often considered frequency independent, increasing linearly with temperature⁷. However, for gels such as lightly crosslinked styrene-butadiene rubber¹⁰⁶, poly(dimethylsiloxane) (PDMS) gels with dangling chains and branched structures¹⁰⁷, and PA gels with lower crosslinker concentration^{4,7}, G' increases with frequency in the high-frequency regime. This reflects the distribution of entanglement relaxation times: increasing the frequency temporarily traps an increasing number of entanglements that contribute to G' . Temperature may affect dynamic moduli spectra in a manner that is beyond the ideal-rubber elasticity prefactor for these gels. This motivates time-temperature superposition (TTS) for extending spectra and determining the activation energy for entanglement disengagement.

The horizontal shift factor a_T and vertical shift factors b_T for TTS are obtained via

$$b_T G^*(\omega, T) = G^*(\omega a_T, T_0), \quad (3.1)$$

where $G^*(\omega a_T, T_0)$ denotes the modulus at the reference temperature and shifted frequency ωa_T ⁷⁴; ωa_T is related to the temperature dependence of the relaxation time, which is primarily attributed to the monomer friction coefficient⁷⁰. Note that b_T has been related to the effective number density of partial chains ν at each temperature by

$$b_T = \frac{T_0 \nu_0}{T \nu}, \quad (3.2)$$

where T_0 is the reference temperature and ν_0 is the effective number density of partial chains at T_0 . Note that ν is adopted here instead of the material density ρ usually used in the literature^{74,108}, because the number density of partial chains contributes to the gel moduli. The correlation between a_T and temperature can be described by either the Arrhenius equation

$$a_T = A e^{E_a/(RT)}, \quad (3.3)$$

where E_a is the apparent activation energy and A is a constant prefactor, or the Williams-Landel-Ferry (WLF) equation

$$\log a_T = \frac{-C_1(T - T_0)}{C_2 + (T - T_0)}, \quad (3.4)$$

where C_1 and C_2 are empirical constants.

The present study examines gelation kinetics and dynamic shear moduli spectra for PA gels with bis-acrylamide crosslinker concentrations that are slightly above the critical gelation concentration, as shown in figure 3.1. Gelation and dynamic moduli data from Adibnia and Hill⁴ are compared to those in the present study. TTS furnishes the apparent activation energy for disentanglements. Creep-recovery provides insights into gel durability. Because of the low crosslinker ratio, distinct rheological characteristics arise from the physical entanglements.

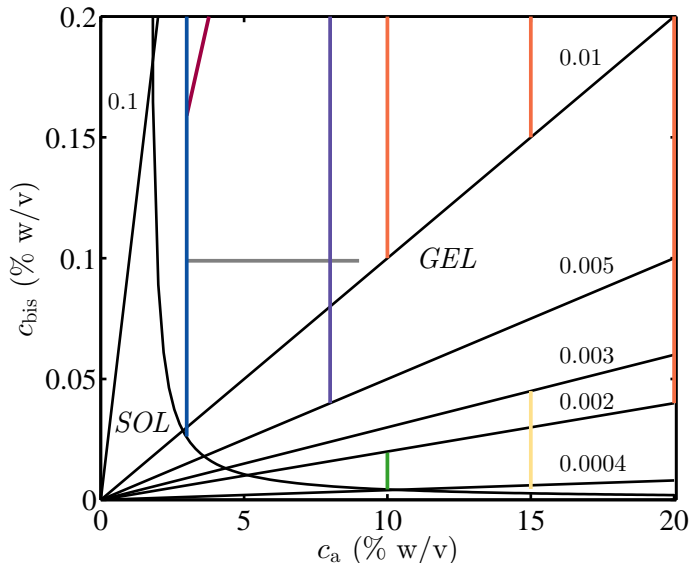


Figure 3.1: Gel-composition map: separation of solutions and gels (black curve); identification of constant crosslinker to monomer ratios (black lines); the monomer and crosslinker concentrations for this study (green), Adibnia and Hill⁴ (blue), Adibnia⁵ (red), Trompette et al.⁶ (grey), Calvet et al.⁷ (violet), Basu et al.⁸ (yellow), and Denisin and Pruitt² (orange).

3.3 Materials and methods

Acrylamide (40% w/v, Fisher Scientific), bis-acrylamide (2% w/v, Fisher Scientific), ammonium persulfate (APS, $\geq 98\%$, Fisher Scientific), N,N,N',N' -tetramethylethylenediamine

(TEMED, 99%, GE Healthcare Life Sciences), and DNA suspension buffer (10 mM Tris-HCl, 0.1 mM EDTA, pH 8.0, Teknova) were used as provided by the manufacturers.

A fixed volume of 40% w/v acrylamide, varying volumes of 0.25% w/v bis-acrylamide solutions and buffer were added to a centrifuge tube to achieve a monomer concentration 1.4 mol l^{-1} while varying the crosslinker ratio as listed in table 3.1. Nitrogen was bubbled through the mixtures for 5 min to remove dissolved oxygen.

To clearly distinguish the samples, a nomenclature B_x is adopted, where x is the ratio of bis-acrylamide crosslinker to acrylamide concentrations (ratio as mmol/mol) in the pre-gel solution.

After adding 10 μl of freshly prepared 10% (w/v) APS⁴ and 3.6 μl TEMED per ml of the pre-gel solution, the mixture was pipetted onto the bottom plate of the parallel-plate sample holder of an ARES-G2 rheometer (TA Instruments), and the 25 mm diameter top plate then lowered to achieve a 0.5 mm gap. An “evaporation blocker” (TA Instruments) and silicone oil were used to minimize evaporation. Oscillatory shear during gelation was applied at 21°C (angular frequency $\omega = 1 \text{ rad s}^{-1}$ and strain amplitude $\gamma = 1\%$) to ensure a linear viscoelastic response. After the dynamic moduli reach steady values, frequency sweeps were performed in the range $\omega = 0.1\text{--}100 \text{ rad s}^{-1}$ with $\gamma = 1\%$ at temperatures from 21°C to 56°C, controlled using a ThermoCube 10-300 thermoelectric chiller (Solid State Cooling Systems). The axial force for TTS was set to 0 N, and the top-plate position at each temperature was corrected according to the sample-holder expansion. Creep-recovery tests in the linear viscoelastic regime were undertaken after returning the temperature to 21°C.

In addition, bis-crosslinked gels with $c_a \approx 1.3 \text{ mol l}^{-1}$ and crosslinker ratios in the range 0.2–0.9 mmol/mol were synthesized by dissolving acrylamide powder in RO water instead of diluting the foregoing 40% acrylamide solution. For these eight samples, frequency sweeps were undertaken following $\approx 1800 \text{ s}$ of gelation.

Table 3.1: Compositions of bis-crosslinked polyacrylamide gels.

Sample	A (%)	Bis-A/A (mmol/mol)	A (mol l^{-1})	Bis-A (mmol l^{-1})
$B_{0.2}$	10	0.2	1.4	0.28
$B_{0.4}$	10	0.4	1.4	0.56
$B_{0.6}$	10	0.6	1.4	0.84
$B_{0.8}$	10	0.8	1.4	1.12

⁴ $\frac{\text{mass of APS (g)}}{\text{volume of water (ml)}} \times 100\%$.

3.4 Results and discussion

3.4.1 Gelation kinetics

Storage modulus G' time series for bis-crosslinked gels at a fixed monomer concentration during gelation are plotted in figure 3.2. G' first increases to a maximum, and then decreases before reaching a plateau. The maximum value occurs at ≈ 1300 s. This is the time at which the majority of the effective crosslinks have formed. Beyond the maximum, relaxation is evident because the gels are viscoelastic materials. The maximum occurs earlier for gels with a lower ratio c_{bis}/c_a , and the percentage reduction following the maximum decreases from ≈ 27 to 6.3% for samples B_{0.2}–B_{0.8}. These characteristics are not evident from studies of PA gels with a higher crosslinker ratio (appendix 3.B).

The top-right panel of figure 3.2 shows G' when $t \leq 1200$ s, and least-squares fits of the empirical model^{7,109}

$$G'(t) = G'_\infty \frac{t^n}{t^n + \theta^n}, \quad (3.5)$$

where G'_∞ is the storage modulus when $t \rightarrow \infty$ (assuming no relaxation occurs), θ is the time at which $G'(t) = G'_\infty/2$, and n is a fitting exponent. The mid-point slope

$$P = \left. \frac{dG'}{dt} \right|_{t=\theta} = \frac{nG'_\infty}{4\theta} \quad (3.6)$$

is customarily adopted to quantify the gelation kinetics⁷.

Dashed lines in the top-right panel of figure 3.2 show that P increases with the crosslinker ratio. This suggests that a higher concentration of localized clusters accelerates the formation of elastically effective crosslinks by shortening partial chains.

As shown in the bottom left panel of figure 3.2, loss moduli time series $G''(t)$ at short times have the same qualitative characteristics as $G'(t)$. G'' decreases with increasing crosslinker ratio for samples B_{0.4}–B_{0.8}, suggesting that the networks with higher crosslinker ratio have higher crosslinking efficiency. G'' for B_{0.4}, however, is larger than for B_{0.2}, suggesting that an increasing number of defect structures increases the viscosity and, therefore, the loss modulus. The loss tangent (bottom right panel) falls below 1 upon gelation, with a substantial decrease at early times. The dependence of the loss tangent on the crosslinker ratio is very closely related to the reciprocal of storage modulus, since the loss modulus has a relatively weak dependence on the crosslinker ratio.

The left panel of figure 3.3 shows the mid-point slope P and gelation half time θ for a series of gels synthesized with crosslinker ratios in the range 0.2–0.9 mmol/mol, all with $c_a \approx 1.3$ mol l⁻¹. P increases linearly with the crosslinker ratio with θ first decreasing and

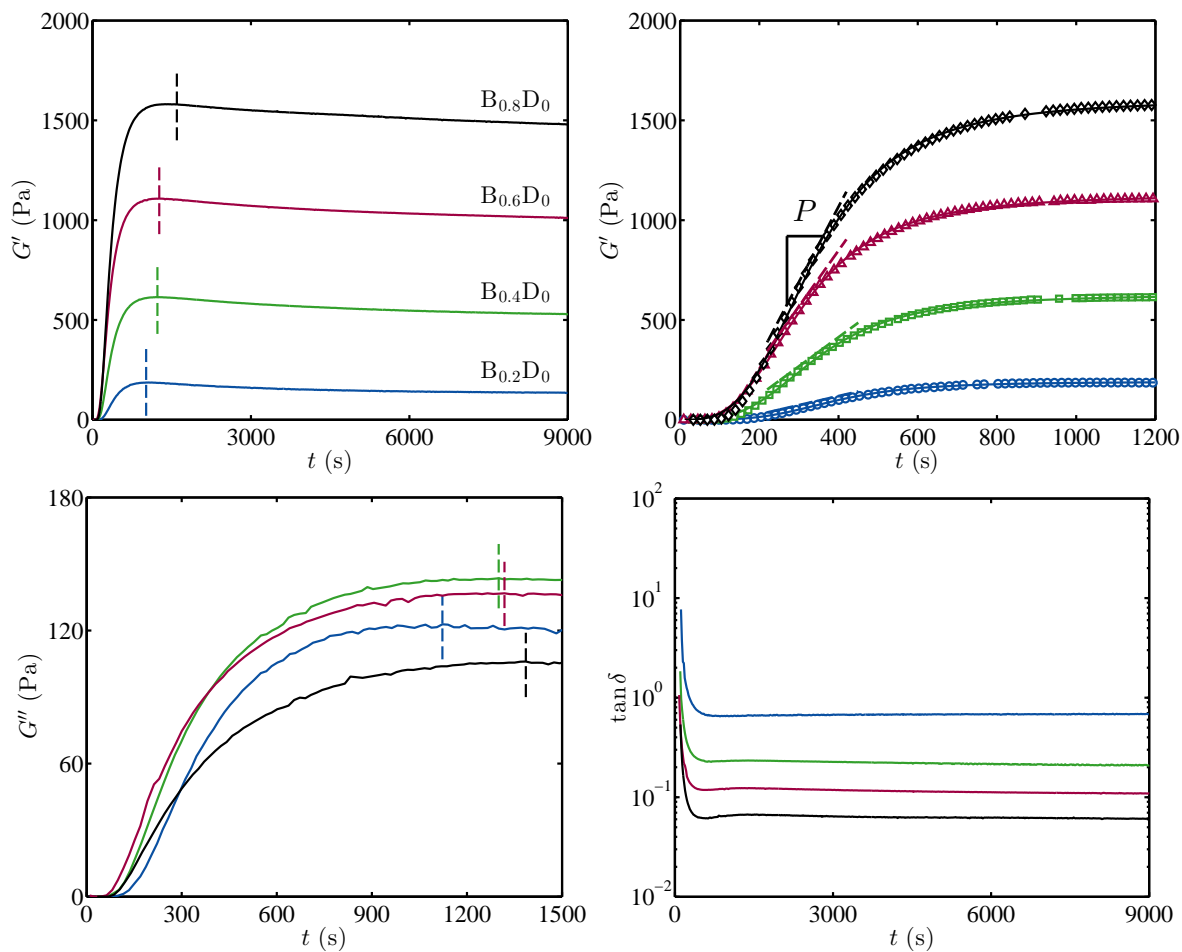


Figure 3.2: Storage modulus G' (top left), least-squares fit of Eqn. (3.5) (top right), loss modulus G'' (bottom left), and loss tangent (bottom right) for bis-crosslinked gels during gelation: $\omega = 1 \text{ rad s}^{-1}$, $T = 21^\circ\text{C}$. Disturbances from the application of silicone oil have been removed.

then increasing with increasing crosslinker ratio. However, for bis-crosslinked gels with a higher ratio c_{bis}/c_a , an increase in P corresponds to a decrease in θ ^{4,7}. An explanation for the trend in this study is that physical entanglements that do not relax at $\omega = 1 \text{ rad s}^{-1}$ contribute to the network, decreasing θ and increasing P when $c_{\text{bis}}/c_a \leq 0.8 \text{ mmol/mol}$. These entanglements may be formed by long dangling ends in the gel network and polymer chains in the solvent.

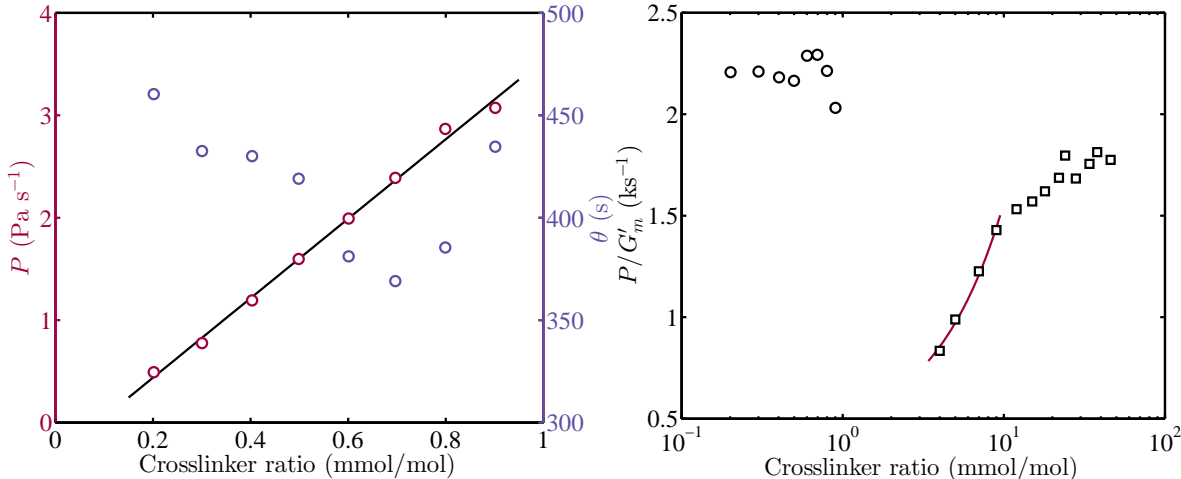


Figure 3.3: Left: The mid-point slope P (left axis) and gelation half time θ (right axis) for bis-crosslinked gels with varying crosslinker ratio: $\omega = 1 \text{ rad s}^{-1}$, $T = 21^\circ\text{C}$. Right: The network-formation rate of bis-crosslinked gels with crosslinker ratios 0.2–0.9 mmol/mol (circles, $c_a \approx 1.3 \text{ mol l}^{-1}$) at $\omega = 1 \text{ rad s}^{-1}$ and crosslinker ratios 4–46 mmol/mol (squares, $c_a \approx 0.42 \text{ mol l}^{-1}$) at $\omega = 10 \text{ rad s}^{-1}$ ⁴. The line identifies the linear region with crosslinker ratio less than 10 mmol/mol .

To further analyze the effect of entanglements on gelation, P scales with the maximum value of the storage modulus G'_m : the ratio P/G'_m , which has units of reciprocal time, furnishing a metric that we loosely refer to as a network-formation rate. As shown in the right panel of figure 3.3, this network-formation rate for bis-crosslinked gels with a higher ratio c_{bis}/c_a increases approximately linearly with the bis-crosslinker ratio. For bis-crosslinked gels with a lower ratio c_{bis}/c_a , however, the rate is practically independent of the crosslinker ratio. This confirms that entanglements may weaken the variation in P with c_{bis}/c_a , imparting a constant P/G'_m .

The storage moduli of bis-crosslinked gels with $c_a \approx 1.3 \text{ mol l}^{-1}$ at $\omega = 0.1 \text{ rad s}^{-1}$ are plotted in the left panel of figure 3.4. The plateau modulus G_N^0 of the gels should exist at lower frequencies as shown in appendix 3.E, and the values are $\approx 3\text{--}15\%$ smaller than

$G'_{0.1} \equiv G'(\omega = 0.1)$ for samples B_{0.4}–B_{0.8}. For sample B_{0.2}, G'_N is $\approx 60\%$ smaller than $G'_{0.1}$. $G'_{0.1}$ is approximately linear in the crosslinker ratio, with a weak positive quadratic contribution, which reflects a weak increase in the crosslinking efficiency. As reported by Adibnia and Hill⁴, Calvet et al.⁷, and Basu et al.⁸, the linear region for G'_N occurs at a lower ratio c_{bis}/c_a for gels with a higher monomer concentration. The results obtained here extend the $G'_{0.1}$ versus c_{bis}/c_a relationship to the lower crosslinker ratio region for $G'_{0.1}$.

Note that $G'_{0.1}$ vanishes when $c_{\text{bis}}/c_a \approx 0.127$ mmol/mol, thus identifying the percolation threshold. The crosslinking efficiency, as measured by

$$G'_{0.1}/G'_{Nideal} \times 100\% \approx 11.1c_{\text{bis}}/c_a + 15.2 - 2.1c_a/c_{\text{bis}},$$

increases from zero (at the percolation threshold) to $\approx 23\%$ when $c_{\text{bis}}/c_a \approx 0.9$ mmol/mol. Note that the affine model was adopted to calculate the plateau modulus for ideal networks. Despite the efficiency vanishing when approaching the percolation threshold, the linear contribution to $G'_{0.1}$ with respect to c_{bis}/c_a indicates that $\sim 15\%$ of the bis-acrylamide crosslinker in the pre-gel solution produces elastically active partial chains. The next section examines in more detail how the storage modulus depends on dynamic entanglements, which are particularly significant in very weakly crosslinked samples.

As shown in the right panel of figure 3.4, with the same $G'_1 \equiv G'(\omega = 1)$, $\tan \delta$ for bis-crosslinked gels with crosslinker ratios in the range 0.2–0.9 mmol/mol is larger than for gels with crosslinker ratios in the range 22–46 mmol/mol⁴. This suggests that networks with the same number of effective crosslinks have distinctly different microstructures. There are more physical entanglements in networks formed with lower crosslinker ratio. These dissipate energy with more liquid-like characteristics. On the other hand, networks formed with higher crosslinker ratio have shorter dangling ends, whereas other defects, such as crosslinker-crosslinker shortcuts, produce non-ideal networks.

3.4.2 Dynamic moduli spectra and time-temperature superposition

Loss moduli of bis-crosslinked gels with $c_a \approx 1.3$ mol l⁻¹ are plotted versus the crosslinker ratio in the top-left panel of figure 3.5. At each of the three widely separated frequencies, G'' is a relatively weak function of the crosslinker ratio. At lower frequencies, G'' exhibits a maximum that suggests a competition between an increasing concentration of defect structures (increasing dissipation) and the increasing efficiency with which crosslinkers contribute to the network elasticity (decreasing dissipation) when increasing the crosslinker ratio. At

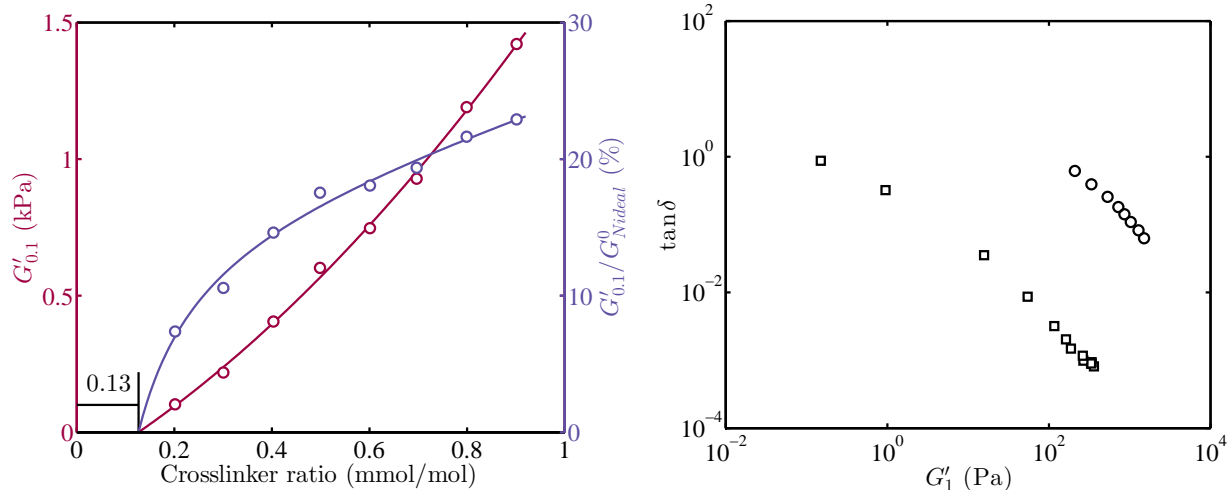


Figure 3.4: Left: G' at $\omega = 0.1 \text{ rad s}^{-1}$ (left axis) and crosslinking efficiency (right axis) at $T = 21^\circ\text{C}$ for bis-crosslinked gels with varying crosslinker ratio. Right: G' versus $\tan \delta$ at $\omega = 1 \text{ rad s}^{-1}$ for bis-crosslinked gels with crosslinker ratios 0.2–0.9 mmol/mol (circles, $c_a \approx 1.3 \text{ mol l}^{-1}$) and crosslinker ratios 4–46 mmol/mol (squares, $c_a \approx 0.42 \text{ mol l}^{-1}$)⁴.

higher frequencies, defects are more tightly coupled to the network, via entanglements and hydrodynamic interactions, so G'' decreases with increasing c_{bis}/c_a according to the strongly increasing network connectivity. The loss tangent $\tan \delta$ is plotted in the top-right panel of figure 3.5. As expected from the foregoing storage and loss moduli, this decreases significantly with increase crosslinker ratio. Qualitative characteristics of the loss-tangent spectra (bottom panel) vary with the crosslinker ratio.

Dynamic moduli for bis-crosslinked gels with $c_a \approx 1.4 \text{ mol l}^{-1}$ at various temperatures ($T = 21$ to 56°C with $\omega = 0.1$ – 100 rad s^{-1}) are shown in the panels on the right-hand-side of figure 3.6. Temperature has a very weak influence on the qualitative characteristics of these spectra. The spectra for gel with the weakest crosslinking density have no plateau, with a loss tangent that is close to one over the entire frequency range. For this sample, temperature affects the storage and loss moduli quantitatively. The spectra for gels with higher crosslinker ratio have a broader plateau and relatively smaller loss tangent.

The spectra can be organized by applying time-temperature superposition. Vertical and horizontal shifts were applied using the TTS function of the TA instruments Trios software. Master curves, with the reference temperature $T_0 = 21^\circ\text{C}$, are plotted in the left panels of figure 3.6. Note that varying the temperature imparts spatial and temporal thermal changes in the sample and rheometer. These can adversely impact the measurements, so our efforts to minimize the resulting instrumental effects are detailed in appendix 3.D.

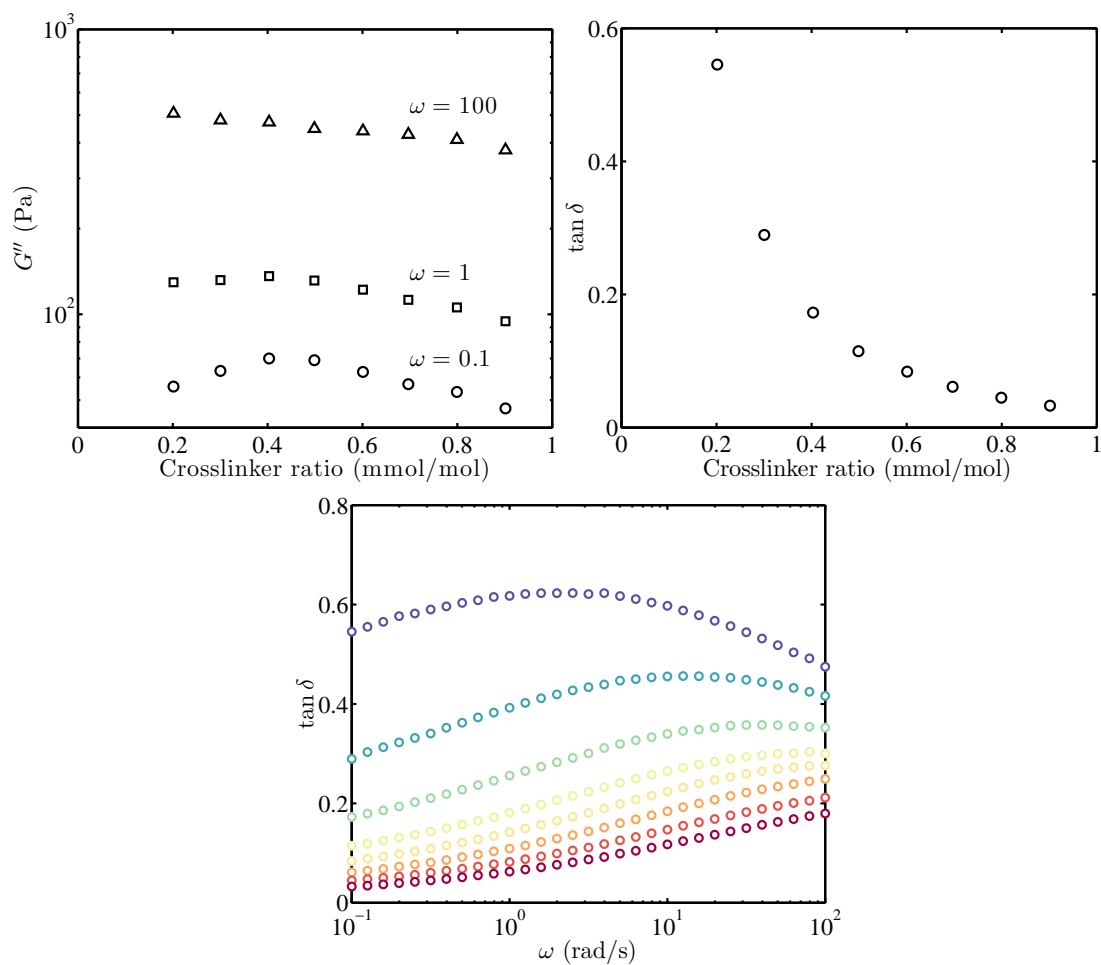


Figure 3.5: G'' at $\omega = 0.1, 10, 100$ rad s $^{-1}$ (top left) and loss tangent at $\omega = 0.1$ rad s $^{-1}$ (top right) for bis-crosslinked gels with varying crosslinker ratio at $T = 21^\circ\text{C}$. Bottom: Loss-tangent spectra for bis-crosslinked gels with varying crosslinker ratio (increasing from blue to red) at $T = 21^\circ\text{C}$.

Despite the subtle temperature dependence of the dynamic moduli, the entanglements have systematic responses to temperature. For example, there is quantitative evidence of entanglements disengaging when increasing the temperature, altering G' at higher frequencies and G'' at all frequencies.

TTS for samples B_{0.4}–B_{0.8} exhibits a rubbery plateau at low frequencies. The increase in G' with frequency identifies the role of physical entanglements. These are elastically ineffective in the plateau region, but increasingly contribute to the elasticity at higher frequencies due to their finite relaxation time. As expected from the considerations of how crosslinking efficiency varies with crosslinker ratio, the frequency dependence of the storage modulus decreases with increasing cross-linking efficiency. At the lowest crosslinking efficiency (sample B_{0.2}), there is no plateau, suggesting that the dominant contribution to the storage modulus (at the frequencies probed) is due to entanglements.

The loss modulus G'' for all samples increases as a power-law in ω . The exponent indicates shear thinning, furnishing a real-part of the complex viscosity

$$\eta' = G''/\omega \sim \omega^{-0.7}.$$

Shear thinning occurs in non-dilute polymer solutions and high-molecular weight polymer melts³, which is caused by the conformational change of polymer chains¹¹⁰. In the linear viscoelastic regime, increasing the frequency reduces the time available for the dissipative relaxation modes of network defects, so that a larger portion of the network strain must be born by non-dissipative elastic strain, i.e., chain stretching, causing shear thinning.

Loss-tangent spectra before and after TTS are shown in figure 3.7. Interestingly, $\tan \delta$ for samples B_{0.4}–B_{0.8} decreases with increasing temperature. This principally reflects the decrease in G'' with respect to temperature. Note that the changes in G'' with respect to temperature are much larger than can be expected from the temperature dependence of the solvent shear viscosity. Here, the temperature dependence of G'' reflects an increase in the relaxation rate of defect structures when increasing the temperature.

Dynamic moduli spectra for a sample B_{0.1} at $T = 21^\circ\text{C}$ are shown in figure 3.8. Here, a crossover of the storage and loss moduli emerges, below which the sample behaves as a viscoelastic liquid. The exponents at lower frequencies are ≈ 0.8 and ≈ 0.6 for G' and G'' respectively. These are smaller than for the Maxwell model because crosslinks presumably hinder polymer chain relaxation.

For the most weakly crosslinked gel B_{0.2}, $\tan \delta$ is practically temperature and frequency independent, even though the storage and loss moduli for this sample have the strongest

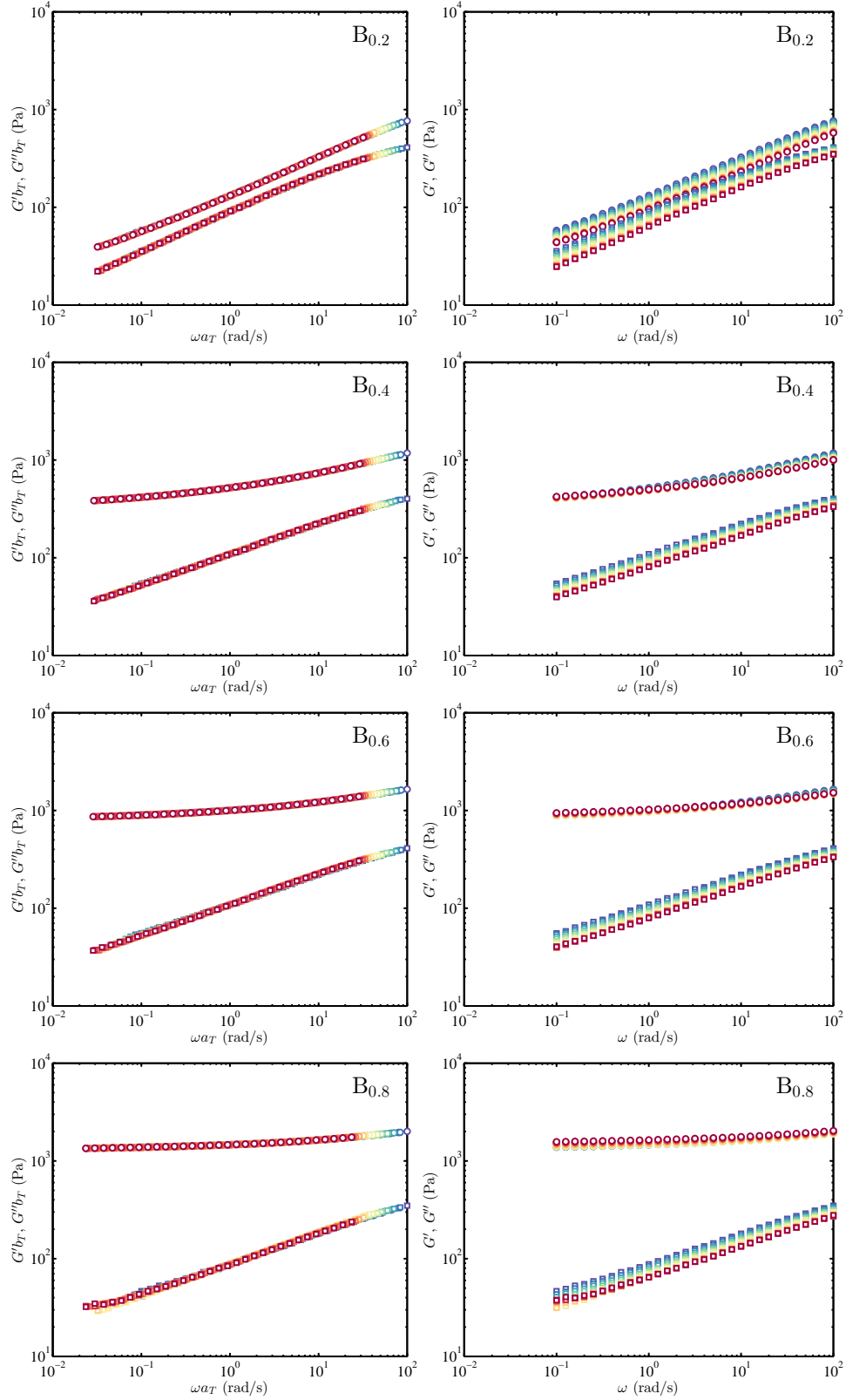


Figure 3.6: G' (circles) and G'' (squares) spectra for bis-crosslinked gels following TTS with reference temperature 21°C (temperature increases from blue to red).

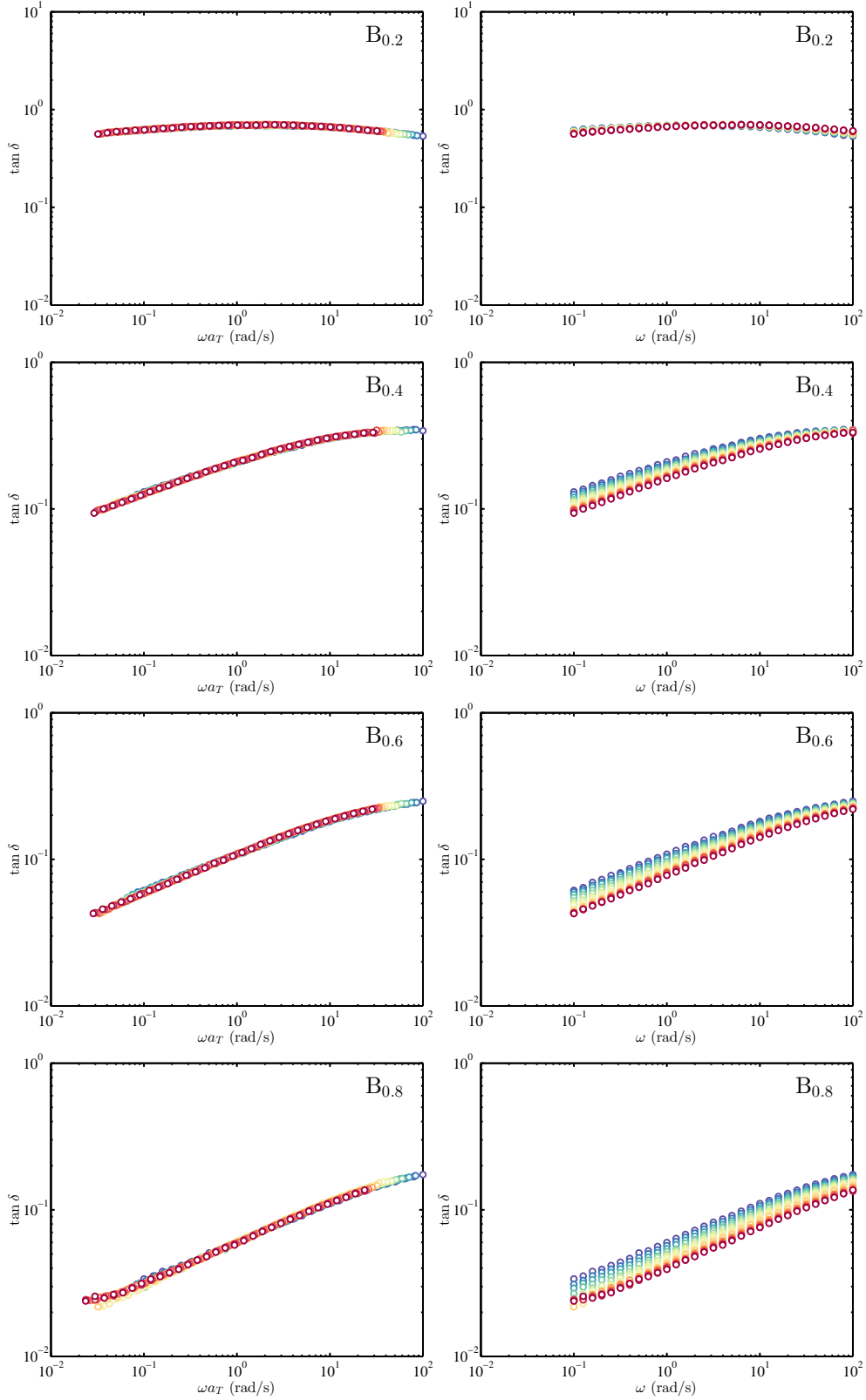


Figure 3.7: Loss-tangent spectra for bis-crosslinked gels following TTS with reference temperature 21°C (temperature increases from blue to red).

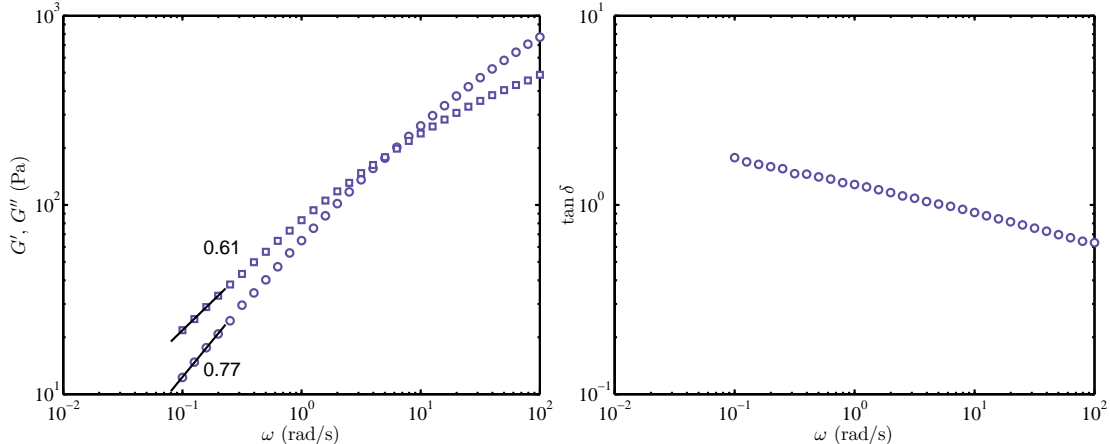


Figure 3.8: G' (circles) and G'' (squares) spectra (left), and loss-tangent spectrum (right) for sample B_{0.1}: $T = 21^\circ\text{C}$.

variations with temperature and frequency. This qualitatively distinct characteristic principally arises from the storage and loss moduli having the hallmark of a critical gel: the storage and loss moduli having the same power-law frequency dependence^{69,111,112}

$$G' \sim G'' \sim \omega^\Delta.$$

Critical gels have been predicted by theory, and demonstrated experimentally, to have a scaling exponent $\Delta = 2/3 - 1$ (theoretical)⁷³ and $\Delta = 0.46 - 0.8$ (experimental)^{69,112,113}.

As shown in figure 3.9, a master curve can be constructed by shifting the dynamic moduli spectra with crosslinker ratios 0.2–0.9 mmol/mol. The so-called time-concentration superposition works well for $c_{\text{bis}}/c_a = 0.4 - 0.9$ mmol/mol gels, whereas spectra for gels with a lower crosslinker ratio cannot be superposed. The horizontal and vertical shift factors do not exhibit a power-law correlation above the critical gel concentration. Moreover, the exponent $\Delta \approx 0.38$, suggesting that bis-crosslinked gels with low crosslinker ratio do not exhibit the universal sol-gel transition identified in earlier studies. This may be because the smaller ratio c_{bis}/c_a imparts more entanglements, causing $\tan \delta$ to be smaller than the theoretical value¹¹¹ (≈ 1.96). Also, sample B_{0.2} has a crosslinker ratio that is somewhat higher than the critical value ≈ 0.13 inferred from figure 3.4. Spectra for the gel with a crosslinker ratio ≈ 0.13 may exhibit larger exponents in G' and G'' .

3.4.3 Activation energy and scaled effective crosslink number

As shown in the left panel of figure 3.10, the temperature dependence of the horizontal shift factors a_T for each sample can be well described by the WLF equation Eqn. (3.4). The

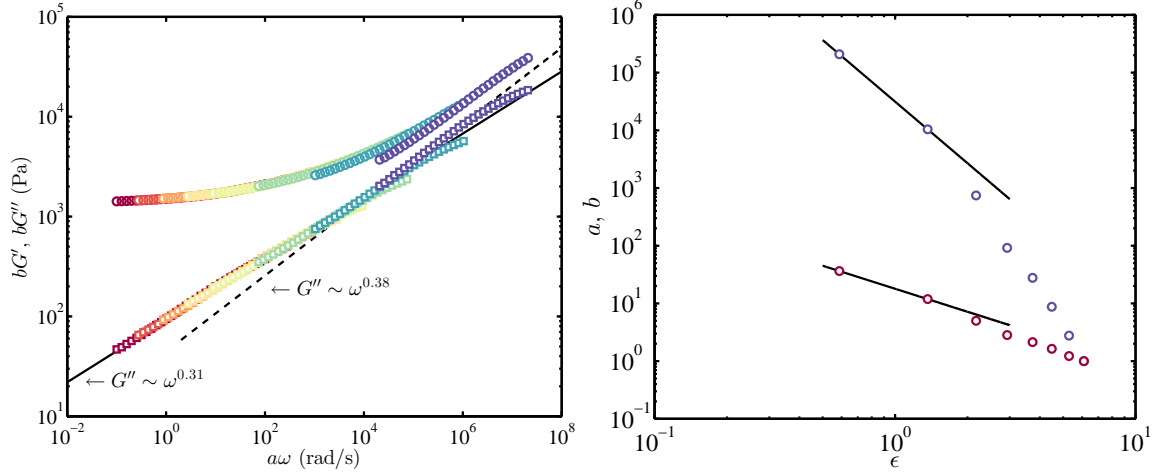


Figure 3.9: Left: Time-concentration superposition of G' (circles) and G'' (squares) for bis-crosslinked gels with crosslinker ratios 0.2–0.9 mmol/mol, referenced to sample B_{0.9}. Right: The horizontal and vertical shift factors are plotted versus $\epsilon = (c_{\text{bis}} - c_c)/c_c$ with the critical bis-acrylamide concentration at the gel point $c_c/c_a = 0.127$. Lines are power-laws (to guide the eye) with exponents -3.5 and -1.3 for a and b .

physical entanglement underlying this temperature dependence of the relaxation times is reminiscent of the relaxation in polymer melts at temperatures in the range $T_g - T_g + 100$ K, and in concentrated polymer solutions. The reference temperature obtained from the fitting is $T_0 \approx 294.15$ K with $C_1 \approx 1.15, 1.12, 1.11, 1.30$, and $C_2 \approx 45.4, 37.7, 35.2, 34.9$ K for samples B_{0.2}–B_{0.8}.

The temperature-dependent apparent activation energy according to Shangguan et al.¹¹⁴

$$E_a = 2.303RC_1C_2 \frac{T^2}{(C_2 + T - T_0)^2}, \quad (3.7)$$

where the parameters C_1 , C_2 and T_0 are from the WLF fitting above, is plotted (lines) in the right panel of figure 3.10. Note that the symbols in this panel are according to local Arrhenius fits to neighbouring triplets of data points in the left panel. It is shown that the activation energy varies between ≈ 15 and 60 kJ mol⁻¹ (6.1 – 25 $k_B T$). We interpret this energy as the potential barrier required to disengage entanglements.

For physical crosslinks, such as micelles formed by hydrophobic chains, $E_a \approx 25$ – 58 $k_B T$, and for ionic bonds, $E_a \approx 29$ – 124 $k_B T$ ^{115,53}. For terminal relaxation in polymer melts, $E_a \approx 2$ – 20 $k_B T$ ^{116,117,114}. The apparent activation energy for the entanglements in our chemically crosslinked gels at lower temperature is therefore comparable to the maximum for entangled polymer networks. This can be attributed to (i) network hindrance, which

is consistent with E_a increasing with the crosslinker ratio, and (ii) the weaker temperature dependence of E_a when closer to the percolation threshold.

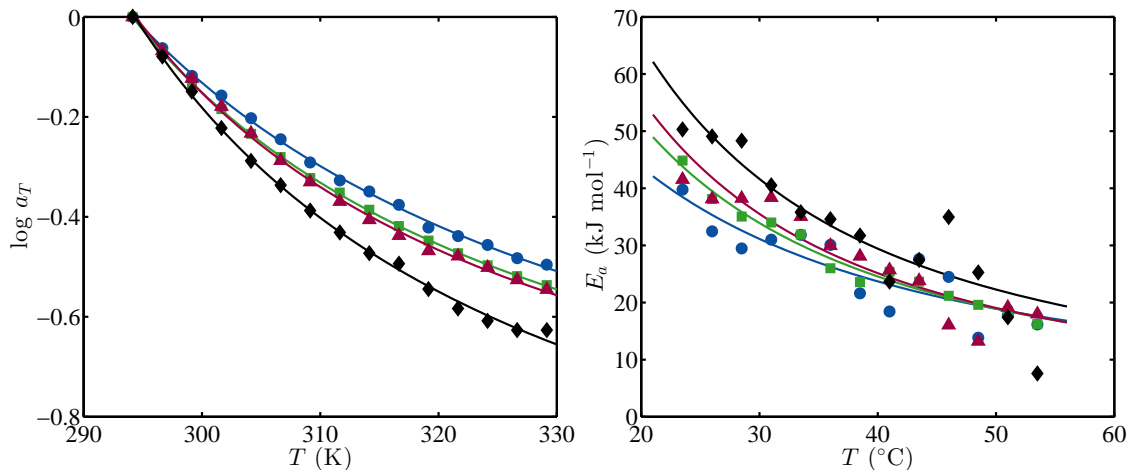


Figure 3.10: Horizontal shift factors a_T (with WLF fits, left) and temperature-dependent apparent activation energy (lines are Eqn. (3.7) and symbols are calculated from local Arrhenius fits to data triplets in the left panel, right) for bis-crosslinked gels: B_{0.2} (circles), B_{0.4} (squares), B_{0.6} (triangles), B_{0.8} (diamonds).

According to Eqn. (3.2), the number of effective crosslinks are obtained from the vertical shift factor b_T via

$$\frac{N}{N_0} = \frac{T_0 V}{b_T T V_0}, \quad (3.8)$$

where N and V are the number of effective crosslinks and gel volume (estimated from the linear expansion of water) at each temperature, and N_0 and V_0 are the number of crosslinks and gel volume at the reference temperature T_0 . As shown in figure 3.11, $N \approx N_0$, suggesting that changes in temperature do not significantly influence the number of effective crosslinks in bis-crosslinked gels.

3.4.4 Creep and recovery in the linear viscoelastic regime

At the beginning of creeps tests, the compliance fluctuated for ≈ 1 s due to the coupling of instrument inertia to sample elasticity¹¹⁸. This “inertio-elastic” regime was removed from the reported creep data. For samples B_{0.2}–B_{0.8}, an initial, practically instantaneous increase in the compliance is followed by $J(t)$ approaching a constant. The creep compliance can be fitted with the Burgers model in which a Maxwell element is connected in series with a

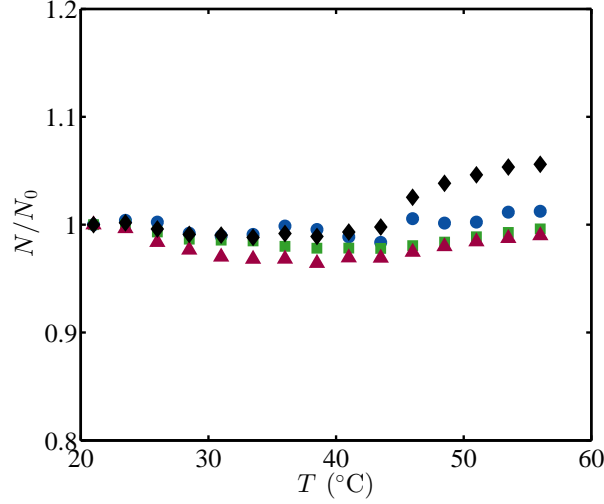


Figure 3.11: Scaled effective crosslink number versus temperature according to the vertical shift factor b_T for bis-crosslinked gels: B_{0.2} (circles), B_{0.4} (squares), B_{0.6} (triangles), B_{0.8} (diamonds).

Kelvin-Voigt element:

$$J(t) = J_0 + t/\eta_M + (1 - e^{-t/\tau})/G_K, \quad (3.9)$$

where $J_0 = 1/G_M$ is the instantaneous compliance, the second term is the irrecoverable compliance, and the third term is the retarded elastic compliance with $\tau = \eta_K/G_K$. G_M and η_M are the modulus and viscosity of the Maxwell spring and dashpot, and G_K and η_K are their counterparts for the Kelvin-Voigt spring and dashpot.

As shown in table 3.2, G_M increases with the crosslinker ratio in the same manner as the plateau modulus G_N^0 . The retardation time τ is related to the relaxation of partial chains⁷⁹. This decreases with increasing crosslinker ratio due to the shorter partial-chains in stiffer gels having shorter relaxation times. J_0/J_{tot} is reported in table 3.2 as a ratio of the instantaneous compliance to the total compliance applied to the sample during the creep.

After removing the stress at $t = t_0$, most of the compliance is recovered immediately, as expected for elastic solids. The recovery can be modelled with the Weibull function^{77,119}

$$J(t) = J_\infty + J_{de}e^{-[(t-t_0)/\eta_r]^{\alpha_r}}, \quad (3.10)$$

where J_∞ is the irrecoverable compliance, J_{de} is the delayed elastic compliance, η_r is the scale parameter, and α_r is the shape parameter. The percentage of the irrecoverable compliance J_∞/J_{tot} decreases with increasing c_{bis}/c_a . For samples B_{0.4}–B_{0.8}, the compliance is fully recovered. For sample B_{0.1}, however, $J(t)$ during the creep continues to increase with most

of the compliance being unrecoverable. These are expected from the crossover that exits in the dynamic moduli for this sample (figure 3.8).

Table 3.2: Best-fit parameters of the Burgers model and Weibull function at 21°C.

Sample	G_M (kPa)	η_M (kPa s)	G_K (kPa)	η_K (kPa s)	τ (s)	J_0/J_{tot} (%)	J_∞/J_{tot} (%)
B _{0.1}	0.069	0.54	0.018	0.47	25.9	3.27	66.7
B _{0.2}	0.14	12.2	0.074	1.24	16.9	19.4	8.90
B _{0.4}	0.50	549	1.62	11.8	7.27	68.4	0.44
B _{0.6}	0.94	2510	6.87	42.4	6.17	83.4	0.96
B _{0.8}	1.47	8000	23.2	137	5.90	91.4	-0.72

3.5 Conclusions

A rheological study of bis-crosslinked polyacrylamide hydrogels in the linear viscoelastic regime was undertaken. Unlike similar studies of polyacrylamide hydrogels in the literature, the gels synthesized here have an unusually low crosslinker ratio. When approaching the percolation threshold, these gels have many features, including a broad spectrum of relaxation times. This motivates the time-temperature and time-concentration superposition analyses undertaken, both of which provide new insights into the microstructures.

Gelation kinetics reveal rapid increases in the storage and loss moduli with time, with the loss tangent decreasing monotonically. The steady-state loss tangents are approximately several orders of magnitude higher than for polyacrylamide gels in the literature with lower monomer concentration and higher crosslinker ratio. The formation rate of elastically effective-crosslinks increases with crosslinker ratio, with the plateau modulus being weakly quadratic (superlinear) in the crosslinker ratio. The network-formation rate is approximately independent of the crosslinker ratio, suggesting that physical entanglements significantly contribute to the storage modulus during gelation.

Time-concentration superposition of spectra above the apparent percolation threshold furnished a master plot of the dynamic moduli in which the storage modulus has a low-frequency plateau and a high-frequency power law with exponent ~ 0.38 . The loss modulus is a single power law with an exponent equal to that for the high-frequency storage modulus, with no crossover.

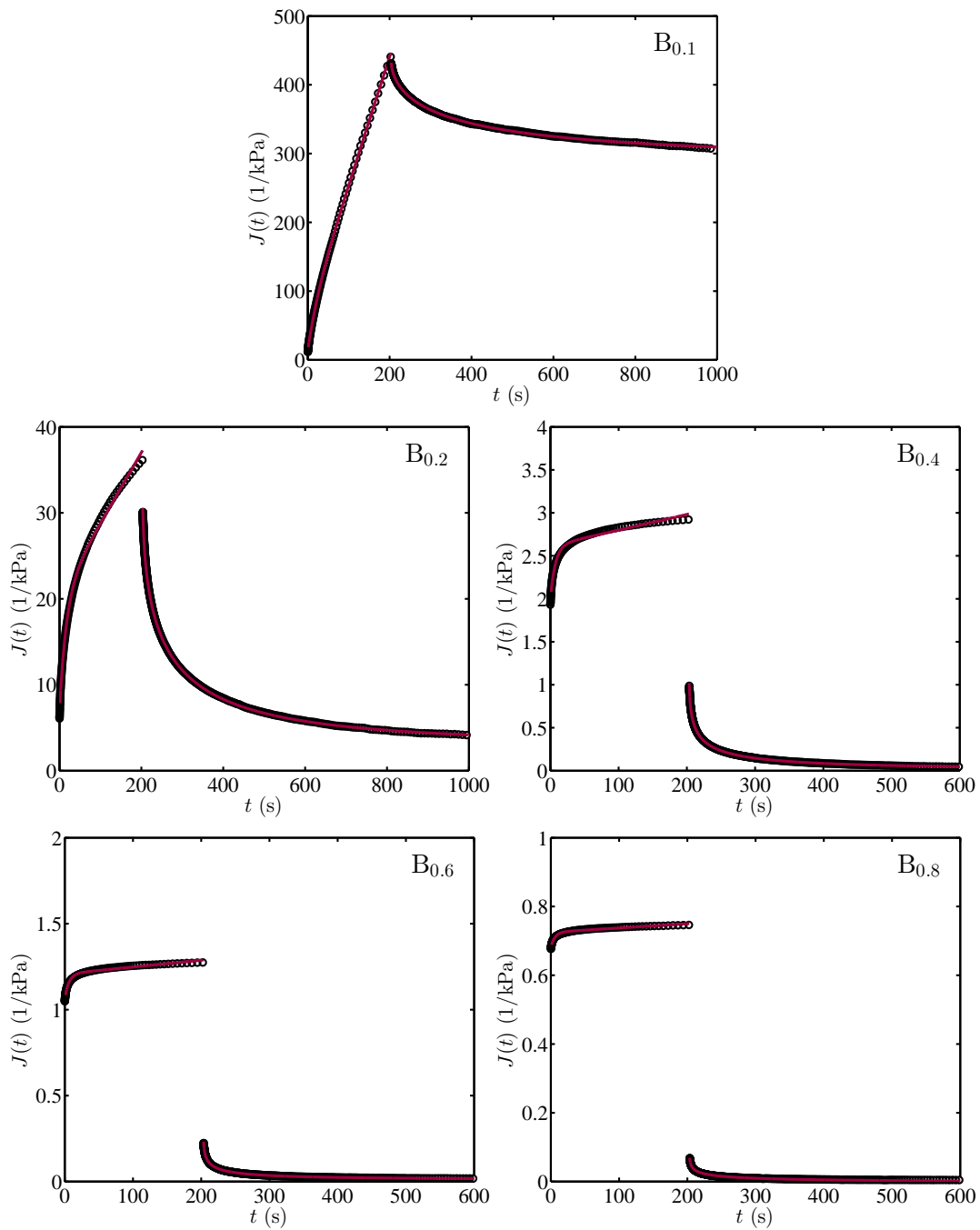


Figure 3.12: Creep-recovery for bis-crosslinked gels: $T = 21^\circ\text{C}$.

Horizontal shift factors from time-temperature superposition furnished the apparent activation energy for disentanglement. The average value is comparable to literature reports for polymer melts at temperatures well above T_g . This suggests that the permanent bis-crosslinks hinder entanglement release. The effective crosslink number, which is ascertained from the vertical shift factors, was found to be practically independent of the temperature. Creep-recovery tests reaffirm that the gels are viscoelastic solids at crosslinker ratios above the critical percolation threshold value, although the gels in this study have very low crosslinker ratios.

Appendix

3.A Detailed protocols for bis-crosslinked hydrogel synthesis and rheology

Bis-crosslinked hydrogel synthesis

1. Using disposable transfer pipettes, take about 2 ml of 40% w/v acrylamide and 2 ml of 2% w/v bis-acrylamide stock solutions stored at 4°C . Wait \approx 40 min for the solutions to reach room temperature.
2. Prepare the rheometer according to the instrument manual.
3. Prepare 800 μ l of 0.25% w/v bis-acrylamide solution by mixing 100 μ l of 2% w/v bis-acrylamide solution and 700 μ l of RO water. Vortex mix the solutions for 10 s.
4. Add appropriate volumes of DNA suspension buffer (see table 3.A.1) to a centrifuge tube.
5. Add 72.4 μ l of 40% w/v acrylamide and appropriate volumes of 0.25% w/v bis-acrylamide solution (see table 3.A.1) to the centrifuge tube.
6. Cover the centrifuge tube with masking tape to reduce evaporation during degassing. Insert a 100 μ l pipette tip attached to a nitrogen gas cylinder to the mixture and bubble nitrogen through the mixture (at 0.4 SFPH) for 5 min to remove dissolved oxygen. The remaining solution has a volume \approx 280 μ l.
7. Weigh 0.05 g APS powder in a glass vial and add 500 μ l of RO water to form a 10% APS solution. Vortex mix the solution for 20 s.
8. Add 2.8 μ l of the 10% APS solution to the tube and blend the mixture with the pipette tip 30 times.

9. Add 1 μl of TEMED to the tube and blend the mixture with a 1000 μl pipette tip 10 times. Deposit 270 μl of the mixture onto the bottom plate of the parallel-plate sample holder. Note that an extra 10% mixture volume is required to ensure the correct filling of the mixture between the parallel plates.
10. Apply a 2 rad/s angular velocity to the bottom plate to achieve even spreading of the pre-gel solution and remove bubbles. Lower the top plate to achieve a 0.5 mm gap with the “evaporation blocker”.
11. Measure gelation kinetics by subjecting the sample to a prescribed oscillatory strain. After ≈ 860 s, apply silicone oil to the sample edges using a disposable transfer pipette.

Rheology protocols

1. Gelation kinetics: The temperature during gelation was set to 21°C. A *conditioning options step* that maintains a constant axial force of 0 N during gelation with a sensitivity of 0.01 N was set before an *oscillation time step*. This step can make the upper plate adjust itself to avoid compression or tension on the sample during its transition from a liquid to solid. This decreases the number of G' and G'' data points acquired during gelation, because the adjustment requires additional time. During the *oscillation time step*, the angular frequency was set to $\omega = 1 \text{ rad s}^{-1}$ with strain amplitude $\gamma = 1\%$ to achieve a linear viscoelastic response. Measurements were terminated when dynamic moduli settled to steady values (≈ 9000 s).
2. Time-temperature superposition: A *conditioning options step* that maintains a constant axial force of 0 N during TTS was set before a *oscillation temperature sweep step*. In future, an average expansion coefficient ($\mu\text{m}/^\circ\text{C}$) that is the sum of the geometry thermal expansion coefficient and the linear thermal expansion coefficient of water can be set without checking the *Move stage to maintain starting gap* box. In this case, the actual gap thickness can be adopted to calculate results. During the *oscillation temperature sweep step*, the soak time was set to 600 s for the gel equilibrium at each temperature. Frequency sweeps were performed in the range $\omega = 0.1\text{--}100 \text{ rad s}^{-1}$ with $\gamma = 1\%$. Temperatures from 21 to 56°C were used with the temperature step 2.5°C.
3. Post time-temperature superposition: The temperature was reduced to 21°C with a 1200 s soak time to achieve thermal equilibrium. A frequency sweep $\omega = 0.1\text{--}100 \text{ rad s}^{-1}$ with $\gamma = 1\%$ was performed afterwards. A *conditioning options step* that

maintains a constant axial force of 0 N during the temperature reduction was set before the step.

4. Creep-recovery test: 60 s equilibrium time with a *locked* motor state was set during *conditioning transducer step* to ensure complete stress relaxation. The *transducer zeroing* box should be checked and the *transducer zero time* was set to *med range*. The *conditioning stress control step* was followed so the motor displacement achieves the desired stress. A *step (transient) creep step* was set afterward with the *duration time* for the creep test selected to be 200 s with a small stress in the linear viscoelastic regime. A *step (transient) creep step* without stress was then set for the sample recovery.

Table 3.A.1: Solution volumes for bis-crosslinked gel synthesis.

Sample	40% w/v acrylamide (μl)	0.25% w/v bis-acrylamide (μl)	Buffer (μl)
B _{0.1}	72.4	2.50	215.1
B _{0.2}	72.4	5.02	212.58
B _{0.4}	72.4	10.0	207.6
B _{0.6}	72.4	15.0	202.6
B _{0.7}	72.4	17.6	200.0
B _{0.8}	72.4	20.0	197.6

3.B Bis-crosslinked gels with higher crosslinker ratio

Figure 3.B.1 shows the rheological time series during the gelation of a bis-crosslinked gel with a commercially available mass ratio 19:1 (crosslinker ratio ≈ 24 mmol/mol). These dynamics are qualitatively different from the gels studied in the main text, which have much smaller crosslinker ratios. Here, G' and G'' increase monotonically with time due to the relatively small contribution of entanglements to the network. Consequently, the storage modulus is constant over the entire frequency range ($G_N^0 \approx 200$ Pa) and the loss tangent is much smaller than for gels having smaller crosslinker ratios. Despite these gels being elastic solids, the crosslinking efficiency at this low monomer concentrations can be very low due to clusters that are rich in bis-acrylamide^{4,31,103} and the low probability of bis-acrylamide linking to polymer chains⁸.

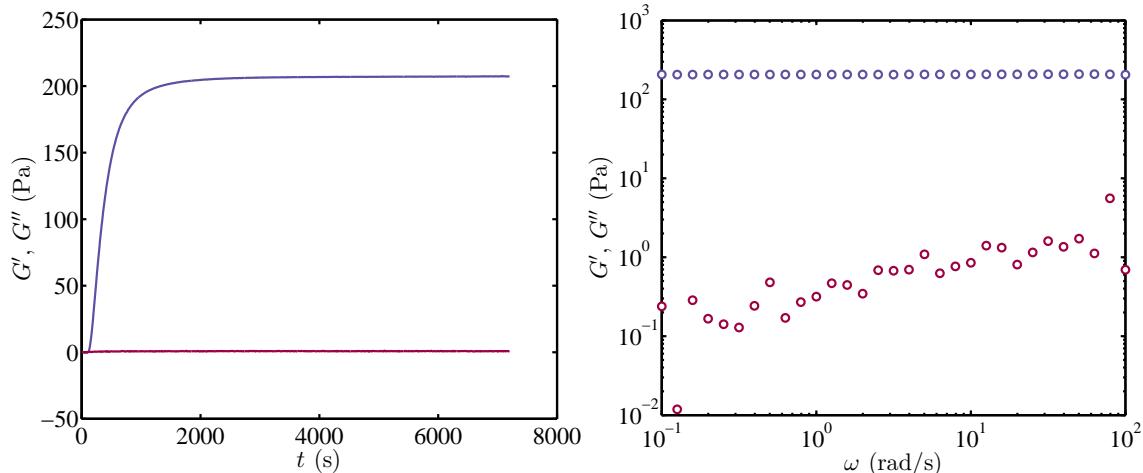


Figure 3.B.1: G' (violet) and G'' (red) during gelation at $\omega = 1 \text{ rad s}^{-1}$ (left) and G' and G'' spectra (right) for a bis-crosslinked gel: monomer concentration $\approx 3\%$ w/v; crosslinker ratio $\approx 24 \text{ mmol/mol}$ at 21°C .

3.C Sensitivity of rheological measurements to instrument setup

Experimental conditions during gel synthesis and rheological testing were found to affect dynamic spectra. For example, a larger nitrogen flow rate used for pre-gel solution degassing increased the moduli, as shown in the left panel of figure 3.C.1. When the flow rate is low, oxygen dissolved in the pre-gel solution cannot be completely removed. However, increasing the flow rate also increases evaporation of water in the pre-gel solution, concentrating the solution and, therefore, increasing the moduli. To minimize these effects, the flow rate was set to 0.4 SFPH.

The right panel of figure 3.C.1 shows that the axial force applied to gels during testing also influences the dynamic moduli spectra. With an increase in the compression force, G' and G'' of $B_{0.4}$ increase at high frequencies. Note, however, that G' and G'' are independent of the compressive force at lower frequencies.

The gap thickness for rheological tests is recommended by the instrument manufacturer (TA instruments) to be set between 0.5 and 2 mm. A smaller gap may impart an uneven gaps or shear heating that could cause a temperature rise.

As shown in the left panel of figure 3.C.2, unlike what is shown in the main text, dynamic moduli during gelation without the “evaporation blocker” and silicone oil first decrease and then increases with time. This shows that the evaporation causes the moduli to increase.

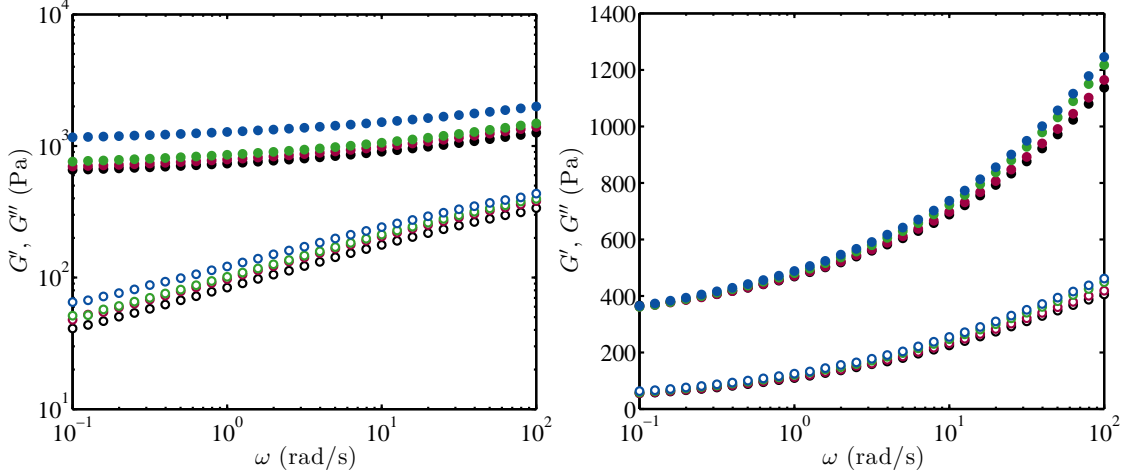


Figure 3.C.1: Left: G' (filled) and G'' (open) for $B_{0.7}$ formed with increasing nitrogen flow rate (from bottom to top) at $T = 21^\circ\text{C}$. Right: G' and G'' (linear-log) of $B_{0.4}$ under different axial forces (-2, 0, 2, 4 N from bottom to top) at $T = 21^\circ\text{C}$.

According to Eqn. (2.4), $\sigma_0 \sim R^{-3}$ and $G' \sim \sigma_0$, so $G'_m = G'_a(R_a/R_m)^3$ (G'_m : measured storage modulus; G'_a : actual storage modulus; R_m : measured plate radius; R_a : actual plate radius that is smaller than R_m because of under-filling due to evaporation). On the other hand, gel shrinkage increases the stiffness, giving $G'_a = G'_{a_0}(R_m/R_a)$ (G'_{a_0} : actual storage modulus before evaporation). Thus, $G'_m = G'_{a_0}(R_a/R_m)^2$, indicating a decrease in the measured G' , which is opposite to the observed increase in G' with time. This shows that another influence increases G' . This may arise from the extra torque imposed on the sample due to surface tension between the viscoelastic gel (loss tangent is 0.3) and the geometry¹²⁰.

Using RO water instead of DNA suspension buffer slows gelation, as shown in the right panel of figure 3.C.2, but increases the effective crosslink density arising from the same amount of bis-acrylamide. This is because TEMED (pH = 8.0–8.5) is more efficient in the buffer with pH = 8.0, which decreases the average polymer chain length and gel elasticity.

The repeatability of gel formation was examined after fixing all experimental parameters to assess the precision of the synthesis and measurement. 15 samples were run at different times. The top-right panel of figure 3.C.3 shows G' of these samples. Due to the different sample intervals, G' , G'' , and $\tan \delta$ (from 5 samples) are used to plot error bars (identifying the population range) during gelation. The errors mainly arise from random errors in pipette measurements and rheometer measurements.

Uncertainties in pipetting volumes for the pre-gel preparation propagate to the bis-acrylamide and acrylamide concentrations, effective crosslink density, and the elastic mod-

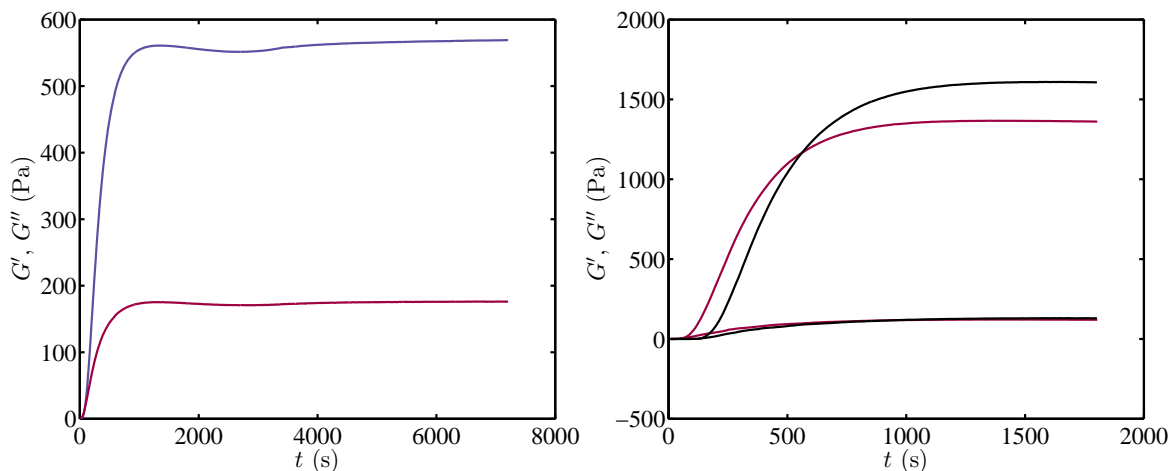


Figure 3.C.2: Left: G' (violet) and G'' (red) during gelation without the evaporation blocker (silicone oil was applied to the sample perimeter at 3500 s): $\omega = 1 \text{ rad s}^{-1}$, $T = 21^\circ\text{C}$. Right: Comparison of gelation kinetics when using RO water (black) and DNA suspension buffer (red) to form pre-gel solutions: $\omega = 1 \text{ rad s}^{-1}$, $T = 21^\circ\text{C}$.

ulus. If we assume the effective crosslink density varies with the monomer/acrylamide concentration with scaling $c_a^{3.34}$, and is linear in the crosslinker/bis-acrylamide concentration, then the uncertainty (standard deviation) in G' due to these errors is estimated to be 3.4%. These are comparable to the total uncertainties shown in figure 3.C.3, which are 4.7%.

Table 3.C.1: Error propagation analysis for pre-gel solution preparation.

Pipetting	Uncertainty (standard deviation)
200 μl buffer	0.45%
72 μl 40% w/v acrylamide	0.85%
100 μl 2% w/v bis-acrylamide	0.83%
700 μl RO water	0.22%
17 μl 0.25% w/v bis-acrylamide	0.73%

If Q is affected by a , b , and c as $Q = a^n b \cdots c$

$$\delta Q/Q = \pm \sqrt{n^2(\delta a/a)^2 + (\delta b/b)^2 + \cdots + (\delta c/c)^2}$$

There are also systematic errors in experimental procedures to consider. For example, pre-gel solution degassing increases the acrylamide and bis-acrylamide concentrations by $\approx 3\%$. An average gap compensation factor was adopted for TTS of DNA- and dual-crosslinked gels in chapter 4. This introduces errors because this factor is actually temperature dependent. Since only one sample for each bis-crosslinked gel was used for TTS, systematic instrumental

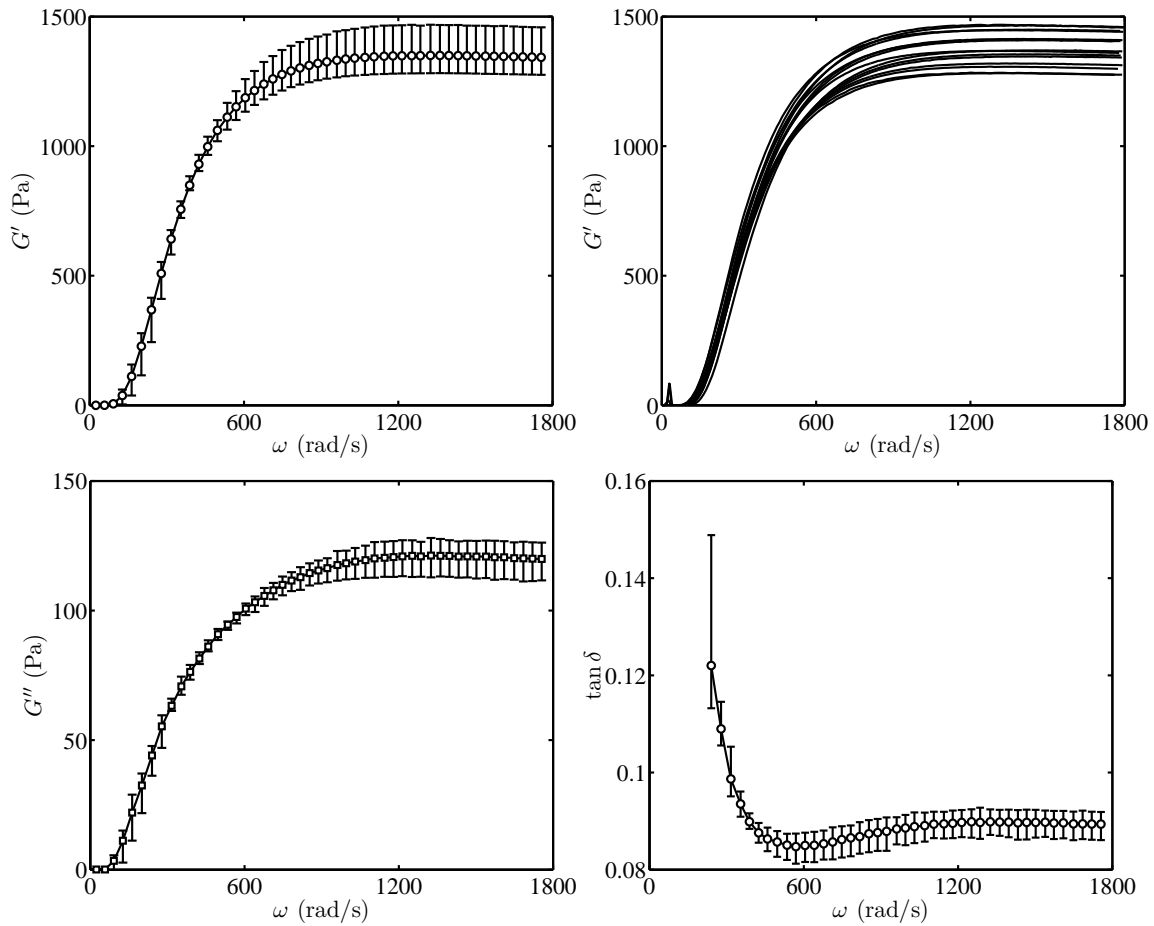


Figure 3.C.3: Analysis of errors in the dynamic moduli and loss-tangent (data from 5 samples) spectra for bis-crosslinked acrylamide hydrogels with composition the same as for sample B_{0.7}. G' from 15 samples are shown in the top-right panel. Error bars identify the maximum and minimum values.

errors due to changing temperature may be present. These are examined in more detail below.

3.D Gap-compensation factor

The stainless steel sample holder in the rheometer undergoes thermal expansion in response to the temperature changes required for TTS. This changes the gap thickness with respect to the value that the instrument expects based on isothermal operation. To minimize such errors, calibration should be undertaken to ascertain gap-compensation factors at each temperature used for TTS measurements.

The factors vary slightly with the applied axial force, and with the time allowed to reach thermal equilibrium at each temperature. As shown in figure 3.D.1, with an axial force of 0 N, the gap-compensation factor is $2.75 \mu\text{m}/^\circ\text{C}$, whereas an axial force of 0.75 N furnishes $2.66 \mu\text{m}/^\circ\text{C}$, so the difference due to the axial force is very small.

When the instrumental thermal settling time is set to 600 s, as used for all the subsequent TTS measurements in the study, the gap-compensation factor is somewhat larger than the value when a shorter settling time of 900 s is adopted. This is because when the temperature is set to increase, it rises to a higher value than the set one, so the longer time allows the expansion reach equilibrium. Furthermore, when the temperature is low, *e.g.*, 23.5°C , the compensation factor is smaller than the average value. The axial force and equilibrium time adopted in the calibration and actual experiments should be kept the same.

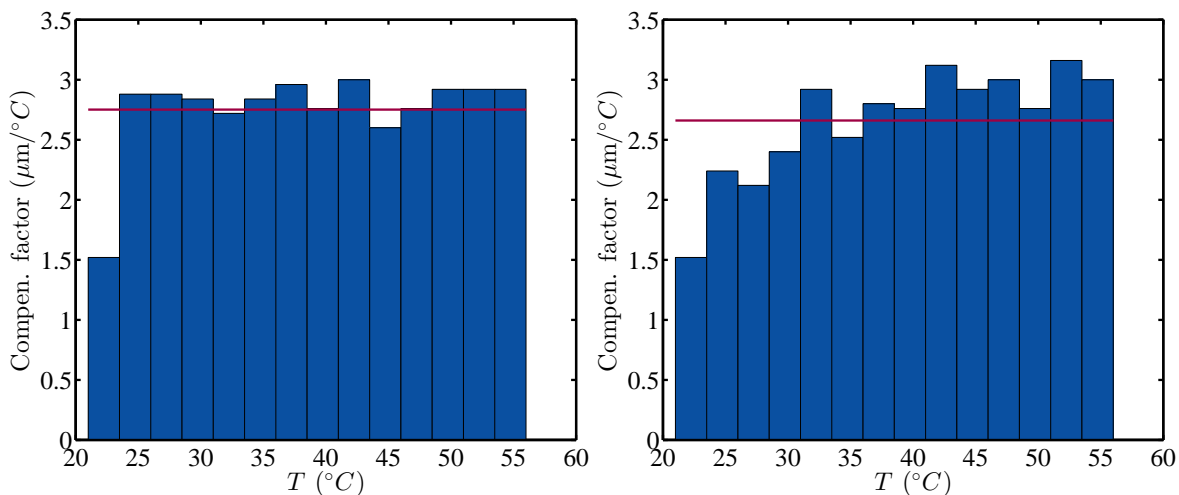


Figure 3.D.1: Gap-compensation factor with a normal/axial force 0 N (left) and 0.75 N (right). Red lines are the average.

Two methods can be used to eliminate the geometry-expansion artifact:

- Constant axial force: maintaining a constant axial force during temperature changes causes the rheometer head to rise in response to thermal expansion. In this case, no thermally induced compressional force is applied to the gel. The actual gaps must be corrected by subtracting thickness increment in each temperature range obtained in calibration from the apparent gaps.
- Constant gap: applying a prescribed gap-compensation factor following temperature changes causes the rheometer head to move to maintain a constant, prescribed gap thickness. Here, an averaged (temperature independent) gap-compensation factor was adopted.

For bis-crosslinked gels, the first method was used. Figure 3.D.2 shows the actual gap thickness for bis-crosslinked gels with various crosslinker ratios. Red squares are the gel thickness when only the linear expansion coefficient of water is used to account for the sample expansion, which are smaller than the actual thickness calculated by the first method (black circles).

The difference between the two methods is examined in figure 3.D.3 by comparison of the apparent activation energy and scaled effective number density of partial chains. Results with a constant gap-compensation factor are noisier than with a constant force, but the systematic variations with respect to temperature are consistent.

As shown in figure 3.D.4, if the compensation for thermal expansion of the sample holder is not applied, unlike the gap thickness obtained after calibration (black circles) that keeps constant, the gap thickness of bis-crosslinked gels obtained from the rheometer head position (black triangles) increases with temperature. This is because bis-crosslinked gels are more elastic, so the expansion of the top plate generates a compressional force. The resilience of the gel raises the top plate. DNA-crosslinked gels that will be mentioned in chapter 4 (red triangles) are more like viscous liquids, especially at higher temperatures, the measured gap thickness does not change, showing that the gel is pushed to the edge of the top plate. Note that G' of these gels are similar (≈ 800 Pa).

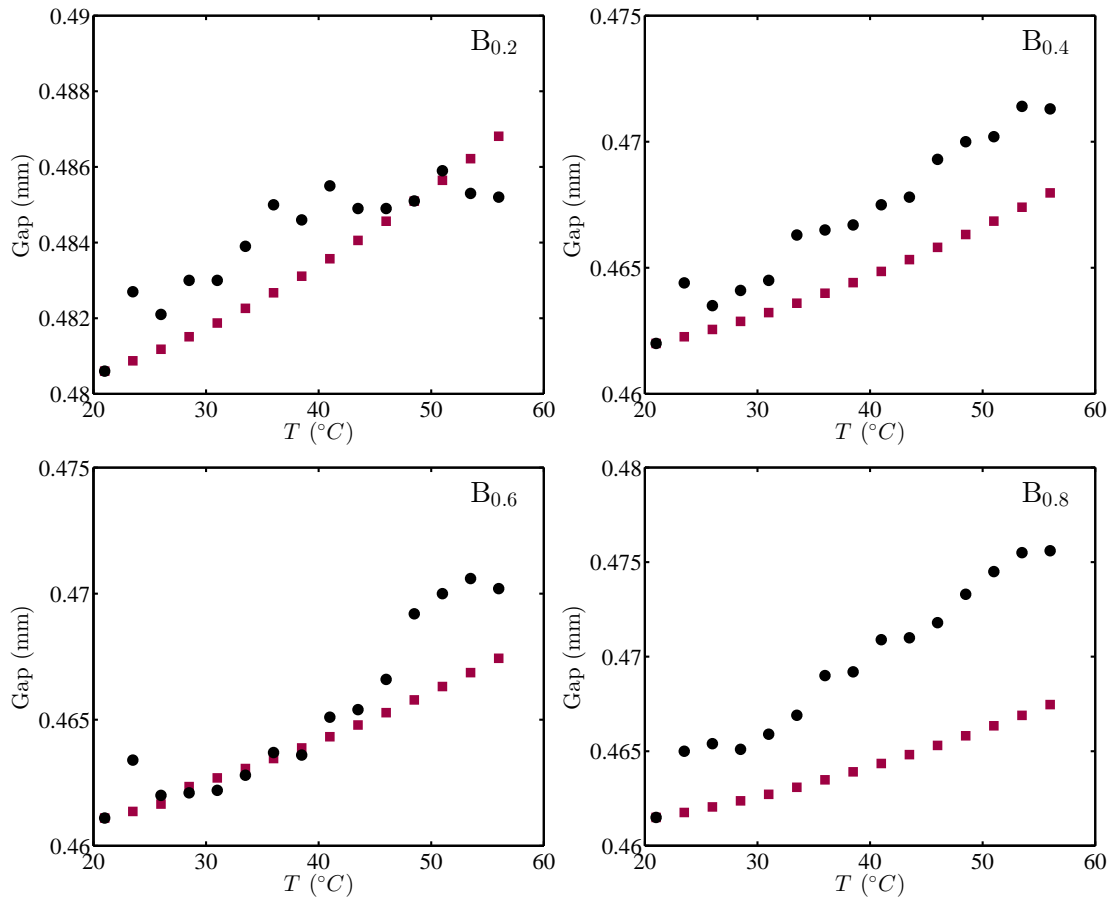


Figure 3.D.2: Comparison of gaps obtained by subtracting thickness increment in each temperature range obtained in calibration from the apparent gaps under a constant force (circles) and gaps calculated according to the thermal expansion of water (squares).

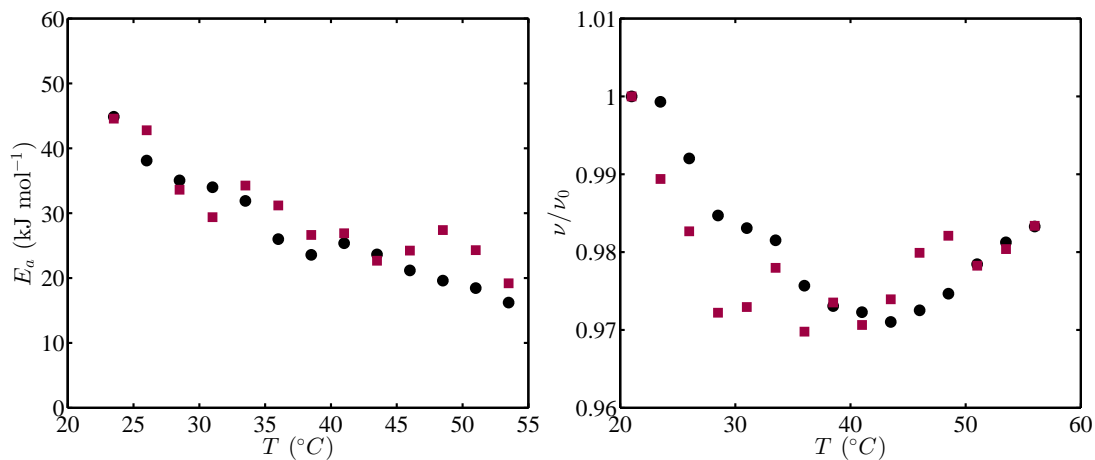


Figure 3.D.3: Comparison of the apparent activation energy (left) and scaled effective number density of partial chains (right) under a constant force (circles) and under a constant gap-compensation factor (squares) for sample B_{0.4}.

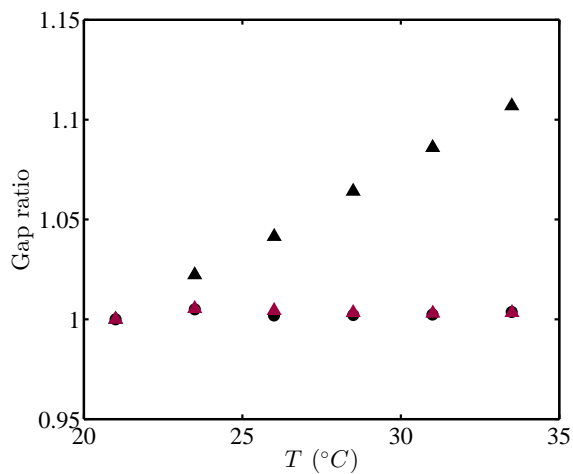


Figure 3.D.4: The ratio of gap thickness at each temperature and at 21 $^{\circ}\text{C}$ for bis-crosslinked (black triangles) and DNA-crosslinked (red triangles) gels without calibration. Black circles are ratios for a bis-crosslinked gel obtained by the constant axial force calibration method.

3.E Transformation between creep compliance and dynamic moduli spectra

Converting the time dependent creep compliance $J(t)$ to the dynamic moduli spectra G' and G'' is an alternative approach to efficiently extend the spectra to lower frequencies, which can be achieved by Fourier transformation (see chapter 2) using the TA instruments Trios software.

Figure 3.E.1 shows that for bis-crosslinked gels, G' and G'' from the creep compliance at low frequencies are very close to the spectra extended by TTS, thus validating TTS. Note, however, that G'' at higher frequencies is significantly higher than the directly measured loss moduli. This is likely due to “creep ringing” caused by the coupling of instrument inertia and sample elasticity in the initial stages of the creep measurements⁸².

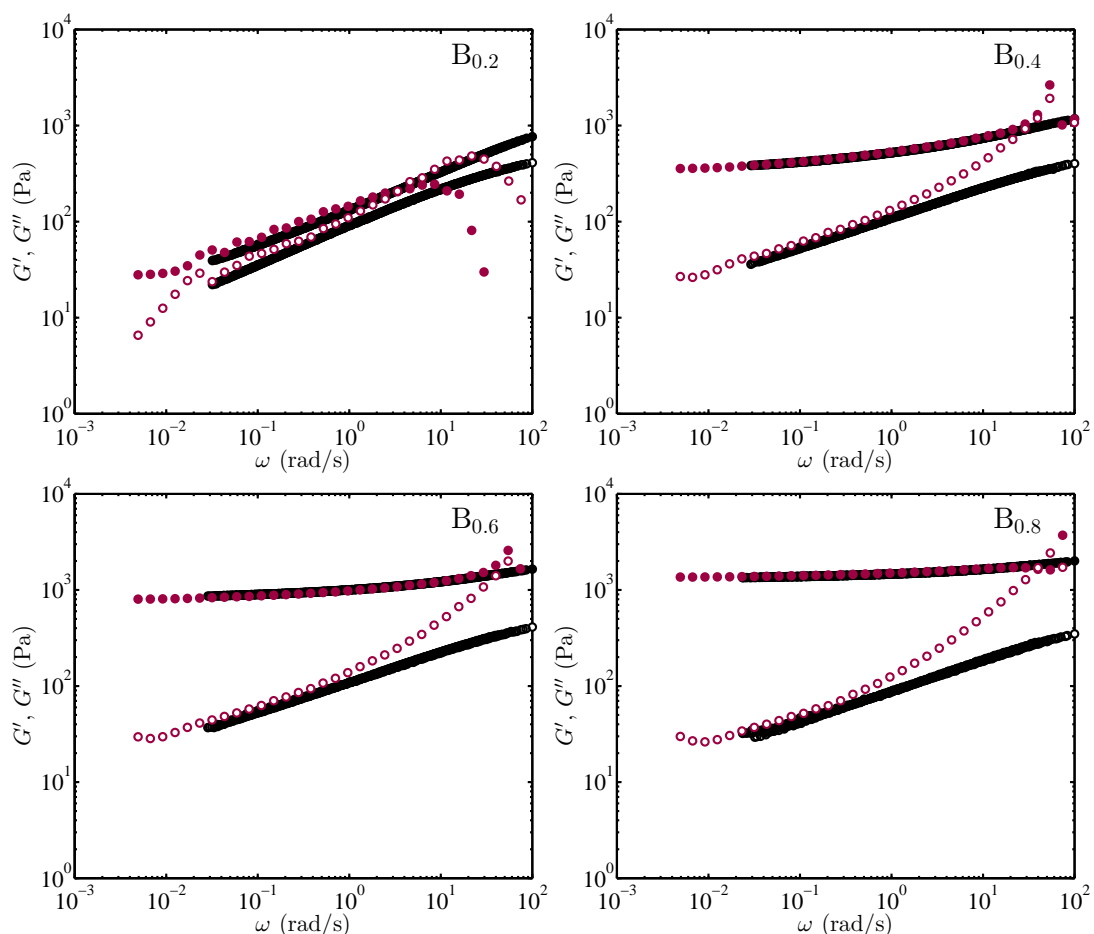


Figure 3.E.1: Comparison of G' (filled) and G'' (open) spectra obtained from TTS (black) and Fourier transformation of creep compliance data (red) for bis-crosslinked gels.

Linear viscoelasticity of complementary-DNA-strand crosslinked polyacrylamide hydrogels

4.1 Preface

DNA-crosslinked polyacrylamide hydrogels have demonstrated potential as “smart” hydrogels that can respond to specific molecules because of their molecular recognition ability and base-pair reversibility. However, the rheological properties of these gels have not been studied in detail. The rheological properties at long timescales are particularly important because they affect the material durability and whether they may be considered “gels”. This chapter examines the rheology of complementary-DNA-strand crosslinked polyacrylamide, with and without chemical/covalent bis-acrylamide crosslinking. Linear viscoelastic responses were measured during and following gelation. These show that gelation with DNA crosslinkers is faster and more efficient than chemical crosslinking. Time-temperature superposition unifies the rheological spectra of DNA-crosslinked and dual-crosslinked gels at low frequencies, furnishing the apparent activation energy for DNA-crosslink disengagement. The apparent activation energy is temperature-independent when the gels are solid-like, but decreases with increasing temperature when the gels become liquid-like. DNA-crosslinked gels behave like elastic-solids on short timescales with dynamic moduli depart from the Maxwell model at low frequencies, exhibiting smaller power-law exponents due to the multiple base-pair structure. The moduli of dual-crosslinked gels exhibit permanent-crosslinking characteristics at low frequencies.

4.2 Introduction

DNA-crosslinked polyacrylamide (PA) hydrogels are physical gels crosslinked by hydrogen bonds and base stacking between double-stranded DNA. Unlike chemically crosslinked PA gels, such as those crosslinked by bis-acrylamide (bis), DNA crosslinks are transient, and their length and sequence are programmable. These impart distinct characteristics, such as heating and cooling reversibility, a tunable melting point, and crosslink dissociation achieved by a “toehold” segment in DNA strands¹⁹. When aptamers are adopted as the “toehold” region, crosslinks are dissociated when the aptamer binds to target molecules, such as adenosine and human thrombin⁴⁶. Such gels have demonstrated potential for drug delivery^{11,12}, molecular separation⁴⁵, tissue engineering¹⁵, and biosensing^{13,14}.

In the foregoing applications, it is important to know mechanical and rheological properties, such as the elastic modulus, the timescales on which the gels are solid and liquid behaving, and durability under load. These aspects of DNA-crosslinked hydrogels are not well understood. Furthermore, to arrest creep and prevent dissolution, permanent chemical crosslinks into networks are necessary^{13,14}. The viscoelastic properties of gels with coexisting bis- and DNA-crosslinks have not been studied, so there is much to learn from linear and nonlinear rheological analysis.

Among the studies of the mechanical properties of DNA-crosslinked hydrogels, Lin et al.¹⁹ and Lin et al.¹²¹ correlated Young’s modulus of DNA-crosslinked PA gels with DNA concentration using video-microscopy of an embedded steel ball subjected to a magnetic force. Using the same method, Jiang et al.²⁰ showed that Young’s modulus of such gels can be varied from 100 Pa to 30 kPa according to the length of crosslinker, monomer concentration, and degree of crosslinking. Chippada et al.²¹ developed a method to determine the shear modulus, Young’s modulus, and Poisson ratio by applying force or torque to embedded magnetic micro-needles. Previtera et al.¹²² demonstrated a stiffness-tuning process by adding various amounts of DNA to gels supported on an elastic cushion and measuring the cushion displacement. In each of these microrheological testing platforms, gel viscosities and/or shear moduli were obtained at short times. The value presented as the shear modulus of 10% w/v DNA-crosslinked gels²⁰ was found to exceed the plateau storage modulus of an ideal network by $\approx 80\%$.

Spectral rheological characterization, as furnished by a macroscale rheometer, is a powerful tool for studying the relaxation of the transient crosslinks^{115,60}. In contrast to the foregoing microrheological platforms, much larger sample volumes are required. Nevertheless, dynamic moduli spectra can be extended using time-temperature superposition (TTS)

to rigorously probe the microstructure over a wide range of relevant time scales. This permits the materials to be unambiguously identified as a liquid or gel^{25,23}.

Topuz and Okay¹²³ and Okay¹²⁴ reported dynamic moduli during gelation, and dynamic moduli spectra, of chemically crosslinked double-strand DNA hydrogels. In these studies, DNA served as the polymer chains, so its influence on the rheological response is different than when it is the crosslinker, as addressed in the study presented below.

The activation energy of physical crosslinking influences the gel melting temperature and yield stress. Moreover, some physical- and dual-crosslinked gels can exhibit self-healing properties, achieved by introducing breakable crosslinks. Dynamic, reversible crosslinking dissipates energy and provides a mechanism with which to restore gel structure and mechanical properties^{51,52,53,57,125,126}. Knowledge of the activation energy can help to predict whether a gel has the foregoing self-healing ability⁵³.

One way to determine the activation energy is by applying TTS. However, there is controversy over the applicability of TTS for physically crosslinked gels¹⁰⁵. For example, Noro et al.¹²⁷ superposed the dynamic moduli for a thermosensitive gel crosslinked by hydrogen bonds. However, Nair et al.¹²⁸ were unable to superpose both the storage and loss moduli. An Arrhenius plot linking the shift factor and temperature had previously been applied to physical gels to obtain the activation energy¹²⁹. For example, Peng et al.¹¹⁵ correlated temperature with the zero-shear viscosity using the Arrhenius equation, obtaining the energy required to disengage the hydrophobic chains from micelles ($\approx 25\text{--}58 k_B T$ for different hydrophobic tail numbers). Similarly, Sun et al.⁵³ reported the apparent activation energy of weak and strong ionic bonds in polyampholyte hydrogels ($\approx 29\text{--}124 k_B T$), and Kim et al.¹³⁰ demonstrated that the activation energies for network formation in nanoemulsions obtained from rheological tests and dynamic light scattering are similar. DNA-crosslinked gels may have unique viscoelastic properties compared to physical gels crosslinked by hydrogen bonds, ionic bonds or micelles, because of a large activation energy arising from multiple-base-pair association.

Introducing permanent bis-crosslinking into DNA-crosslinked networks complicates the viscoelastic response. Recent studies have examined the rheological properties of gels with dual crosslinked architectures. For example, Loveless et al.¹³¹ reported that multiple types of crosslinks affect the mechanical properties of poly(4-vinylpyridine) gels additively. Narita et al.⁶⁰ reported frequency-sweep spectra for poly(vinyl alcohol) (PVA) crosslinked with borate ions as physical crosslinkers, with and without glutaraldehyde as a chemical crosslinker. They identified an associative-Rouse mode, theoretically described by Indei and Takimoto⁷¹

(evident by G' and G'' spectra scaling as $\omega^{1/2}$) for the physical crosslinking in dual gels. Long et al.¹³² developed a theory to describe the linear mechanical response of dual-crosslinked PVA gels, predicting torsional rheometry data. To the best of our knowledge, however, no mechanical or rheological properties of PA gels in which DNA- and bis-crosslinks coexist have been reported. In addition to dynamic shear moduli, creep-recovery tests in the linear viscoelastic regime may help to elucidate the recoverable strain⁷⁷. Fitting models, such as the Burgers model, to such data can also furnish insights into self-healing^{51,78,79}.

In the present study, we applied bulk rheological testing in the linear viscoelastic regime to DNA-crosslinked gels and dual-crosslinked gels. Schematics of the gel synthesis and comparison with bis-crosslinked gels are shown in figure 4.1. Two acrydite-modified DNA strands were complemented to a third DNA strand to form the DNA crosslinks. The third strand contains an aptamer segment that can bind to adenosine. The base sequences of DNA are adopted from Yang et al.¹². With or without bis-, DNA-crosslinkers are copolymerized with acrylamide as the monomer. The procedure is modified from Lin et al.¹⁹ to achieve dual-crosslinked gels by forming DNA-crosslinking centres before acrylamide polymerization. This modification is necessary because bis-acrylamide crosslinks are difficult to introduce if the monomer is polymerized before hybridizing the DNA crosslinks. Using dynamic rheology during gelation, gelation kinetics were examined, and frequency-sweep spectra at different temperatures following gelation were used to ascertain the complementary DNA-crosslink dynamics and apparent activation energy.

4.3 Materials and methods

Acrylamide (40% w/v, Fisher Scientific), bis-acrylamide (2% w/v, Fisher Scientific), acrydite-modified oligonucleotides (standard desalting, Integrated DNA Technologies), ammonium persulfate (APS, $\geq 98\%$, Fisher Scientific), N,N,N',N' -tetramethylethylenediamine (TEMED, 99%, GE Healthcare Life Sciences), and DNA suspension buffer (10 mM Tris-HCl, 0.1 mM EDTA, pH 8.0, Teknova) were used as provided by the manufacturer.

Acrydite-modified DNA Strand A, acrydite-modified Strand B, and “LinkerAdap” were prepared as 5 mM solutions in DNA suspension buffer. Different volumes of Strand A, Strand B, and “LinkerAdap” solutions, as well as DNA suspension buffer, were first added to a centrifuge tube, and then, after 2 min for the three DNA strands to combine, a fixed volume of 40% w/v acrylamide and different volumes of 0.25% w/v bis-acrylamide solutions were added to the tube to achieve a constant monomer concentration 1.4 mol l^{-1} and varying

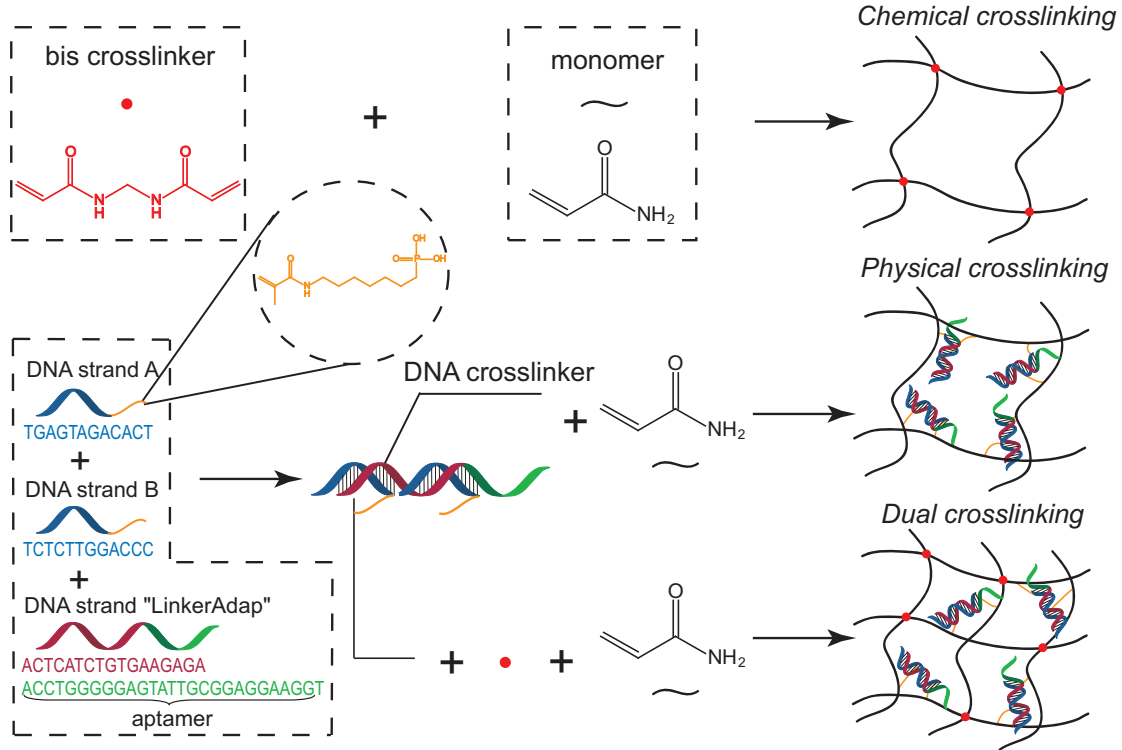


Figure 4.1: Schematics of the chemical-, physical-, and dual-crosslinked hydrogel formation.

physical to chemical crosslinker ratios, as summarized in table 4.1. Nitrogen was bubbled through the mixture for 5 min to remove dissolved oxygen, prior to centrifugation at $\approx 1,000 \times g$ for 2 min to collect liquid transferred to the tube wall during degassing. In this pre-gel solution, base pairs form between Strand A and “LinkerAdap”, and between Strand B and “LinkerAdap”, thus forming what we term “DNA crosslinkers”, which, similarly to bis-acrylamide crosslinkers, are tetra-functional, but with a significantly higher molecular weight.

To clearly distinguish the samples, we adopt a nomenclature B_xD_y , where x is the ratio of the bis-acrylamide crosslinker concentration to the acrylamide concentration (ratio as mmol/mol) in the pre-gel solution, and y is the ratio of the DNA-crosslinker concentration to the acrylamide concentration (ratio as mmol/mol) in the pre-gel solution.

After adding 10 μl of freshly prepared 10% (w/v) APS¹ and 3.6 μl TEMED per ml of pre-gel solution, the mixture was pipetted onto the bottom plate of a parallel-plate sample holder of an ARES-G2 rheometer (TA Instruments), and the 25 mm diameter top plate was then lowered to achieve a 0.5 mm gap. An “evaporation blocker” and silicone oil applied to the sample edge were used to minimize evaporation. Oscillatory shear during gelation

¹ $\frac{\text{mass of APS (g)}}{\text{volume of water (ml)}} \times 100\%$.

was applied at 21°C with an angular frequency $\omega = 1 \text{ rad s}^{-1}$ and strain amplitude $\gamma = 1\%$ to ensure a linear viscoelastic response. After the dynamic moduli reached steady values, frequency sweeps were performed in the range $\omega = 0.1\text{--}100 \text{ rad s}^{-1}$ with $\gamma = 1\%$ from 21°C to 56°C, controlled using a ThermoCube 10-300 thermoelectric chiller (Solid State Cooling Systems). An average gap compensation factor that is the sum of the sample holder expansion and the gel expansion was set $\approx 2.9 \mu\text{m}/^\circ\text{C}$ for TTS. Creep-recovery tests in the linear viscoelastic regime were undertaken after returning the temperature to 21°C.

Figure 4.2 shows several DNA- and dual-crosslinked hydrogels ($B_0D_{0.8}$, $B_{0.2}D_{0.6}$, $B_{0.4}D_{0.4}$, and $B_{0.6}D_{0.2}$) after rheological tests. These are transparent and solid-like in appearance. The right panel shows a two-layer (each layer with $\approx 0.5 \text{ mm}$ thickness) dual-crosslinked hydrogel ($B_{0.1}D_{0.4}$) can be extended without breaking, thus highlighting its characteristic ductility.

Table 4.1: Compositions of DNA- and dual-crosslinked polyacrylamide gels.

Sample	A (%)	Bis-A/A (mmol/mol)	DNA/A (mmol/mol)	A (mol l^{-1})	DNA+Bis-A (mmol l^{-1})
$B_0D_{0.2}$	10	0	0.2	1.4	0.28
$B_0D_{0.4}$	10	0	0.4	1.4	0.56
$B_0D_{0.6}$	10	0	0.6	1.4	0.84
$B_0D_{0.8}$	10	0	0.8	1.4	1.12
$B_{0.6}D_{0.2}$	10	0.6	0.2	1.4	1.12
$B_{0.4}D_{0.4}$	10	0.4	0.4	1.4	1.12
$B_{0.2}D_{0.6}$	10	0.2	0.6	1.4	1.12
$B_{0.1}D_{0.4}$	10	0.1	0.4	1.4	0.70

4.4 Results and discussion

4.4.1 Gelation kinetics

Figure 4.3 shows time series of the storage and loss moduli for DNA-crosslinked gels with various DNA-crosslinker ratios, c_{DNA}/c_a^2 . The storage modulus G' clearly increases systematically with the DNA-crosslinker ratio, whereas the loss moduli are practically independent of the DNA-crosslinker ratio. As gelation progresses, G' reaches maximum values at $t \sim 1000 \text{ s}$, and then decreases on a time scale that is about an order of magnitude slower.

² $\frac{\text{amount of substance of DNA}}{\text{amount of substance of acrylamide}}$ (mmol/mol).

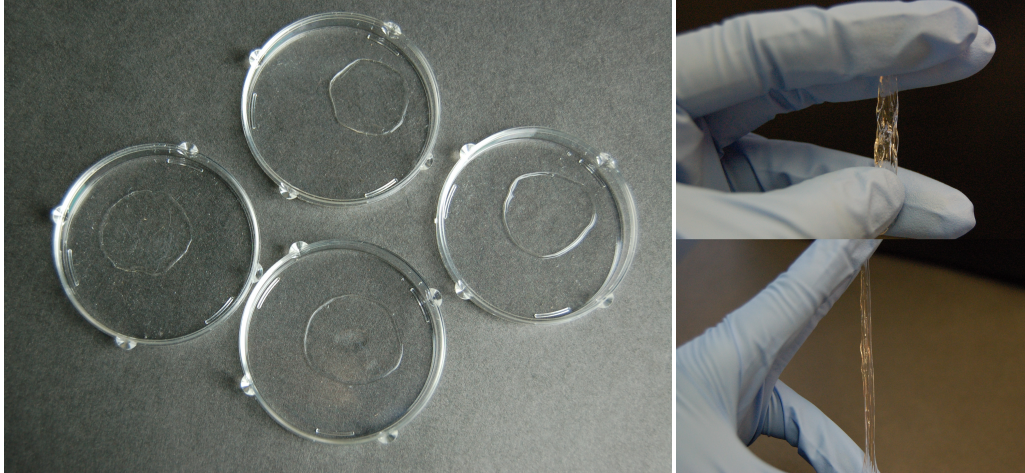


Figure 4.2: Left: DNA- and dual-crosslinked polyacrylamide hydrogels after rheological testing. Right: Ductility of a dual-crosslinked polyacrylamide hydrogel demonstrated before (top) and after (bottom) stretching.

The qualitative characteristics of the G' time series are similar to those of dual-crosslinked gels (see figure 4.4) and gels with bis-only crosslinking (see chapter 3).

The loss modulus G'' is qualitatively different from bis-only gels, showing a local maximum in the initial stage of gelation. This is because the DNA crosslinker has a higher molecular weight, increasing the interaction or coupling between DNA crosslinkers. With the growth of polymer chains connected to DNA crosslinkers, the cluster size increases, causing aggregation and a transition from a dilute to an entangled solution. Thus, a rapid increase in the dissipated energy occurs, as measured by G'' . When clusters attach to the growing network, they contribute to the elasticity, and the internal friction between the solvent and the network reduces, decreasing G'' . Fluctuations in the G'' time series arise from instrumental adjustments of the top plate that are required to maintain a constant axial force (set to 0 N).

Note that the dual-crosslinked gels in figure 4.4 have a fixed total crosslinker ratio. The storage moduli increase systematically with the DNA-crosslinker ratio, and are somewhat higher than for DNA-only crosslinked gels with the same DNA-crosslinker ratio. Thus, the bis- and DNA-crosslinking contributions to the storage moduli are additive, as examined in greater detail below. The loss moduli for dual-crosslinked gels and DNA-crosslinked gels are all very similar, with the exception of the DNA-only crosslinked gel with the highest DNA ratio (sample B₀D_{0.8}), and an ostensibly higher loss modulus. Despite the storage and loss moduli all exhibiting a slow relaxation, their ratio, reported in the figures as loss-tangent time

series, rapidly establish steady-state values during the relaxation of the dynamic moduli.

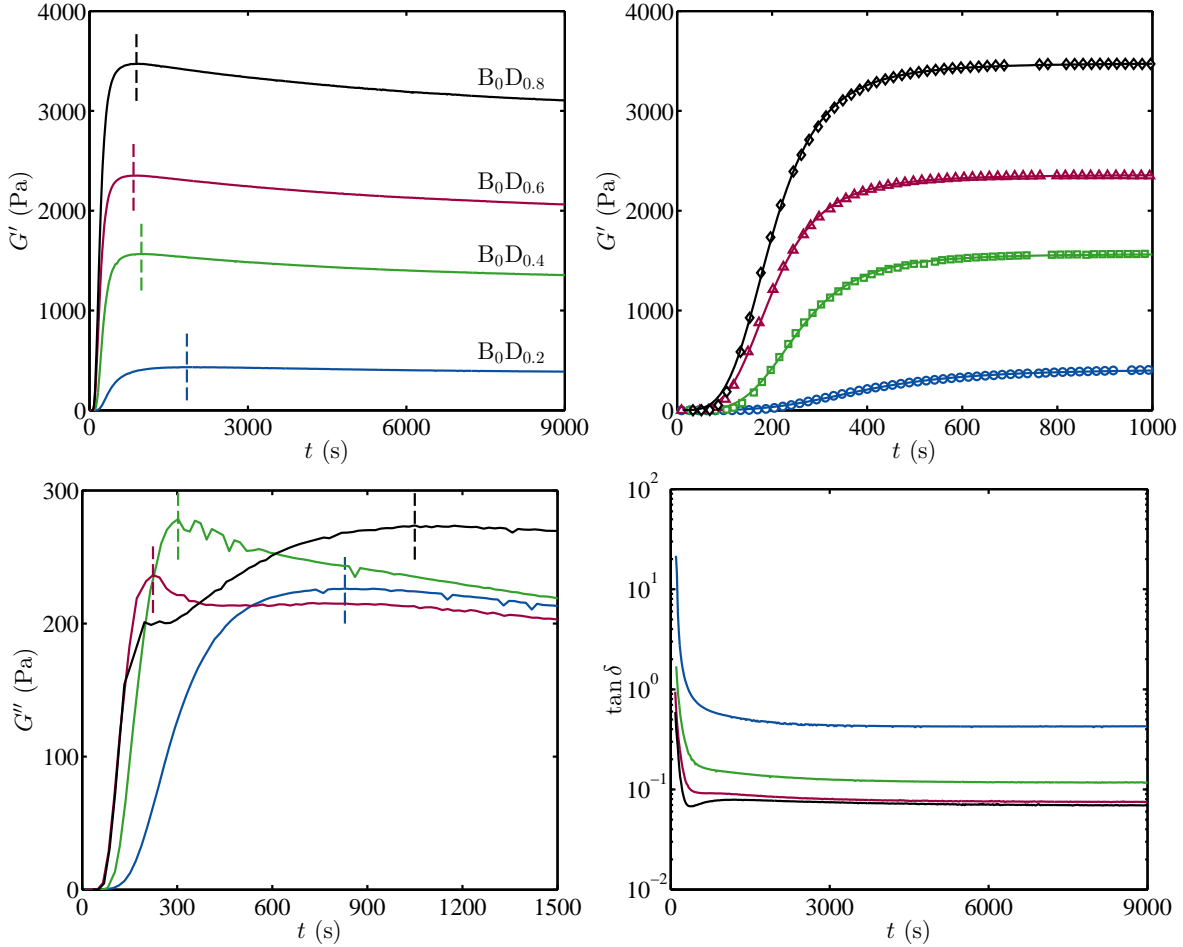


Figure 4.3: Storage modulus G' (top left), least-squares fit of Eqn. (3.5) (top right), loss modulus G'' (bottom left), and loss tangent (bottom right) for DNA-crosslinked gels during gelation: $\omega = 1 \text{ rad s}^{-1}$, $T = 21^\circ\text{C}$. Disturbances attributed to the application of silicone oil have been removed.

The storage-moduli time series in the top-right panel of figure 4.3 are used to fit Eqn. (3.5), furnishing quantitative metrics on the formation rate of effective crosslinks P at the gelation half-time θ , which are plotted in figure 4.5. The top-left panel compares P and θ for DNA-crosslinked gels with those for bis-crosslinked gels having the same acrylamide monomer concentration. P for both gels is linear in the crosslinker ratio with θ first decreasing and then remaining constant or increasing with increasing crosslinker ratio. However, since P scales with the maximum value of the storage modulus G'_m , the ratio P/G'_m , which has units of reciprocal time, furnishes a metric that we loosely refer to as a network-formation rate. As shown in the bottom-left panel, this rate for bis-crosslinked gels (circles, asterisks, triangles)

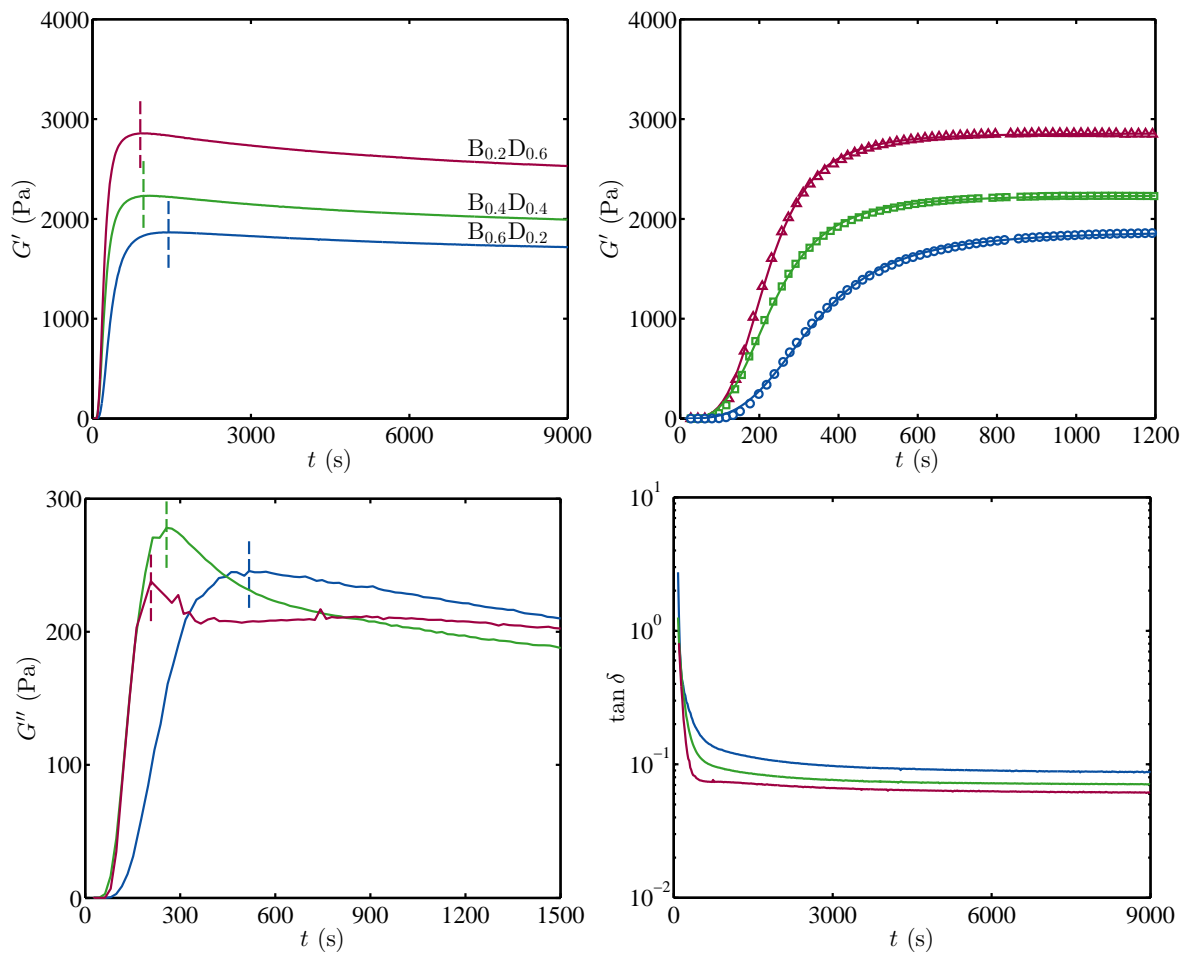


Figure 4.4: Storage modulus G' (top left), least-squares fit of Eqn. (3.5) (top right), loss modulus G'' (bottom left), and loss tangent (bottom right) for dual-crosslinked gels during gelation: $\omega = 1 \text{ rad s}^{-1}$, $T = 21^\circ\text{C}$. Disturbances attributed to the application of silicone oil have been removed.

is practically independent of the crosslinker ratio, and is weakly dependent on the amount of TEMED in the pre-gel solution. As mentioned in chapter 3, the constant value of P/G'_m for bis-crosslinked gels is attributed to physical entanglements in the network. For DNA-crosslinked gels (squares), however, the rate increases approximately linearly with c_{DNA}/c_a when $c_{\text{DNA}}/c_a \leq 0.6$ mmol/mol. This is because, unlike bis-acrylamide crosslinkers, the DNA crosslinker mass is equivalent to $\approx 7\text{--}27\%$ of the monomer mass from $\text{B}_0\text{D}_{0.2}$ to $\text{B}_0\text{D}_{0.8}$. Thus, there is an increasing number of pre-formed oligomers in the network, which may accelerate the formation of elastically effective crosslinks and offset the effect of entanglements on P . The higher TEMED concentration creates more clusters in the early gelation stage, increasing the network-formation rate.

For the dual-crosslinked gels (right panels in figure 4.5), P increases quadratically with the fraction of crosslinkers that are DNA, transiting smoothly from the pure bis- and pure DNA-crosslinking limits. This suggests a weakly nonlinear superposition of the rates expected from the bis- and DNA-crosslinked gels.

4.4.2 Dynamic moduli spectra and time-temperature superposition

Dynamic moduli spectra for DNA- and dual-crosslinked gels at various temperatures ($T = 21$ to 56°C with $\omega = 0.1\text{--}100$ rad s^{-1}) are shown in the panels on the right-hand-side of figure 4.6 and figure 4.7. Due to the transient DNA crosslinks, temperature has a strong influence. The spectra can be neatly organized by applying time-temperature superposition (TTS). Vertical and horizontal shifts were applied using the TTS function of the TA instruments Trios software to overlap spectra at low frequencies. Master curves with the reference temperature $T_0 = 21^\circ\text{C}$ are plotted in the panels on the left-hand-side of figures 4.6 and 4.7. Note that systematic upturns in G' and G'' appear at higher frequencies following TTS because of segments—including acrydite and four extra bases—that connect Strand A and Strand B to polyacrylamide, which act like branches to the polymers. Thus, the relaxation time of partial chains increases, and the moduli at higher frequencies increase earlier. The upturn has also been observed in the rheological spectra of reversible gels following TTS^{133,134,135,136}. Noro et al.¹³⁷ demonstrated that the deviation can be elucidated by shifting the G'' upturn at each temperature according to the temperature dependence of the solvent viscosity.

For DNA-only gels, a rubbery plateau is present at high frequencies. The plateau modulus G_N^0 can be estimated from G' at the frequency where G'' has a local minimum¹³⁸. Figure 4.8 shows that G_N^0 defined in this manner for DNA-crosslinked gels is higher than for bis-

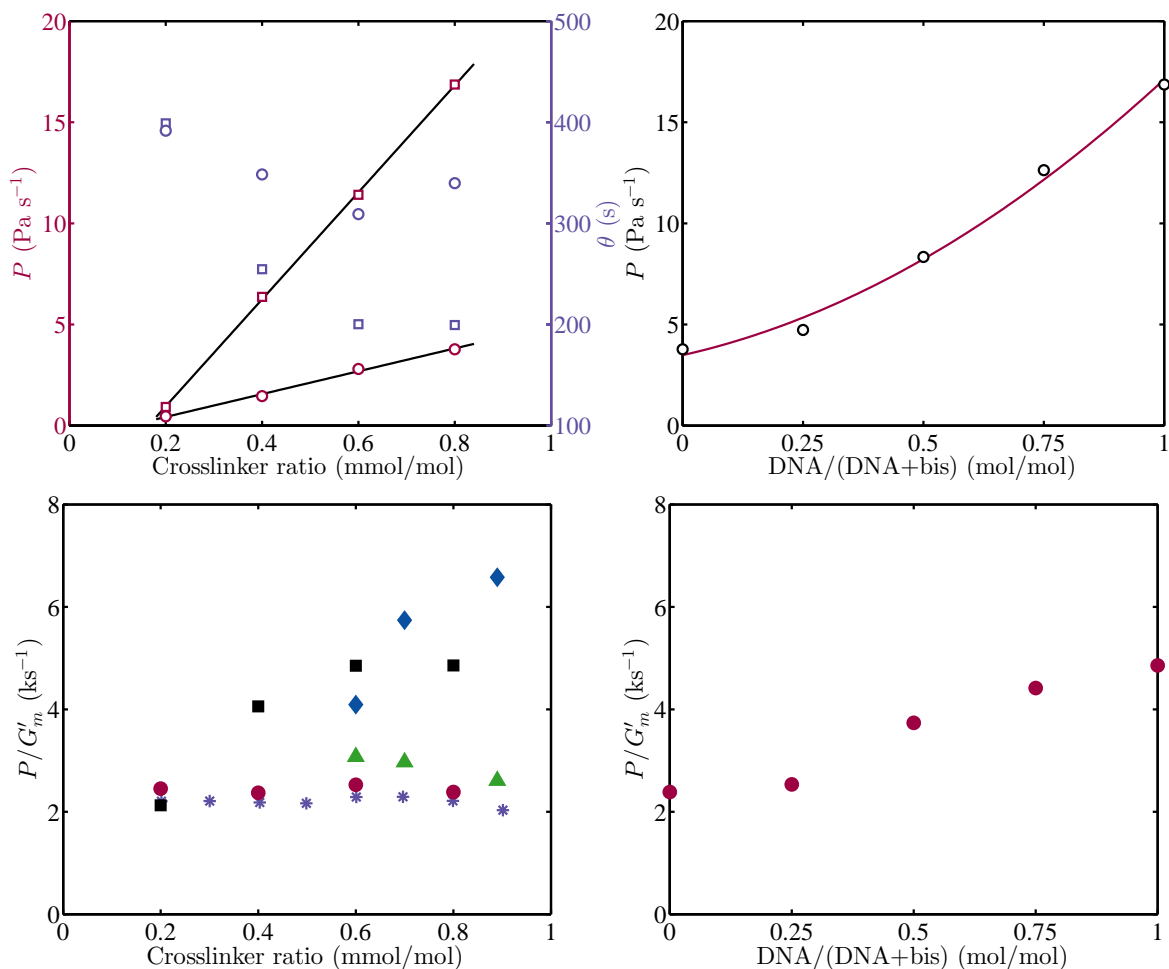


Figure 4.5: Top left: Mid-point slope P (left axis) and gelation half time θ (right axis) versus crosslinker ratio for bis- (circles) and DNA-crosslinked (squares) gels: $\omega = 1 \text{ rad s}^{-1}$, $T = 21^\circ\text{C}$. Top right: P for dual-crosslinked gels with a fixed total crosslinker ratio equal to that for sample $B_0D_{0.8}$. Bottom left: Network-formation rate versus crosslinker ratio for bis-crosslinked gels (circles), DNA-crosslinked gels (squares), bis-crosslinked gels with a higher TEMED concentration (triangles), DNA-crosslinked gels with a higher TEMED concentration (diamonds), bis-crosslinked gels with monomer concentration 1.3 mol l^{-1} (asterisk): $\omega = 1 \text{ rad s}^{-1}$, $T = 21^\circ\text{C}$. Bottom right: The network-formation rate for dual-crosslinked gels with a fixed total crosslinker ratio equal to that for sample $B_0D_{0.8}$.

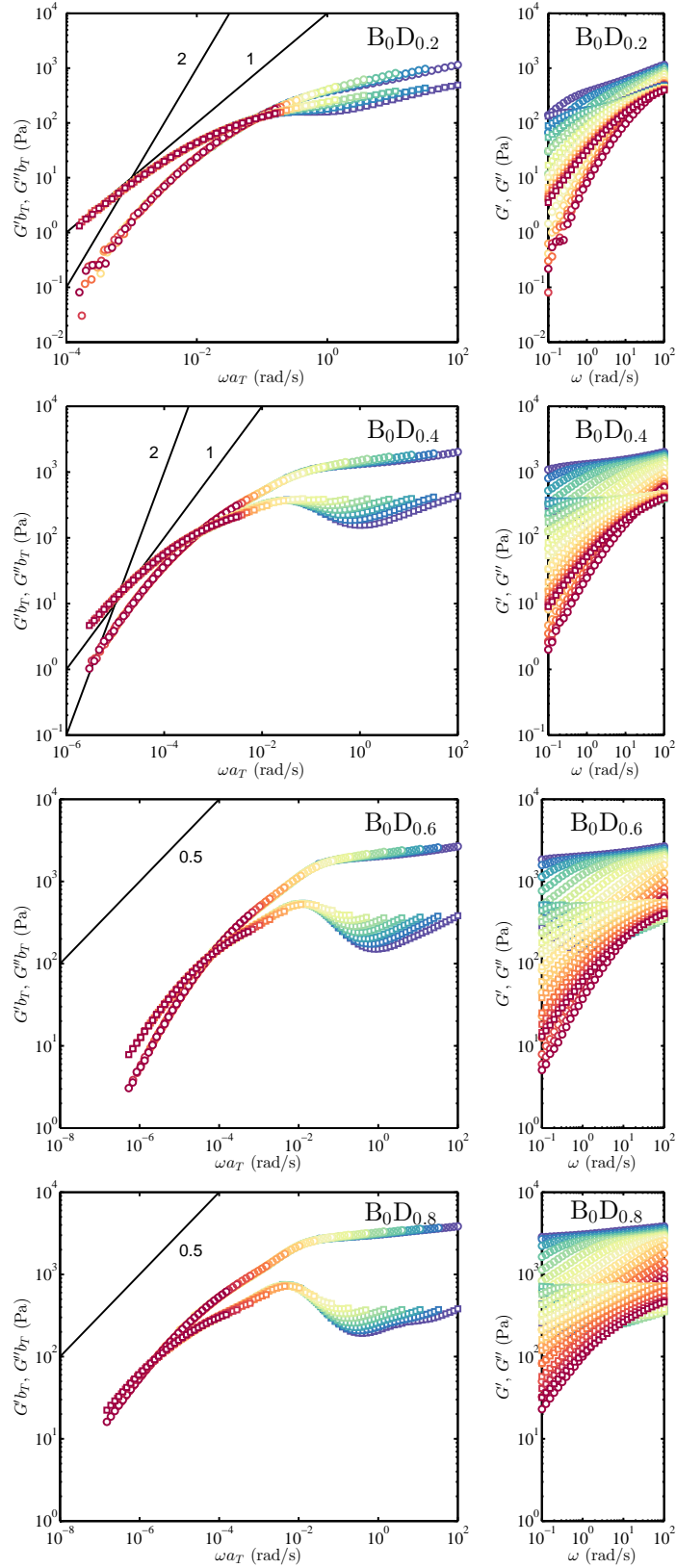


Figure 4.6: G' (circles) and G'' (squares) spectra for DNA-crosslinked gels following TTS with reference temperature 21°C (temperature increases from blue to red).

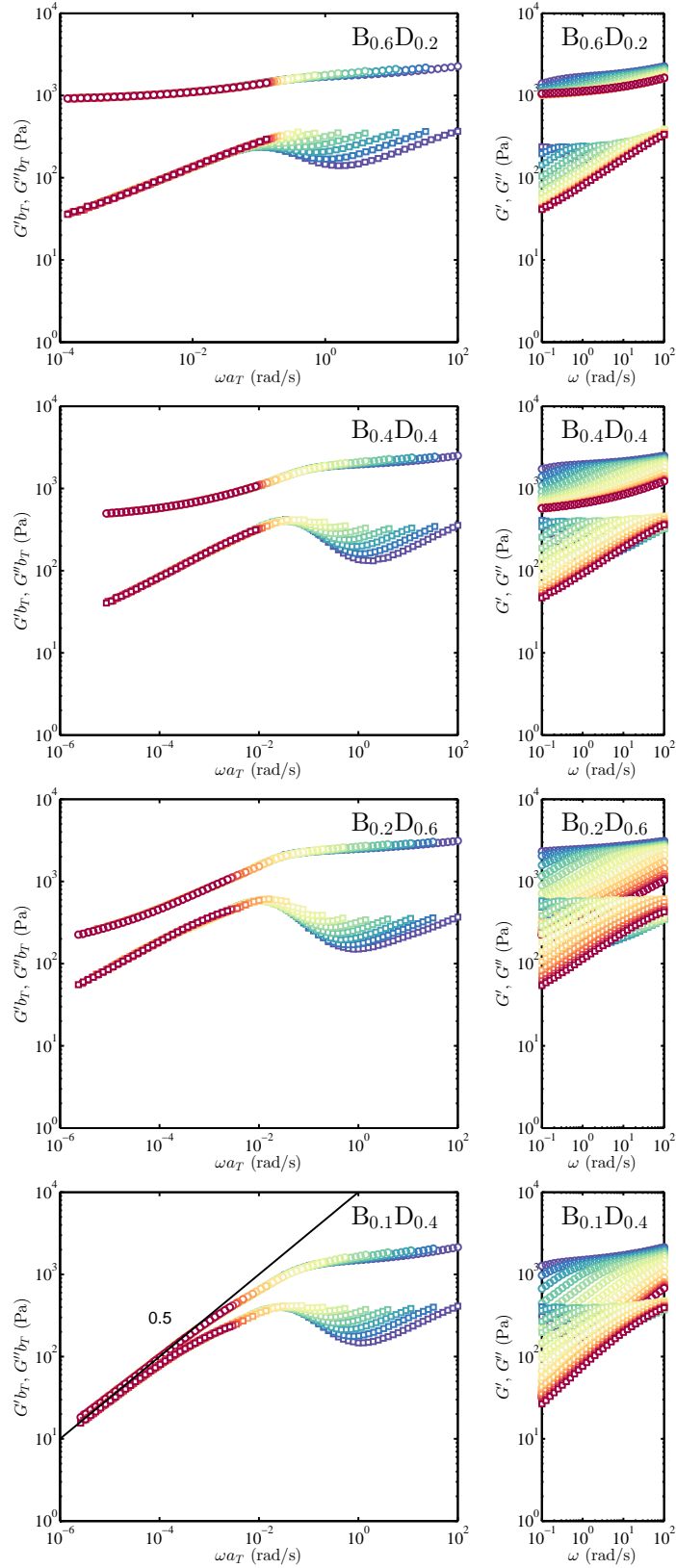


Figure 4.7: G' (circles) and G'' (squares) spectra for dual-crosslinked gels following TTS with reference temperature 21°C (temperature increases from blue to red).

crosslinked gels with same crosslinker ratio, indicating that physical crosslinking produces a more elastically effective network than chemical crosslinking. This might be explained by the larger size and mass of the DNA crosslinks, which makes the connection of localized clusters more efficient, decreasing the number of dangling ends. Moreover, the larger size likely separates polymer chains growing from the crosslinking centre, thus avoiding self-termination and reducing defects, such as loops. For bis-crosslinked gels, G_N^0 is approximately linear in the crosslinker ratio, with a weak positive quadratic contribution, whereas for DNA-crosslinked gels, the correlation between G_N^0 and crosslinker ratio is linear, without weak increase in the crosslinking efficiency.

Note that G_N^0 of bis-crosslinked gels vanishes when $c_{\text{bis}}/c_a \approx 0.18$ mmol/mol, which we identify as the percolation threshold. The crosslinking efficiency, as measured by

$$G_N^0/G_{Nideal}^0 \times 100\% \approx 12.5c_{\text{bis}}/c_a + 19.4 - 3.9c_a/c_{\text{bis}}$$

increases from zero (at the percolation threshold) to $\approx 24\%$ when $c_{\text{bis}}/c_a \approx 0.8$ mmol/mol. Despite the efficiency vanishing when approaching the percolation threshold, the linear contribution to G_N^0 with respect to c_{bis}/c_a indicates that $\sim 19\%$ of bis-acrylamide crosslinker in the pre-gel solution produces elastically active partial chains.

For DNA-crosslinked gels, the crosslinking efficiency reaches a plateau earlier than that for bis-crosslinked gels. The plateau modulus vanishes when $c_{\text{DNA}}/c_a \approx 0.12$ mmol/mol, which we identify as the percolation threshold. The crosslinking efficiency, as measured by

$$G_N^0/G_{Nideal}^0 \times 100\% \approx 62.8 - 7.4c_a/c_{\text{DNA}}$$

increases from zero (at the percolation threshold) to $\approx 54\%$ when $c_{\text{DNA}}/c_a \approx 0.8$ mmol/mol. Despite the efficiency vanishing when approaching the percolation threshold, the linear contribution to G_N^0 with respect to c_{DNA}/c_a indicates that $\sim 63\%$ of DNA crosslinker in the pre-gel solution produce elastically active partial chains.

For dual-crosslinked gels having the same total crosslinker ratio as B₀D_{0.8}, G_N^0 and G_N^0/G_{Nideal}^0 increase with increasing $c_{\text{DNA}}/c_{\text{bis}}$ ³, showing that blending DNA crosslinkers with bis-acrylamide crosslinkers increases the effective crosslink density. Table 4.2 summarizes metrics obtained for DNA- and dual-crosslinked gels. A higher crosslinker ratio lowers the molecular weight of polymer between crosslinks and decreases the mesh size $l = (2k_B T/G_N^0)^{1/3}$. Moreover, the ratio of the mesh size to the estimated Flory radius R_F of partial chains for DNA-crosslinked gels are larger than for bis-crosslinked gels, indicating

³ $\frac{\text{amount of substance of DNA}}{\text{amount of substance of bis-acrylamide}}$ (mol/mol).

that DNA crosslinking is more effective at stretching partial chains between crosslinking centres.

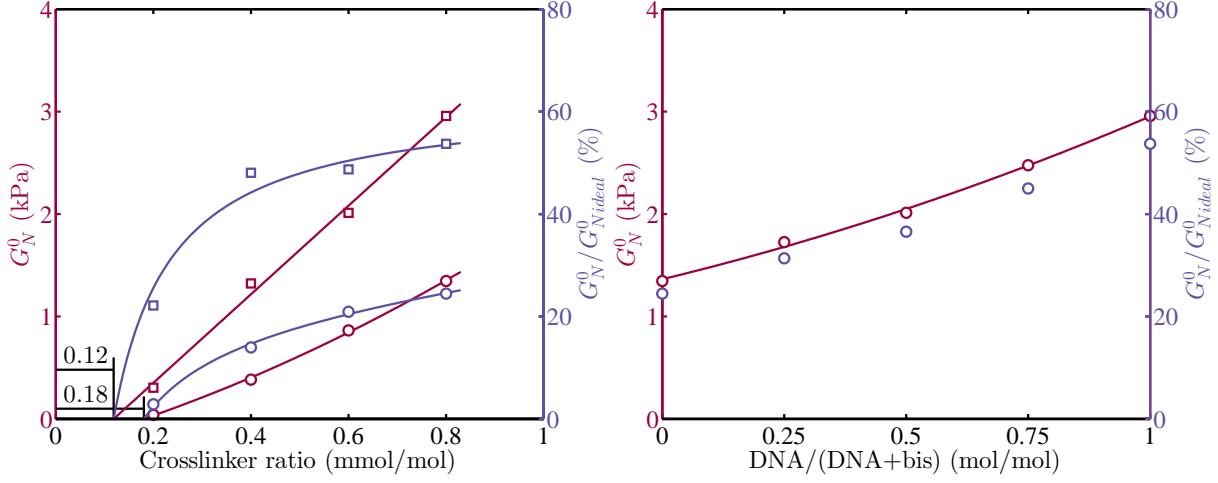


Figure 4.8: Left: Plateau modulus (left axis) and crosslinking efficiency (right axis) at $T = 21^\circ\text{C}$ versus crosslinker ratio for bis- (circles) and DNA-crosslinked (squares) gels. Right: The plateau modulus (left axis) and crosslinking efficiency (right axis) for dual-crosslinked gels with a fixed total crosslinker ratio equal to that for sample $B_0D_{0.8}$ at $T = 21^\circ\text{C}$.

For DNA-crosslinked gels beyond the plateau region, a crossover angular frequency ω_c exists in the master spectra, below which the gels become viscoelastic liquids ($G' < G''$). The average crosslink lifetime τ_c is often approximated by $2\pi\omega_c^{-1}$ ¹³⁹. At 21°C , τ_c increases with the effective DNA crosslink density n_{DNA} (figure 4.9), indicating slower partial-chain relaxation. In the low-frequency regime, G' and G'' increase as a power-law in ω . The power-law exponents for G' and G'' increase with decreasing frequency. The maximum exponents obtained from low-frequency regimes are shown in table 4.2, which are smaller than predicted by the Maxwell model (for which $G' \sim \omega^2$, $G'' \sim \omega^1$) in the terminal regimes. This deviation is explained by the associative-Rouse model of Indei and Takimoto⁷¹. In this model, the gel network comprises as polymer chains with multiple associative stickers, and the terminal or longest relaxation time τ_A is proportional to $\tau_X \bar{N}^2$, where \bar{N} is the average number of associated stickers per chain, and τ_X is the time for an associated sticker to return to its equilibrium state (identified by the peak in G'').

In the Maxwell model, τ_A and τ_X coincide (with small \bar{N}), so only the terminal relaxation mode is observed. However, the associative-Rouse model applies when \bar{N} is large, reducing the power-law exponents between the plateau and terminal regimes. Because the multiple base pairs in DNA crosslinks impart a much higher association rate than dissociation rate

(increasing \bar{N} and imparting a broad distribution of relaxation times), the associative-Rouse model is appropriate for DNA-crosslinked gels. Progressing from $B_0D_{0.2}$ to $B_0D_{0.8}$, the increase of power-law exponents with decreasing frequency becomes slower, showing that \bar{N} increases with the DNA-crosslinker ratio. Figure 4.9 shows that τ_X increases with the effective DNA crosslink density. The same trend was found by Narita et al.⁶⁰ and Jongschaap et al.¹⁴⁰. Narita et al.⁶⁰ attributed this to the increasing number of elastically inactive crosslinks, and Jongschaap et al.¹⁴⁰ noted that (i) only the dissociation of terminal stickers releases stress, and (ii) the fraction of terminal stickers decreases with increasing \bar{N} .

There is no crossover of G' and G'' for dual-crosslinked gels at low frequencies, because the bis-acrylamide crosslinks impart permanent elastic connectivity. τ_X for dual-crosslinked gels is mainly affected by transient DNA crosslinking, as shown in figure 4.9. Except for $B_{0.4}D_{0.4}$, the coexistence of permanent crosslinks increases τ_X , because permanent crosslinks between DNA crosslinks hinder stress release. The exception of $B_{0.4}D_{0.4}$ may be due to random errors arising from the synthesis of $B_0D_{0.4}$ and $B_{0.4}D_{0.4}$. Moreover, the power-law exponent of G' at low frequencies for dual-crosslinked gels decreases with decreasing $c_{\text{DNA}}/c_{\text{bis}}$, and the exponent of G' first increases and then decreases with increasing frequency. Two plateaus are present in the spectra for dual-crosslinked gels. A high-frequency plateau indicates the presence of physical and chemical crosslinking, whereas only chemical crosslinking contributes to the low-frequency plateau. Loveless et al.¹³¹ also demonstrated that the crosslinks with longer lifetimes in a multi-crosslinked network control its mechanical properties at low frequencies. For $B_{0.1}D_{0.4}$, which has the largest ratio $c_{\text{DNA}}/c_{\text{bis}}$, the exponents for G' and G'' are close to those of the associative-Rouse model: $G' \sim G'' \sim \omega^{1/2}$ when $2\pi\tau_A^{-1} \ll \omega \ll 2\pi\tau_X^{-1}$. This is because τ_A for $B_{0.1}D_{0.4}$ is practically infinite due to chemical crosslinking, whereas $\tau_X \approx 200$ s. Unlike pure DNA-crosslinked gels, permanent crosslinks in $B_{0.1}D_{0.4}$ impart a significant disparity between $2\pi\tau_A^{-1}$ and $2\pi\tau_X^{-1}$, but unlike other dual-crosslinked gels, the bis-crosslinker ratio is too low to dominate the low-frequency dynamics.

G' and G'' from the dynamic spectra as a function of temperature are re-plotted in figure 4.10. Note that the frequency is the one used to define where G' is the plateau modulus at 21°C. It is shown that G' decreases with increasing temperature, whereas G'' increases to a maximum and then decreases. The crossover temperature for G' and G'' , which indicates the gel-sol transition temperature for DNA-crosslinked gels, increases with increasing DNA-crosslinker ratio. This is because the melting temperature of DNA crosslinkers is only determined by the DNA sequence; thus, the fraction of DNA crosslinks that are dissociated is the same for different gels at each temperature. With a higher DNA crosslink ratio, the

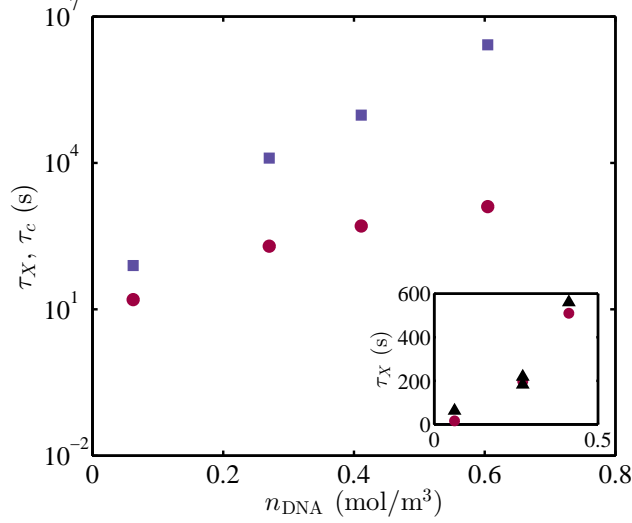


Figure 4.9: τ_X (circles) and τ_c (squares) of DNA-crosslinked gels at $T = 21^\circ\text{C}$ versus effective crosslink density. The inset compares τ_X for DNA-crosslinked (circles) and dual-crosslinked (triangles) gels.

fraction of DNA crosslinks needed to maintain the solid state is smaller, so the transition of the gel to a liquid-like state occurs at a higher temperature. For dual-crosslinked gels, G' and G'' have no crossover point, and reach a plateau with increasing temperature, indicating permanent crosslinks. The temperature at which the plateau region begins is found to increase with $c_{\text{DNA}}/c_{\text{bis}}$.

In figure 4.11, $\tan \delta$ for DNA-crosslinked gels decreases with increasing DNA-crosslinker ratio, exhibiting more solid-like behaviour. Moreover, $\tan \delta$ first decreases to a minimum, and then increases with frequency. In the low-frequency regime, $\tan \delta > 1$, indicating that gels are viscous fluids. For dual-crosslinked gels (figure 4.12), $\tan \delta < 1$ at all frequencies, because of the chemical crosslinking. Moreover, except for B_{0.1}D_{0.4}, $\tan \delta$ decreases with decreasing frequency at low frequencies, confirming that chemical crosslinks control the low-frequency dynamics.

4.4.3 Activation energy and scaled effective crosslink number

Figures 4.13 and 4.14 furnish the apparent activation energy E_a for DNA crosslinks from linear fitting of $\ln a_T$ to $1/T$ for physically and dually cross-linked samples, and multiplying the best-fit slope by $R \approx 8.31 \text{ J mol}^{-1} \text{ K}^{-1}$. Arrhenius behaviour with a constant E_a occurs at low temperatures, but the curves becomes non-Arrhenius at high temperatures, with E_a obtained from neighbouring triplets of data points decreasing with increasing temperature.

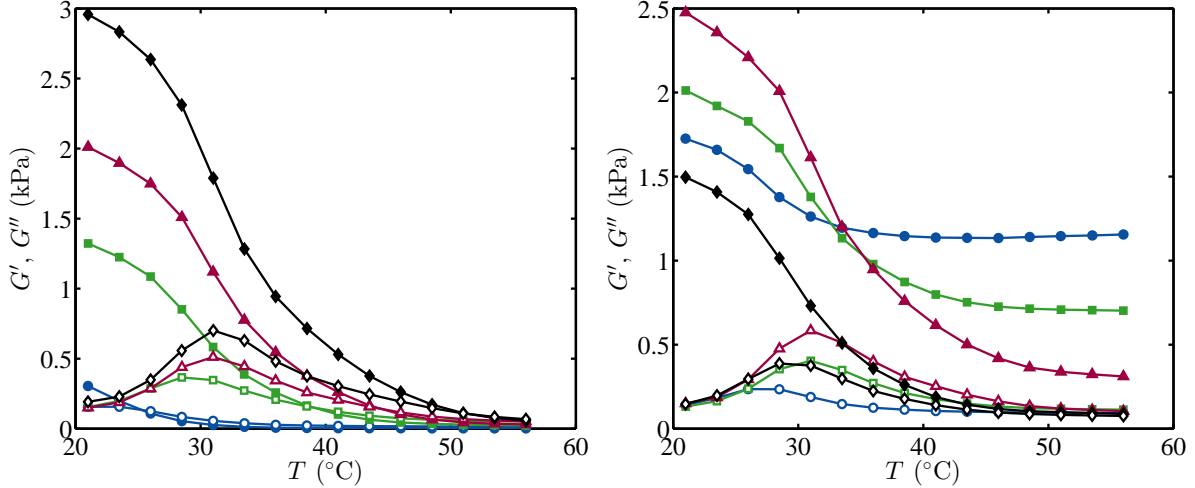


Figure 4.10: G' (filled) and G'' (open) moduli at the frequencies furnishing G_N^0 at 21°C plotted versus temperature. Left: DNA-crosslinked gel samples $B_0D_{0.2}$ (circles), $B_0D_{0.4}$ (squares), $B_0D_{0.6}$ (triangles), and $B_0D_{0.8}$ (diamonds). Right: dual-crosslinked gel samples $B_{0.6}D_{0.2}$ (circles), $B_{0.4}D_{0.4}$ (squares), $B_{0.2}D_{0.6}$ (triangles), and $B_{0.1}D_{0.4}$ (diamonds).

The maximum E_a for both DNA- and dual-crosslinked gels is $\approx 318 \text{ kJ mol}^{-1}$ ($\approx 130 k_B T$). This indicates that, at low temperatures, E_a that controls the crosslink dissociation rate is not affected by the DNA-crosslinker ratio or the chemical crosslinks. There are 24 complementary base pairs in one DNA crosslink, with each crosslink comprising two sets (12 for each) of base pairs between DNA strands and two “LinkerAdap” moieties. Note that crosslinks disengage only when one set breaks. According to Panjkovich and Melo¹⁴¹, the bond energy of 12 base pairs in Strand A or Strand B obtained from three different thermodynamic studies is $350 \pm 50 \text{ kJ mol}^{-1}$ ($\approx 143 k_B T$). Because the activation energy for DNA-double-strand hybridization is $\approx 9 k_B T$ ¹⁴², our data show that the bond energy (subtracting $9 k_B T$ from $143 k_B T$) is equal to that for ≈ 10 base pairs. Thus, when 10 out of 12 of the base pairs in one set are broken, the double-stranded DNA may be not stable, causing the dissociation. This is consistent with the assumption that the DNA crosslinks have a much higher association than dissociation rate.

Beyond the Arrhenius region, E_a begins to decrease when the effective crosslink density is below the critical value for a solid-like network and the continuous gel network no longer exists. Thus, the polymer chain relaxation does not need to overcome the bond energy of base pairs. When all crosslinks are dissociated, E_a may reach a constant, reflecting the dissociation barrier for an entangled polymer solution. The transition from Arrhenius to non-Arrhenius behaviour occurs at a lower temperature for gels with a smaller ratio c_{DNA}/c_a ,

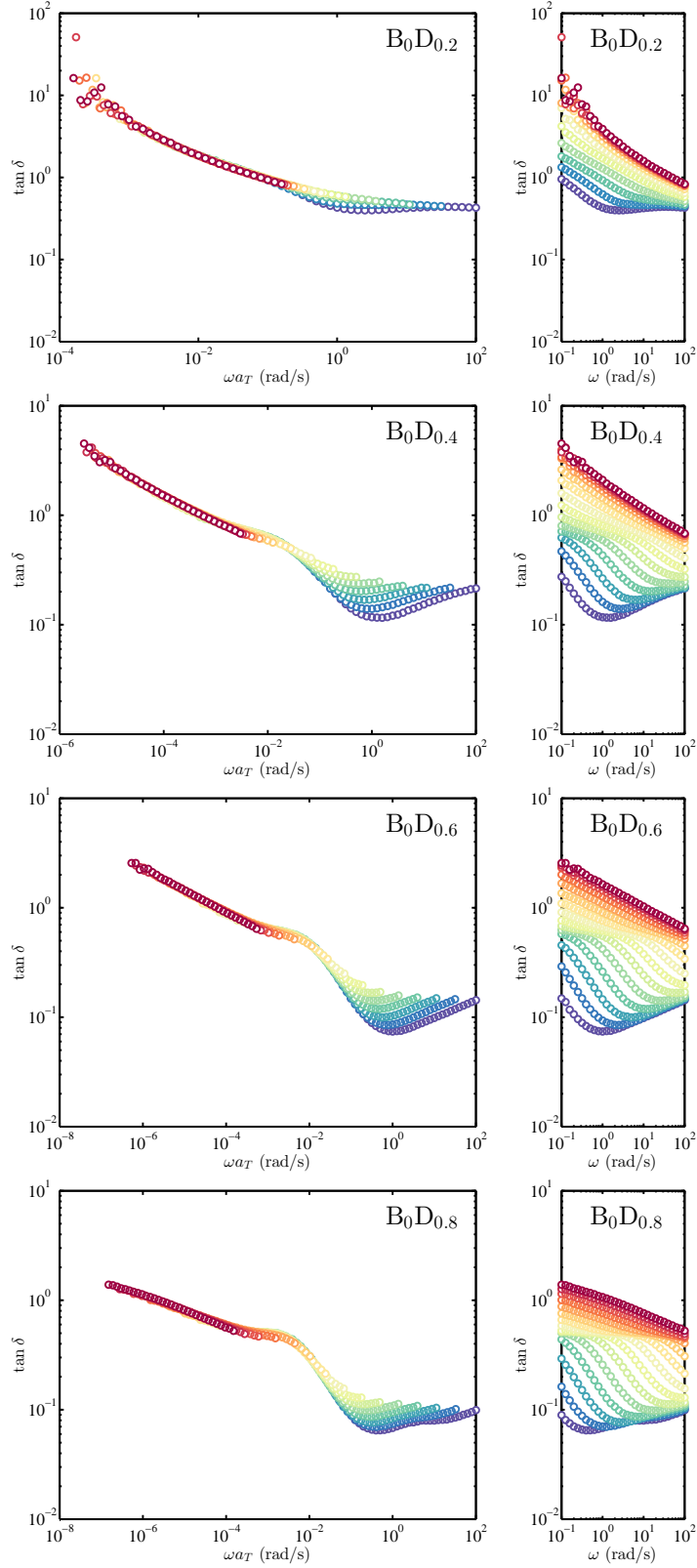


Figure 4.11: Loss tangent spectra for DNA-crosslinked gels following TTS with reference temperature 21°C (temperature increases from blue to red).

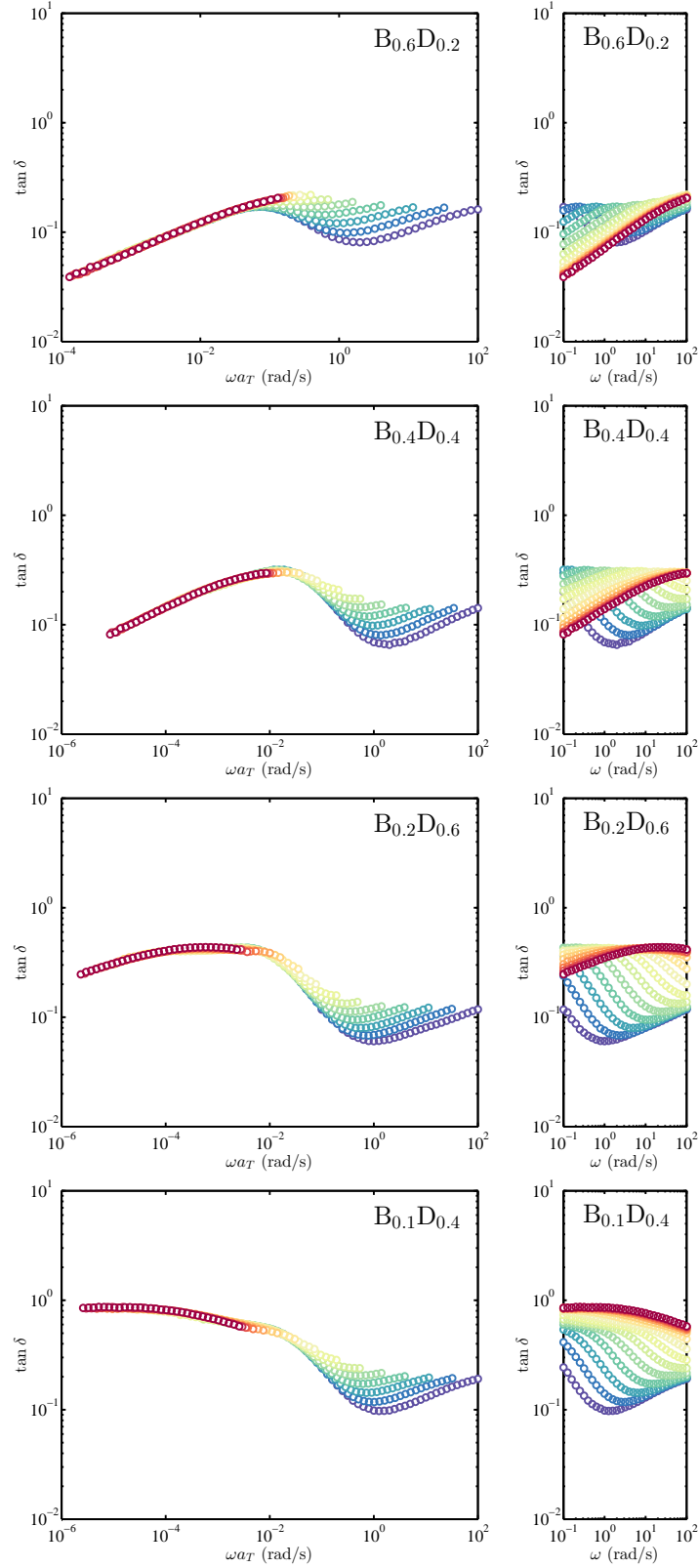


Figure 4.12: Loss tangent spectra for dual-crosslinked gels following TTS with reference temperature 21°C (temperature increases from blue to red).

because with a lower DNA-crosslinker ratio the gels are more easily transferred to liquids. This is confirmed by the left panel of figure 4.15, in which the transition temperature is close to the crossover temperature for G' and G'' in figure 4.10. Moreover, inflection points are found in the E_a versus T curves for $B_0D_{0.2}$ and $B_0D_{0.4}$. This is because inflection points also exist in the melting curves of double-stranded DNA, indicating its melting temperature at which a half of DNA strands are denatured. The melting temperatures reported by the manufacturer for Strand A and Strand B are 34°C and 38°C, respectively.

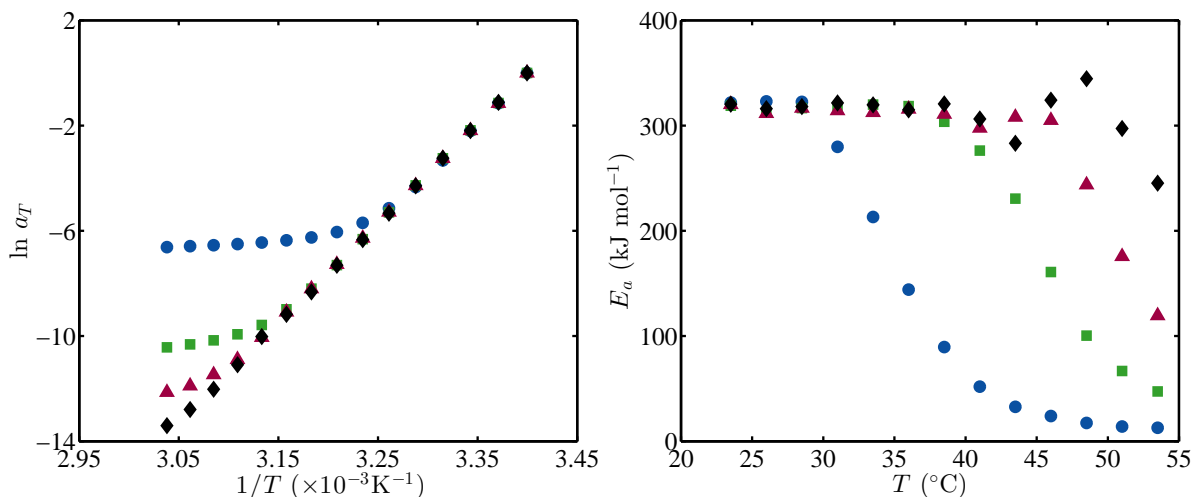


Figure 4.13: Arrhenius plots of the horizontal shift factor (left) and apparent activation energy versus temperature (right) for DNA-crosslinked gels: $B_0D_{0.2}$ (circles); $B_0D_{0.4}$ (squares); $B_0D_{0.6}$ (triangles); $B_0D_{0.8}$ (diamonds).

E_a for dual-crosslinked gels have a similar temperature dependence. The transition from Arrhenius to non-Arrhenius behaviour is compared with the temperature at which G' and G'' for dual-crosslinked gels reach constants. As shown in the right panel of figure 4.15, the transition occurs at a lower temperature than the temperature at which the majority of DNA crosslinks in dual-crosslinked gels are dissociated. Moreover, the difference between transition temperature for DNA-crosslinked gels and dual-crosslinked gels with the same DNA-crosslinker ratio increases with DNA-crosslinker ratio (from $B_{0.6}D_{0.2}$ to $B_{0.2}D_{0.6}$). For example, E_a of $B_0D_{0.6}$ begins to decrease at 46°C, whereas for $B_{0.2}D_{0.6}$ the activation energy decreases when the temperature is above 36°C. This may be because in the dual-crosslinked networks, DNA- and bis-crosslinks are not distributed homogeneously. A portion of the polymer chains is prevented from disconnecting from networks by bis-acrylamide crosslinks, whereas the rest can further disconnect. Thus, the DNA-crosslink concentration that can cause the disconnection of polymer chains in $B_{0.2}D_{0.6}$ may be less than in $B_0D_{0.6}$, resulting

in a lower transition temperature than for $B_0D_{0.6}$.

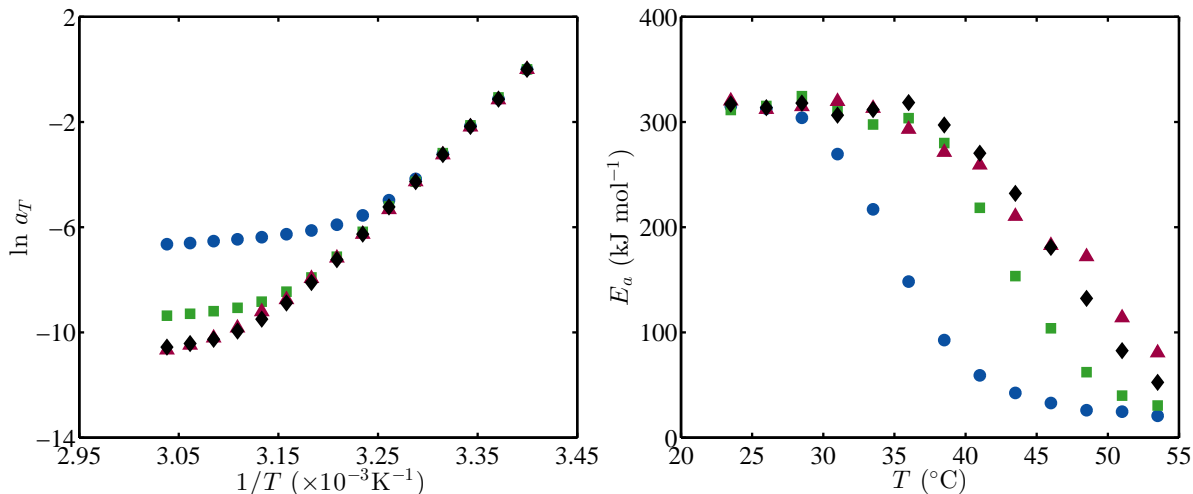


Figure 4.14: Arrhenius plots of the horizontal shift factor (left) and apparent activation energy versus temperature (right) for dual-crosslinked gels: $B_{0.6}D_{0.2}$ (circles); $B_{0.4}D_{0.4}$ (squares); $B_{0.2}D_{0.6}$ (triangles); $B_{0.1}D_{0.4}$ (diamonds).

Figure 4.16 shows that for DNA-crosslinked gels, the scaled number of effective crosslinks N/N_0 increases beyond the temperature at which the gel becomes liquid-like. Gels with a lower DNA-crosslinker ratio have a larger increase in N/N_0 before N/N_0 reaches a constant. This may be because, after the gel becomes liquid-like, polymer chains form entanglements that contribute to G' as effective crosslinks with a shorter relaxation time than for DNA crosslinks, and the number of these entanglements is larger than DNA crosslinks. For $B_0D_{0.2}$, N is ≈ 2.5 times as large as N_0 , showing that more entanglements are formed after the gel-sol transition of gels with longer partial chains. On the other hand, the increasing crosslink number may arise from the increase in the partial chain radius of gyration with temperature. When partial chains extend, the homogeneity of the network may increase, imparting more elastically effective crosslinks from entanglement. Except for $B_{0.1}D_{0.4}$, N/N_0 for dual-crosslinked gels is close to 1 and temperature independent, because the permanent bis-acrylamide crosslinks prevent the gels behaving as liquids at low frequencies and hinder entanglement. For sample $B_{0.1}D_{0.4}$, the effect of permanent crosslinks is very small, increasing N/N_0 .

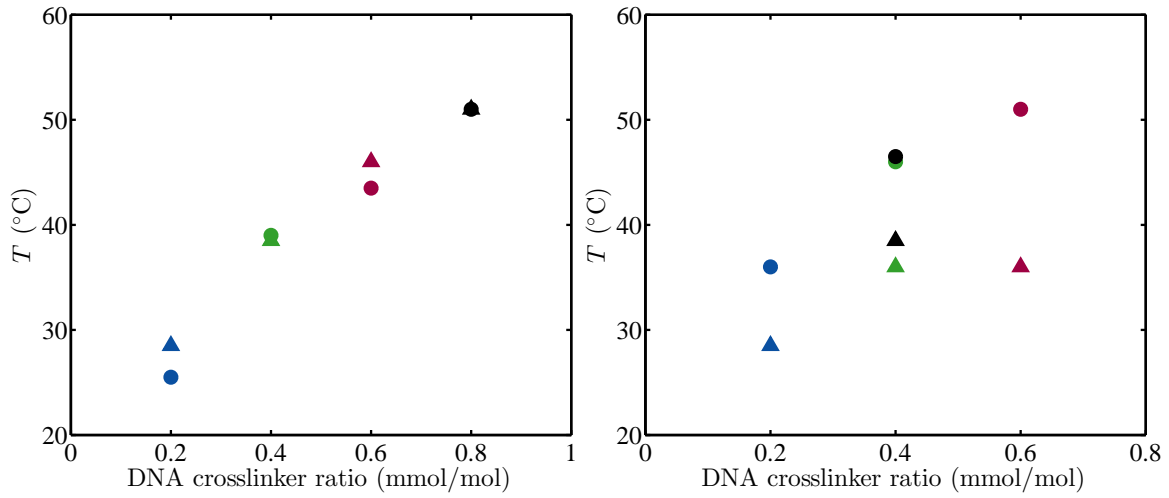


Figure 4.15: Left: Crossover temperature for G' and G'' (circles) and transition temperature from Arrhenius to non-Arrhenius behaviour (triangles) versus DNA-crosslinker ratio for samples $B_0D_{0.2}$ (blue), $B_0D_{0.4}$ (green), $B_0D_{0.6}$ (red), $B_0D_{0.8}$ (black). Right: Temperature at which G' and G'' reach a constant (circles) and transition temperature from Arrhenius to non-Arrhenius behaviour (triangles) versus DNA-crosslinker ratio for samples $B_{0.6}D_{0.2}$ (blue), $B_{0.4}D_{0.4}$ (green), $B_{0.2}D_{0.6}$ (red), $B_{0.1}D_{0.4}$ (black).

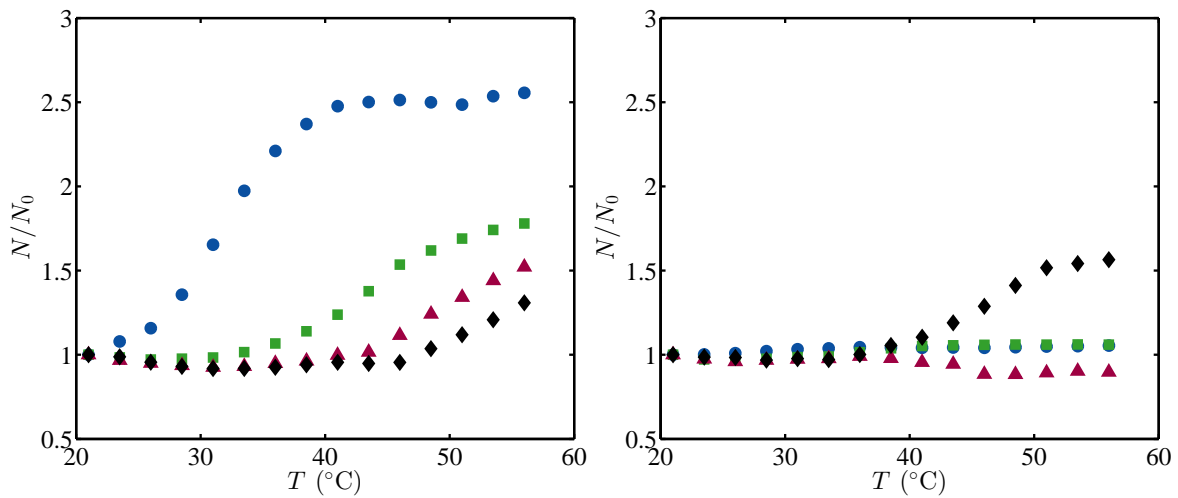


Figure 4.16: Scaled effective crosslink number versus temperature according to the vertical shift factor b_T for DNA-crosslinked (left) and dual-crosslinked (right) gels. Symbols are the same as in figures 4.13 and 4.14.

4.4.4 Roles of physical and chemical crosslinks in dual-crosslinked networks

To examine the roles of physical and chemical crosslinks in dual-crosslinked networks, the spectrum for each dual-crosslinked gel is compared to the sum of spectra for gels with only physical or chemical crosslinking (each having the same crosslinker ratio as in the dual-crosslinked gel) in figure 4.17. The plateau modulus for dual-crosslinked gels is larger than the summed spectra, suggesting that there are more effective crosslinks in the dual-crosslinked networks than the sum of the individual networks. However, G' at high frequencies and G'' for each dual-crosslinked gel are smaller than the summed spectra, indicating fewer entanglements. This is because, in the low crosslinker ratio region, the crosslinking efficiency increases with crosslinker ratio, as discussed above, so, a portion of the entanglements in the individual networks become effective crosslinks in the dual-crosslinked network.

Figure 4.18 illustrates that spectra from the subtraction of the physical gel spectra from the dual-crosslinked gels spectra have smaller upturns in G' and G'' at high frequencies. This may be because the upturns in dual- and DNA-crosslinked gels cancel. The subtracted plateau modulus is larger than that for bis-crosslinked gels, and G'' at lower frequencies are significantly larger than those for bis-crosslinked gels. This is because the bis-acrylamide in dual-crosslinked networks is more efficient at forming crosslinks with fewer defects than in individual networks. Note that since only one sample for each composition was measured and the fractional uncertainties of G' and G'' are $\sim 4.7\%$ and $\sim 3.8\%$, the adding and subtracting may enhance the errors and impart inaccurate comparisons.

4.4.5 Creep and recovery in the linear viscoelastic regime

Unlike bis-crosslinked gels, DNA-crosslinked gels are more viscous. The compliance $J(t)$ increases with a decreasing slope before reaching a linear regime in which the material deforms as a viscous fluid (figure 4.19). After removing the stress, the compliance decreases until it reaches equilibrium, and a part of the compliance is irreversible. The percentage of irreversible compliance from fitting Eqn. (3.10) decreases with increasing DNA-crosslinker ratio. For gels having both chemical and physical crosslinks, as shown in figure 4.20, recoverability is enhanced. The irrecoverable compliance fraction J_∞/J_{tot} is smaller for the gel having a larger bis-acrylamide portion. It also behaves more like an elastic solid during creep, showing that permanent chemical crosslinks arrest creep and increase the recoverable compliance.

Table 4.3 summarizes parameters obtained from fitting Eqn. (3.9) for DNA- and dual-

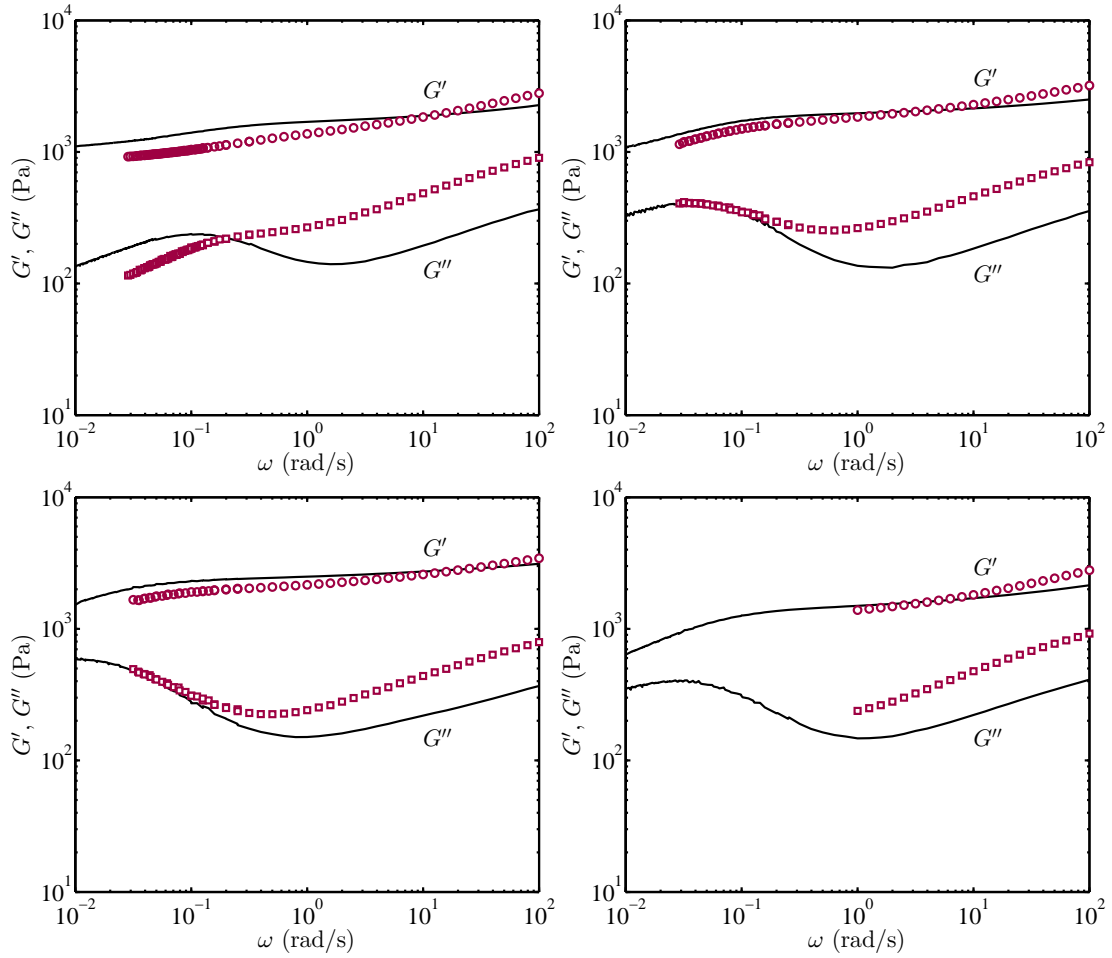


Figure 4.17: Adding G' (circles) and G'' (squares) spectra for bis-crosslinked gels to DNA-crosslinked gels at $T = 21^\circ\text{C}$. Top left: $B_{0.6}D_{0.2}$ (lines); adding $B_{0.6}D_0$ to $B_0D_{0.2}$ (symbols). Top right: $B_{0.4}D_{0.4}$ (lines); adding $B_{0.4}D_0$ to $B_0D_{0.4}$ (symbols). Bottom left: $B_{0.2}D_{0.6}$ (lines); adding $B_{0.2}D_0$ to $B_0D_{0.6}$ (symbols). Bottom right: $B_{0.1}D_{0.4}$ (lines); adding $B_{0.1}D_0$ to $B_0D_{0.4}$ (symbols).

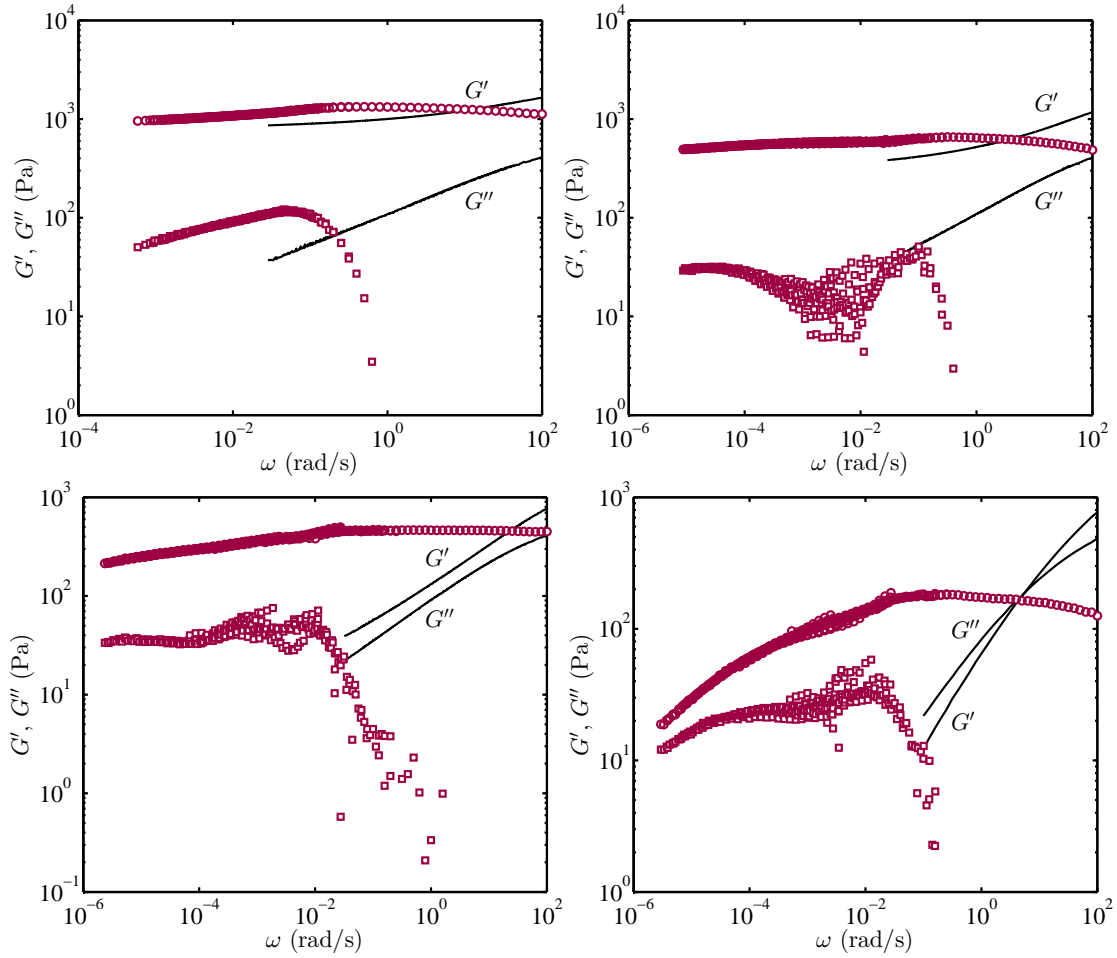


Figure 4.18: Subtracting G' (circles) and G'' (squares) spectra for DNA-crosslinked gels from those for dual-crosslinked gels at $T = 21^\circ\text{C}$. Top left: $B_{0.6}D_0$ (lines); subtracting $B_0D_{0.2}$ from $B_{0.6}D_{0.2}$ (symbols). Top right: $B_{0.4}D_0$ (lines); subtracting $B_0D_{0.4}$ from $B_{0.4}D_{0.4}$ (symbols). Bottom left: $B_{0.2}D_0$ (lines); subtracting $B_0D_{0.6}$ from $B_{0.2}D_{0.6}$ (symbols). Bottom right: $B_{0.1}D_0$ (lines); subtracting $B_0D_{0.4}$ from $B_{0.1}D_{0.4}$ (symbols).

crosslinked gels. Gels with a larger value of G_N^0 have a larger Maxwell spring modulus G_M , imparting a higher stiffness at short times. The viscosity of the Maxwell dashpot η_M , indicating the compliance that is reversible after removing the stress, increases with c_{DNA}/c_a in DNA-crosslinked gels, but decreases with increasing $c_{\text{DNA}}/c_{\text{bis}}$ for dual-crosslinked gels. For Kelvin-Voigt elements, G_K is found to increase with c_{DNA}/c_a in DNA-crosslinked gels, indicating a more elastic network. Also, G_K for DNA-crosslinked gels is smaller than that for bis-crosslinked gels, confirming that bis-crosslinked gels are more solid-like at long times. The retardation time τ is influenced by the relaxation time for DNA crosslinks and the fluctuation of partial chains. For example, τ for DNA-crosslinked gels first increases and then decreases with increasing DNA-crosslinker ratio. This is because the relaxation time for DNA crosslinks is smaller for the gel with a lower DNA-crosslinker ratio, but the partial chains need a longer time to relax. The two effects produce a maximum retardation time.

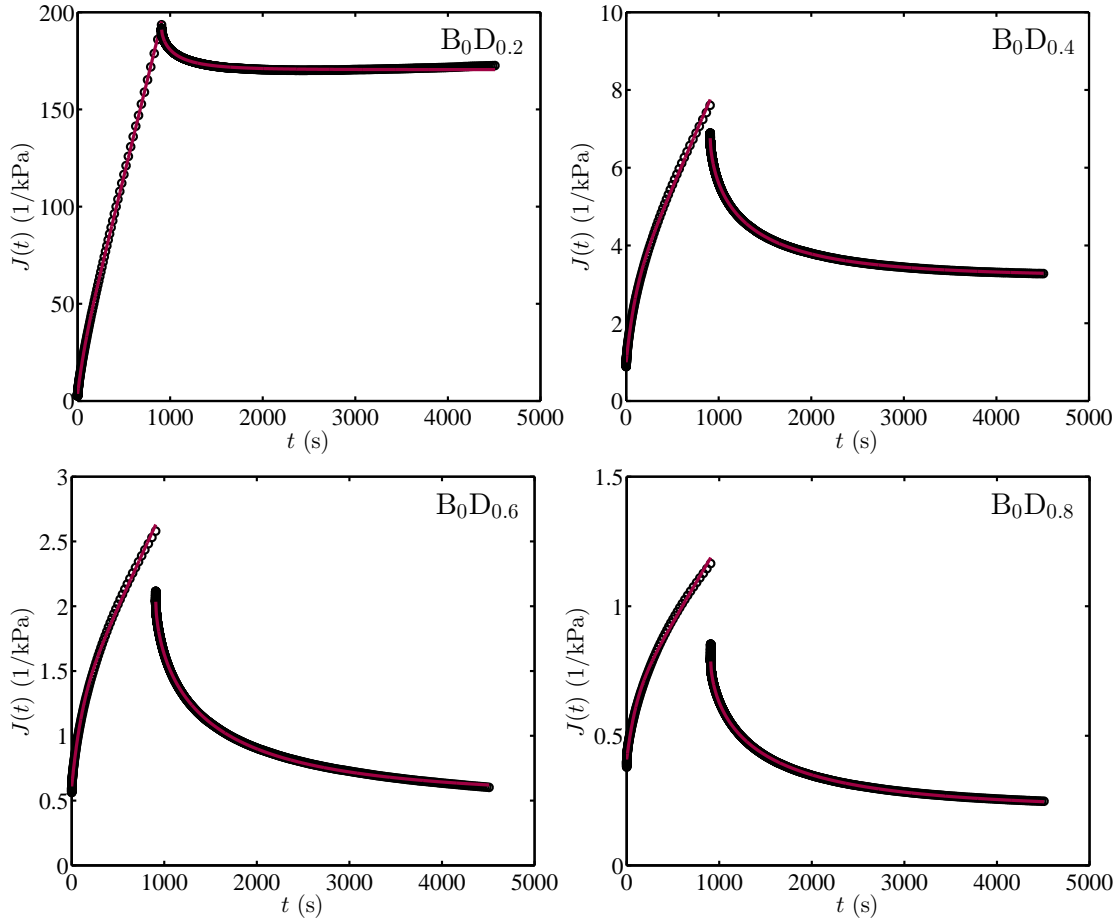


Figure 4.19: Creep-recovery for DNA-crosslinked gels: $T = 21^\circ\text{C}$.

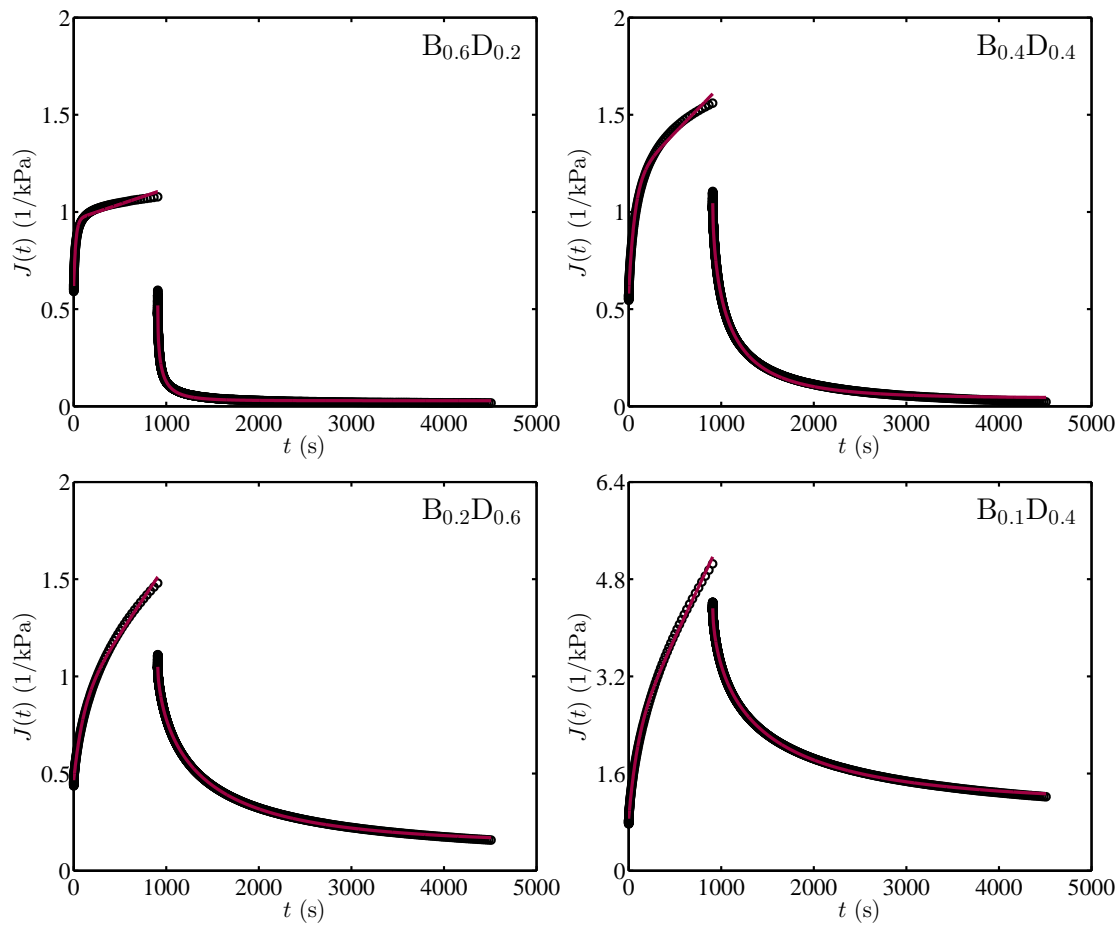


Figure 4.20: Creep-recovery for dual-crosslinked gels: $T = 21^\circ\text{C}$.

4.5 Conclusions

Polyacrylamide hydrogels having DNA- and dual-crosslinking were synthesized using complementary DNA strands as the physical crosslinker and bis-acrylamide as the chemical crosslinker. Using rheometry, gelation by DNA crosslinking was found to be faster and more efficient than bis-crosslinking. The loss moduli for DNA- and dual-crosslinked gels have a distinct peak in the early stages of gelation, which we attributed to the large size of the DNA-crosslinking centres.

TTS was applied to DNA- and dual-crosslinked gels with extended spectra exhibiting distinct characteristics. Unlike polymer melts, vertical shift factors need to be applied to physically crosslinked gels. Dynamics of DNA-crosslinked gels depart further from the Maxwell model when increasing the DNA-crosslinker ratio, with dual-crosslinked gels reflecting transient and permanent crosslinking. When transient dynamics control the network, the spectra scale as $G' \sim \omega^{1/2}$ and $G'' \sim \omega^{1/2}$ at low frequencies, whereas dynamic moduli spectra for gels with a large bis-acrylamide portion are similar to those for bis-only-crosslinked gels. A rheological determination of the apparent activation energy for DNA crosslinking furnished $\approx 318 \text{ kJ mol}^{-1}$, which corresponds to thermodynamic estimates for 10 of the 12 base-pairs. The correction between the horizontal shift factor and temperature transforms from Arrhenius to non-Arrhenius when the DNA-crosslinked gels become liquid-like. The effective crosslink number obtained from the vertical shift factor increases with temperature after the gel-sol transition. The permanent crosslinks in dual-crosslinked gel networks are found to hinder the relaxation of DNA crosslinks. Creep-recovery tests show that permanent crosslinks can also arrest creep and increase the recoverable compliance.

This study shows that DNA-crosslinked hydrogels have viscoelastic properties that depend greatly on the deformation timescales, behaving as elastic solids on short timescales. According to the definition of Almdal et al.²⁵, DNA-crosslinked gels with the crosslinker ratio larger than 0.4 mmol/mol used in this study may be considered gels. By introducing chemical crosslinking, they regain the frequency-independent elastic properties of chemically crosslinked gels, and are much less sensitive to temperature. Moreover, DNA-crosslinked gels are a good model to study the mechanical properties and swelling/dissolving of physical gels, since the activation energy for the crosslink disengagement is programmable.

Table 4.2: Analysis of gel samples at 21°C.

Sample	P (Pa s ⁻¹)	G_N^0 (Pa)	M_l^a (kDa)	l (nm)	R_F^c (nm)	l/R_F	G_N^0/G_{Nideal}^0 (%) ^d	τ_X (s)	τ_c (h)	Expon. ^e for G'	Expon. for G''	E_a^{max} (kJ mol ⁻¹)
B _{0.2} D ₀	0.46	39	6224	59.1	124.0	0.48	2.9	-	-	-	0.36	39.8
B _{0.4} D ₀	1.46	384	637	27.7	32.5	0.85	14	-	-	-	0.31	44.9
B _{0.6} D ₀	2.80	864	283	21.1	20.2	1.05	21	-	-	-	0.31	41.5
B _{0.8} D ₀	3.77	1346	182	18.2	15.5	1.17	24	-	-	-	0.31	50.3
B ₀ D _{0.2}	0.92	305	802	29.9	37.2	0.80	22	16	0.02	1.76	0.96	322
B ₀ D _{0.4}	6.36	1323	185	18.3	15.7	1.17	48	197	3.49	1.41	0.83	319
B ₀ D _{0.6}	11.4	2011	122	15.9	12.3	1.30	49	510	26.5	0.90	0.69	320
B ₀ D _{0.8}	16.9	2957	83	14.0	9.78	1.43	54	1272	731	0.67	0.55	320
B _{0.6} D _{0.2}	4.73	1726	142	16.8	13.4	1.25	31	63	-	0.03	0.31	315
B _{0.4} D _{0.4}	8.34	2012	122	15.9	12.3	1.30	37	183	-	0.05	0.29	311
B _{0.2} D _{0.6}	12.6	2476	99	14.9	10.9	1.37	45	561	-	0.14	0.30	320
B _{0.1} D _{0.4}	7.23	1496	163	17.6	14.6	1.20	43	219	-	0.46	0.46	317

^aThe molecular weight of partial chains $M_l = cRT/G_N^0$ with c the concentration of acrylamide monomers (g m⁻³).

^bUsing the effective crosslink number density $n = G_N^0/(2k_B T)$, $l = n^{-1/3}$.

^c $R_F \sim a_m N^{0.588}$ with $a_m \approx 0.154$ nm the C-C bond length and $N = M_l/M$ the number of repeating units between crosslinks (M is the molecular weight of a repeating unit).

^d $G_{Nideal}^0 = 2n_{(DNA+bis)}k_B T$ (ideal affine network).

^eExponents for G' and G'' are obtained from 4–8 data points in the low-frequency regime of master spectra.

Table 4.3: Best-fit parameters for the Burgers model and Weibull function at 21°C.

Sample	G_M (kPa)	η_M (kPa·s)	G_K (kPa)	η_K (kPa·s)	τ (s)	J_0/J_{tot} (%)	J_∞/J_{tot} (%)
B ₀ D _{0.2}	0.28	5.12	0.069	5.29	76.7	1.86	88.1
B ₀ D _{0.4}	1.01	181	0.58	56.5	97.8	13.1	42.2
B ₀ D _{0.6}	1.64	642	1.64	176	107	23.6	21.0
B ₀ D _{0.8}	2.45	1642	4.42	439	99.3	35.1	18.7
B _{0.6} D _{0.2}	1.62	6278	2.93	65.5	22.3	57.4	2.67
B _{0.4} D _{0.4}	1.72	2043	1.71	114	66.6	37.2	2.73
B _{0.2} D _{0.6}	2.15	1403	2.51	263	105	31.5	9.52
B _{0.1} D _{0.4}	1.17	309	0.73	70.8	97.0	16.9	22.1

Appendix

4.A Detailed protocols for DNA- and dual-crosslinked hydrogel synthesis and rheology

DNA- and dual-crosslinked hydrogel synthesis

1. Prepare “LinkerAdap” DNA strand, acrydite-modified DNA Strand A, and acrydite-modified DNA Strand B as 5 mM solutions in DNA suspension buffer (10 mM Tris-HCl, 0.1 mM EDTA, pH 8.0).
2. Use a vortex mixer to dissolve lyophilized DNA. Centrifuge the tubes containing DNA solution at $\approx 2,300 \times g$ (4,500 rpm for Sorvall Primo Centrifuge, Thermo Scientific) for 3 min to collect liquid transferred to the tube wall. Store DNA solutions at 4°C (long-term storage should be undertaken at -20°C).
3. Using disposable transfer pipettes, take about 2 ml of 40% w/v acrylamide and 2 ml of 2% w/v bis-acrylamide stock solutions stored at 4°C . Wait ≈ 40 min for the solutions to reach room temperature.
4. Prepare the rheometer according to the instrument manual.
5. Prepare 800 μl of 0.25% w/v bis-acrylamide solution by mixing 100 μl of 2% w/v bis-acrylamide solution and 700 μl of RO water. Vortex mix the solutions for 10 s.
6. Add different volumes of Strand A, Strand B, and “LinkerAdap” solutions as well as DNA suspension buffer (see table 4.A.1) to a centrifuge tube and stir it for 10 s.
7. Wait 2 min for the three DNA strands to combine.
8. Add 72.4 μl of 40% w/v acrylamide and appropriate volumes of 0.25% w/v bis-acrylamide solution (see table 4.A.1) to the centrifuge tube. Note that for “LinkerAdap” strand used for this study, only $\approx 71\%$ of the strands are full-length. The remaining 29% would be a mixture of truncated strands with deletions on their 5’

end. For acrydite-modified Strand A and Strand B, $\approx 89\%$ of the strands are full-length. Therefore, the concentrations of DNA crosslinkers with complete structures are smaller than what are shown in table 4.1. HPLC purification is recommended for future studies.

9. Cover the centrifuge tube with masking tape to reduce evaporation during degassing. Insert a $100\ \mu\text{l}$ pipette tip attached to a nitrogen gas cylinder to the mixture and bubble nitrogen through the mixture (at 0.4 SFPH) for 5 min to remove dissolved oxygen.
10. Centrifuge the tube at $\approx 1,000 \times g$ (3,000 rpm for Sorvall Primo Centrifuge, Thermo Scientific) for 2 min to collect liquid transferred to the tube wall during degassing. The remained solution has a volume $\approx 270\ \mu\text{l}$. Do not shake the tube afterwards to avoid the solution attaching to the tube wall.
11. Weigh 0.05 g APS powder in a glass vial and add $500\ \mu\text{l}$ of RO water to form a 10% APS solution. Vortex mix the solution for 20 s.
12. Add $2.7\ \mu\text{l}$ of the 10% APS solution to the tube and blend the mixture with the pipette tip 30 times.
13. Add $0.96\ \mu\text{l}$ of TEMED to the tube and blend the mixture with a $1000\ \mu\text{l}$ pipette tip 10 times. Deposit $270\ \mu\text{l}$ of the mixture onto the bottom plate of the parallel-plate sample holder. Note that an extra 10% mixture volume is required to ensure the correct filling of the mixture between the parallel plates.
14. Apply a 2 rad/s angular velocity to the bottom plate to achieve even spreading of the pre-gel solution and remove bubbles. Lower the top plate to achieve a 0.5 mm gap with the “evaporation blocker”.
15. Measure gelation kinetics by subjecting the sample to a prescribed oscillatory strain. After ≈ 660 s, apply silicone oil to the sample edges using a disposable transfer pipette.

The setting of experimental procedures

1. Gelation kinetics: The temperature during gelation was set to 21°C . A *conditioning options step* that maintains a constant axial force of 0 N with a sensitivity of 0.01 N during gelation was set before an *oscillation time step*. This step can make the upper plate adjust itself to avoid compression or tension on the sample during its transition from a liquid to solid. This decreases the number of G' and G'' data points acquired

during gelation, because the adjustment requires additional time. During the *oscillation time step*, the angular frequency was set to $\omega = 1 \text{ rad s}^{-1}$ with strain amplitude $\gamma = 1\%$ to achieve a linear viscoelastic response. Measurements were terminated when dynamic moduli settled to steady values ($\approx 9000 \text{ s}$).

2. Time-temperature superposition: An average expansion coefficient ($\approx 2.9 \mu\text{m}/^\circ\text{C}$) that is the sum of the geometry thermal expansion coefficient and the linear thermal expansion coefficient of water. The *move stage to maintain starting gap* box was checked, thereby the upper plate can rise with increasing temperature to avoid compression or tension on the sample. During the *oscillation temperature sweep step*, the soak time was set to 600 s for the gel equilibrium at each temperature. Frequency sweeps were performed in the range $\omega = 0.1\text{--}100 \text{ rad s}^{-1}$ with $\gamma = 1\%$. Temperatures from 21 to 56°C were used with the temperature step 2.5°C.
3. Post time-temperature superposition: The temperature was reduced to 21°C with a 1200 s soak time to achieve thermal equilibrium. The same expansion coefficient used for TTS was set during the temperature reduction. A frequency sweep $\omega = 0.1\text{--}100 \text{ rad s}^{-1}$ with $\gamma = 1\%$ was performed afterwards.
4. Creep-recovery test: 480 s equilibrium time with a *locked* motor state was set during *conditioning transducer step* to ensure complete stress relaxation. The soft gel with $G_N^0 \approx 300 \text{ Pa}$ may need a longer equilibrium time. The *transducer zeroing* box should be checked and the *transducer zero time* was set to *precision*. The *conditioning stress control step* was followed so the motor displacement achieves the desired stress. A *step (transient) creep step* was set afterward with the *duration time* for the creep test selected to be 900 s to achieve a strain and stress in the linear viscoelastic regime. A *step (transient) creep step* without stress was then set for the sample recovery.

4.B Dynamic moduli spectra of gels before and after time-temperature superposition

Since creep-recovery tests were undertaken after TTS, moduli spectra for the gels after the temperature reaching equilibrium at 21°C were monitored. It is found that for bis-crosslinked gels, there is no significant influence of temperature increase and decrease on the gel dynamic moduli spectra. However, for DNA- and dual-crosslinked gels, the elastic

Table 4.A.1: Solution volumes for DNA- and dual-crosslinked gel synthesis.

Sample	40% w/v acrylamide (μl)	5 mM DNA ^a (μl)	0.25% w/v bis-acrylamide (μl)	Buffer (μl)
B ₀ D _{0.2}	72.4	16.2	0	169.0
B ₀ D _{0.4}	72.4	32.4	0	120.4
B ₀ D _{0.6}	72.4	48.6	0	71.8
B ₀ D _{0.8}	72.4	64.8	0	23.2
B _{0.6} D _{0.2}	72.4	16.2	15.0	154.0
B _{0.4} D _{0.4}	72.4	32.4	10.0	110.4
B _{0.2} D _{0.6}	72.4	48.6	5.02	66.78
B _{0.1} D _{0.4}	72.4	32.4	2.50	117.9

^aEqual volumes of “LinkerAdap”, Strand A, and Strand B

modulus at $\omega = 0.1 \text{ rad s}^{-1}$ decreases by 3.4–24.5% after TTS, suggesting that not all of the physical crosslinks dissociated when increasing temperature can re-form. Moreover, since an average expansion coefficient is set for TTS, there might be compression or tension applied to the samples, imparting creep to physical gels, reducing G' and G'' .

4.C Experimental condition effect on dynamic moduli spectra and time-temperature superposition

It is found that the sample thickness for the rheological tests has influences on TTS for DNA-crosslinked gels. Figure 4.C.1 shows that with the increase of gap thickness, the upturn in the G'' spectrum is enhanced. This may be because the thin gap confines the relaxation of partial chains having branches in the solvent. Arrhenius plots of DNA-crosslinked gels with different sample thicknesses and/or TEMED concentrations are shown in the bottom-right panel of figure 4.C.1. The activation energies are close to each other. The TEMED concentration used to polymerize the gels as the accelerator affects the frequency at which G' is considered the plateau modulus (figure 4.C.2). It is shown that with less TEMED, this frequency is lower for both DNA- and dual-crosslinked gels. This may be because the reptation of polymer chains in the network formed with less TEMED is more pronounced. Furthermore, the coexistence of bis-acrylamide crosslinks has little influence on the frequency.

The method that maintains a constant force during TTS was applied to a DNA-crosslinked

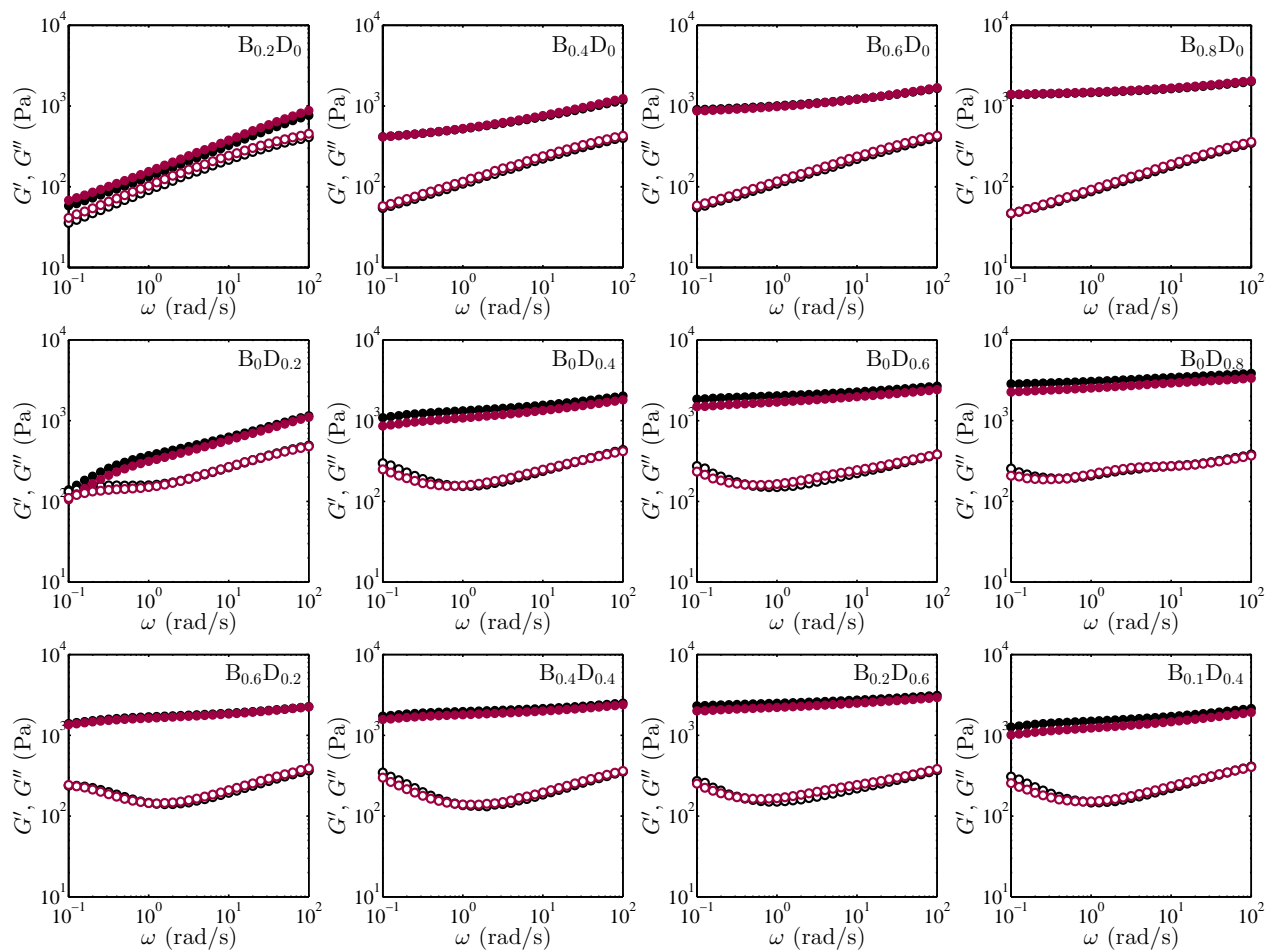


Figure 4.B.1: G' (filled) and G'' (open) spectra for bis-, DNA-, and dual-crosslinked gels at $T = 21^\circ\text{C}$ before (black) and after (red) TTS.

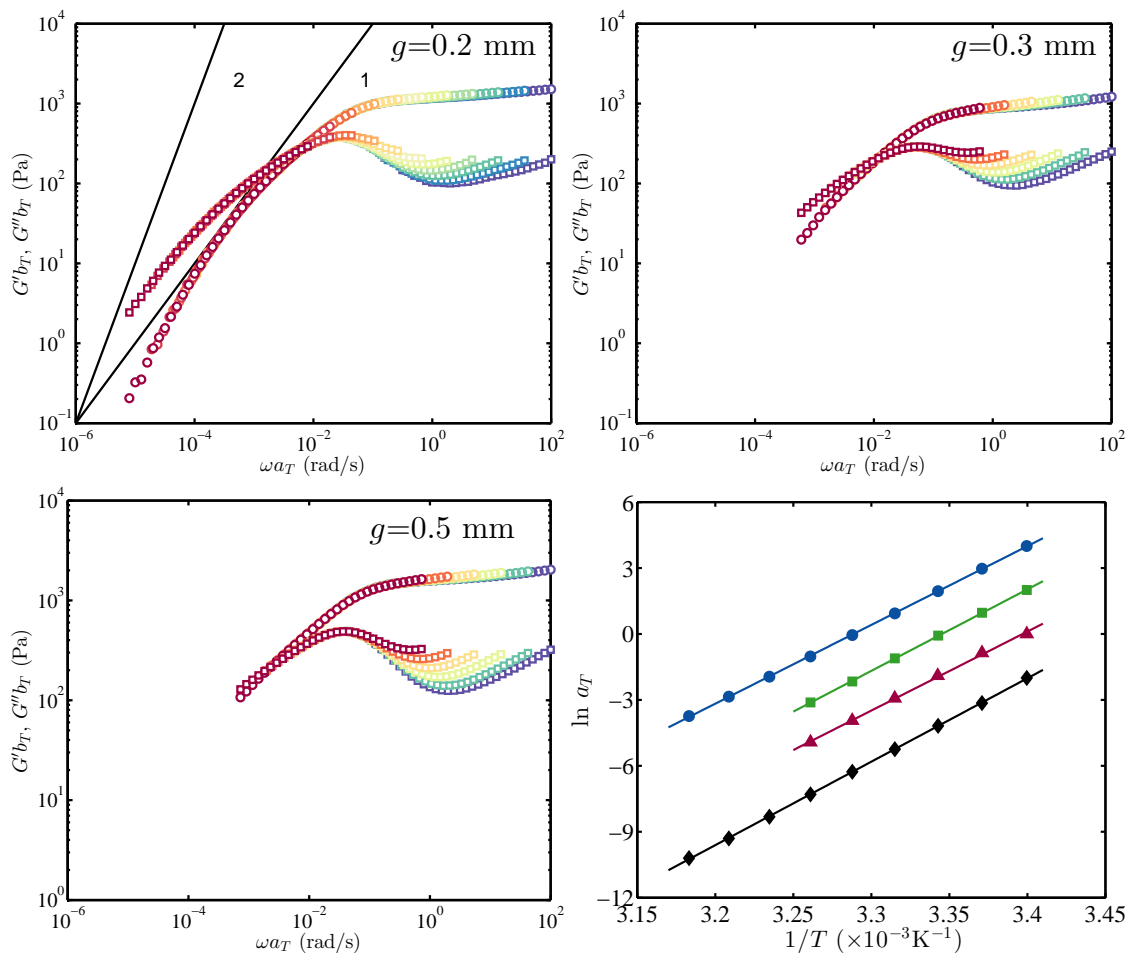


Figure 4.C.1: G' (circles) and G'' (squares) spectra for DNA-crosslinked gels with different sample gap thicknesses (top left, top right, and bottom left). Arrhenius plots (bottom right) for DNA-crosslinked gels with different sample gap thicknesses and/or TEMED concentrations (circles: $g = 0.2$ mm; squares: $g = 0.3$ mm; triangles: $g = 0.5$ mm; diamonds: $g = 0.5$ mm with lower TEMED concentration). An arbitrary factor 2 separates otherwise overlapping lines.

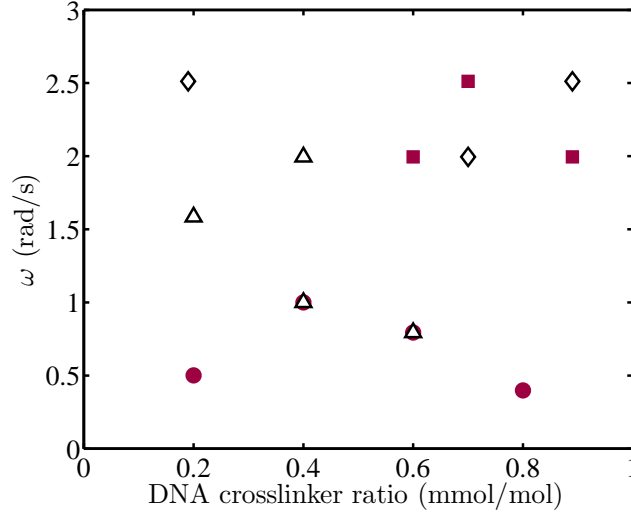


Figure 4.C.2: The angular velocity at which G'' is at the local minimum for DNA-crosslinked gels (circles), DNA-crosslinked gels with a high TEMED concentration (squares), dual-crosslinked gels (triangles), and dual-crosslinked gels with a high TEMED concentration (diamonds).

gel. However, the top-left panel of figure 4.C.3 shows that at a higher temperature, the rise of the rheometer head is insufficient because the gel softens. This could compress the gels and affect dynamic moduli spectra at higher temperatures, especially for softer DNA gels. The method that maintains a constant gap (see section 3.D) was adopted for DNA- and dual-crosslinked gels. The gap compensation factor was set as the sum of the average expansion coefficient obtained from calibration and the average linear expansion coefficient of water. Using this method, the upper plate rises according to the temperature increase. However, adopting the average value of the geometry and water expansion coefficient also introduce errors. For example, the gel actually expands less at the lower temperature, increasing the sample thicknesses used to calculate the moduli. Also, the upper plate may move up or down with respect to the position where the axial force is zero, imparting additional compression or tension. The bottom-left panel shows that the scaled effective number density of partial chains obtained using this method is smaller than the values from the method that maintains a constant force.

The bottom-right panel shows that peaks in G'' during the initial stage of gelation are sharper for gels formed with higher TEMED concentration. This is because the higher concentration of TEMED accelerates polymerization, forming more local clusters with higher viscosity. The viscosity decreases when those clusters connect to the continuous network.

However, with a lower concentration of TEMED, polymer-chain growth and the connection of clusters to the network occur at the same time, which smooth peaks in G'' .

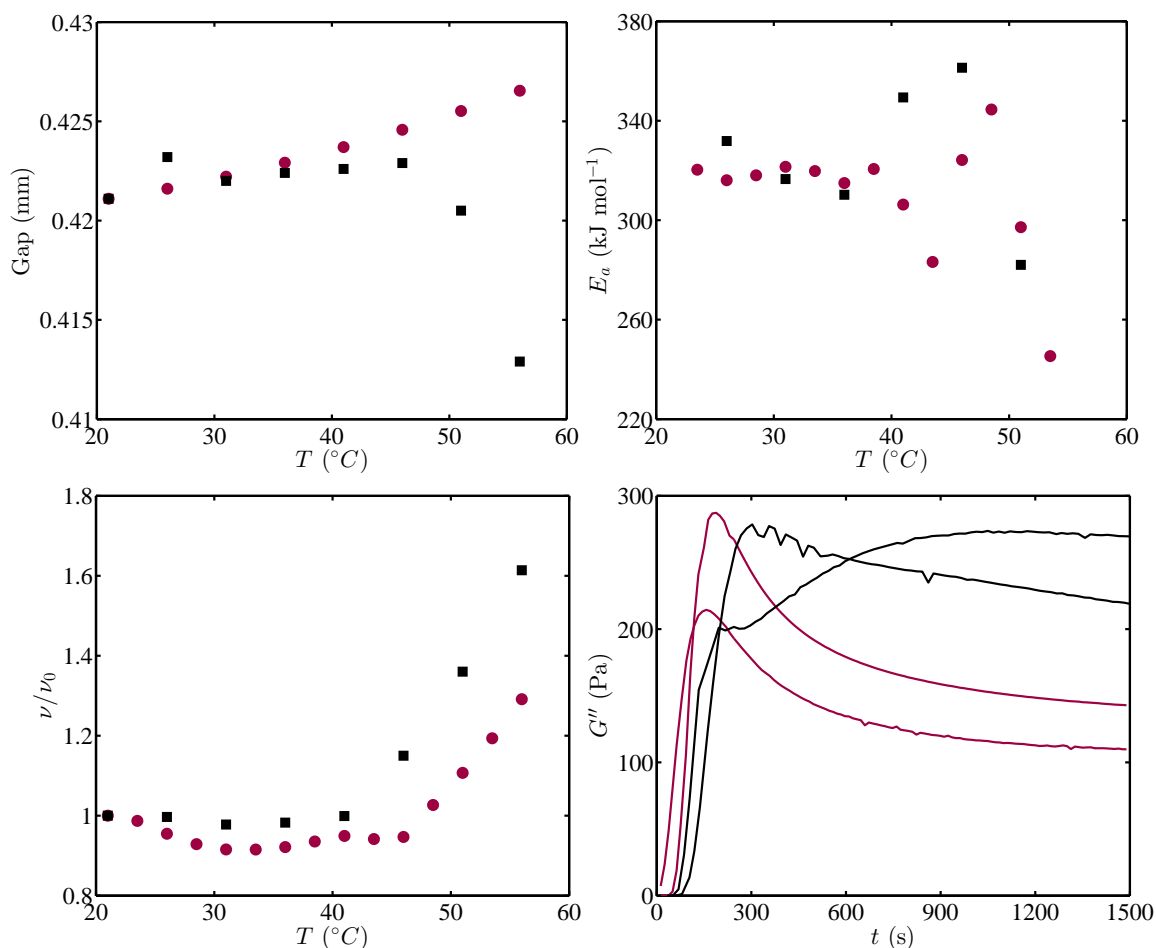


Figure 4.C.3: Top left: Comparisons of gaps obtained from subtracting gap compensation factors at difference temperatures from the apparent gaps under a constant force (squares) and gaps obtained according to the expansion of water for a DNA-crosslinked gel (circles). Comparison of the apparent activation energy (top right) and scaled effective number density of partial chains (bottom left) under a constant force (squares) and under a constant gap compensation factor (circles). Bottom right: G'' during gelation for pre-gel solution with a low (black) and high (red) TEMED concentration.

4.D Creep compliance model

The compliance during creep tests for bis-, DNA-, and dual-crosslinked gels are all fitted by the Burgers model in chapters 3 and 4, because it is more convenient to compare the fitting

parameters. However, for more solid-like gels, such as bis-crosslinked and dual-crosslinked gels with a smaller ratio $c_{\text{DNA}}/c_{\text{bis}}$, the Burgers model is not quite suitable for creep in the probed time range. It is found that fitting the creep data with one Maxwell element in series with two Kelvin-Voigt elements

$$J(t) = J_0' + \frac{1}{\eta_{M'}}t + \frac{1}{G_{K1}}(1 - e^{-t/\tau_1}) + \frac{1}{G_{K2}}(1 - e^{-t/\tau_2}) \quad (4.1)$$

yields smaller squared 2-norm of the residual, as shown in figure 4.D.1. Table 4.D.1 shows parameters extracted from the two models. It is found that η_M obtained with one Maxwell element in series with two Kelvin-Voigt elements is larger than from the Burgers model, showing a smaller irrecoverable compliance. Also, the modulus of the Kelvin-Voigt spring increases, indicating a better description of elasticity at long times. The retardation time from the Burgers model is between the two retardation times obtained from Eqn. (4.1). According to Barry¹⁴³, because breaking and reforming of secondary bonds do not occur at the same rate, a spectrum of retardation times exists. For bis-crosslinked gels, the distribution of the retardation time may be caused by the different fluctuation rates of entanglements and partial chains. For dual-crosslinked gels, the two retardation times may represent the permanent crosslinks and transient crosslinks.

Table 4.D.1: Best-fit parameters for two creep models: Eqn. (3.9) and Eqn. (4.1).

Sample	G_M (kPa)	η_M (kPa s)	G_K (kPa)	τ (s)	$G_{M'}$ (kPa)	$\eta_{M'}$ (kPa s)	G_{K1} (kPa)	τ_1 (s)	G_{K2} (kPa)	τ_2 (s)
B _{0.8} D ₀	1.47	8000	23.2	5.90	1.48	12930	35.1	17.7	38.2	1.90
B _{0.4} D _{0.4}	1.72	2043	1.71	66.6	1.78	3014	1.78	123	6.70	13.2

4.E Transformation between creep compliance and dynamic moduli spectra

Figures 4.E.1 and 4.E.2 show that for DNA- and dual-crosslinked gels, G' and G'' transformed from the creep compliance are smaller than those obtained from TTS. This is because the moduli decrease after TTS, as shown in appendix 4.B. However, their qualitative shapes are similar, demonstrating that it is reasonable to overlap dynamic moduli spectra at low frequency in TTS. Like bis-crosslinked gels, G'' transformed from creep compliance at higher frequencies is also significantly higher than the directly measured loss moduli.

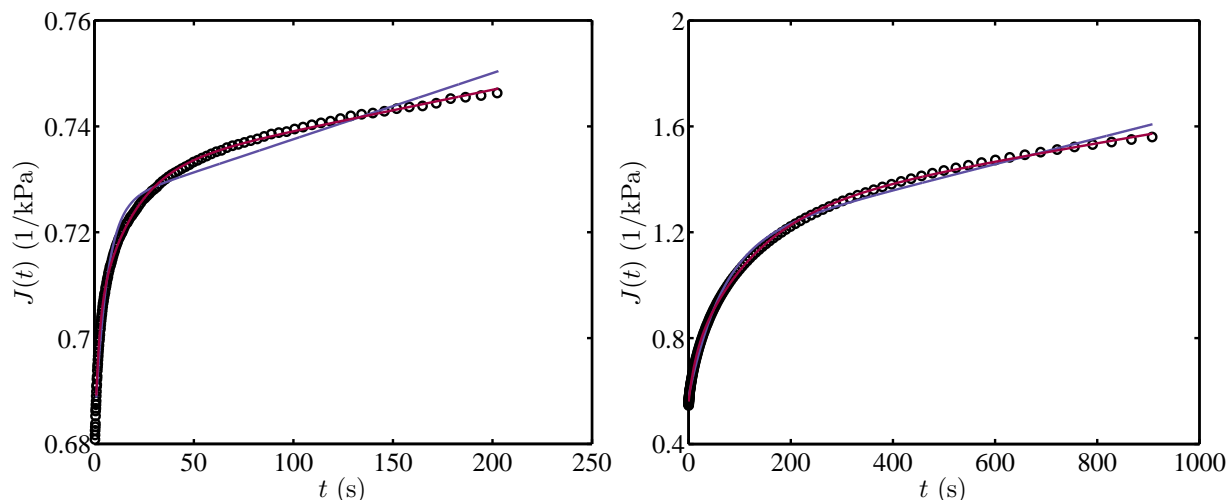


Figure 4.D.1: Creep for a bis-crosslinked $B_{0.8}D_0$ (left) and a dual-crosslinked $B_{0.4}D_{0.4}$ (right) gels fitted by one Maxwell element in series with one Kelvin-Voigt element (violet) and one Maxwell element in series with two Kelvin-Voigt elements (red) at $T = 21^\circ\text{C}$.

4.F Strain-sweep test

Strain-sweep tests with $\gamma = 0.1\text{--}100\%$ were undertaken with bis-, DNA-, and dual-crosslinked gels after creep-recovery tests (figure 4.F.1). G' and G'' are both initially constant, indicating that the strain is in the linear viscoelastic region, and then G' decrease with increasing strain. The decrease occurs at a smaller strain for bis-crosslinked or DNA-crosslinked gels with a larger G' . Moreover, the decrease occurs at larger strains for DNA-crosslinked gels than for bis-crosslinked gels with similar G' , which can be confirmed by that G' of $B_{0.6}D_{0.2}$ decreases at a smaller strain compared to other dual-crosslinked gels. This may be because the two types of gels have different microstructure changes under larger strains. Stress versus strain in the linear viscoelastic regime are shown in figure 4.F.2. With a decrease in the loss tangent at short times, the area under the curves decreases, indicating more solid-like properties.

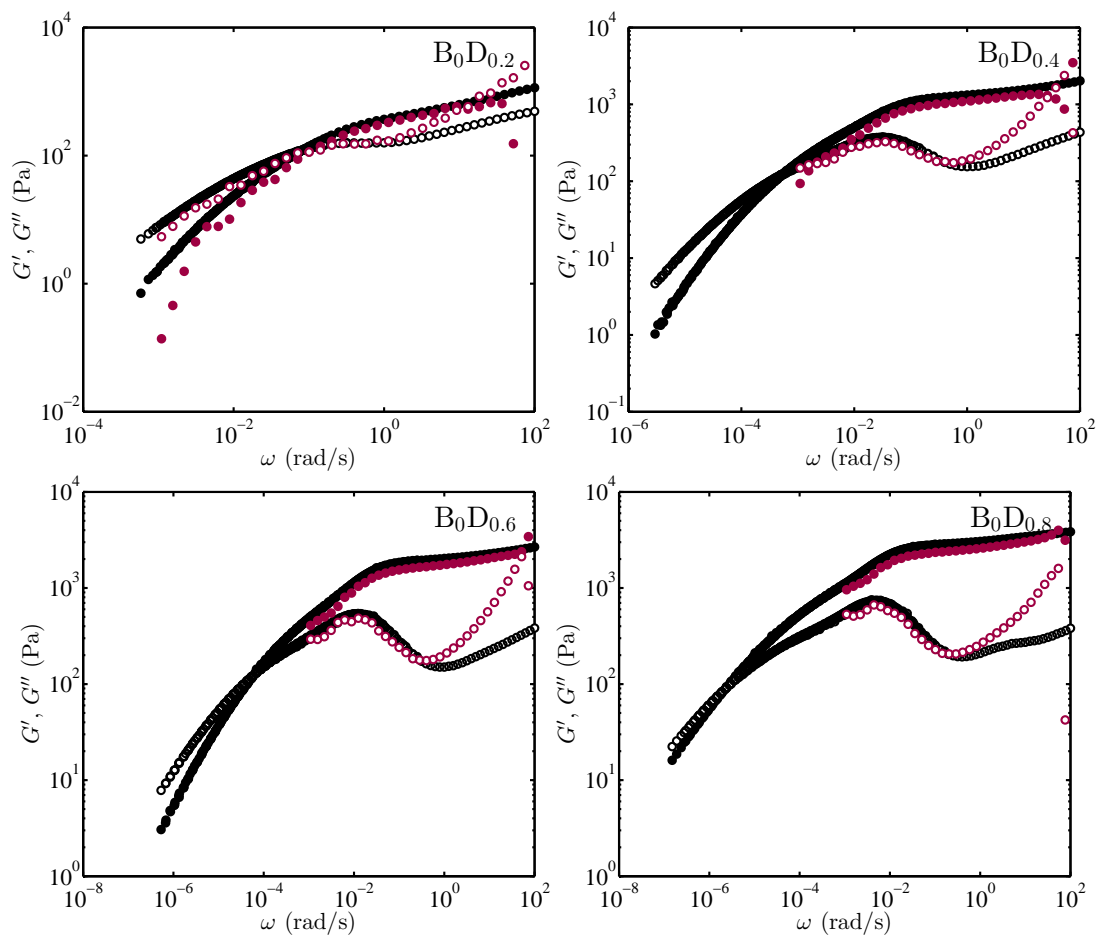


Figure 4.E.1: Comparison of G' (filled) and G'' (open) spectra obtained from TTS (black) and Fourier transformation of creep compliance data (red) for DNA-crosslinked gels.

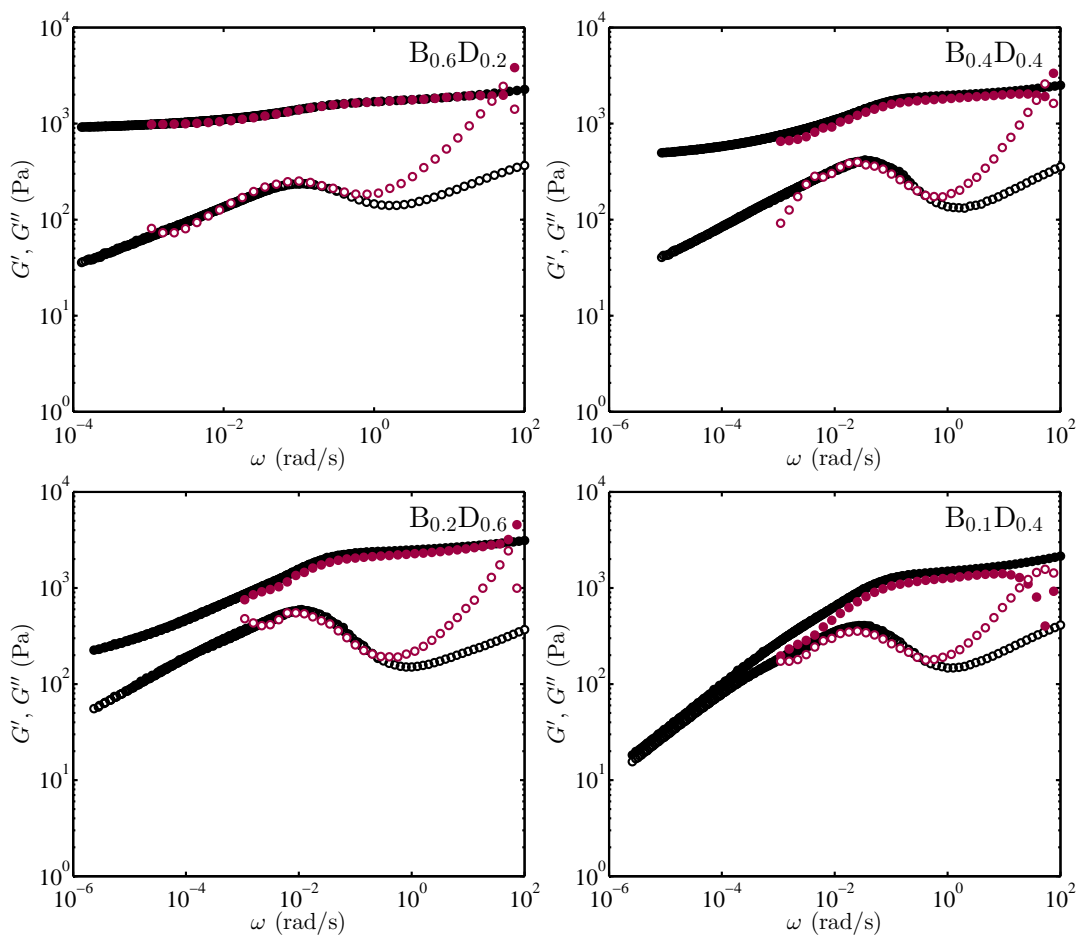


Figure 4.E.2: Comparison of G' (filled) and G'' (open) spectra obtained from TTS (black) and Fourier transformation of creep compliance data (red) for dual-crosslinked gels.

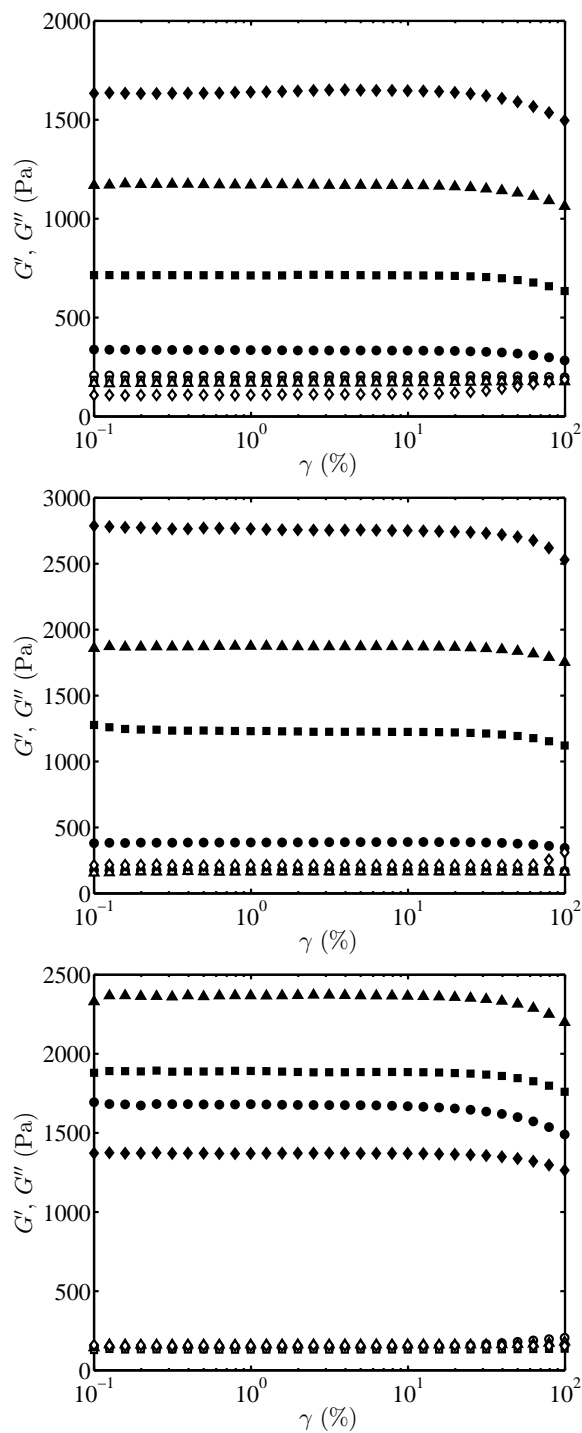


Figure 4.F.1: Strain-sweep tests performed at $\omega = 6.28$ rad/s for bis-crosslinked gel samples $B_{0.2}D_0$ (circle), $B_{0.4}D_0$ (squares), $B_{0.6}D_0$ (triangles), and $B_{0.8}D_0$ (diamonds); at $\omega = 1$ rad/s for DNA-crosslinked gel samples $B_0D_{0.2}$ (circles), $B_0D_{0.4}$ (squares), $B_0D_{0.6}$ (triangles), and $B_0D_{0.8}$ (diamonds); at $\omega = 1$ rad/s for dual-crosslinked gel samples $B_{0.6}D_{0.2}$ (circle), $B_{0.4}D_{0.4}$ (squares), $B_{0.2}D_{0.6}$ (triangles), and $B_{0.1}D_{0.4}$ (diamonds) at $T = 21^\circ\text{C}$.

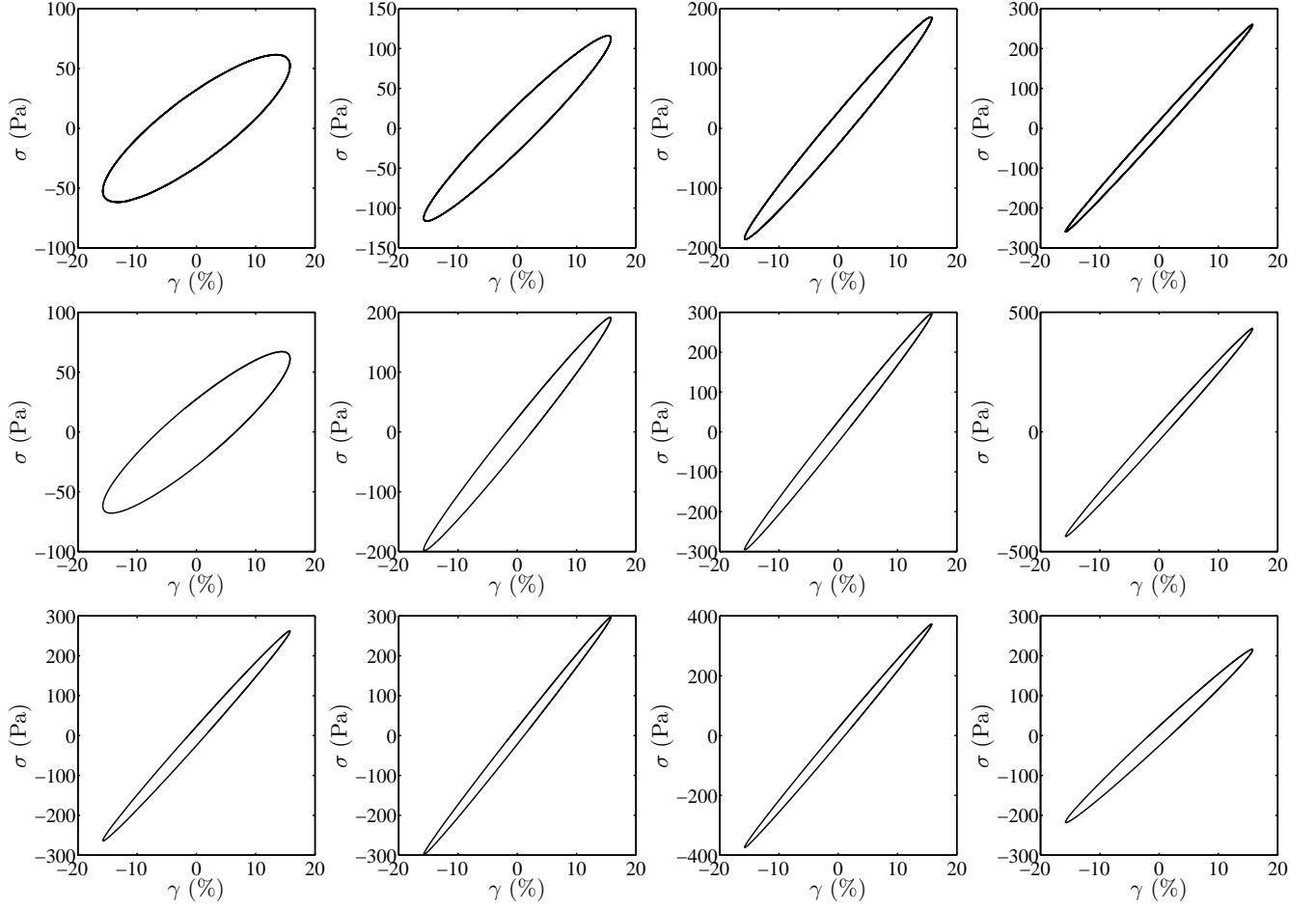


Figure 4.F.2: Stress versus strain during oscillatory cycles in the linear viscoelastic region at $T = 21^\circ\text{C}$. Top row from left to right: bis-crosslinked gel samples from $B_{0.2}D_0$ to $B_{0.8}D_0$; middle row from left to right: DNA-crosslinked gel samples from $B_0D_{0.2}$ to $B_0D_{0.8}$; bottom row from left to right: dual-crosslinked gel samples $B_{0.6}D_{0.2}$, $B_{0.4}D_{0.4}$, $B_{0.2}D_{0.6}$, $B_{0.1}D_{0.4}$.

Swelling of complementary-DNA-strand crosslinked polyacrylamide hydrogels

5.1 Preface

Unlike bis-acrylamide crosslinked gels, the swelling of physically crosslinked gels is not well understood. In this chapter, the swelling of DNA-crosslinked polyacrylamide gels with and without chemical/covalent bis-crosslinking is studied. DNA-crosslinked gels dissolve, and the swelling ratio (prior to dissolution) increases with the gel plateau modulus. This is interpreted by DNA crosslinks dissociating during swelling, further enhancing the swelling ability. The release of DNA strands to the buffer during swelling is identified by UV-vis spectroscopy. For dual-crosslinked gels, permanent crosslinks prevent gel dissolution, while the dissociation of DNA crosslinks imparts a larger swelling ratio than bis-crosslinked gels with the same plateau modulus. The hydrodynamic pore sizes obtained from swelling, and mesh sizes from the plateau modulus, are of the same order of magnitude. A theoretical interpretation incorporating a DNA crosslink formation probability was undertaken to establish the relationship between the bond energy of a crosslink, the polymer-solvent interaction parameter, plateau modulus, and equilibrium swelling ratio. With rheological studies in chapter 4, mechanical properties and microstructures of the gels were examined. These pave the way for future applications in drug delivery and biosensing.

5.2 Introduction

Hydrogels *swell* in solvents, but are generally not considered to *dissolve*, even in good solvents. According to the Flory-Rehner theory, a cross-linked polymer expands by a polymer-solvent mixing force that is resisted by the network elasticity. Gerlach and Arndt²⁹ showed the Flory–Rehner equation describing isotropic swelling of an uncharged gel from a dry/solvent-free state. If an uncharged gel is initially in a hydrated state and assumed to deform as a localized-phantom-network, then the equilibrium swelling ratio satisfies

$$G_N^0 \left(\frac{1}{S}\right)^{1/3} = -\frac{k_B T}{\Omega} \left[\ln \left(1 - \frac{\phi_0}{S}\right) + \frac{\phi_0}{S} + \chi \left(\frac{\phi_0}{S}\right)^2 \right], \quad (5.1)$$

where G_N^0 and ϕ_0 are the plateau modulus and polymer volume fraction (in the initial, as-prepared state), S is the equilibrium volume swelling ratio, Ω is the volume of a solvent molecule, χ is the Flory-Huggins interaction parameter, and $k_B T$ is the thermal energy. Note that charge on the polymer backbone and ions in the solvent significantly influence the swelling capacity^{94,29}.

Comparing swelling experiments with the foregoing theory has established that χ for polyacrylamide (PA) gels decreases with increasing temperature in the range 10–30°C⁹⁰. This is because polyacrylamide solutions have an upper critical solution temperature (UCST) below 0°C and do not have a lower critical solution temperature (LCST) below 100°C^{144,145}. Also, χ has been found to be smaller for softer gels, with a transition from good- to poor-solvent behaviour when increasing the polymer volume fraction^{89,90}. In the Flory-Huggins theory of polymer-solvent mixing, the number of monomers per polymer chain cannot be assumed infinite as for gels. Thus, χ ascertained from the Flory-Huggins model applied to polymer gels is slightly different than for polymer solutions⁸⁹.

In studies of the swelling of chemically-crosslinked gels, Tanaka and Fillmore⁹⁵ found that the characteristic swelling time is proportional to the square of the linear dimension. The cooperative diffusion coefficient has been obtained from swelling experiments on gel cylinders and disks from the approach to equilibrium. These agree with values obtained from light-scattering spectroscopy^{96,97}. Biot’s theory of linear poroelasticity can describe swelling when the effect of fluid transport on the gel deformation is strong. This has been applied to free-standing and constrained hydrogel layers⁹⁸, showing that the time to reach equilibrium for a constrained gel is longer than for free swelling.

The foregoing theories are for gels crosslinked by permanent covalent bonds²³. For physical gels that have transient crosslinks, such as hydrogen bonds, ionic interactions, and helix

conformation, the swelling behaviour is more complicated. This is because the modulus has a different dependence on the swelling ratio⁶⁶. Some physical gels have been found to dissolve. For example, unassociated molecular chains in a gellan gel were released from gels placed in a large volume of distilled water, with the gels swelling infinitely so that they become completely dispersed^{43,23}. This can be suppressed by using an ionic solvent instead of distilled water. The electrostatic repulsion between negative groups (carboxyl) in gellan molecules is shielded by cations, such as calcium, promoting the formation of helix- and junction-zones¹⁴⁶. Poloxamer 407 gels crosslinked by micelle formation dissolve, because dilution of the polymer imparts a concentration below the critical-gelation concentration³⁰. Due to dilution and dispersion of gels, physically crosslinked hydrogels are limited to relatively short-acting drug delivery systems³⁰. Nevertheless, some physical gels do not dissolve. For example, Yang et al.¹⁴⁷ reported the swelling ratio of poly(acrylic acid) that is physically crosslinked by hydrophobic association and silica nanoparticles. These gels initially swell, reaching a plateau, and then deswell before reaching equilibrium. They attributed the swelling ratio decrease to leaching of un-reacted monomers and un-crosslinked polymers.

Swelling of dual-crosslinked gels is affected by both kinds of crosslinks. For example, Shibayama et al.⁵⁹ showed that increasing the borate-ion concentration in PVA dual-crosslinked gels first decreases the equilibrium swelling ratio because of the increase in crosslinking density. However, a further increase in the ion concentration increases swelling due to increasing intrachain electrostatic repulsion. Dual networks have been used to prolong drug release, *e.g.*, adding chemical crosslinks to gellan gels slows release¹⁴⁸.

DNA- and dual-crosslinked gels have demonstrated potential for drug delivery, tissue engineering, and biosensing^{11,12,13,14,15,16}. These gels are often required to reach equilibrium in a buffer before use. Thus, whether DNA-crosslinks dissociate is important for applications. Physical gels prepared by applying heating and cooling cycles to DNA solutions dissolve in water because swelling breaks physical crosslinks formed by hydrogen bonds between double-stranded DNA¹⁴⁹. A high concentration of salt (0.1 M) can slow this process and stabilize such gels for many days. When preparing polyacrylamide hydrogels crosslinked by complementary DNA strands¹⁵⁰, phosphate buffered saline (PBS) containing calcium and magnesium has been adopted as the buffer. Here, divalent cations in the buffer stabilize DNA hybridization. However, the reason for the hybridization instability and the influence of DNA-crosslinker concentration is unclear. A thermodynamic model has been developed to describe the phase transition of physical gels in the solvent, showing that gels with a smaller activation energy for crosslink disengagement and a smaller χ are easier to dissolve¹⁰¹.

However, swelling of DNA-crosslinked gels and the influence of permanent bis-acrylamide crosslinks on the swelling is presently unknown.

The pore size is important in many applications, and often reflects the gel microstructure. Among the many methods to determine the pore size, including permeability, swelling kinetics, light scattering, electron microscopy, rubber elasticity, equilibrium swelling theory, and electrophoresis⁴⁰, the pore size can vary significantly with the measurement method^{40,96,100,37}. Pore sizes of soft gels with a very low crosslinker ratio have not been widely reported.

In the present study, the swelling of DNA- and dual-crosslinked PA gels are studied in PBS to understand the swelling mechanism and ascertain the pore size. Figure 5.1 illustrates the proposed mechanism for DNA- and dual-crosslinked hydrogel swelling, with photos of dual-crosslinked gels before and after swelling. Gels with only chemical crosslinks are used as references, and to ascertain the χ parameter for the PA-solvent interaction. A theoretical interpretation is undertaken, introducing a phenomenological DNA-crosslink forming probability for swelling of DNA- and dual-crosslinked gels.

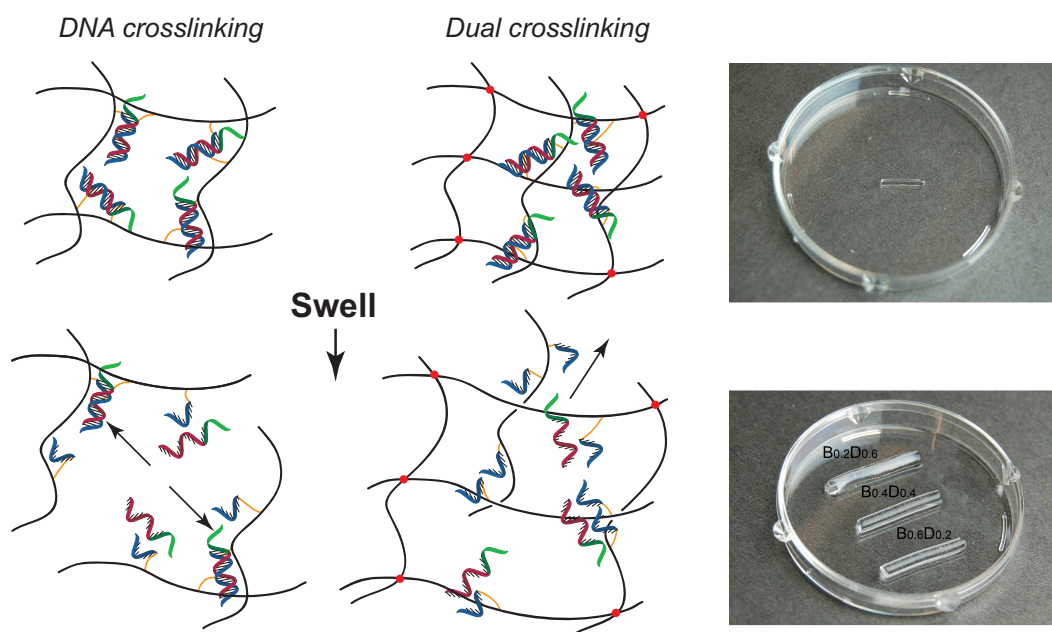


Figure 5.1: Schematics of DNA- and dual-crosslinked polyacrylamide hydrogel swelling, and dual-crosslinked polyacrylamide hydrogel cylinders before (top) and after (bottom) swelling.

5.3 Materials and methods

Acrylamide (40% w/v, Fisher Scientific), bis-acrylamide (2% w/v, Fisher Scientific), acrydite-modified oligonucleotides (standard desalting, Integrated DNA Technologies), ammonium persulfate (APS, $\geq 98\%$, Fisher Scientific), N,N,N',N' -tetramethylethylenediamine (TEMED, 99%, GE Healthcare Life Sciences), DNA suspension buffer (10 mM Tris-HCl, 0.1 mM EDTA, pH 8.0, Teknova), and Dulbecco's Phosphate Buffered Saline with calcium and magnesium (PBS, Sigma) were used as provided by the manufacturer.

The synthesis of bis-, DNA-, and dual-crosslinked hydrogels is according to the methods set out in chapters 3 and 4. Note that bis-crosslinked gels were synthesized by dissolving acrylamide powder in RO water instead of diluting the 40% acrylamide solution. The pre-gel solutions were injected into compliant Tygon S3TM plastic tubes: a 3/32" inner diameter for bis-crosslinked gels; and a 1/16" inner diameter for DNA- and dual-crosslinked gels, being careful to avoid trapping bubbles. Tape was used to seal the tube ends. After approximately 2.5 hours for gelation, cylindrical gels were gently squeezed from the tubes and cut using a razor blade into shorter cylinders having an aspect ratio ≈ 6.3 . Each cylinder was weighed on a petri dish. To prevent the gel breaking, PBS (volume ≈ 100 times the gel volume) was first poured into the petri dish, and then the liquid and cylinder were poured into a centrifuge tube. During the subsequent swelling, the gels were transferred back to the petri dish, weighed, and then transferred to a new centrifuge tube containing fresh PBS. This sequence was repeated for each gel until either a constant weight was achieved or the gel fractured, breaking into small pieces. Before weighing, PBS in the petri dish and on the gel surface was gently removed using a pipette with a 100 μl tip. The gels were too fragile to dry using tissue or filter paper. A lid on the petri dish was used to slow evaporation.

The mass swelling ratio is reported as

$$S_w(t) = \frac{m(t)}{m_0}, \quad (5.2)$$

where m_0 is the initial (as prepared) gel mass, and $m(t)$ is the gel mass after being immersed in PBS for a time t . The volume swelling ratio $S_v(t)$ can be calculated from $S_w(t)$ as detailed in appendix 5.C. PBS into which DNA- and dual-crosslinked gels were swollen was transferred to a quartz cuvette and scanned using an UV-vis spectrophotometer (Ultrospec 2100 pro) in the range 190–400 nm. The UV-vis spectra were compared with that for a blank containing only PBS. The concentration of DNA strands in each tube $c(t)$ was calculated from the absorbance at 260 nm according to Beer's law:

$$A = \epsilon cL, \quad (5.3)$$

where c is the concentration (mol l^{-1}) of DNA strands (c is the same for Strand A, Strand B, and “LinkerAdap”), ε is the sum of molar extinction coefficients for three DNA strands, and L is the path length. The accumulated concentration $c_a(t)$ was obtained by summing $c(t) = n_D/V_P$ at previous times, where n_D is the moles of released DNA and V_P is the PBS volume, which is the same at each t . V_P is assumed the same before and after immersing the gel. The fraction of DNA strands remaining in the gel is calculated as

$$P(t) = 1 - \frac{c_a(t)}{c_{tot}}, \quad (5.4)$$

where c_{tot} is the ratio of the total moles of DNA strands used to form a gel cylinder to the PBS volume V_P . Plateau moduli G_N^0 in the following sections were obtained from rheological tests performed on samples having the same composition. S_v and P for the gels were averaged from 4–5 samples and reported with error bars identifying the maximum and minimum values.

5.4 Results and discussion

5.4.1 Swelling of bis-crosslinked hydrogels

Figure 5.2 shows that bis-crosslinked gels swell and reach equilibrium. The volume swelling ratio at equilibrium decreases with increasing crosslinker ratio, showing that stiffer gels have a smaller swelling ratio, as expected from the Flory-Rehner theory. The main component in PBS is 0.14 M NaCl with 0.90 mM Ca^{2+} and 0.49 mM Mg^{2+} . The volume swelling ratio at equilibrium for bis-crosslinked gels in PBS is larger than in RO water, as shown in appendix 5.B.

For the isotropic swelling of a cylindrical gel with infinite length, swelling ratio near equilibrium is

$$S_v = \left[\frac{a}{r_0} + \left(1 - \frac{a}{r_0}\right) B e^{-t/\tau} \right]^3, \quad (\text{long times}) \quad (5.5)$$

where r_0 is the initial cylinder radius, $a = r_0 S_{eq}^{1/3}$ is the cylinder radius at equilibrium, τ is the swelling relaxation time, and B is a parameter related to the cooperative diffusion coefficient D ⁹⁶. Figure 5.2 shows that τ decreases with increasing G_N^0 , indicating that stiffer gels reach equilibrium faster, and stiffer gels have a larger diffusion coefficient because of the shorter partial chain.

For one-dimensional swelling of a thin rectangular gel, the thickness change can be used to estimate the cooperative diffusion coefficient in the initial stage of swelling via linear

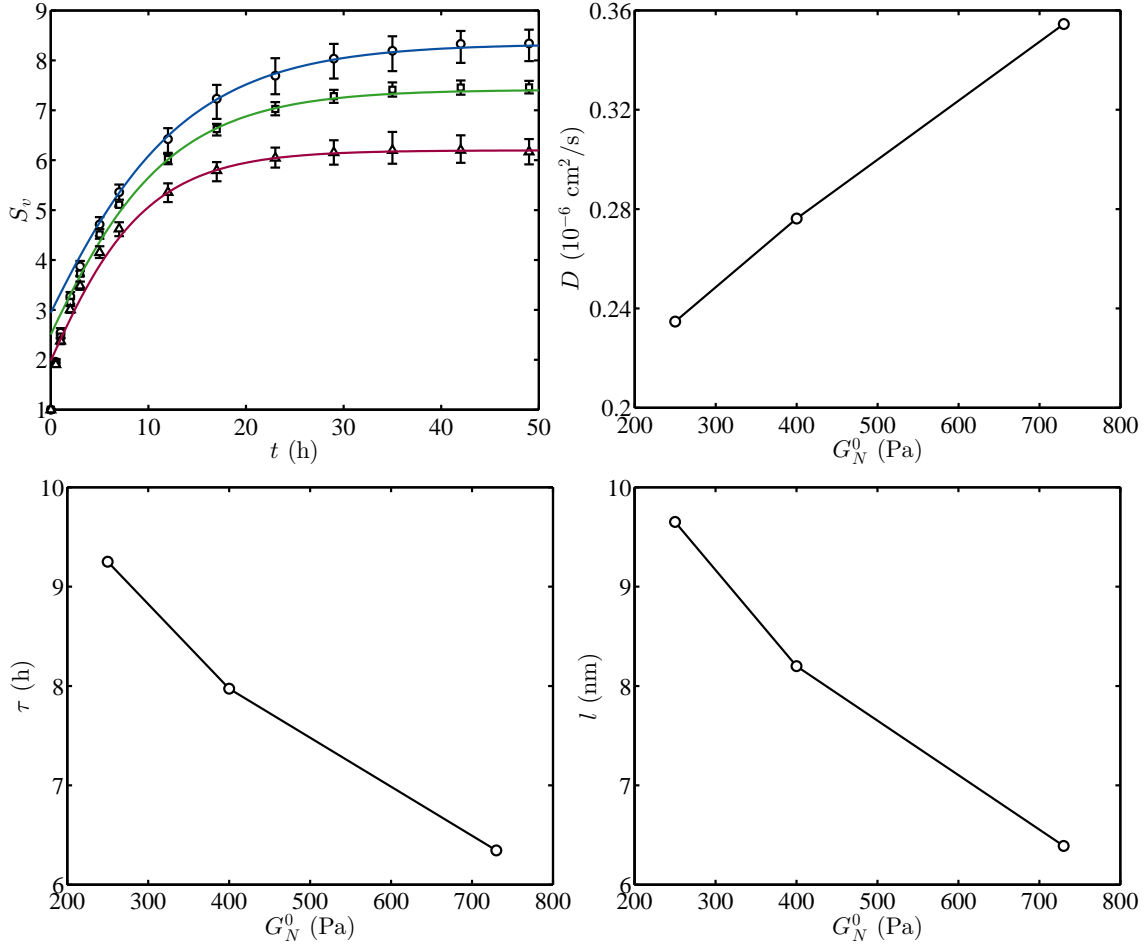


Figure 5.2: Top left: Swelling of bis-crosslinked gels with $G_N^0 = 250$ Pa (circles), $G_N^0 = 400$ Pa (squares), and $G_N^0 = 730$ Pa (triangles) in PBS. Lines are least-squares fits of Eqn. (5.5). Top right: Cooperative diffusion coefficient versus G_N^0 . Bottom left: Swelling relaxation time versus G_N^0 . Bottom right: Pore size from D in the top-right panel (Eqn. (5.7)) versus G_N^0 .

poroelastic theory⁹⁸. It has been shown that for gels with Poisson’s ratio $\nu \approx 0.33$, plots of $\Delta H(t)/H_0$ versus \sqrt{t}/H_0 for one-dimensional and three-dimensional swelling nearly overlap in the early swelling stage ($\Delta H(t)$: thickness change; H_0 : initial thickness). Also, $\Delta H(\infty)$ (thickness change at equilibrium) for constrained gels is $(1 + \nu)/(1 - \nu)$ times as large as that for free-standing gels. For a gel cylinder, it is assumed that the effect of sample geometry is negligible in the initial stage of swelling, permitting following equation to be used to estimate the cooperative diffusion coefficient (as shown in the top-left panel of figure 5.3):

$$\frac{r(t) - r_0}{r_0} = \frac{2(a - r_0)(1 + \nu)}{r_0^2(1 - \nu)} \sqrt{\frac{Dt}{\pi}}, \text{ (short times)} \quad (5.6)$$

where r_0 is the initial cylinder radius, a is the cylinder radius at equilibrium, and $r(t) = r_0 S_v(t)^{1/3}$.

Poisson’s ratio $\nu \approx 0.33$ has been reported from free-standing and constrained swelling of poly(*N*-isopropylacrylamide) gels with $G_N^0 \approx 1300$ Pa⁹⁸. However, ν obtained from mechanical tests of PA gels is often ≈ 0.5 ^{21,151,152}. Thus, both Poisson’s ratios are used to estimate the cooperative diffusion coefficient and hydrodynamic pore size. Figure 5.3 shows that the diffusion coefficient in the early swelling stage increases with the gel stiffness. The hydrodynamic pore size can be defined as

$$l = \frac{k_B T}{6\pi\eta D}, \quad (5.7)$$

where η is the solvent viscosity, and $k_B T$ is the thermal energy⁹⁶. As shown in the bottom panel of figure 5.3, the pore size obtained from the initial swelling stage is 1.5–5 times larger than the pore size near equilibrium stage. This may be because fluid displacement is not considered in Eqn. (5.5). Moreover, the mesh size obtained from G_N^0 , $l = (2k_B T/G_N^0)^{1/3}$, is between the pore sizes from the initial swelling stage when using $\nu = 0.33$ and $\nu = 0.5$. This is because gel networks are heterogenous, so there are differences between the hydrodynamic pore size from swelling and the distance between elastically effective crosslinks. For example, the solvent will prefer to flow through larger pores.

5.4.2 Swelling of DNA- and dual-crosslinked hydrogels

Unlike permanently crosslinked gels, the surface of the DNA-crosslinked gels at some stage of swelling becomes stickier and more viscous, with the appearance of cracks, indicating dissolution. Eventually, the cylinder fractures into small pieces, further accelerating dissolution. Note that after macroscopic dissolution, transfer of the gel between the centrifuge

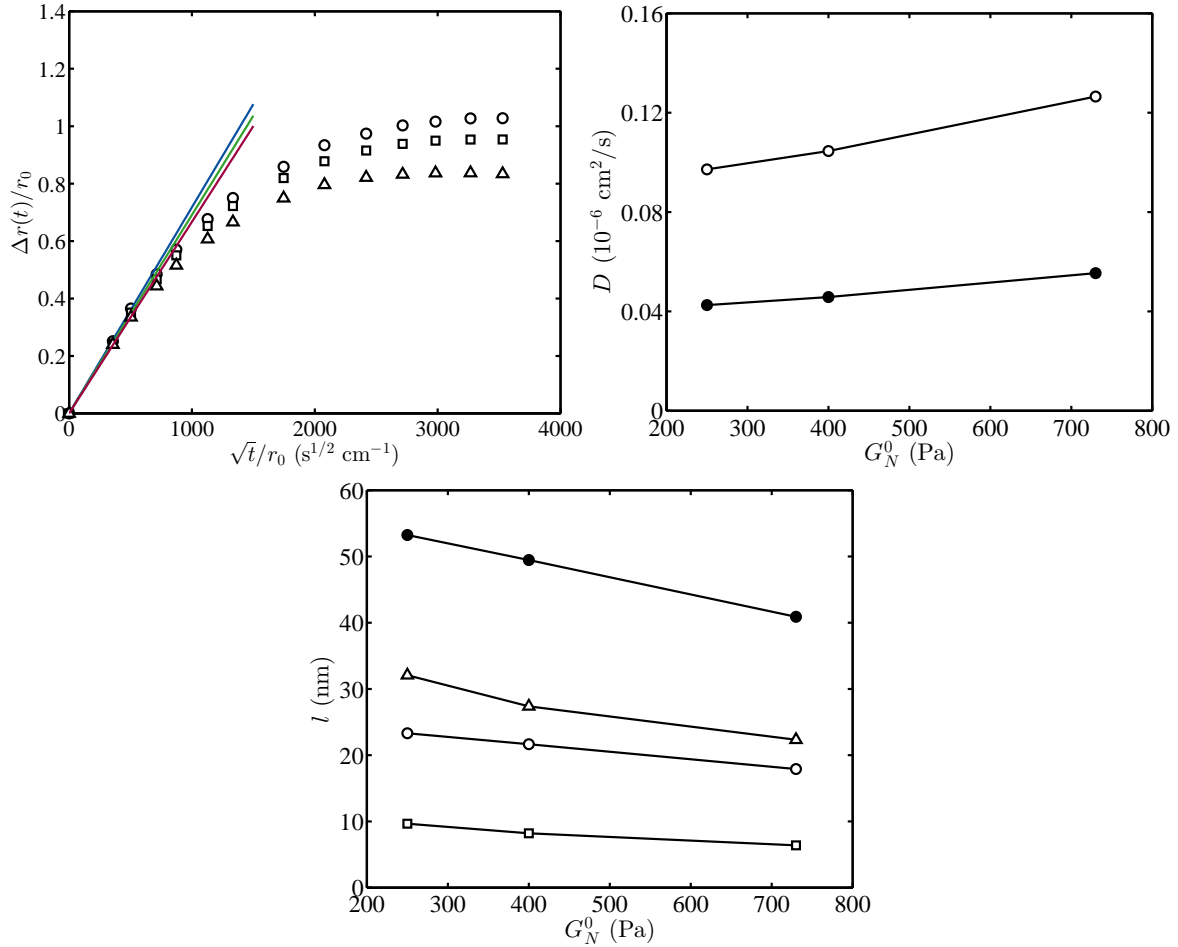


Figure 5.3: Top left: Fitting of Eqn. (5.6) to the initial stage of swelling $G_N^0 = 250$ Pa (circles and blue line), $G_N^0 = 400$ Pa (squares and green line), and $G_N^0 = 730$ Pa (triangles and red line). Top right: Cooperative diffusion coefficient calculated with $\nu = 0.33$ (open circles) and $\nu = 0.5$ (filled circles) versus G_N^0 . Bottom: Pore (mesh) size obtained from D in the top-right panel with $\nu = 0.33$ (open circles) and $\nu = 0.5$ (filled circles), from D in the top-right panel of figure 5.2 (squares), and from $l = (2k_B T / G_N^0)^{1/3}$ (triangles) versus G_N^0 .

tube and petri dish promotes fracture and dissolution. The dissolution of DNA-crosslinked gels in quiescent fluid, *i.e.* undisturbed, would be slower than shown below, because there is no advective enhancement of diffusive mass transfer.

Figure 5.4 shows that the volume swelling ratio for samples B₀D_{0.4}, B₀D_{0.6}, and B₀D_{0.8} in PBS initially increases, and then decreases until the gel mass can no longer be measured. An explanation for the dissolution is that as the distance between transient DNA crosslinks increases the probability for hydrogen-bond formation between DNA strands decreases, causing the gradual dissociation of DNA crosslinks and the release of polymer chains with Strand A and Strand B into the solvent. Because of the decrease in DNA crosslink concentration, the propensity of the gel to absorb solvent is enhanced by swelling, further increasing the dissociation, leading to complete dissolution. It is also shown that the dissolution slows with increasing DNA-crosslinker ratio. This may be because gels with a larger DNA-crosslinker ratio have a longer average crosslink lifetime.

To examine the swelling kinetics of DNA-crosslinked gels, the following empirical formula was fit to S_v versus t data before gel fracture:

$$S_v = S' - A_s e^{-t/\tau} + at, \quad (5.8)$$

where τ is the swelling relaxation time, S' is a constant, and A_s is the swelling amplitude. The parameter a quantifies the dissolution rate. The fits show that a increases with decreasing DNA-crosslinker ratio (0.20, 0.43, and 0.78 1/h), showing the softer DNA-crosslinked gels dissolve faster. The cooperative diffusion coefficient for DNA-crosslinked gels in the initial stage of swelling is obtained from Eqn. (5.6) and plotted in figure 5.5. Because gel dissolution is not prominent in the initial swelling stage, the gel radius at equilibrium for DNA-crosslinked gels is estimated by assuming the gels do not dissolve. Similarly to bis-crosslinked gels, D for DNA-crosslinked gels increases with the gel stiffness. Moreover, the relaxation time obtained from fitting the whole swelling curve before dissolution (Eqn. (5.8)) increases with the gel stiffness, which is opposite of bis-crosslinked gels. This is because softer gels require less time to fracture and dissolve. The mesh sizes of DNA-crosslinked gels obtained from rheological tests are close to hydrodynamic pore sizes calculated using $\nu = 0.5$.

Figure 5.6 shows the fraction $1 - P$ of DNA strands released to PBS. This is obtained from the absorbance of PBS at 260 nm (detailed in appendix 5.D). The ratio increases with time, suggesting that “LinkerAdap” DNA strands and polymer chains attached to DNA strands are gradually released. Before gel fracture, the release rate decreases with time. Note that in the initial swelling stage DNA strands that are not part of the network are released to the

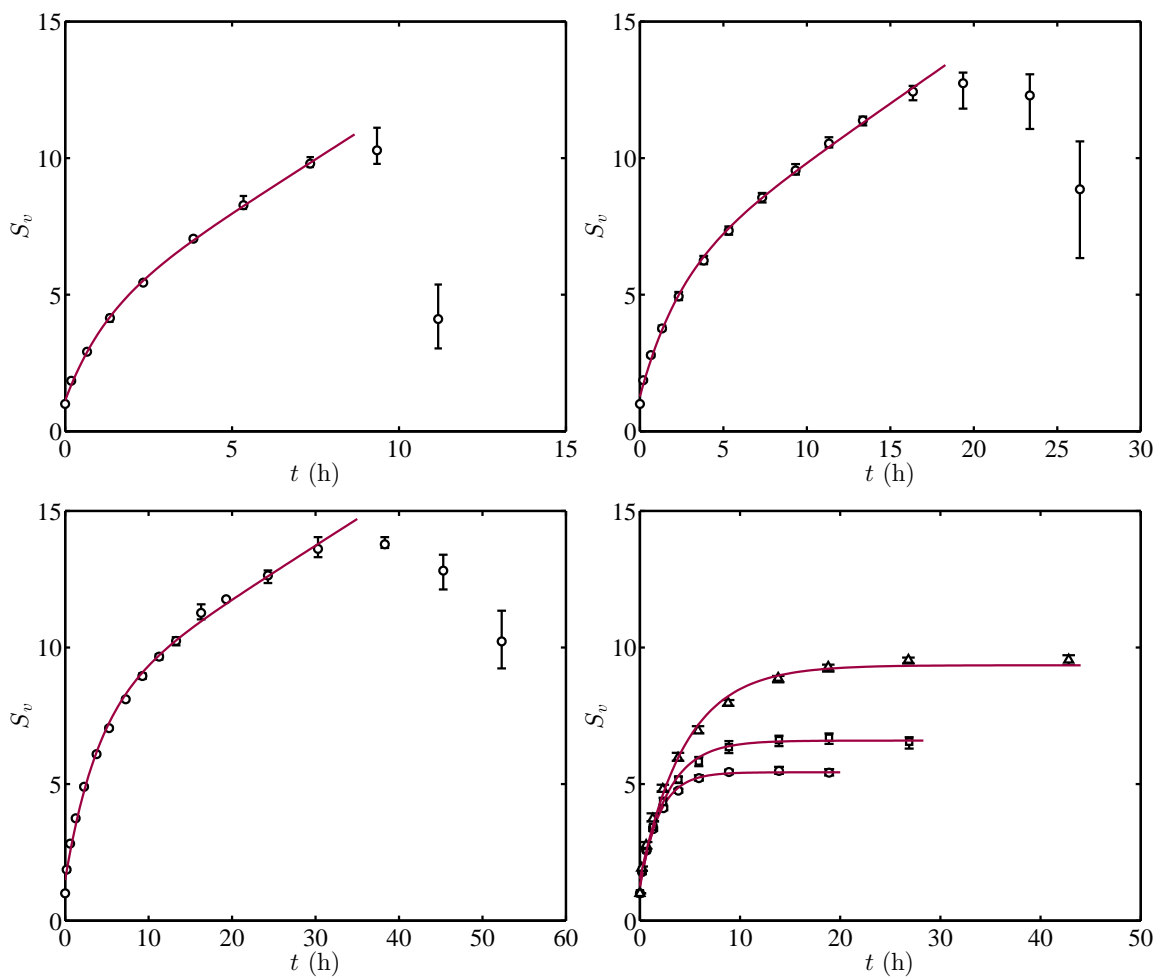


Figure 5.4: Swelling and dissolution of DNA-crosslinked gels in PBS: $B_0D_{0.4}$ (top left); $B_0D_{0.6}$ (top right); $B_0D_{0.8}$ (bottom left). Bottom right: Swelling of dual-crosslinked gels in PBS before the swelling-ratio decrease: $B_{0.6}D_{0.2}$ (circles); $B_{0.4}D_{0.4}$ (squares); $B_{0.2}D_{0.6}$ (triangles). Lines are least-squares fits of empirical Eqn. (5.8).

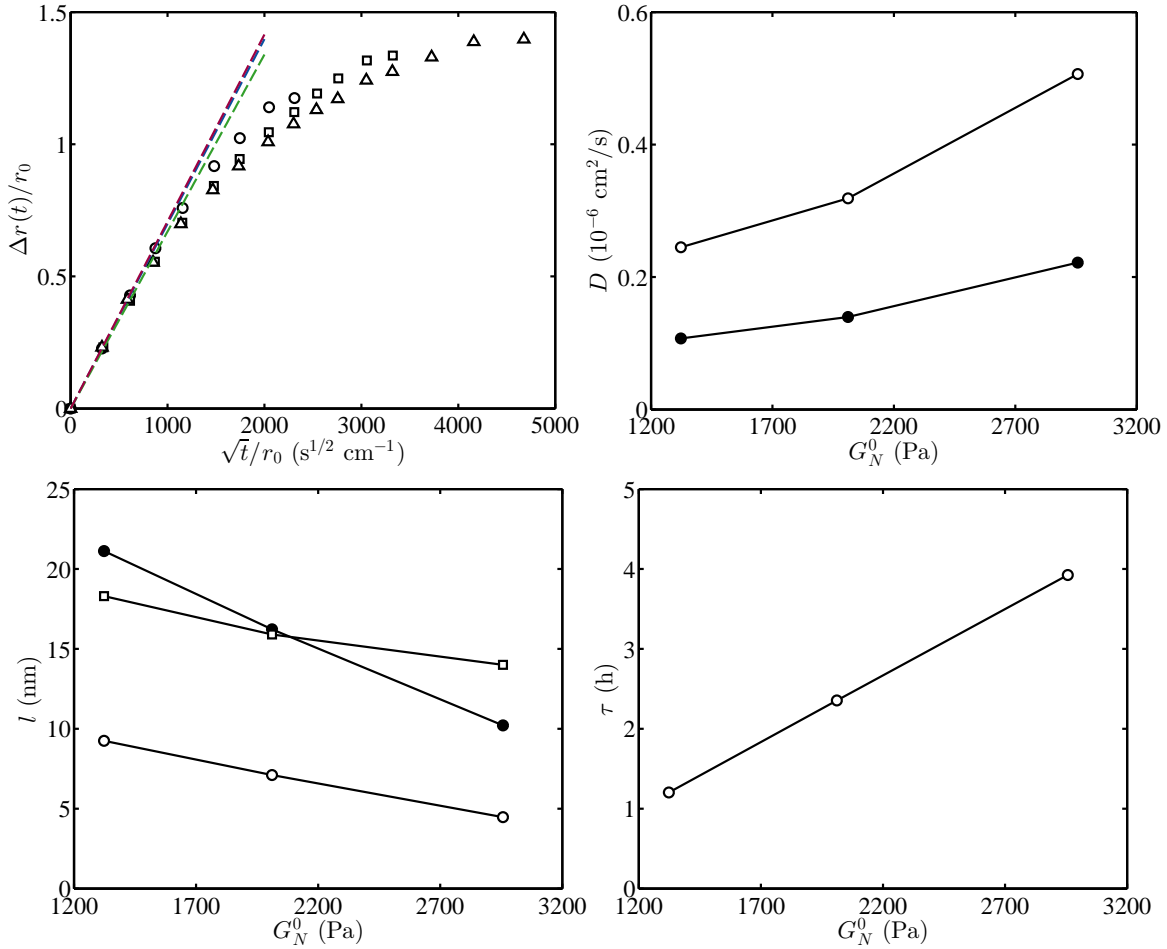


Figure 5.5: Top left: Fitting of Eqn. (5.6) to the initial stage of swelling B₀D_{0.4} (circles and blue line), B₀D_{0.6} (squares and green line), and B₀D_{0.8} (triangles and red line). Top right: Cooperative diffusion coefficient calculated with $\nu = 0.33$ (open circles) and $\nu = 0.5$ (filled circles) versus G_N^0 . Bottom left: Pore (mesh) size from D in the top-right panel with $\nu = 0.33$ (open circles) and $\nu = 0.5$ (filled circles), and from $l = (2k_B T / G_N^0)^{1/3}$ (squares) versus G_N^0 . Bottom right: Swelling relaxation time from empirical Eqn. (5.8) versus G_N^0 .

solvent, contributing to the absorbance at 202 nm and 260 nm. Moreover, unpolymerized acrylamide and polyacrylamide that is not connected to the network are also released during swelling, causing a higher absorbance. After fracture, the release rate first increases and then decreases to a constant. This is because when the gel breaks into small pieces, the surface area increases, promoting dissolution. The absorbance eventually becomes constant when the gel becomes very small fragments. Note that gel breakage is likely accelerated by the disturbances that accompany the measurements.

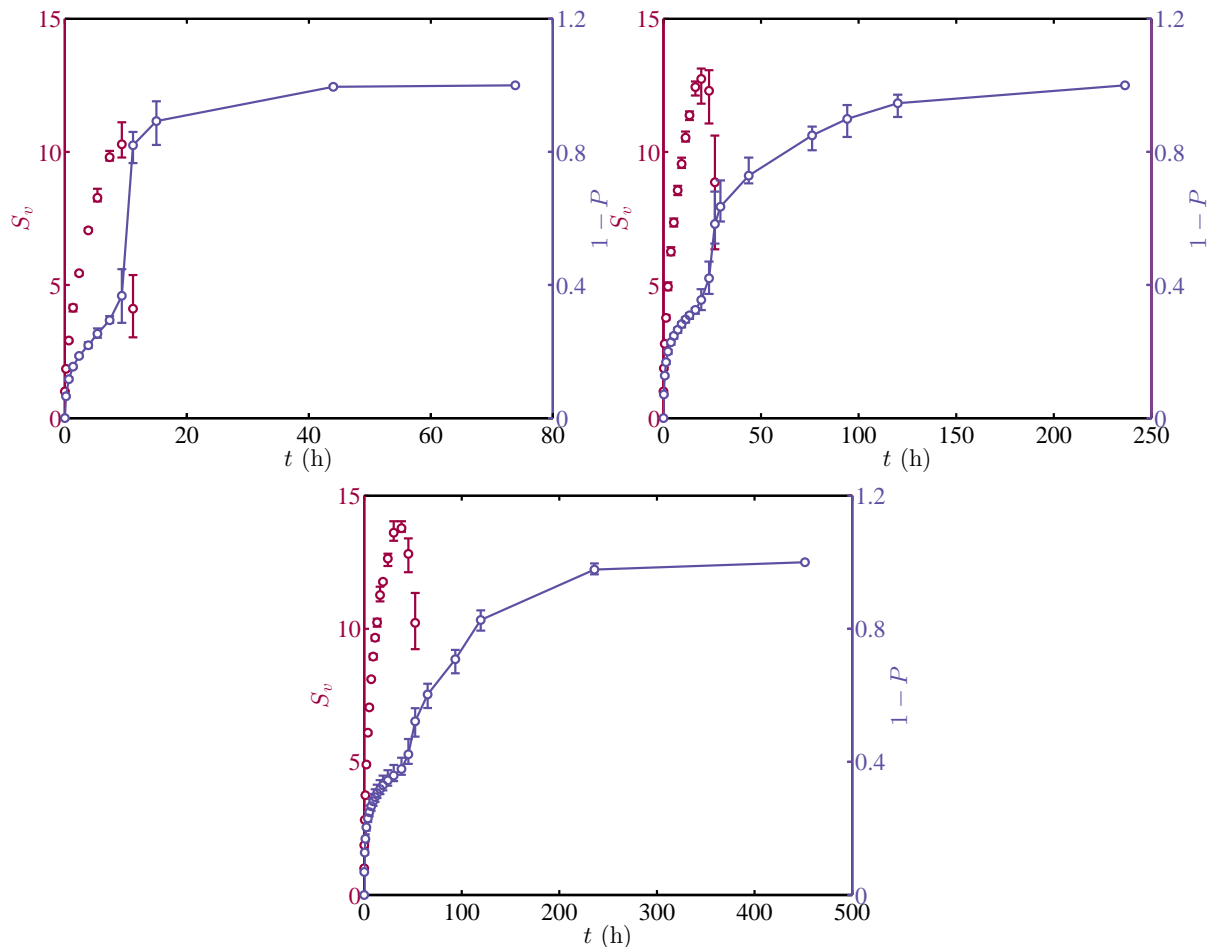


Figure 5.6: Time series of the volume swelling ratio (left axis) and the fraction of DNA strands released to PBS (right axis) for samples $B_0D_{0.4}$ (top left), $B_0D_{0.6}$ (top right), and $B_0D_{0.8}$ (bottom).

Because of permanent crosslinks, dual-crosslinked gels $B_{0.6}D_{0.2}$, $B_{0.4}D_{0.4}$, and $B_{0.2}D_{0.6}$ do not dissolve. As shown in figure 5.1, the gel volume at equilibrium increases with c_{DNA}/c_{bis} . Figure 5.8 shows that S_v first increases and then decreases, eventually reaching a constant. The relaxation time τ obtained from fitting Eqn. (5.8) to the data also increases

with $c_{\text{DNA}}/c_{\text{bis}}$. Note that a in the equation is set to 0 for dual-crosslinked gels, since the rate of DNA-crosslink dissolution and release is suppressed by permanent crosslinks. The eventual decrease in gel-volume indicates the release of polymer chains that were initially linked to the network only by DNA crosslinks. These chains may arise from the inhomogeneous distribution of bis-acrylamide and DNA crosslinks when gels were cast. This also causes the decrease of activation energy for DNA-crosslinker disengagement in dual-crosslinked gels with increasing temperature, as highlighted in chapter 4. Moreover, polymer chains that are not connected to the continuous network diffuse from the gel to the solvent. Noteborn et al.¹⁵³ and Yang et al.¹⁴⁷ use this reasoning to explain the swelling ratio decreasing after reaching the maximum swelling ratio.

Figure 5.7 shows the cooperative diffusion coefficient, the pore size of dual-crosslinked gels, and relaxation time before reaching the maximum volume swelling ratio. These all have the similar trends as for DNA-crosslinked gels. The cooperative diffusion coefficient for $B_{0.6}D_{0.2}$ and $B_{0.4}D_{0.4}$ are smaller than for pure DNA-crosslinked gels with the same plateau modulus. As mentioned in chapter 4, there might be less defects in DNA-crosslinked gels than in bis-crosslinked gels. The DNA-crosslinked gels network are more homogenous, with a smaller hydrodynamic pore sizes.

The fraction of DNA strands released to the solvent $1 - P$ for dual-crosslinked gels increases with swelling time, reaching a constant, as shown in figure 5.8. Unlike DNA-crosslinked gels, the release rate keeps decreasing because no fracture occurs in dual-crosslinked gels. “LinkerAdap” DNA strands and polymer chains with DNA Strand A and Strand B are gradually released until equilibrium is achieved. The values of P suggest 40–50% of DNA strands are immobilized in gel networks by bis-acrylamide crosslinks. Note that $1 - P$ may be smaller than the fraction of DNA crosslinks that are dissociated, because the portion of dissociated DNA Strand A and Strand B that are connected to polymer chains cannot be released to PBS due to the permanent bis-acrylamide crosslinking.

The fraction of DNA strands left in the dual-crosslinked gels P calculated in different ways are compared in figure 5.9. In addition to UV absorbance, dual-crosslinked gels were dried after swelling tests and weighed. The mass ratio of dried gel to the monomer used to form the gel is shown as circles, which is $\approx 80\%$. If the decrease in S_v is attributed to the gel mass loss, triangles in figure 5.9 illustrate that the value of P is also close to $\approx 80\%$. P ascertained from the two gravimetric methods is larger than from UV absorbance, because they are based on the mass loss of polymer rather than DNA crosslinks. The number of dissociated DNA crosslinks needed to release one polymer chain may be larger than one.

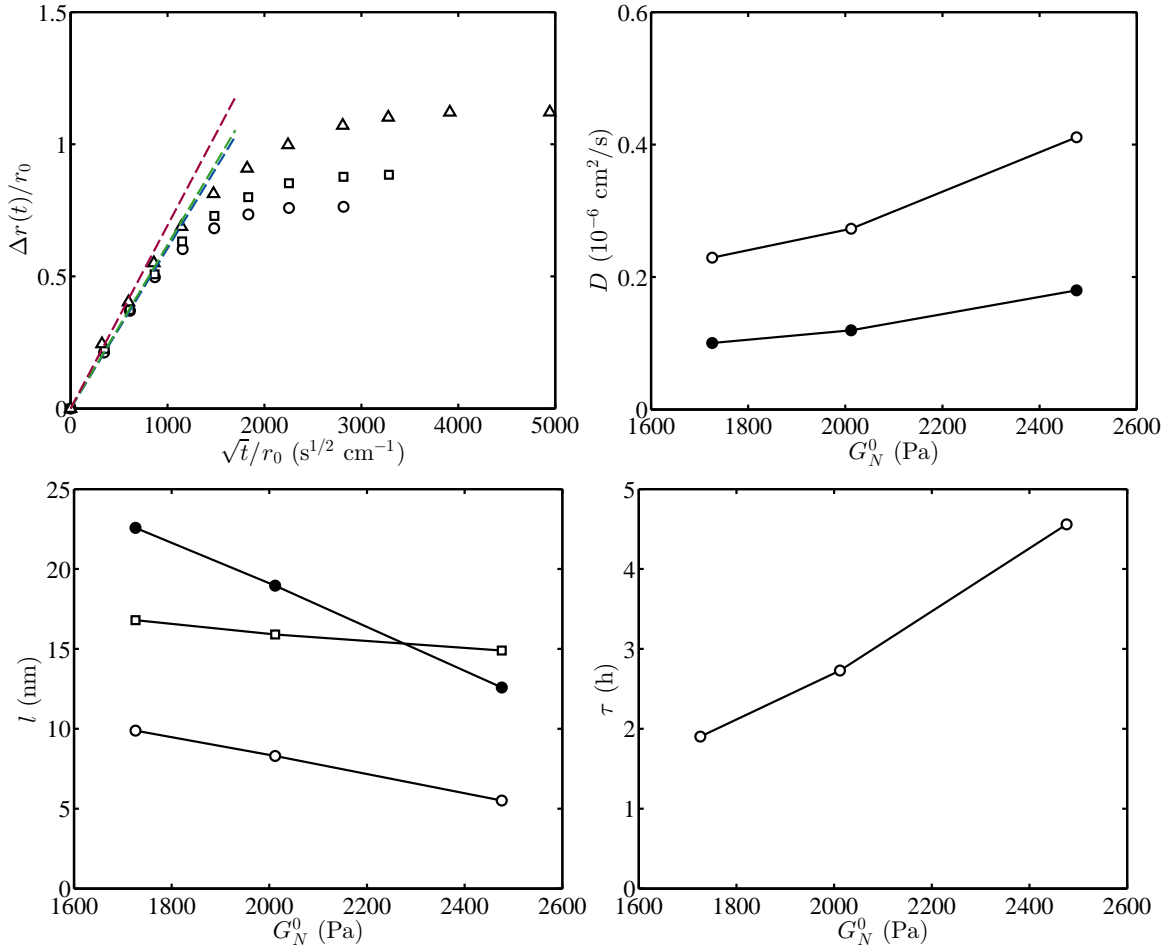


Figure 5.7: Top left: Fitting of Eqn. (5.6) to the initial stage of swelling $B_{0.6}D_{0.2}$ (circles and blue line), $B_{0.4}D_{0.4}$ (squares and green line), and $B_{0.2}D_{0.6}$ (triangles and red line). Top right: Cooperative diffusion coefficient calculated with $\nu = 0.33$ (open circles) and $\nu = 0.5$ (filled circles) versus G_N^0 . Bottom left: Pore (mesh) size from D in the top-right panel with $\nu = 0.33$ (open circles) and $\nu = 0.5$ (filled circles), and from $l = (2k_B T / G_N^0)^{1/3}$ (squares) versus G_N^0 . Bottom right: Swelling relaxation time from fitting Eqn. (5.8) versus G_N^0 .

Also, $1 - P$ obtained from UV absorbance includes un-reacted DNA strands, decreasing the number of DNA strands immobilized in the network. Furthermore, if elastically inefficient crosslinks are assumed to be released, the diamonds indicate that P is in the range 30–40%. The smallest P is obtained from this method, because a portion of crosslinks that do not contribute to gel elasticity may still be connected to the network.

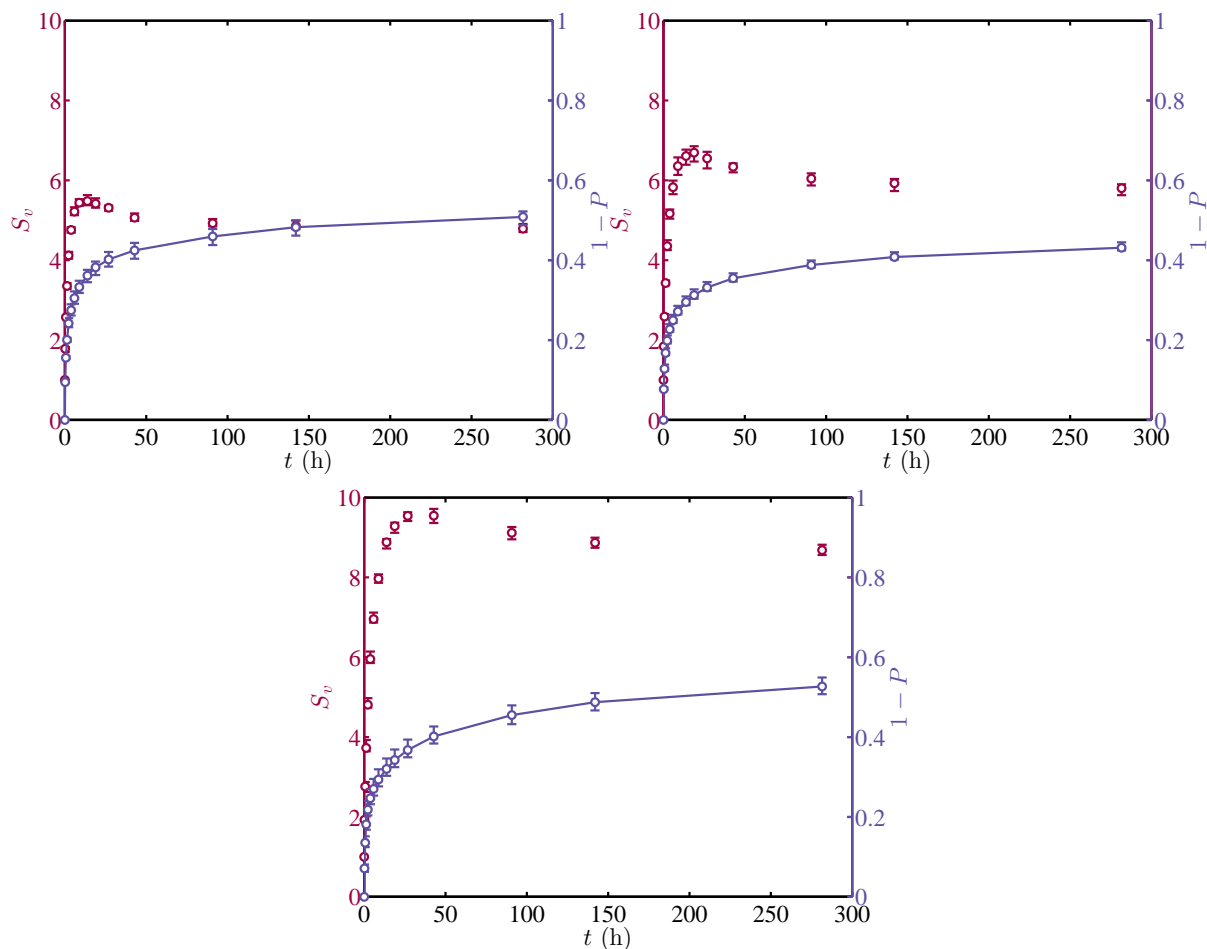


Figure 5.8: Time series of the volume swelling ratio (left axis) and the fraction of DNA strands released to PBS (right axis) for samples $B_{0.6}D_{0.2}$ (top left), $B_{0.4}D_{0.4}$ (top right), and $B_{0.2}D_{0.6}$ (bottom) during swelling.

In figure 5.10, the plateau modulus and equilibrium swelling ratio for bis-crosslinked gels in PBS are fitted using Eqn. (5.1) and extrapolated to the larger gel stiffness. From fitting we find $\chi = 0.4837 \pm 0.0013$, showing that PBS acts as a good solvent for polyacrylamide at $\approx 22.5^\circ\text{C}$. From Livney et al.⁹ and Konda et al.¹⁰, the swelling ratios at equilibrium for bis-crosslinked gels are found to deviate from the fitting curve. This may be because for soft hydrogels having high water contents in this study, assumptions for Flory-Huggins

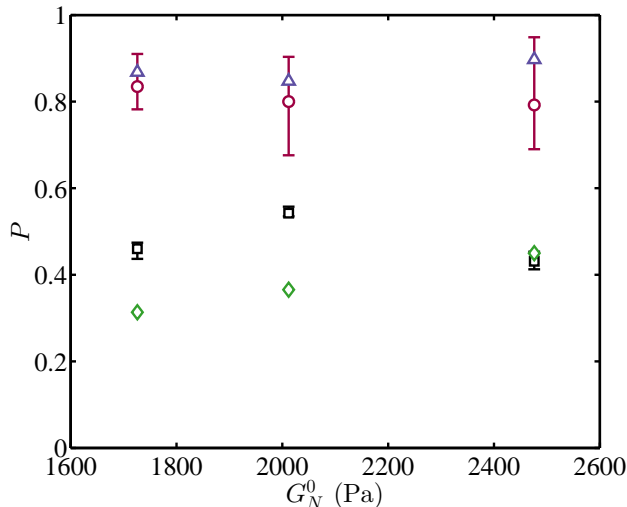


Figure 5.9: The fraction of DNA strands/polymer chains left in dual-crosslinked gels from drying the gels (circles); UV-vis (squares); the decrease of S_v (triangles); the crosslinking efficiency (diamonds).

theory such as solutions need to be sufficiently concentrated or the assumption for the rubber elasticity theory that end-to-end vectors of polymer chains follow Gaussian distribution are not valid. Another possible reason for our gels having smaller equilibrium swelling ratio is that the mass of gel after casting includes polymer chains that are not connected to the network. Thus, the initial mass used to calculate swelling ratios is larger than the gel mass, imparting smaller swelling ratios. The maximum swelling ratios for DNA-crosslinked gels before fracture are plotted in figure 5.10. Unlike permanently crosslinked gels, the maximum swelling ratio for DNA-crosslinked gels increases with the plateau modulus and is larger than for bis-crosslinked gels with the same plateau modulus. With more DNA crosslinks, the gel can swell to a larger volume before the DNA-crosslinker concentration is low enough to cause the fracture. For dual-crosslinked gels, the maximum swelling ratio before decreasing increases with increasing $c_{\text{DNA}}/c_{\text{bis}}$, confirming that the dissociation of transient crosslinks promotes swelling. It is also shown that the maximum swelling ratio for dual-crosslinked gels is below that for DNA-crosslinked gels, but above the fitting curve for bis-crosslinked gels.

5.4.3 Theoretical interpretation

To predict the equilibrium swelling ratio for gels with transient crosslinks (*e.g.*, DNA-crosslinked gels) crosslink dissociation should be considered in the Flory-Rehner model.

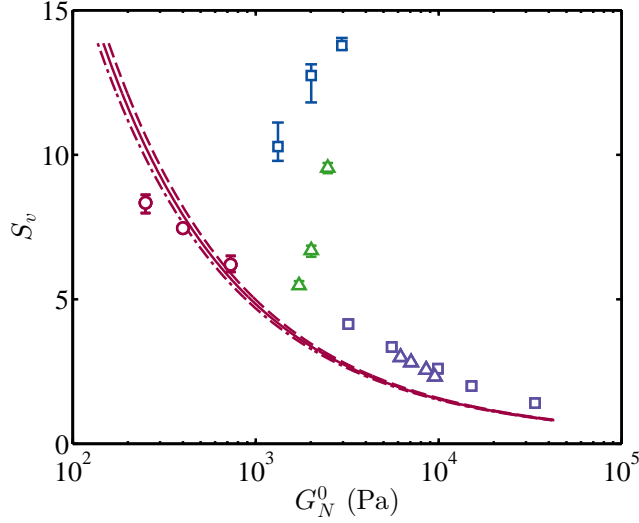


Figure 5.10: Swelling ratio at equilibrium/prior to dissolution/prior to decreasing versus plateau modulus for bis-crosslinked gels (red circles), DNA-crosslinked gels (blue squares), and dual-crosslinked gels (green triangles) in PBS. The curve is the least-squares fit of Eqn. (5.1) (solid: average; dashed: maximum; dash-dot: minimum). Violet squares and triangles are the swelling ratio at equilibrium for bis-crosslinked gels from Livney et al.⁹ and Konda et al.¹⁰

We therefore define the probability of forming a crosslink with average end-to-end distance $r = r_0\lambda$ as $p(r)$. This may be considered the fraction of crosslinks in an associated state, so $p(r)$ transits from 1 when $r = r_0$ to 0 as $r \rightarrow \infty$. A function that satisfies these requirements is

$$p(r) = 1 - \tanh\left(\frac{r - r_0}{\delta}\right).$$

Assuming the gel is prepared with an initial volume fraction ϕ_0 and volume V_0 , the stretch ratio for isotropic swelling is $\lambda = (\phi_0/\phi)^{1/3}$ with

$$V = \frac{V_0\phi_0}{\phi},$$

where V is the solution volume and ϕ is the polymer volume fraction. The number of crosslinks contributes a free energy per unit volume

$$k_B T p(r) \Delta\epsilon n \phi,$$

where $\Delta\epsilon (> 0)$ is the bond energy of a crosslink, and n is the number of available crosslinking sites per unit of dry polymer volume. The free energy A of the gel relative to the as-prepared

state is

$$\frac{A}{k_B T} = -p(r)f\Delta\epsilon n\phi V + \chi\phi(1-\phi)V + (1-\phi)\ln(1-\phi)V + \frac{[p(r)f + 1 - f]n\phi V r_0^2(\lambda^2 - 1)3}{Nb^2} \frac{3}{2},$$

with

$$\frac{\partial p(r)}{\partial \phi} = -\frac{\partial p(r)}{\partial r} \frac{\phi_0^{1/3} r_0}{3} \phi^{-4/3} = D(\phi),$$

where

$$\frac{\partial p(r)}{\partial r} = -\text{sech}^2\left(\frac{r-r_0}{\delta}\right) \frac{1}{\delta},$$

evaluating $\partial A/\partial \phi = 0$ gives

$$0 = -D\Delta\epsilon n f - \chi - \frac{\ln(1-\phi)}{\phi^2} - \frac{1}{\phi} + \frac{3Dn f}{2} \left[\left(\frac{\phi_0}{\phi}\right)^{2/3} - 1 \right] - [fp(r) + 1 - f]n\phi_0^{2/3}\phi^{-5/3},$$

where f is the fraction of crosslinks that are transient.

The top panel of figure 5.11 shows the correlation between $p(r)$ and λ . For a dual-crosslinked gel, $p(r)$ applies to the transient crosslinks. The parameters are set as $\phi_0 = 0.0693$, $n = 1/N/3.5$, $b = 1.54 \times 10^{-10}$ m, $N = 1720$, $r_0 = b\sqrt{N}$.

The bottom-left panel of figure 5.11 shows that with $\chi = 0.4837$ and $\Delta\epsilon = 130k_B T$, $\partial A/\partial \phi = 0$ has two roots. The left one is unstable, whereas the right one is stable. The stable root is larger than ϕ_0 , indicating gel collapse, which is not observed for DNA-crosslinked gels. Thus, the unstable root is the only equilibrium state, predicting dissolution. For the dual-crosslinked network, as shown in the bottom-right panel of figure 5.11, the left root indicates a stable equilibrium that predicts the swelling ratio.

Figure 5.12 shows that the isotropic swelling ratio λ obtained from the unstable equilibrium increases with the bond energy of a crosslink $\Delta\epsilon$, δ , and Flory-Huggins interaction parameter χ . The unstable root occurs when $p(r) \approx 0$, so the gel must fracture before it can reach equilibrium. As shown in the right-bottom panel of figure 5.12, the equilibrium swelling ratio increasing with the modulus is consistent with the experimental swelling ratio when gels fracture. This trend is unique for gels with transient crosslinks. For dual-crosslinked networks, adjusting the fraction of transient crosslinks f captures the experimental trend that the equilibrium swelling ratio increases with $c_{\text{DNA}}/c_{\text{bis}}$. Note that the swelling ratios before decreasing are adopted as the experimental equilibrium swelling ratios for dual-crosslinked gels. The value of f used to fit experimental data is larger than the fraction of DNA crosslinker used to synthesize the gels, because the crosslinking efficiency for DNA crosslinkers is larger than that for bis-acrylamide crosslinkers. It is also shown that for gels with the same composition, the equilibrium swelling ratio decreases with increasing modulus. The

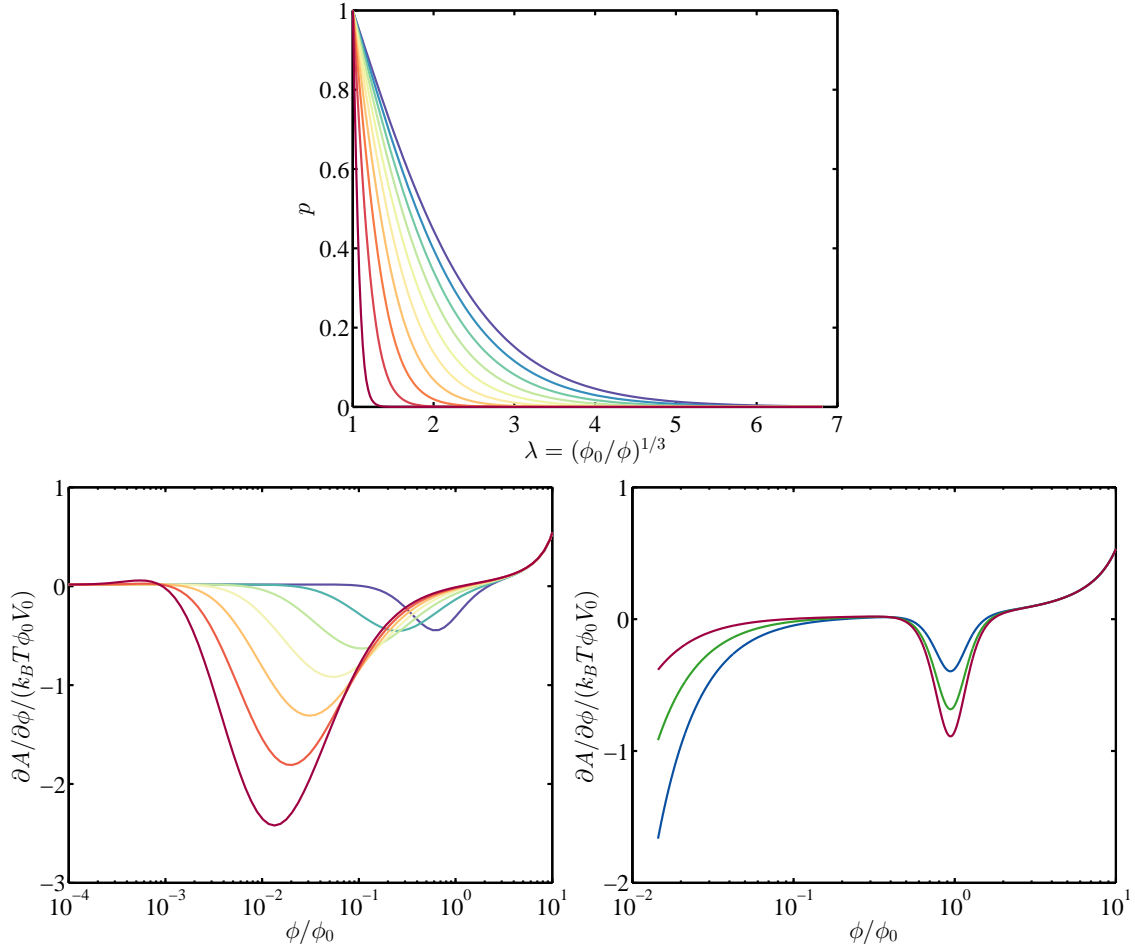


Figure 5.11: Top: Phenomenological probability function p versus λ with $\delta = 0.1\text{--}1.6r_0$ (from red to blue). Bottom left: $\partial A/\partial\phi$ versus ϕ/ϕ_0 with $\delta = 0.3\text{--}2.1r_0$ (from blue to red). Bottom right: $\partial A/\partial\phi$ versus ϕ/ϕ_0 for $B_{0.6}D_{0.2}$ with $\delta = 0.1r_0$ and $f = 2/5$ (blue), $B_{0.4}D_{0.4}$ with $\delta = 0.15r_0$ and $f = 2/3$ (green), and $B_{0.2}D_{0.6}$ with $\delta = 0.15r_0$ and $f = 6/7$ (red).

quantitative validity of the model for dual-crosslinked gels needs to be further explored with more experimental data.

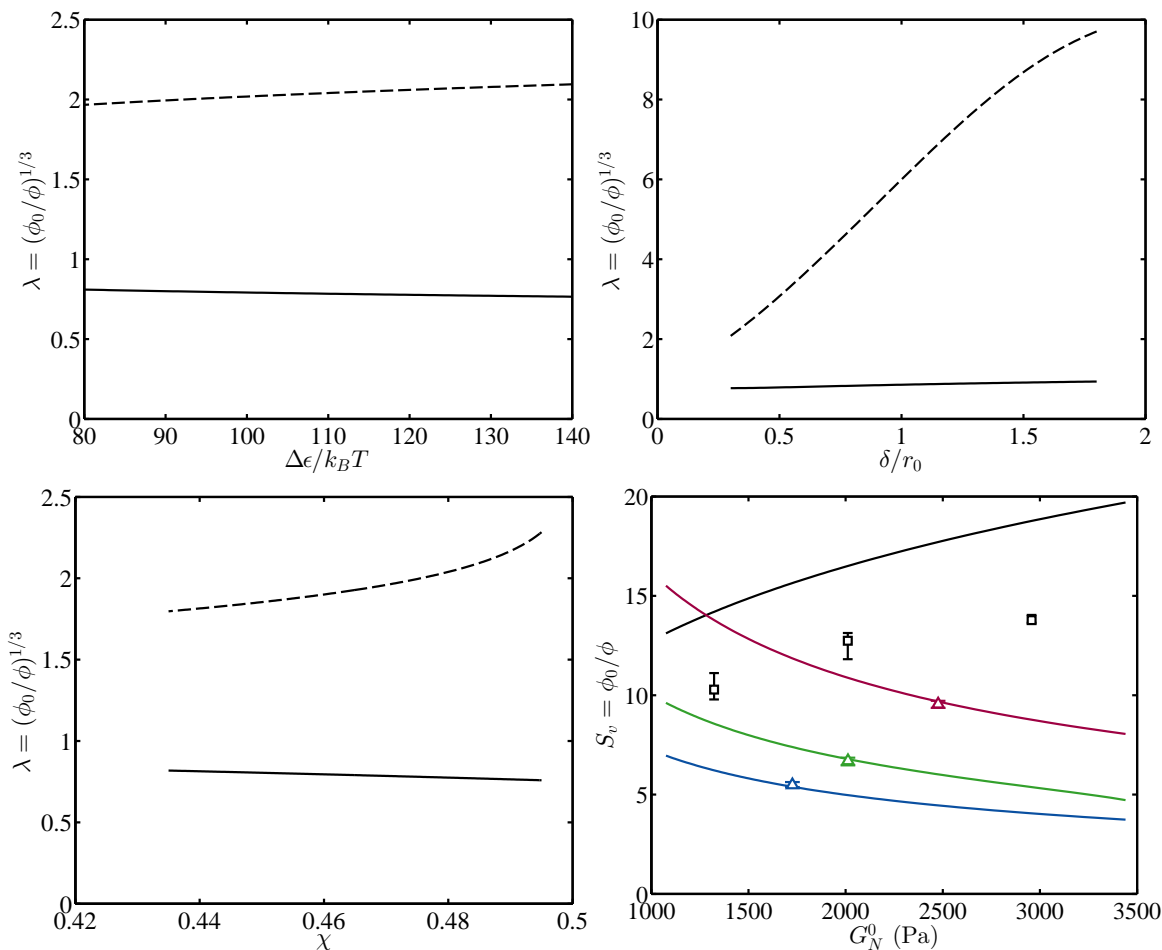


Figure 5.12: The correlation between λ and $\Delta\epsilon$ (top left); λ and δ (top right); λ and χ (bottom left). Solid and dashed lines are from the stable and unstable roots. Bottom right: Swelling ratio at equilibrium $S_v = \phi_0/\phi$ versus gel plateau modulus G_N^0 for DNA-crosslinked gels (black lines) and dual-crosslinked gel samples $B_{0.6}D_{0.2}$ with $f = 2/5$ (blue), $B_{0.4}D_{0.4}$ with $f = 2/3$ (green), and $B_{0.2}D_{0.6}$ with $f = 6/7$ (red). Squares and triangles are experimental swelling ratios for DNA- and dual-crosslinked gels.

5.5 Conclusions

Swelling of polyacrylamide hydrogels with bis-, DNA-, and dual-crosslinking were studied. Unlike bis-crosslinked gels, DNA-crosslinked gels formed by copolymerization dissolve during swelling, making them unsuitable for drug delivery, because toxic acrylamide cannot

be removed without dissolution. The volume swelling ratio for DNA-crosslinked gels prior to dissolution increases with the DNA-crosslinker ratio, because DNA crosslinks dissociate during swelling, enhancing the swelling capacity. The release of DNA strands to the buffer during swelling was established using UV-vis spectroscopy. The hydrodynamic pore sizes determined by Biot's theory are different from mesh sizes obtained from the elastic modulus, confirming a heterogeneous gel network. In dual-crosslinked gels, permanent crosslinks prevent gel dissolution, while DNA crosslinks dissociated, imparting a larger swelling ratio than bis-crosslinked gels with the same plateau modulus. A greater fraction of DNA crosslinks in the dual network imparts a larger solvent uptake capacity. The swelling ratio for dual-crosslinked gels decreases before reaching equilibrium, demonstrating the transfer of polymer chains to the solvent. A theoretical model was proposed to capture qualitative trends in the swelling of DNA-crosslinked gels. This shows that the bond energy and the polymer-solvent interaction parameter influence the equilibrium swelling ratio. The model also captures the correlation between the fraction of crosslinks that are transient and equilibrium swelling ratio for dual-crosslinked gels.

Appendix

5.A Dissolution and reformation of DNA-crosslinked gels

After adding RO water to vials containing DNA-crosslinked gels with different crosslinker ratios, swelling and dissolution occurs. The gel with lowest crosslinker ratio $B_0D_{0.2}$ dissolves first and swells with the smallest swelling ratio before dissolution. Samples $B_0D_{0.6}$ and $B_0D_{0.8}$ continue to swell after adding 1.5 ml of RO water. The dissolved sample $B_0D_{0.2}$ forms a gel after the DNA-crosslinker concentration reaches the critical concentration for gelation via evaporation. This re-formation suggests that gel dissolution is caused by DNA denaturation rather than breaking of DNA chains.

5.B Accumulated UV-vis spectra

Accumulated UV-vis spectra for PBS containing DNA- and dual-crosslinked gels shown in figure 5.B.1 and figure 5.B.2 have the a standard peak for DNA at 260 nm. The spectra are accumulated to show the absorbance trend at 260 nm during swelling. These are not the actual spectra because the absorbance at lower wavelengths is not linear in the concentration when the absorbance is greater than 1.5.

5.C Conversion of mass swelling ratio to volume swelling ratio

For bis-crosslinked gels, it is assumed that all monomers are polymerized. As the gel was prepared, the mass of buffer is $m_b = 10m$, and the mass of the gel is $m_g = m$. The density of buffer is $\rho_b = 1$ g/ml and the density of polyacrylamide is $\rho_g = 1.443$ g/ml¹⁵⁴. If the gel volume is assumed as the sum of each component volume, and the mass of bis-acrylamide is

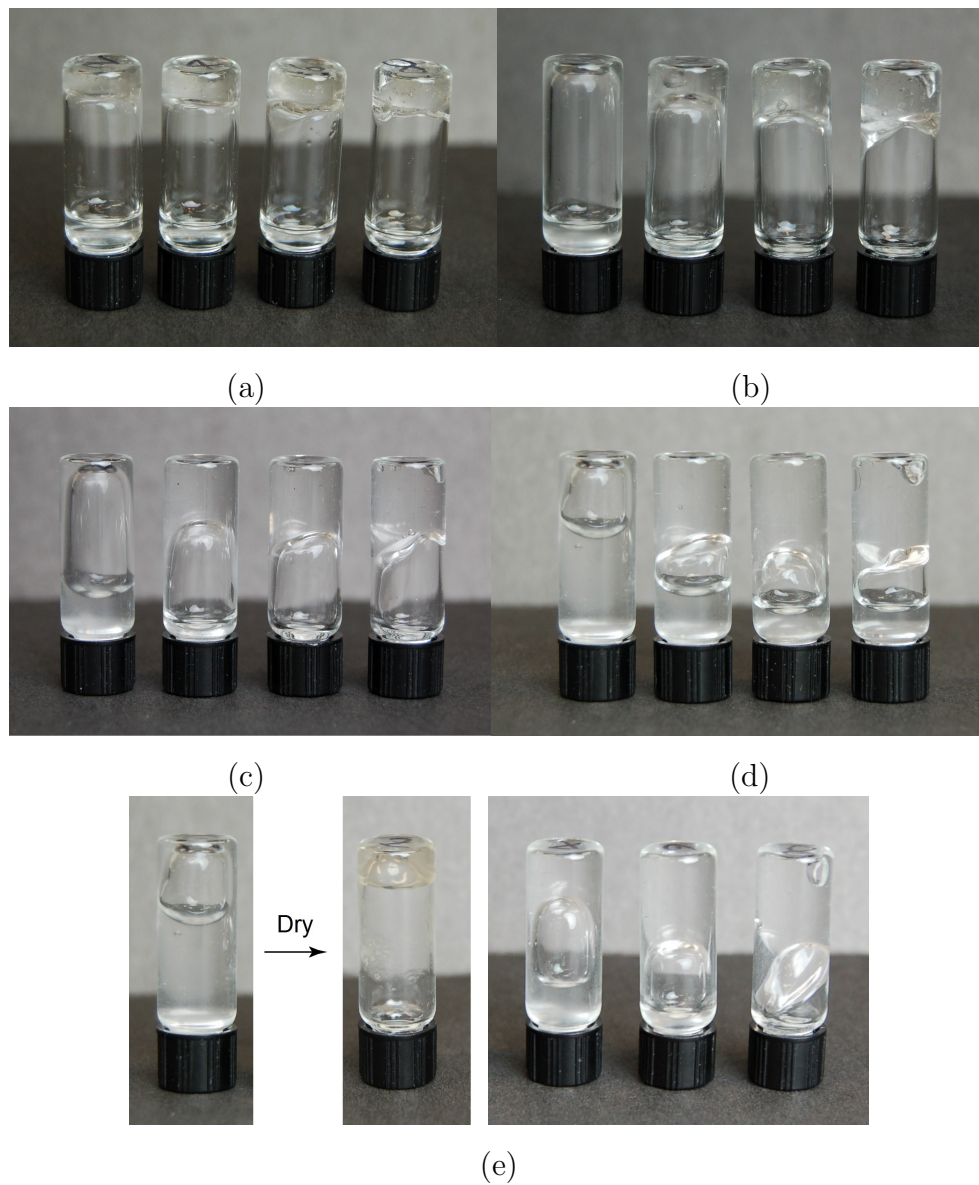


Figure 5.A.1: Swelling of DNA-crosslinked polyacrylamide hydrogels before (a) and after adding 0.5 ml (b), 1 ml (c), and 1.5 ml (d: after 2 weeks; e: after 5 weeks) RO water. From left to right: $B_0D_{0.2}$, $B_0D_{0.4}$, $B_0D_{0.6}$, and $B_0D_{0.8}$.

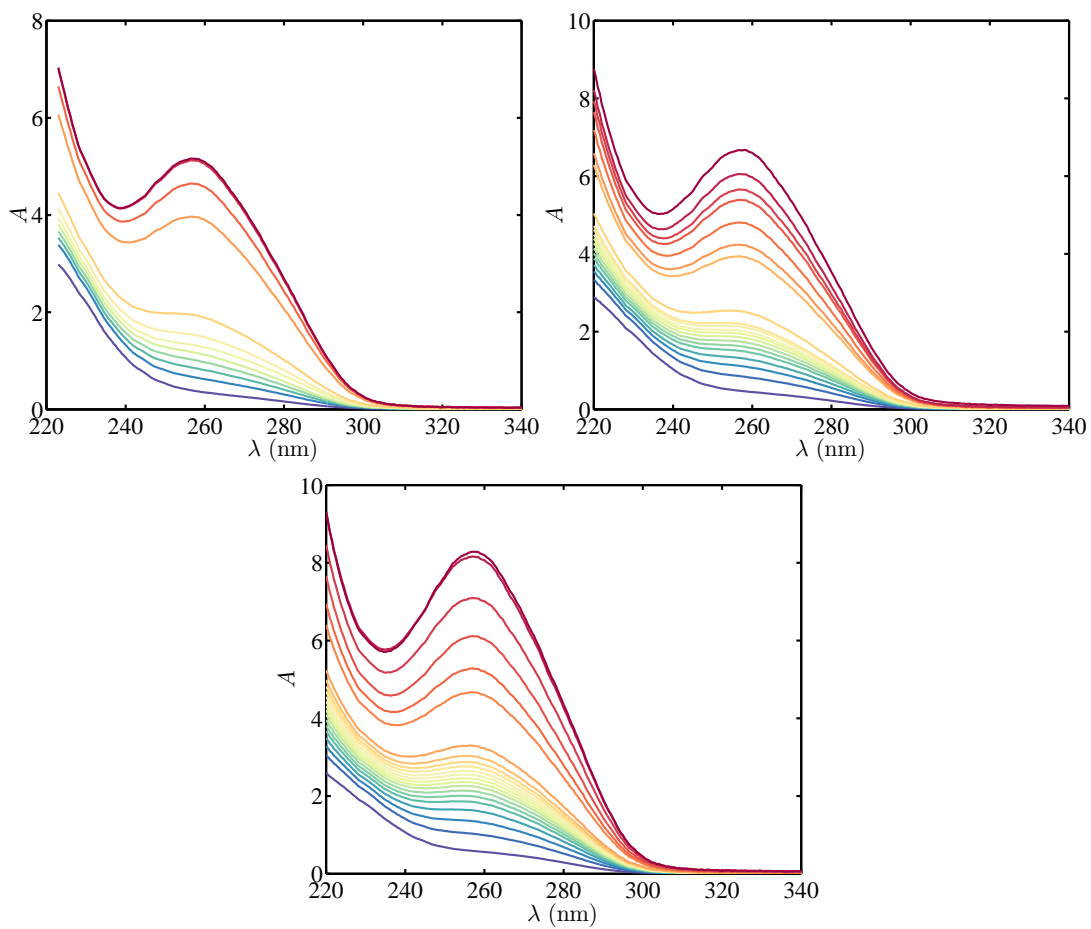


Figure 5.B.1: Accumulated UV-vis spectra for PBS containing gels during swelling (from blue to red) for $B_0D_{0.4}$ (top left), $B_0D_{0.6}$ (top right), and $B_0D_{0.8}$ (bottom).

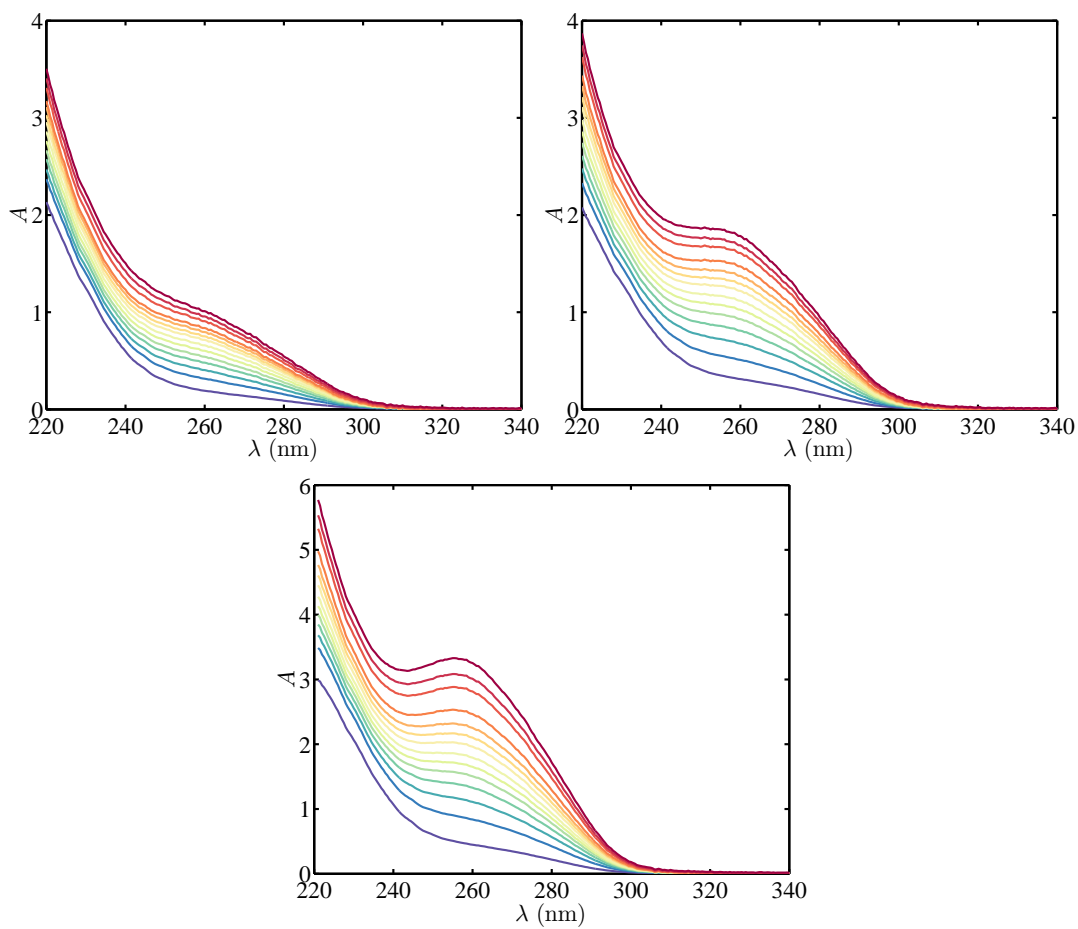


Figure 5.B.2: Accumulated UV-vis spectra for PBS containing gels during swelling (from blue to red) for $B_{0.6}D_{0.2}$ (top left), $B_{0.4}D_{0.4}$ (top right), and $B_{0.2}D_{0.6}$ (bottom).

neglected, then

$$V_0 = \frac{m_b}{\rho_b} + \frac{m_g}{\rho_g} = \frac{10m}{1} + \frac{m}{1.443} = 10.693m.$$

At time t , the mass swelling ratio S_w and the total gel mass are related by

$$m_{tot} = S_w 11m.$$

The mass of buffer is

$$m_b = m_{tot} - m_g = S_w 11m - m.$$

The total volume is

$$V_{tot} = \frac{S_w 11m - m}{\rho_b} + \frac{m}{\rho_g} = 11m S_w - 0.307m.$$

The volume swelling ratio is

$$S_v = \frac{V_{tot}}{V_0} = \frac{11m S_w - 0.307m}{10.693m} = 1.02871 S_w - 0.02871.$$

For DNA-crosslinked gels, the mass of DNA crosslinker is not negligible. The densities of Strand A (ρ_{SA}), Strand B (ρ_{SB}), and “LinkerAdap” (ρ_{SC}) are 1.69067 g/ml, 1.70292 g/ml, 1.71125 g/ml, respectively; the molecular weights of Strand A (M_{SA}), Strand B (M_{SB}), and “LinkerAdap” (M_{SC}) are 5169.5 g/mol, 5072.4 g/mol, and 13765.9 g/mol, respectively.

Taking the as-prepared volume of the gel to be V_0 ml, for B₀D_{0.8} (as an example), the buffer volume is

$$V_{b0} = V_0 - \frac{0.1V_0}{1.443} - V_0 \times 1.1167 \times 10^{-6} \left(\frac{M_{SA}}{\rho_{SA}} + \frac{M_{SB}}{\rho_{SB}} + \frac{M_{SC}}{\rho_{SC}} \right) = 0.915V_0.$$

The total mass is

$$m_0 = V_{b0} \times 1 + 0.1V_0 + V_0 \times 1.1167 \times 10^{-6} (M_{SA} + M_{SB} + M_{SC}) = 1.0418V_0.$$

At time t , P denotes the fraction of DNA crosslinkers in the gel, which can be obtained from the UV-vis absorbance. The fraction of polyacrylamide in the gel network is approximately $0.5 + 0.5P$, when $P > 0.5$, because the fraction of polymer chains disconnected from the network is half of the fraction of crosslinks needed to break these chains. If the network is assumed homogeneous, the total mass of the gel is $m_{tot} = S_w 1.0418V_0$, $m_g = (0.5 + 0.5P)0.1V_0$, and $m_D = 0.0268P$, the volume of buffer is

$$V_b = \frac{S_w 1.0418V_0 - (0.5 + 0.5P)0.1V_0 - 0.0268PV_0}{1}.$$

Therefore, the total volume

$$\begin{aligned}
 V_{tot} &= V_b + \frac{(0.5 + 0.5P)0.1V_0}{1.443} + 1.1167 \times 10^{-6}V_0P \left(\frac{M_{SA}}{\rho_{SA}} + \frac{M_{SB}}{\rho_{SB}} + \frac{M_{SC}}{\rho_{SC}} \right) \\
 &= (1.0418S_w - 0.01535 - 0.02643P)V_0.
 \end{aligned}$$

The volume swelling ratio

$$S_v = 1.0418S_w - 0.01535 - 0.02643P.$$

S_v for other DNA-crosslinked gels can be obtained using the same method. If the mass of bis-acrylamide is neglected, S_v for dual-crosslinked gels can be obtained using the correlations for DNA-crosslinked gels with the same DNA-crosslinker ratio.

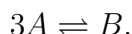
5.D Calibration of DNA absorbance and determination of the DNA combination time

The left panel of figure 5.D.1 shows the correlations between the DNA-strand concentration and UV-vis absorbance at 260 nm arising from the heterocyclic rings in nucleotides. Extinction coefficients for DNA strands obtained from the slope of least-squares fits are 161,000 l mol⁻¹ cm⁻¹ for Strand A, 154,000 l mol⁻¹ cm⁻¹ for Strand B, and 370,000 l mol⁻¹ cm⁻¹ for “LinkerAdap”. If three strands are assumed separated when polymer chains with DNA strands are released to PBS, the sum of extinction coefficients for three strands is 685,000 l mol⁻¹ cm⁻¹, which can be used to convert the absorbance of PBS to the DNA-crosslinker concentration. Note that in the early stage of swelling, the actual concentration of released DNA strands may be larger than that converted from the absorbance. This is because DNA Strand A and Strand B that are connected to polymer chains cannot be released to PBS until the polymer chains are disconnected from the network, lowering the actual extinction coefficient. The spectra for PBS with each DNA strand concentration are shown in the right panel. In addition to peaks at 260 nm, there are also peaks around 202 nm.

To examine the impact of polyacrylamide chains and acrylamide that are not polymerized on the spectra for PBS with dissolved DNA gels, the UV-vis absorbance for PBS with different concentrations of PA and acrylamide are shown in figures 5.D.2 and 5.D.3. The spectrum for a polyacrylamide solution has peaks around 202 nm that can be attributed to carbon-carbon double bonds. The UV-vis absorbance at the peaks is linear with the polyacrylamide concentration when the concentration is low, and the absorbance at 260 nm is

linear with the polyacrylamide concentration. The value of A is smaller and negligible compared to that for DNA strands. The absorbance at the peak and a 260 nm for the acrylamide solution is about ten times larger than for PA solution. The unpolymerized acrylamide may affect the determination of DNA concentrations if the polymerization conversion is low.

The combination of Strand A, Strand B, and “LinkerAdap” can be simplified if we assume no side reactions occur:



The reaction conversion X is

$$1 - X = \frac{c_A - c_{A'}}{c_{A0} - c_{A'}},$$

where c_{A0} is the initial concentration, and $c_{A'}$ is the final concentration. The left panel of figure 5.D.4 shows $1 - X$ versus time. The reaction reaches equilibrium after 110 s, and the conversion is 27% at the reactant concentration. If the reaction is a third-order reaction, then

$$-r_A = k_a c_A^3 - k_d c_B = k_a \left(c_A^3 - \frac{k_d}{k_a} c_B \right) = k_a \left(c_A^3 - \frac{c_B}{K_c} \right) = k_a \left(c_A^3 - \frac{c_{A0} - c_A}{3K_c} \right),$$

where K_c is the equilibrium constant, giving

$$-\frac{dc_A}{dt} = k_a \left(c_A^3 + \frac{c_A}{3K_c} - \frac{c_{A0}}{3K_c} \right).$$

Letting $c_{A0} - c_{A'} = a$, $c_{A'} = b$,

$$c_A = a(1 - X) + b,$$

so,

$$-a \frac{d(1 - X)}{dt} = k_a [a(1 - X) + b]^3 + \frac{1}{3K_c} \left[a(1 - X) + b - \frac{a + b}{3K_c} \right].$$

Using the three-point differentiation formulas, $d(1 - X)/dt$ can be obtained as:

Initial point:

$$\left. \frac{d(1 - X)}{dt} \right|_{t_0} = \frac{1}{2\Delta t} [-3(1 - X_0) + 4(1 - X_1) - (1 - X_2)]$$

Interior points:

$$\left. \frac{d(1 - X)}{dt} \right|_{t_i} = \frac{1}{2\Delta t} [(1 - X_{i+1}) - (1 - X_{i-1})]$$

Last point:

$$\left. \frac{d(1 - X)}{dt} \right|_{t_{51}} = \frac{1}{2\Delta t} [(1 - X_{49}) - 4(1 - X_{50}) + 3(1 - X_{51})]$$

Because absorbance at 260 nm for a double-stranded DNA is 80% of the sum of absorbance for each single-stranded DNA, $1 - X$ can be calculated from the absorbance during the reaction. The right panel of figure 5.D.4 shows that $d(1 - X)/dt$ versus $1 - X$ is fitted well by the correlation for a third-order reaction, which means the reaction can be considered as Strand A and Strand B combining with “LinkerAdap” at the same time.

5.E Effect of solvent on the swelling ratio

Gel cylinders with an aspect ratio ≈ 1 were swollen in RO water and PBS. Because of the ions in PBS, the swelling ratio of bis-crosslinked gels in PBS is larger than in RO water, as shown in figure 5.E.1. The Flory-Huggins parameter $\chi \approx 0.4865$ and 0.4834 for PBS and RO water. χ obtained here is the same as obtained from the gel with aspect ratio ≈ 6.3 , confirming that the aspect ratio has no influence on the equilibrium swelling ratio.

5.F Comparing the swelling of DNA-crosslinked gels synthesized varying TEMED concentration

DNA-crosslinked gels were synthesized using a higher concentration of TEMED, which, as mention previously, decreases the effective crosslink concentration and the gel plateau modulus. Thus, gels with the similar crosslinker ratios dissolve faster during swelling than gels synthesized with a lower TEMED concentration. Moreover, the elastically ineffective crosslinks in the gel impart a smaller hydrodynamic pore size. The swelling ratio prior to dissolution is smaller than that for gels with a lower TEMED concentration, but also increases with increasing DNA-crosslinker ratio (figure 5.F.1). The swelling and dissolution kinetics, the parameters obtained from swelling in the early stages, and the release of DNA strands to PBS are shown in figures 5.F.2, 5.F.3, and 5.F.4.

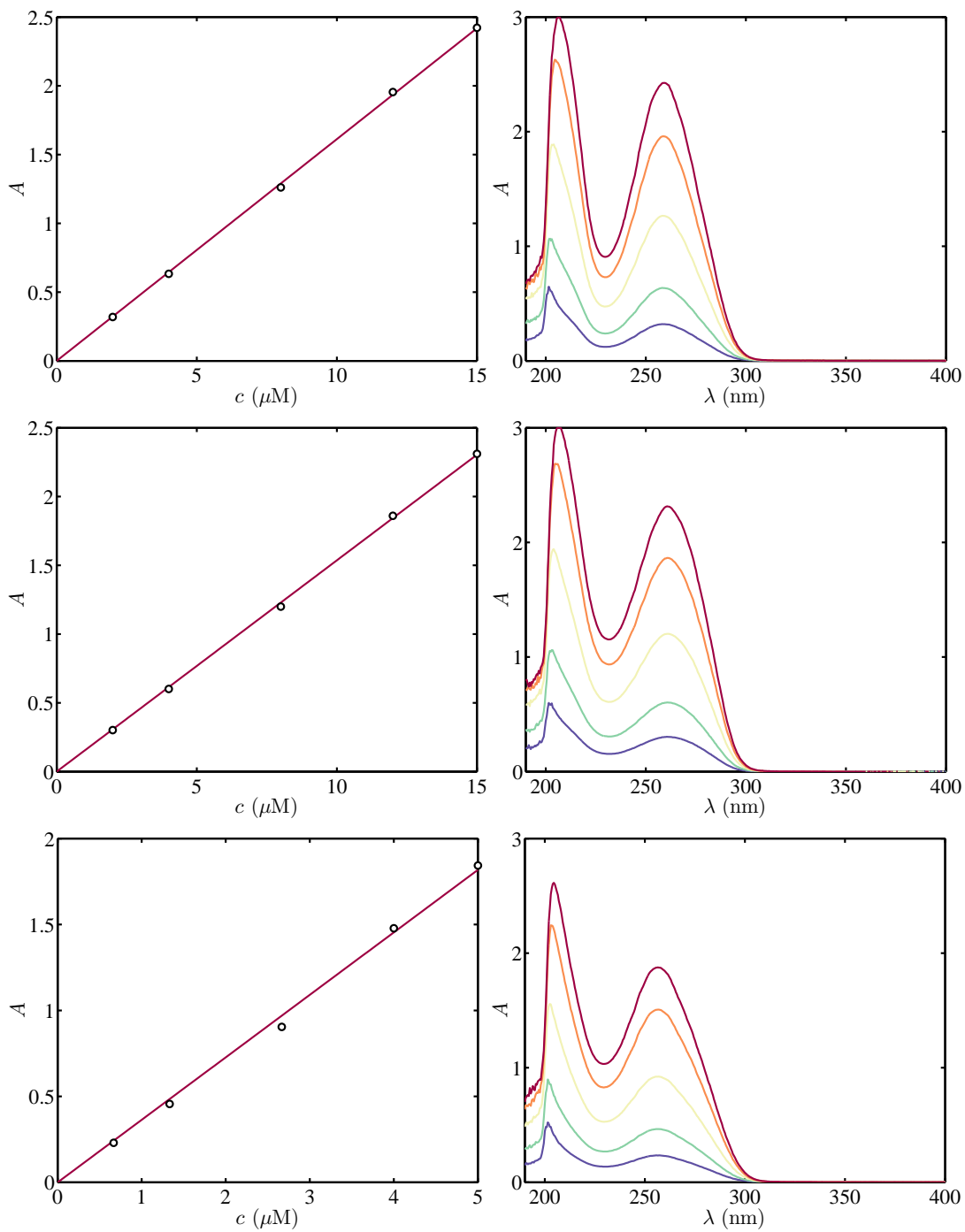


Figure 5.D.1: Left: UV-vis absorbance for DNA solution at 260 nm versus DNA concentration for Strand A (top), Strand B (middle), and “LinkerAdap” (bottom). Right: UV-vis spectra for DNA solution with concentration increasing from blue to red.

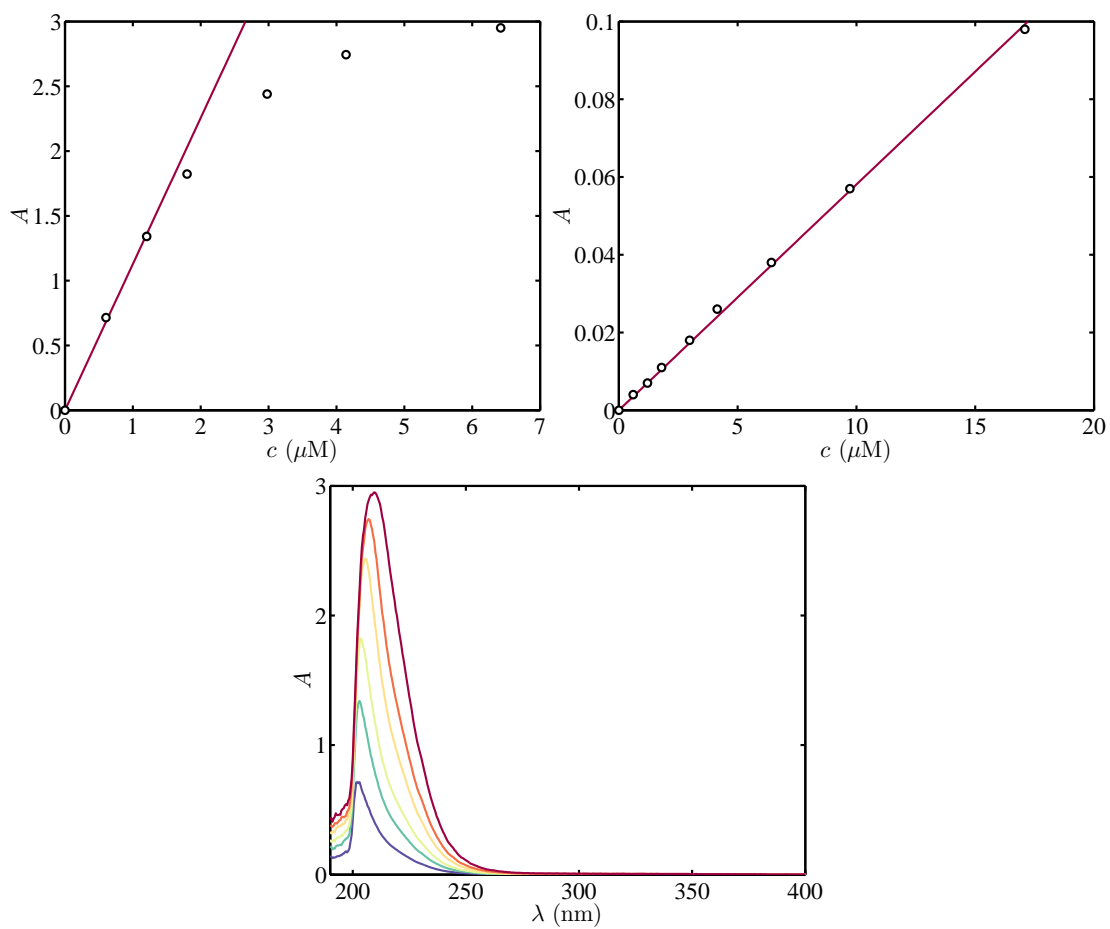


Figure 5.D.2: Top left: UV-vis absorbance for PA solution at the peak versus PA concentration. Top right: UV-vis absorbance for PA solution at 260 nm versus PA concentration. Bottom: UV-vis spectra for PA solution with concentration increasing from blue to red.

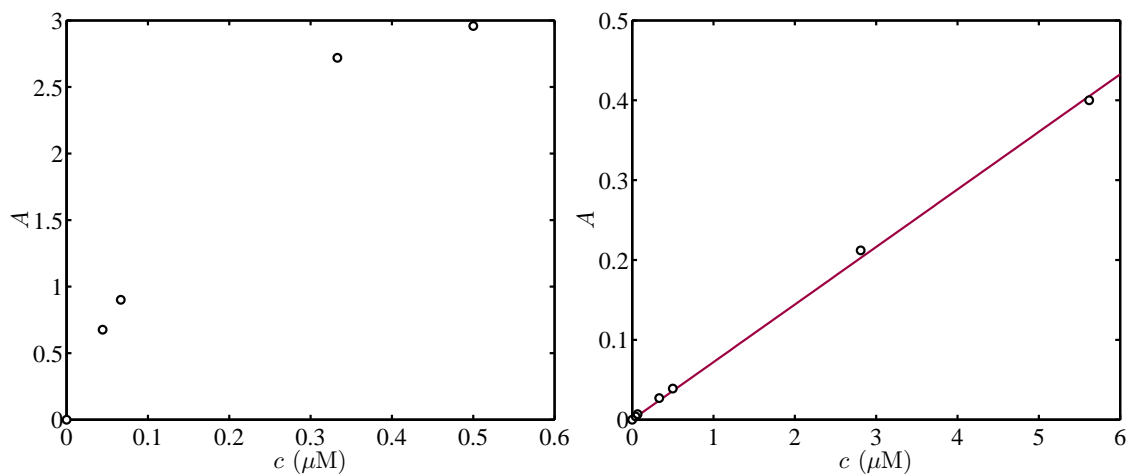


Figure 5.D.3: Left: UV-vis absorbance for acrylamide solution at the peak versus acrylamide concentration. Right: UV-vis absorbance for acrylamide solution at 260 nm versus acrylamide concentration.

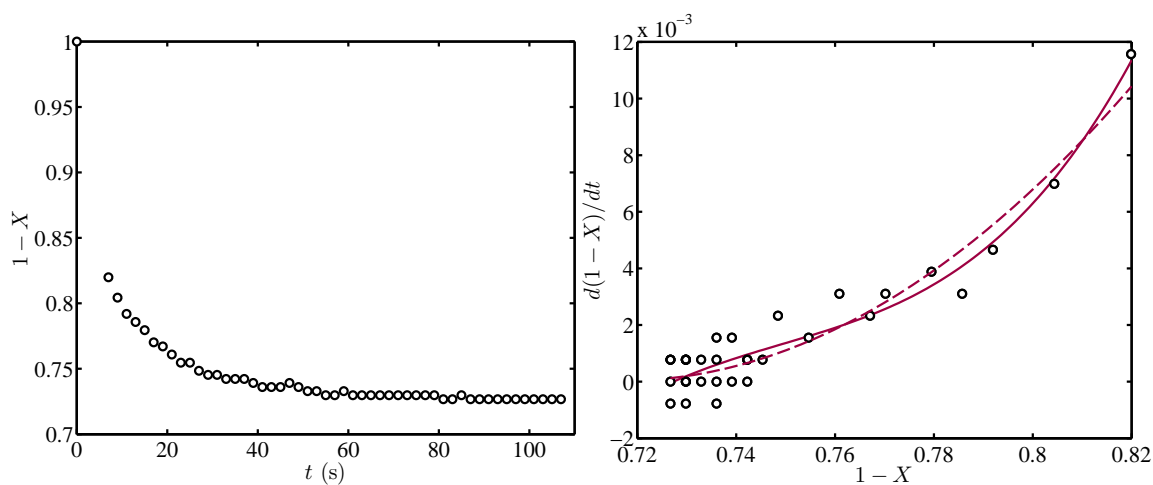


Figure 5.D.4: Left: Kinetics of Strand A, Strand B, and “LinkerAdap” forming DNA crosslinker. Right: The solid curve is the least-squares fit of the $d(1 - X)/dt$ versus $1 - X$ correlation for a third-order reaction, and the dashed curve is the least-squares fit of the $d(1 - X)/dt$ versus $1 - X$ correlation for a second-order reaction.

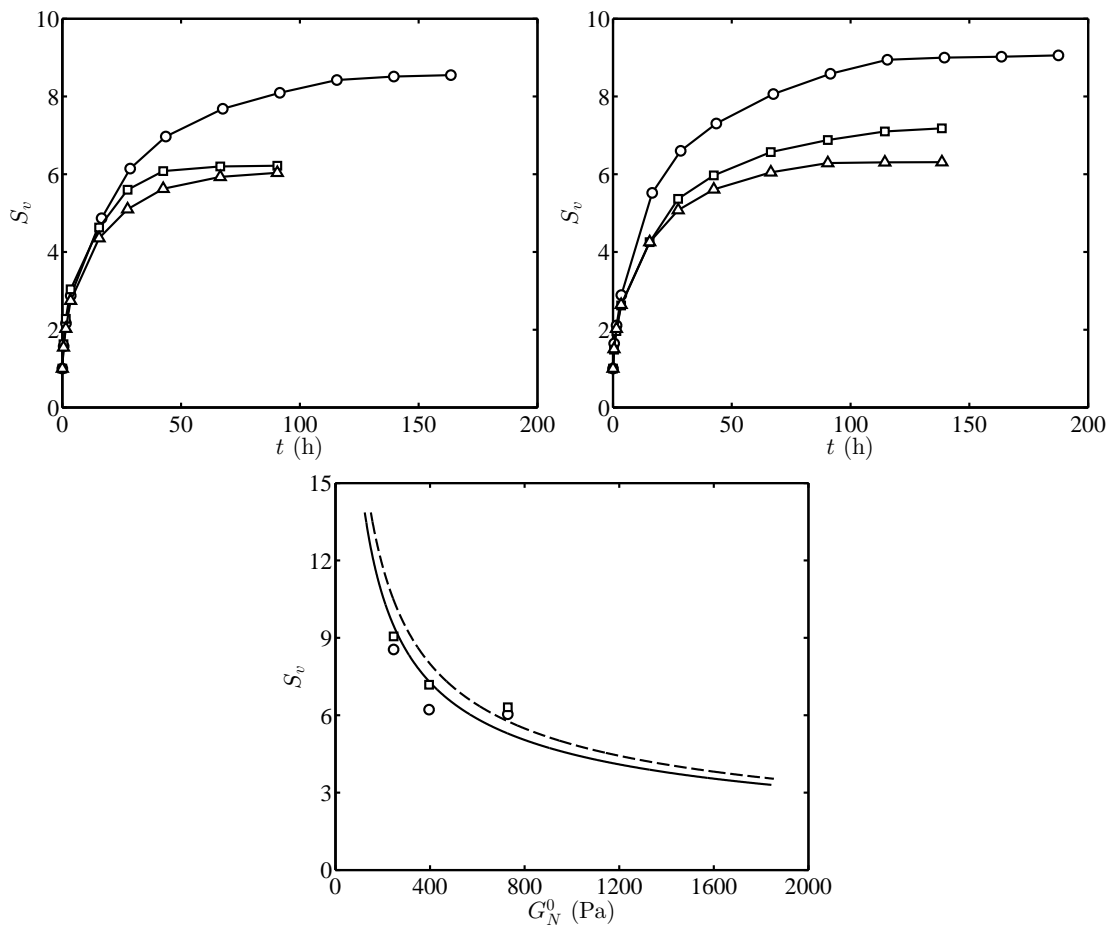


Figure 5.E.1: Top: Swelling of bis-crosslinked gels in RO water (left) and PBS (right). Bottom: Fitting of swelling ratio at equilibrium in RO water (solid) and PBS (dashed) versus G_N^0 with Eqn. (5.1).

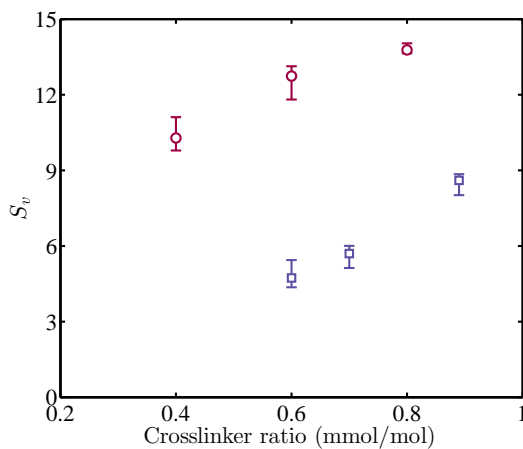


Figure 5.F.1: Swelling ratio prior to dissolution for DNA-crosslinked gels synthesized with a low (circles) and high (squares) TEMED concentration versus crosslinker ratio.

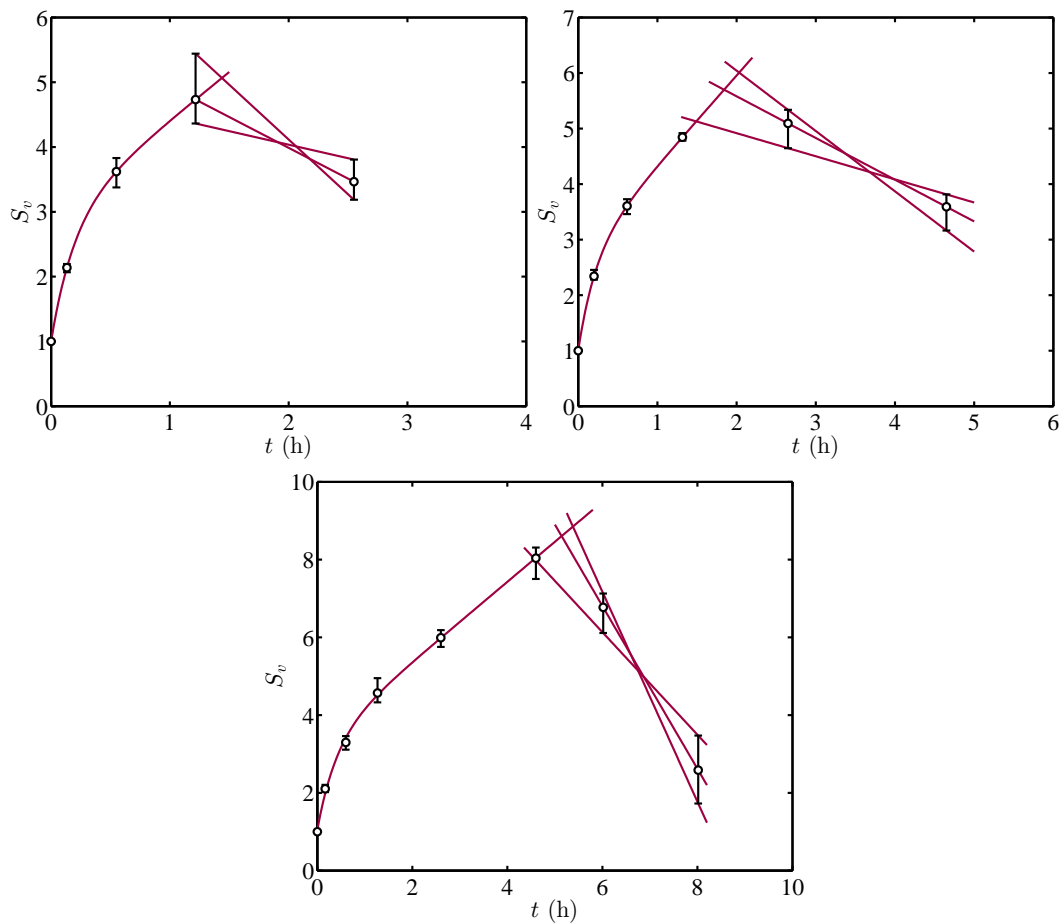


Figure 5.F.2: Swelling and dissolution of DNA-crosslinked gels $B_0D_{0.6}$ (top left), $B_0D_{0.7}$ (top right), and $B_0D_{0.89}$ (bottom) formed with a high TEMED concentration in PBS. Lines before S_v decrease are least-squares fits of empirical Eqn. (5.8). Lines after S_v decrease are used to objectively estimate the maximum S_v .

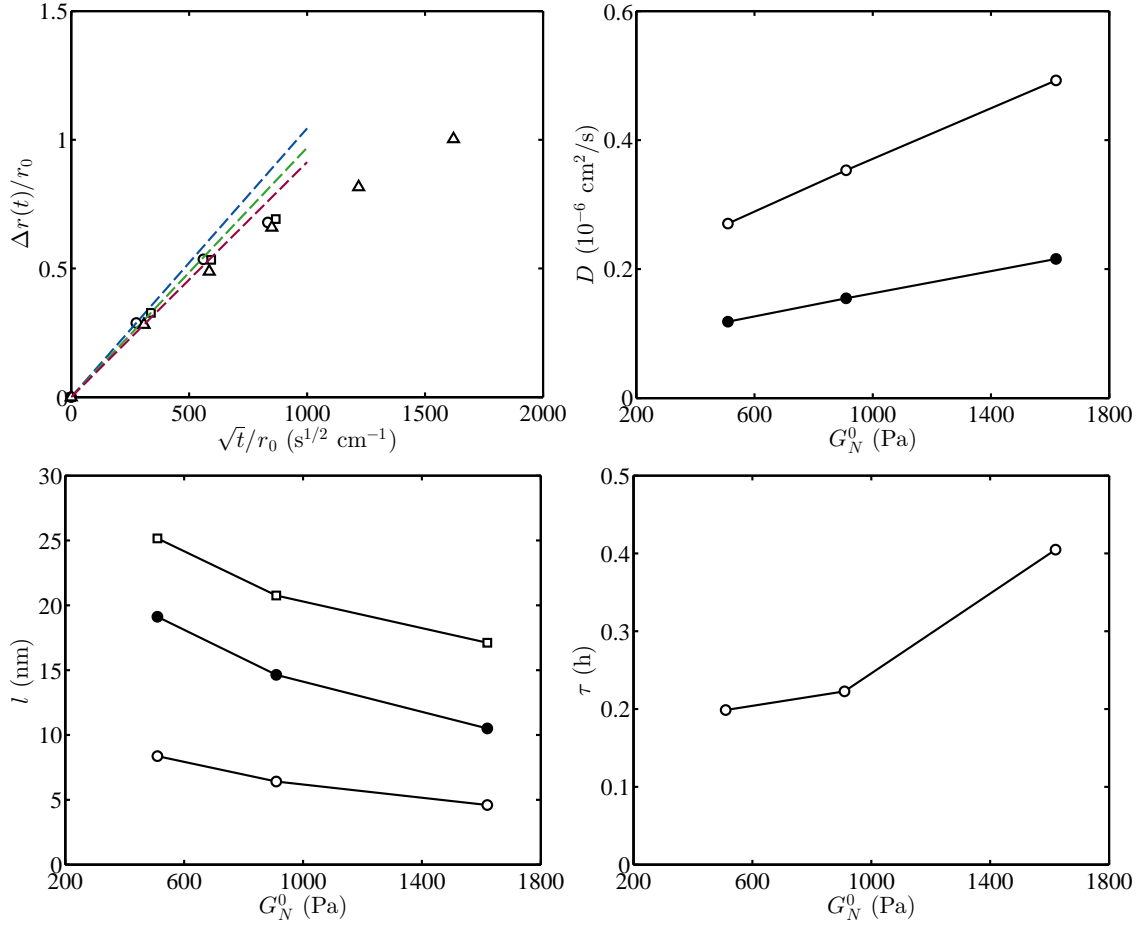


Figure 5.F.3: Top left: Fitting of Eqn. (5.6) to the initial stage of swelling $B_0D_{0.6}$ (circles and blue line), $B_0D_{0.7}$ (squares and green line), and $B_0D_{0.89}$ (triangles and red line). Top right: Cooperative diffusion coefficient calculated with $\nu = 0.33$ (open circles) and $\nu = 0.5$ (filled circles) versus G_N^0 . Bottom left: Pore (mesh) size from D in the top-right panel with $\nu = 0.33$ (open circles) and $\nu = 0.5$ (filled circles), and from $l = (2k_B T / G_N^0)^{1/3}$ (squares) versus G_N^0 . Bottom right: Swelling relaxation time from fitting Eqn. (5.8) versus G_N^0 .

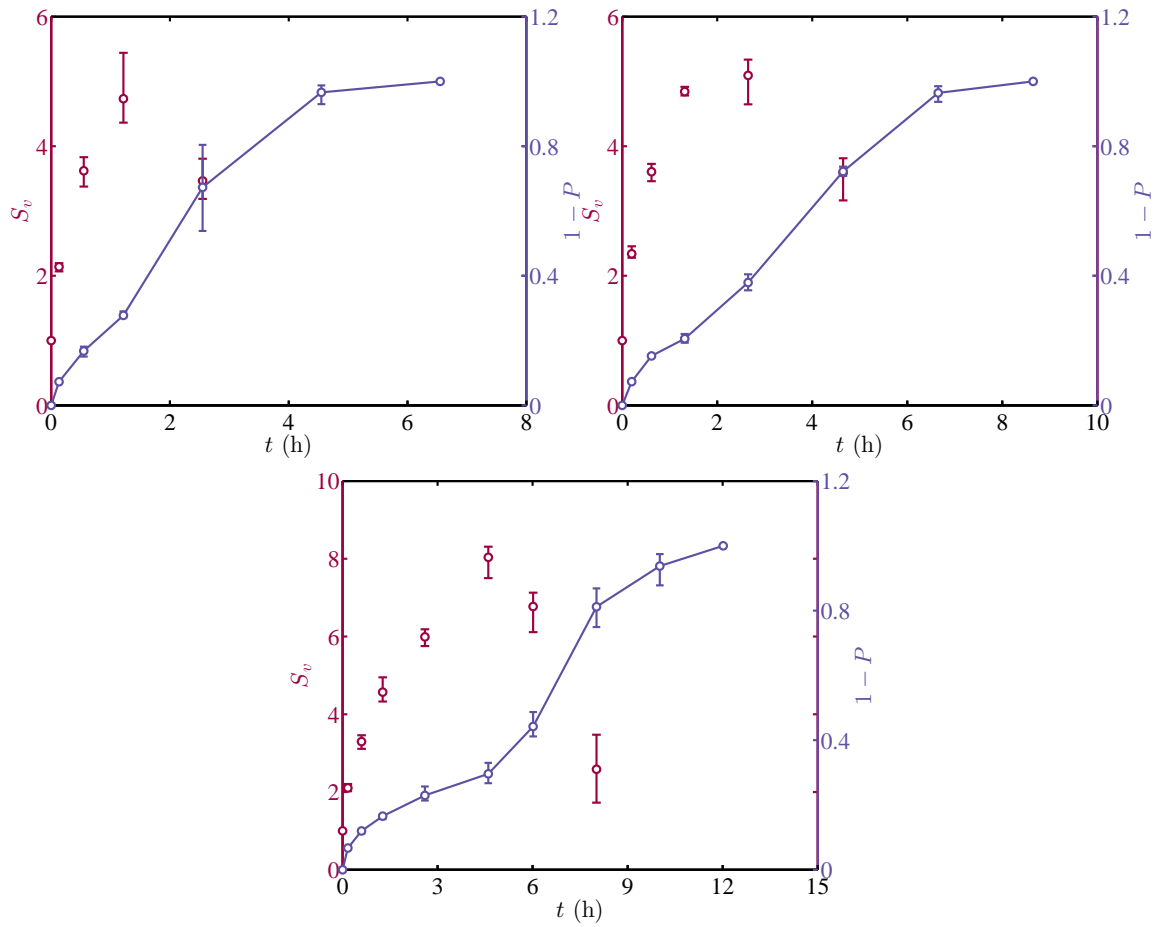


Figure 5.F.4: Time series of the volume swelling ratio (left axis) and the fraction of DNA strands released to PBS (right axis) for DNA-crosslinked gels formed with more TEMED $B_0D_{0.6}$ (top left), $B_0D_{0.7}$ (top right), and $B_0D_{0.89}$ (bottom) during swelling.

Conclusions and future work

6.1 Summary

The objective of this thesis was to achieve a fundamental understanding of complementary-DNA-strand crosslinked polyacrylamide hydrogels using macrorheological and swelling tests.

Linear viscoelasticity of bis-crosslinked polyacrylamide hydrogels were adopted for benchmark comparisons with DNA-crosslinked gels in chapter 3. These gels were synthesized with unusually low crosslinker ratios to match those used for DNA-crosslinked gels. This imparted physical entanglements that are released at long times. Thus, the loss tangent for these gels are much higher than gels with high crosslinker ratio and the upturns in storage modulus occur at lower frequencies. Time-concentration superposition furnished a master plot of the dynamic moduli in which the storage and loss moduli have high-frequency power-laws with an exponent that is smaller than the universal exponent; time-temperature superposition extended the spectra to lower frequencies and furnished an apparent activation energy for disentanglement that is comparable to literature values for polymer melts at temperatures above the glass transition temperature.

Rheological properties in the linear viscoelastic regime of DNA-crosslinked gels and gels that are crosslinked with both physical (DNA) and chemical (bis-acrylamide) crosslinking were investigated in chapter 4. Gelation by DNA crosslinking was found to be faster and more efficient than bis-crosslinking. The loss moduli for DNA- and dual-crosslinked gels have a distinct peak in the early stages of gelation because of the large size of DNA-crosslinking centres. Time-temperature superposition with both horizontal and vertical shifts was used to extend dynamic moduli spectra. It was found that the dynamics of DNA-crosslinked gels depart further from the Maxwell model when increasing the DNA-crosslinker concentration, with dual-crosslinked gels reflecting transient and permanent crosslinking. When DNA-crosslinked gels behave as elastic solids, the apparent activation energy for DNA-crosslink disengagement is constant, with a temperature-independent crosslink number; when the gels become liquid-like, the activation energy decreases with increasing temperature, with an increase in the crosslink number. Creep-recovery tests were undertaken, showing that per-

manent crosslinks in dual-crosslinked gels can also arrest creep and increase the recoverable compliance.

In chapter 5, swelling of polyacrylamide hydrogels with bis-, DNA-, and dual-crosslinking were studied. DNA-crosslinked gels were found to dissolve in PBS. The volume swelling ratio prior to dissolution increases with the DNA-crosslinker ratio. The release of DNA strands to the buffer during swelling was established using UV-vis spectroscopy. Permanent crosslinks in dual-crosslinked gels prevented gel dissolution. A theoretical model was used to examine the swelling and dissolution of DNA- and dual-crosslinked gels. This captures qualitative experimental trends, namely the correlation between the gel plateau modulus and swelling ratio for DNA- and dual-crosslinked gels.

6.2 Original contributions to knowledge

The original contributions of this thesis to knowledge include:

- Rheological properties of bis-crosslinked gels with low crosslinker ratio are reported, providing microstructural interpretations.
- The apparent activation energy for disentanglement in chemically crosslinked gels is ascertained using time-temperature superposition to be in the range of $25\text{--}6 k_B T$ at temperature in the range of $21\text{--}56^\circ\text{C}$. The horizontal shift factor follows the WLF equation. The physical entanglements increase dynamic moduli at high frequencies and impart a non-universal sol-gel transition with exponent $\Delta \approx 0.38$.
- Time-temperature superposition is shown to be applicable for DNA-crosslinked and dual-crosslinked gels, extending the dynamic spectra to low frequencies. The apparent activation energy for DNA-crosslink disentanglement is reported to be $\approx 130 k_B T$, showing that breaking ≈ 10 out of 12 base pairs between one DNA strand and one “LinkerAdap” moiety can dissociate the DNA crosslink. Below the gel-sol transition temperature, the activation energy is temperature-independent, whereas it decreases with increasing temperature when the temperature is above the transition temperature.
- DNA-crosslinked gels with increasing crosslinker ratio behave like viscous-liquids at times greater than 3–700 h. DNA-crosslinked gel cylinders with a $1/16''$ diameter and an aspect ratio ≈ 6.3 dissolve in PBS buffer with a volume ≈ 100 times the gel volume after 10–40 h.

- The role of chemical crosslinks in dual-crosslinked gel networks was investigated through rheology and swelling tests. It was found that permanent crosslinks can arrest creep and ensure most of the strain caused by the load during creep is recoverable. Chemical crosslinks can also prevent dual-crosslinked gels from dissolving in PBS buffer.
- Existing studies of DNA- and dual-crosslinked gels have focused on the volume or phase change of the gel in response to target molecules. This thesis provides new insights on their durability under load and solvent, which will be useful for applications of such gels.

6.3 Future work

- Distinct features were found for bis-crosslinked gels with low crosslinker ratio in this thesis. However, the definition of “low crosslinker ratio” is ambiguous, because only one monomer concentration was used. Thus it is necessary to study gels with different monomer concentrations and crosslinker concentrations. Thus, the range of monomer and crosslinker concentrations imparting these distinct features can be ascertained.
- Large amplitude oscillatory shear tests were performed for gel samples, but results are not included in this thesis because of the wall-slip effect. This should be addressed in future by using sand-paper coated or serrated sample holders. Also, self-healing of DNA- and dual-crosslinked gels was not proven because of this effect. The gels were not broken even under a very larger strain. After changing the sample holder, dynamic moduli spectra of DNA- and dual-crosslinked gel can be measured under small–large–small strain cycles to verify the self-healing ability.
- Gravimetry was adopted to monitor the gel swelling, which accelerators the gel breakage. Also, the conversion from the mass to volume swelling ratio may introduce errors to the results, because the gel density was estimated. A procedure that can directly measure the gel cylinder size during swelling without disturbance should be developed. A possible method is using a video camera to record images of the cylinder, and adopting ImageJ to analyze the video and obtain the diameter or length change.
- Bis-crosslinked gels should be dried and weighed to obtain the mass loss from polymers that were not connected to networks. This would help to determine the possible errors arise from starting swelling from the as-prepared state other than dried state, and to ascertain the reason for the mass loss in dual-crosslinked gel swelling.

- DNA crosslinkers can be constructed with a different number of base pairs. Thus, whether dynamic moduli spectra at lower frequencies are affected by the activation energy for DNA dissociation, whether the swelling and dissolution of DNA-crosslinked gel with larger activation energy are slower, and whether the activation energy affects the gel self-healing ability can be validated.
- Paper-based polymerized colloidal crystal arrays (PB-PCCAs) can be developed using dual-crosslinked gels. The ratio of DNA crosslinkers to bis-acrylamide crosslinkers could be chosen between 3:1 and 1:1 to form a sensor that can rest on its own weight and exhibit different colour-shifts in response to buffer with and without target molecules.

References

- [1] F. Di Lorenzo and S. Seiffert. Nanostructural heterogeneity in polymer networks and gels. *Polym. Chem.*, 6:5515–5528, 2015.
- [2] A. K. Denisin and B. L. Pruitt. Tuning the range of polyacrylamide gel stiffness for mechanobiology applications. *ACS Appl. Mater. Interfaces*, 8:21893–21902, 2016.
- [3] J. D. Ferry. *Viscoelastic Properties of Polymers*. John Wiley & Sons, Inc., 1980.
- [4] V. Adibnia and R. J. Hill. Universal aspects of hydrogel gelation kinetics, percolation and viscoelasticity from PA-hydrogel rheology. *J. Rheol.*, 60:541–548, 2016.
- [5] V. Adibnia. *Electroacoustic and rheological characterization of hydrogel nanocomposites*. PhD thesis, McGill University, 2017.
- [6] J. L. Trompette, E. Fabrègue, and G. Cassanas. Influence of the monomer properties on the rheological behavior of chemically crosslinked hydrogels. *J. Polym. Sci. B*, 35: 2535–2541, 1997.
- [7] D. Calvet, J. Y. Wong, and S. Giasson. Rheological monitoring of polyacrylamide gelation: importance of cross-link density and temperature. *Macromolecules*, 37:7762–7771, 2004.
- [8] A. Basu, Q. Wen, X. Mao, T. C. Lubensky, P. A. Janmey, and A. G. Yodh. Nonaffine displacements in flexible polymer networks. *Macromolecules*, 44:1671–1679, 2011.
- [9] Y. D. Livney, I. Portnaya, B. Faupin, L. Fahoum, O. Ramon, Y. Cohen, S. Mizrahi, and U. Cogan. Interactions of glucose and polyacrylamide in solutions and gels. *J. Polym. Sci. B Polym. Phys.*, 41:3053–3063, 2003.
- [10] A. Konda, K. Urayama, and T. Takigawa. Strain-rate-dependent Poisson’s ratio and stress of polymer gels in solvents revealed by ultraslow stretching. *Macromolecules*, 44: 3000–3006, 2011.

- [11] T. Liedl, H. Dietz, B. Yurke, and F. Simmel. Controlled trapping and release of quantum dots in a DNA-switchable hydrogel. *Small*, 3:1688–1693, 2007.
- [12] H. Yang, H. Liu, H. Kang, and W. Tan. Engineering target-responsive hydrogels based on aptamer-target interactions. *J. Am. Chem. Soc.*, 130:6320–6321, 2008.
- [13] X. Wang and X. Wang. Aptamer-functionalized hydrogel diffraction gratings for the human thrombin detection. *Chem. Commun.*, 49:5957–5959, 2013.
- [14] B.-F. Ye, Y.-J. Zhao, Y. Cheng, T.-T. Li, Z.-Y. Xie, X.-W. Zhao, and Z.-Z. Gu. Colorimetric photonic hydrogel aptasensor for the screening of heavy metal ions. *Nanoscale*, 4:5998–6003, 2012.
- [15] F. X. Jiang, B. Yurke, R. S. Schloss, B. L. Firestein, and N. A. Langrana. Effect of dynamic stiffness of the substrates on neurite outgrowth by using a DNA-crosslinked hydrogel. *Tissue Eng. Part A.*, 16:1873–1889, 2010.
- [16] F. X. Jiang, B. Yurke, R. S. Schloss, B. L. Firestein, and N. A. Langrana. The relationship between fibroblast growth and the dynamic stiffnesses of a DNA crosslinked hydrogel. *Biomaterials*, 31:1199–1212, 2010.
- [17] F. X. Jiang, B. Yurke, D. Verma, M. Previtera, R. Schloss, and N. A. Langrana. Development of DNA based active macro-materials for biology and medicine: a review. In *Biomaterials Science and Engineering*. InTech, 2011.
- [18] C. Li, X. Zhou, Y. Shao, P. Chen, Y. Xing, Z. Yang, Z. Li, and D. Liu. A supramolecular hydrogel with identical cross-linking point density but distinctive rheological properties. *Mater. Chem. Front.*, 1:654–659, 2017.
- [19] D. C. Lin, B. Yurke, and N. A. Langrana. Mechanical properties of a reversible, DNA-crosslinked polyacrylamide hydrogel. *J. Biomech. Eng.*, 126:104–110, 2004.
- [20] F. X. Jiang, B. Yurke, B. L. Firestein, and N. A. Langrana. Neurite outgrowth on a DNA crosslinked hydrogel with tunable stiffnesses. *Ann. Biomed. Eng.*, 36:1565–1579, 2008.
- [21] U. Chippada, B. Yurke, and N. A. Langrana. Simultaneous determination of Young’s modulus, shear modulus, and Poisson’s ratio of soft hydrogels. *J. Mater. Res.*, 25: 545–555, 2011.

- [22] H. H. Winter and M. Mours. Rheology of polymers near liquid-solid transitions. In *Advances in Polymer Science*. Springer Berlin Heidelberg, 1997.
- [23] K. Nishinari. Some thoughts on the definition of a gel. In *Progress in Colloid and Polymer Science*. Springer Berlin Heidelberg, 2009.
- [24] P. J. Flory. Introductory lecture. *Faraday Discuss. Chem. Soc.*, 57:7–18, 1974.
- [25] K. Almdal, J. Dyre, S. Hvidt, and O. Kramer. Towards a phenomenological definition of the term ‘gel’. *Polym. Gels Netw.*, 1:5–17, 1993.
- [26] P. Gupta, K. Vermani, and S. Garg. Hydrogels: from controlled release to pH-responsive drug delivery. *Drug Discov. Today*, 7:569–579, 2002.
- [27] N. Chirani, L. Yahia, L. Gritsch, F. L. Motta, SoumiaChirani, and S. Faré. History and applications of hydrogels. *J. Biomedical Sci.*, 4:1–23, 2015.
- [28] M. Vert, Y. Doi, K.-H. Hellwich, M. Hess, P. Hodge, P. Kubisa, M. Rinaudo, and F. Schué. Terminology for biorelated polymers and applications (IUPAC Recommendations 2012). *Pure Appl. Chem.*, 84:377–410, 2012.
- [29] G. Gerlach and K.-F. Arndt, editors. *Hydrogel Sensors and Actuators*. Springer Berlin Heidelberg, 2009.
- [30] T. R. Hoare and D. S. Kohane. Hydrogels in drug delivery: progress and challenges. *Polymer*, 49:1993–2007, 2008.
- [31] H. J. Naghash and O. Okay. Formation and structure of polyacrylamide gels. *J. Appl. Polym. Sci.*, 60:971–979, 1996.
- [32] M. Y. Kizilay and O. Okay. Effect of hydrolysis on spatial inhomogeneity in poly(acrylamide) gels of various crosslink densities. *Polymer*, 44:5239–5250, 2003.
- [33] Y. Akagi, J. P. Gong, U.-i. Chung, and T. Sakai. Transition between phantom and affine network model observed in polymer gels with controlled network structure. *Macromolecules*, 46:1035–1040, 2013.
- [34] M. L. Oyen. Mechanical characterisation of hydrogel materials. *Int. Mater. Rev.*, 59:44–59, 2014.

- [35] W. Hennink and C. van Nostrum. Novel crosslinking methods to design hydrogels. *Adv. Drug Deliv. Rev.*, 54:13–36, 2002.
- [36] D. Hunkeler. Mechanism and kinetics of the persulfate-initiated polymerization of acrylamide. *Macromolecules*, 24:2160–2171, 1991.
- [37] A. Chrambach and D. Rodbard. Polyacrylamide gel electrophoresis. *Science*, 172:440–451, 1971.
- [38] J. Baselga, I. Hernandez-Fuentes, I. F. Pierola, and M. A. Llorente. Elastic properties of highly crosslinked polyacrylamide gels. *Macromolecules*, 20:3060–3065, 1987.
- [39] Y. Li and T. Tanaka. Kinetics of swelling and shrinking of gels. *J. Chem. Phys.*, 92:1365–1371, 1990.
- [40] L. M. Lira, K. A. Martins, and S. I. C. d. Torresi. Structural parameters of polyacrylamide hydrogels obtained by the Equilibrium Swelling Theory. *Eur. Polym. J.*, 45:1232–1238, 2009.
- [41] M. Ebara, Y. Kotsuchibashi, K. Uto, T. Aoyagi, Y.-J. Kim, R. Narain, N. Idota, and J. M. Hoffman. Smart hydrogels. In *Smart Biomaterials*. Springer Japan, 2014.
- [42] A. Hayashi and T. Kanzaki. Swelling of agarose gel and its related changes. *Food Hydrocoll.*, 1:317–325, 1987.
- [43] S. Tanaka and K. Nishinari. Unassociated molecular chains in physically crosslinked gellan gels. *Polym. J.*, 39:397–403, 2007.
- [44] S. Nagahara and T. Matsuda. Hydrogel formation via hybridization of oligonucleotides derivatized in water-soluble vinyl polymers. *Polym. Gels Netw.*, 4:111–127, 1996.
- [45] X. He, B. Wei, and Y. Mi. Aptamer based reversible DNA induced hydrogel system for molecular recognition and separation. *Chem. Commun.*, 46:6308–6310, 2010.
- [46] J. Liu. Oligonucleotide-functionalized hydrogels as stimuli responsive materials and biosensors. *Soft Matter*, 7:6757–6767, 2011.
- [47] S. Tombelli, M. Minunni, and M. Mascini. Analytical applications of aptamers. *Biosens. Bioelectron.*, 20:2424–2434, 2005.

- [48] Z. Zhu, C. Wu, H. Liu, Y. Zou, X. Zhang, H. Kang, C. J. Yang, and W. Tan. An aptamer cross-linked hydrogel as a colorimetric platform for visual detection. *Angew. Chem. Int. Ed.*, 49:1052–1056, 2010.
- [49] B. Wei, I. Cheng, K. Q. Luo, and Y. Mi. Capture and release of protein by a reversible DNA-induced sol-gel transition system. *Angew. Chem. Int. Ed.*, 120:337–339, 2008.
- [50] Z. Wei, J. H. Yang, J. Zhou, F. Xu, M. Zrinyi, P. H. Dussault, Y. Osada, and Y. M. Chen. Self-healing gels based on constitutional dynamic chemistry and their potential applications. *Chem. Soc. Rev.*, 43:8114–8131, 2014.
- [51] P. Terech, M. Yan, M. Marechal, G. Royal, J. Galvez, and S. K. P. Velu. Characterization of strain recovery and “self-healing” in a self-assembled metallo-gel. *Phys. Chem. Chem. Phys.*, 15:7338–7344, 2013.
- [52] Q. Wang, J. L. Mynar, M. Yoshida, E. Lee, M. Lee, K. Okuro, K. Kinbara, and T. Aida. High-water-content mouldable hydrogels by mixing clay and a dendritic molecular binder. *Nature*, 463:339–343, 2010.
- [53] T. L. Sun, T. Kurokawa, S. Kuroda, A. B. Ihsan, T. Akasaki, K. Sato, M. A. Haque, T. Nakajima, and J. P. Gong. Physical hydrogels composed of polyampholytes demonstrate high toughness and viscoelasticity. *Nat. Mater.*, 12:932–937, 2013.
- [54] G. H. Deng, C. M. Tang, F. Y. Li, H. F. Jiang, and Y. M. Chen. Covalent cross-linked polymer gels with reversible sol-gel transition and self-healing properties. *Macromolecules*, 43:1191–1194, 2010.
- [55] X. Yan, Q. Chen, L. Zhu, H. Chen, D. Wei, F. Chen, Z. Tang, J. Yang, and J. Zheng. High strength and self-healable gelatin/polyacrylamide double network hydrogels. *J. Mater. Chem. B*, 5:7683–7691, 2017.
- [56] Z. Wei, J. He, T. Liang, H. Oh, J. Athas, Z. Tong, C. Wang, and Z. Nie. Autonomous self-healing of poly(acrylic acid) hydrogels induced by the migration of ferric ions. *Polym. Chem.*, 4:4601–4605, 2013.
- [57] A. Phadke, C. Zhang, B. Arman, C.-C. Hsu, R. A. Mashelkar, A. K. Lele, M. J. Tauber, G. Arya, and S. Varghese. Rapid self-healing hydrogels. *PNAS*, 109:4383–4388, 2012.
- [58] A. B. W. Brochu, S. L. Craig, and W. M. Reichert. Self-healing biomaterials. *J. Biomed. Mater. Res. A*, 96:492–506, 2010.

- [59] M. Shibayama, M. Uesaka, S. Inamoto, H. Mihara, and S. Nomura. Analogy between swelling of gels and intrinsic viscosity of polymer solutions for ion-complexed poly(vinyl alcohol) in aqueous medium. *Macromolecules*, 29:885–891, 1996.
- [60] T. Narita, K. Mayumi, G. Ducouret, and P. Hébraud. Viscoelastic properties of poly(vinyl alcohol) hydrogels having permanent and transient cross-links studied by microrheology, classical rheometry, and dynamic light scattering. *Macromolecules*, 46:4174–4183, 2013.
- [61] K. Mayumi, J. Guo, T. Narita, C. Y. Hui, and C. Creton. Fracture of dual crosslink gels with permanent and transient crosslinks. *Extreme Mech. Lett.*, 6:52–59, 2016.
- [62] R. Long, K. Mayumi, C. Creton, T. Narita, and C.-Y. Hui. Time dependent behavior of a dual cross-link self-healing gel: theory and experiments. *Macromolecules*, 47:7243–7250, 2014.
- [63] M. T. Shaw. *Introduction to Polymer Rheology*. John Wiley & Sons, Inc., 2012.
- [64] T. A. Waigh. Advances in the microrheology of complex fluids. *Rep. Prog. Phys.*, 79:074601, 2016.
- [65] V. Adibnia and R. J. Hill. Electroacoustic spectroscopy of nanoparticle-doped hydrogels. *Macromolecules*, 47:8064–8071, 2014.
- [66] M. Djabourov, K. Nishinari, and S. B. Ross-Murphy. *Physical Gels from Biological and Synthetic Polymers*. Cambridge University Press, 2013.
- [67] P. Cicutta and A. M. Donald. Microrheology: a review of the method and applications. *Soft Matter*, 3:1449–1455, 2007.
- [68] R. E. Mahaffy, C. K. Shih, F. C. MacKintosh, and J. Käs. Scanning probe-based frequency-dependent microrheology of polymer gels and biological cells. *Phys. Rev. Lett.*, 85:880–883, 2000.
- [69] T. H. Larsen and E. M. Furst. Microrheology of the liquid-solid transition during gelation. *Phys. Rev. Lett.*, 100:146001, 2008.
- [70] R. G. Larson. *The Structure and Rheology of Complex Fluids*. Oxford University Press Inc., 1999.

- [71] T. Indei and J.-i. Takimoto. Linear viscoelastic properties of transient networks formed by associating polymers with multiple stickers. *J. Chem. Phys.*, 133:194902, 2010.
- [72] D. Adolf and J. E. Martin. Time-cure superposition during crosslinking. *Macromolecules*, 23:3700–3704, 1990.
- [73] J. E. Martin, D. Adolf, and J. P. Wilcoxon. Viscoelasticity of near-critical gels. *Phys. Rev. Lett.*, 61:2620–2623, 1988.
- [74] L. Rouleau, J.-F. Deü, A. Legay, and F. L. Lay. Application of Kramers-Kronig relations to time-temperature superposition for viscoelastic materials. *Mech. Mater.*, 65:66–75, 2013.
- [75] H. F. Mark. *Encyclopedia of Polymer Science and Technology, Concise*. John Wiley & Sons, Inc., 2007.
- [76] R. Lakes. *Viscoelastic Materials*. Cambridge University Press, 2009.
- [77] Y. Xu, X. Gong, S. Xuan, X. Li, L. Qin, and W. Jiang. Creep and recovery behaviors of magnetorheological plastomer and its magnetic-dependent properties. *Soft Matter*, 8:8483–8492, 2012.
- [78] W. A. Cruz and E. P. G. Areas. Protein-polysaccharide viscoelastic matrices: synergic effects of amylose on lysozyme physical gelation in aqueous dimethylsulfoxide. *Soft Matter*, 5:4240–4249, 2009.
- [79] S. Abdurrahmanoglu and O. Okay. Rheological behavior of polymer-clay nanocomposite hydrogels: Effect of nanoscale interactions. *J. Appl. Polym. Sci.*, 116:2328–2335, 2010.
- [80] R. M. L. Evans, M. Tassieri, D. Auhl, and T. A. Waigh. Direct conversion of rheological compliance measurements into storage and loss moduli. *Phys. Rev. E*, 80:012501, 2009.
- [81] M. Kim, J.-E. Bae, N. Kang, and K. Soo Cho. Extraction of viscoelastic functions from creep data with ringing. *J. Rheol.*, 59:237–252, 2014.
- [82] M. K. Kwon, S. H. Lee, S. G. Lee, and K. S. Cho. Direct conversion of creep data to dynamic moduli. *J. Rheol.*, 60:1181–1197, 2016.

- [83] K. Hyun, M. Wilhelm, C. O. Klein, K. S. Cho, J. G. Nam, K. H. Ahn, S. J. Lee, R. H. Ewoldt, and G. H. McKinley. A review of nonlinear oscillatory shear tests: Analysis and application of large amplitude oscillatory shear (LAOS). *Prog. Polym. Sci.*, 36:1697–1753, 2011.
- [84] S. Khandavalli and J. P. Rothstein. Large amplitude oscillatory shear rheology of three different shear-thickening particle dispersions. *Rheologica. Acta.*, 54:601–618, 2015.
- [85] K. Atalık and R. Keunings. On the occurrence of even harmonics in the shear stress response of viscoelastic fluids in large amplitude oscillatory shear. *J. Non-Newtonian Fluid Mech.*, 122:107–116, 2004.
- [86] T. Domenech and S. S. Velankar. On the rheology of pendular gels and morphological developments in paste-like ternary systems based on capillary attraction. *Soft Matter*, 11:1500–1516, 2015.
- [87] Y. Eom and B. C. Kim. Effects of chain conformation on the viscoelastic properties of polyacrylonitrile gels under large amplitude oscillatory shear. *Eur. Polym. J.*, 85:341–353, 2016.
- [88] S. Cai and Z. Suo. Equations of state for ideal elastomeric gels. *Europhys. Lett.*, 97:34009, 2012.
- [89] J. Li, Y. Hu, J. J. Vlassak, and Z. Suo. Experimental determination of equations of state for ideal elastomeric gels. *Soft Matter*, 8:8121–8128, 2012.
- [90] J. Baselga, I. Hernández-Fuentes, R. M. Masegosa, and M. A. Llorente. Effect of crosslinker on swelling and thermodynamic properties of polyacrylamide gels. *Polym. J.*, 21:467–474, 1989.
- [91] T. Boyde. Swelling and contraction of polyacrylamide gel slabs in aqueous solutions. *J. Chromatogr. A*, 124:219–230, 1976.
- [92] M. Sivanantham and B. V. R. Tata. Swelling/deswelling of polyacrylamide gels in aqueous NaCl solution: Light scattering and macroscopic swelling study. *Pramana - J. Phys.*, 79:457–469, 2012.
- [93] Y. D. Livney, I. Portnaya, B. Faupin, O. Ramon, Y. Cohen, U. Cogan, and S. Mizrahi. Interactions between inorganic salts and polyacrylamide in aqueous solutions and gels. *J. Polym. Sci. B Polym. Phys.*, 41:508–519, 2003.

- [94] O. Okay, S. B. Sariişik, and S. D. Zor. Swelling behavior of anionic acrylamide-based hydrogels in aqueous salt solutions: Comparison of experiment with theory. *J. Appl. Polym. Sci.*, 70:567–575, 1998.
- [95] T. Tanaka and D. J. Fillmore. Kinetics of swelling of gels. *J. Chern. Phys.*, 70:1214–1218, 1979.
- [96] A. Hakiki and J. E. Herz. A study of the kinetics of swelling in cylindrical polystyrene gels: Mechanical behavior and final properties after swelling. *J. Chern. Phys.*, 101:9054–9059, 1994.
- [97] A. Peters and S. J. Candau. Kinetics of swelling of spherical and cylindrical gels. *Macromolecules*, 21:2278–2282, 1988.
- [98] J. Yoon, S. Cai, Z. Suo, and R. C. Hayward. Poroelastic swelling kinetics of thin hydrogel layers: comparison of theory and experiment. *Soft Matter*, 6:6004–6012, 2010.
- [99] C.-Y. Hui and V. Muralidharan. Gel mechanics: a comparison of the theories of Biot and Tanaka, Hocker, and Benedek. *J. Chem. Phys.*, 123:154905, 2005.
- [100] D. L. Holmes and N. C. Stellwagen. Estimation of polyacrylamide gel pore size from Ferguson plots of linear DNA fragments. ii. Comparison of gels with different crosslinker concentrations, added agarose and added linear polyacrylamide. *Electrophoresis*, 12:612–619, 1991.
- [101] Y. An, F. J. Solis, and H. Jiang. A thermodynamic model of physical gels. *J. Mech. Phys. Solids*, 58:2083–2099, 2010.
- [102] S. H. Jeong, K. M. Huh, and K. Park. Hydrogel drug delivery systems. In *Polymers in Drug Delivery*. CRC Press, 2006.
- [103] J. Baselga, M. Llorente, J. Nieto, I. Hernández-Fuentes, and I. Piérola. Polyacrylamide networks. sequence distribution of crosslinker. *Eur. Polym. J.*, 24:161–165, 1988.
- [104] R. A. L. Jones. *Soft Condensed Matter*. Oxford University Press Inc., 2002.
- [105] S. Seiffert and J. Sprakel. Physical chemistry of supramolecular polymer networks. *Chem. Soc. Rev.*, 41:909–930, 2012.

- [106] J. F. Sanders, J. D. Ferry, and R. H. Valentine. Viscoelastic properties of 1,2-polybutadiene—comparison with natural rubber and other elastomers. *J. Polym. Sci. B Polym. Phys.*, 6:967–980, 1968.
- [107] S. K. Patel, S. Malone, C. Cohen, J. R. Gillmor, and R. H. Colby. Elastic modulus and equilibrium swelling of poly(dimethylsiloxane) networks. *Macromolecules*, 25:5241–5251, 1992.
- [108] R. H. Colby, L. J. Fetters, and W. W. Graessley. The melt viscosity-molecular weight relationship for linear polymers. *Macromolecules*, 20:2226–2237, 1987.
- [109] S. Abdurrahmanoglu, V. Can, and O. Okay. Design of high-toughness polyacrylamide hydrogels by hydrophobic modification. *Polymer*, 50:5449–5455, 2009.
- [110] X. Xu, J. Chen, and L. An. Shear thinning behavior of linear polymer melts under shear flow via nonequilibrium molecular dynamics. *J. Chem. Phys.*, 140:174902, 2014.
- [111] F. Chambon and H. H. Winter. Linear viscoelasticity at the gel point of a crosslinking PDMS with imbalanced stoichiometry. *J. Rheol.*, 31:683–697, 1987.
- [112] J. E. Martin, D. Adolf, and J. P. Wilcoxon. Viscoelasticity near the sol-gel transition. *Phys. Rev. A*, 39:1325–1332, 1989.
- [113] M. Adam, M. Delsanti, and D. Durand. Mechanical measurements in the reaction bath during the polycondensation reaction, near the gelation threshold. *Macromolecules*, 18:2285–2290, 1985.
- [114] Y. Shangguan, F. Chen, E. Jia, Y. Lin, J. Hu, and Q. Zheng. New insight into time-temperature correlation for polymer relaxations ranging from secondary relaxation to terminal flow: application of a universal and developed WLF equation. *Polymers*, 9:567–588, 2017.
- [115] J. Peng, R. Dong, B. Ren, X. Chang, and Z. Tong. Novel hydrophobically modified ethoxylated urethanes end-capped by percec-type alkyl substituted benzyl alcohol dendrons: synthesis, characterization, and rheological behavior. *Macromolecules*, 47:5971–5981, 2014.
- [116] M. Rubinstein and R. H. Colby. *Polymer Physics*. Oxford University Press Inc., 2003.

- [117] C. Roland and P. Santangelo. Effect of temperature on the terminal relaxation of branched polydimethylsiloxane. *J. Non-Cryst. Solids*, 307–310:835–841, 2002.
- [118] R. H. Ewoldt and G. H. McKinley. Creep ringing in rheometry or how to deal with oft-discarded data in step stress tests. *Rheol. Bull.*, 76:4–6; 22–24, 2007.
- [119] Y. Jia, K. Peng, X. long Gong, and Z. Zhang. Creep and recovery of polypropylene/carbon nanotube composites. *Int. J. Plast.*, 27:1239–1251, 2011.
- [120] M. T. Johnston and R. H. Ewoldt. Precision rheometry: Surface tension effects on low-torque measurements in rotational rheometers. *J. Rheol.*, 57:1515–1532, 2013.
- [121] D. Lin, B. Yurke, and N. Langranaa. Inducing reversible stiffness changes in DNA-crosslinked gels. *J. Mater. Res.*, 20:1456–1464, 2005.
- [122] M. L. Previtiera, U. Chippada, R. S. Schloss, B. Yurke, and N. A. Langrana. Mechanical properties of DNA-crosslinked polyacrylamide hydrogels with increasing crosslinker density. *Biores Open Access.*, 1:256–259, 2012.
- [123] F. Topuz and O. Okay. Rheological behavior of responsive DNA hydrogels. *Macromolecules*, 41:8847–8854, 2008.
- [124] O. Okay. DNA hydrogels: New functional soft materials. *J. Polym. Sci., Part B: Polym. Phys.*, 49:551–556, 2011.
- [125] J. Cui and A. d. Campo. Multivalent H-bonds for self-healing hydrogels. *Chem. Commun.*, 48:9302–9304, 2012.
- [126] V. Can, Z. Kochovski, V. Reiter, N. Severin, M. Siebenbürger, B. Kent, J. Just, J. P. Rabe, M. Ballauff, and O. Okay. Nanostructural evolution and self-healing mechanism of micellar hydrogels. *Macromolecules*, 49:2281–2287, 2016.
- [127] A. Noro, Y. Matsushita, and T. P. Lodge. Thermoreversible supramacromolecular ion gels via hydrogen bonding. *Macromolecules*, 41:5839–5844, 2008.
- [128] K. P. Nair, V. Breedveld, and M. Weck. Complementary hydrogen-bonded thermoreversible polymer networks with tunable properties. *Macromolecules*, 41:3429–3438, 2008.
- [129] F. Tanaka and S. Edwards. Viscoelastic properties of physically crosslinked networks: Part 2. Dynamic mechanical moduli. *J. Non-Newtonian Fluid Mech.*, 43:273–288, 1992.

- [130] J. Kim, Y. Gao, C. Hebebrand, E. Peirtsegaele, and M. E. Helgeson. Polymer-surfactant complexation as a generic route to responsive viscoelastic nanoemulsions. *Soft Matter*, 9:6897–6910, 2013.
- [131] D. M. Loveless, S. L. Jeon, and S. L. Craig. Rational control of viscoelastic properties in multicomponent associative polymer networks. *Macromolecules*, 38:10171–10177, 2005.
- [132] R. Long, K. Mayumi, C. Creton, T. Narita, and C.-Y. Hui. Rheology of a dual crosslink self-healing gel: Theory and measurement using parallel-plate torsional rheometry. *J. Rheol.*, 59:643–665, 2015.
- [133] Y. Lei and T. P. Lodge. Effects of component molecular weight on the viscoelastic properties of thermoreversible supramolecular ion gels via hydrogen bonding. *Soft Matter*, 8:2110–2120, 2012.
- [134] J. I. Jay, K. Langheinrich, M. C. Hanson, A. Mahalingam, and P. F. Kiser. Unequal stoichiometry between crosslinking moieties affects the properties of transient networks formed by dynamic covalent crosslinks. *Soft Matter*, 7:5826–5835, 2011.
- [135] X. Ma, R. Usui, Y. Kitazawa, H. Kokubo, and M. Watanabe. Photo-healable ion gel with improved mechanical properties using a tetra-arm diblock copolymer containing azobenzene groups. *Polymer*, 78:42–50, 2015.
- [136] S. Tang and B. D. Olsen. Relaxation processes in supramolecular metallogels based on histidine-nickel coordination bonds. *Macromolecules*, 49:9163–9175, 2016.
- [137] A. Noro, Y. Matsushita, and T. P. Lodge. Gelation mechanism of thermoreversible supramacromolecular ion gels via hydrogen bonding. *Macromolecules*, 42:5802–5810, 2009.
- [138] C. Liu, J. He, E. v. Ruymbeke, R. Keunings, and C. Bailly. Evaluation of different methods for the determination of the plateau modulus and the entanglement molecular weight. *Polymer*, 47:4461–4479, 2006.
- [139] M. Piest, X. Zhang, J. Trinidad, and J. F. J. Engbersen. pH-responsive, dynamically restructuring hydrogels formed by reversible crosslinking of PVA with phenylboronic acid functionalised PPO-PEO-PPO spacers (jeffamines[®]). *Soft Matter*, 7:11111–11118, 2011.

- [140] R. J. J. Jongschaap, R. H. W. Wientjes, M. H. G. Duits, and J. Mellema. A generalized transient network model for associative polymer networks. *Macromolecules*, 34:1031–1038, 2001.
- [141] A. Panjkovich and F. Melo. Comparison of different melting temperature calculation methods for short DNA sequences. *Bioinformatics*, 21:711–722, 2005.
- [142] T. E. Ouldridge, P. Šulc, F. Romano, J. P. K. Doye, and A. A. Louis. DNA hybridization kinetics: zippering, internal displacement and sequence dependence. *Nucleic Acids Res.*, 41:8886–8895, 2013.
- [143] B. Barry. The self bodying action of the mixed emulsifier sodium dodecyl sulfate/cetyl alcohol. *J. Colloid Interface Sci.*, 28:82–91, 1968.
- [144] S. Jan and A. Seema. Polymers with upper critical solution temperature in aqueous solution. *Macromol. Rapid Commun.*, 33:1898–1920, 2012.
- [145] A. Kanda, M. Duval, D. Sarazin, and J. François. Theta point of polyacrylamide in aqueous solution and temperature dependence of the molecular dimensions. *Polymer*, 26:406–412, 1985.
- [146] E. Miyoshi, T. Takaya, and K. Nishinari. Gel-sol transition in gellan gum solutions. i. Rheological studies on the effects of salts. *Food Hydrocoll.*, 8:505–527, 1994.
- [147] J. Yang, F.-K. Shi, C. Gong, and X.-M. Xie. Dual cross-linked networks hydrogels with unique swelling behavior and high mechanical strength: Based on silica nanoparticle and hydrophobic association. *J. Colloid Interface Sci.*, 381:107–115, 2012.
- [148] P. Matricardi, C. Cencetti, R. Ria, F. Alhaique, and T. Coviello. Preparation and characterization of novel gellan gum hydrogels suitable for modified drug release. *Molecules*, 14:3376–3391, 2009.
- [149] P. Karacan, H. Cakmak, and O. Okay. Swelling behavior of physical and chemical DNA hydrogels. *J. Appl. Polym. Sci.*, 128:3330–3337, 2013.
- [150] M. L. Previterra and N. A. Langrana. Preparation of DNA-crosslinked polyacrylamide hydrogels. *J. Vis. Exp.*, 0:0, 2014.
- [151] T. Takigawa, Y. Morino, K. Urayama, and T. Masuda. Poisson’s ratio of polyacrylamide (PAAm) gels. *Polymer Gels and Networks*, 4:1–5, 1996.

- [152] T. Boudou, J. Ohayon, C. Picart, and P. Tracqui. An extended relationship for the characterization of Young's modulus and Poisson's ratio of tunable polyacrylamide gels. *Biorheology*, 43:721–728, 2006.
- [153] W. E. M. Noteborn, Y. Gao, W. Jesse, A. Kros, and R. E. Kieltyka. Dual-crosslinked human serum albumin-polymer hydrogels for affinity-based drug delivery. *Macromol. Mater. Eng.*, 302:1700243, 2017.
- [154] J. C. Day and I. D. Robb. Thermodynamic parameters of polyacrylamides in water. *Polymer*, 22:1530–1533, 1981.